Loughborough University

Investigations into the pre-treatment methods for the removal of Nickel (II) and Vanadium (IV) from crude oil

by

Rose Erdoo Ikyereve

A Doctoral Thesis Submitted in partial fulfilment of the requirements for the award of Ph.D. of Loughborough University 2014

Abstract

The efficacy of using zeolitic materials for the removal of nickel (II) and vanadium (IV) ions from solution has been evaluated in order to provide a method for the removal of the metal ions during hydroprocessing of crude oil. Batches of sodium based zeolites with a variety of pore sizes and Si/Al ratios were prepared using standard methods (high causticity solutions and templating agent). Characterisation of the products was carried out using powder X-ray diffraction, infrared spectroscopy, Raman spectroscopy and thermogravimetric analysis to confirm the presence of single zeolitic phases (zeolite A, zeolite X, zeolite Y, sodalite $Na_8 [AlSiO_4]_6Cl_2$ and hydrosodalite $Na_6 [AlSiO_4]_6$. $6H_2O$). In a batch exchange process, divalent nickel and tetravalent vanadium ion solutions of concentration range 0.01M - 0.1M were placed in contact with the zeolite samples at 110°C for a period of 24h.

Nickel (II) exchange was found to occur for all the zeolites at concentrations considered. Zeolite X was found to be most efficient at removing nickel from the solutions while zeolite Y was least efficient. Characterisation of zeolite X after ion exchange using powder X-ray diffraction and scanning electron microscopy showed that the structure of the zeolite had been maintained. Simplistic modelling of powder X-ray diffraction data have shown that the nickel ions are preferentially substituted on one of the four sodium sites.

Vanadium (IV) exchange was also found to occur for all the zeolites at the concentrations considered. Zeolite A was found to be most efficient for the vanadium uptake. Characterisation with PXRD, FTIR and SEM-EDS however, shows that in addition to exchange at the zeolite's normal cation exchange sites, a significant amount of framework silicon species were also exchanged by the vanadium ions thus having a destructive effect on the zeolite framework leading to structural collapse.

Ion exchange of the sodium-based zeolites with potassium and lithium showed that the uptake of nickel and vanadium of the zeolites significantly increased compared to the as- synthesised zeolites. Zeolite Y was surface-modified with the APTES ligand and showed a similar trend to that observed for alkali metal-zeolites; showing significantly greater nickel uptake at lower concentrations.

Nickel-tetraphenylporphrin was synthesised as a mimic for the nickel-asphaltenes found in crude oil and an α-hydrogen donor solvent used to remove the nickel in the presence of zeolite ion exchangers. A similar trend was observed to that seen in aqueous solution, implying the process would be transferrable to a live medium.

Analysis to determine the metal ions present in ashed Nigerian crude samples before and after solvent and/or complexing agent extraction was carried out using inductively coupled plasma mass spectroscopy (ICPMS) and energy fluorescence analysis by X-rays (XRF). The process showed varying amounts of nickel was extracted by the different media along with iron. For nickel, the extent of extraction in the order of increasing % extraction is $H_2O<H_3PO_4<EDTA<IPA$. For iron the order of increasing % extraction was $H_2O=EDTA<H_3PO_4<CH_3OH$ while zinc extraction was in the order $H_2O<H_3PO_4 <CH_3OH=EDTA$.

Acknowledgements

Table of contents

Lists of Abbreviations

LCO	Light Crude Oil
HCO	Heavier Crude Oil
HDM	Hydrodemetallization
HDS	Hydrodesulphurization
HDN	Hydrodenitrogenation
H/C	Hydrogen-to-carbon ratio
AR	Atmospheric residue
PNA	Polynuclear aromatics
CUS	Coordinative unsaturated sites
TEM	Transmission electron microscopy
STM	Scanning tunnelling spectroscopy
SBU	Secondary building units
FAU	Faujasite
LTA	Linde type A
SOD	Sodalite
XRD	X-ray diffraction
PXRD	Powder X-ray diffraction
XRF	X-ray florescence
IR	Infrared
FTIR	Fourier transformed infrared
F	Scattering factor
UV-Raman	Ultraviolet-Raman
CARS	Coherent antistokes Raman scattering
CCD	Charge coupled device
TGA	Thermogravimetric analysis
DTA	Differential thermal analysis
DSC	Differential scanning calorimetry

NMR	Nuclear magnetic resonance
SSNMR	Solid state nuclear magnetic resonance
MAS	Magic angle spinning
CP	Cross polarisation
DP	Direct polarisation
CSA	Chemical shift anisotropy
SSB	Spinning side bands
DI	relaxation delay
DEC	decoupling
FID	Free inductive decay
TOSS	Total suppression of spinning side bands
HR-MAS	High resolution magic angle spinning
SEM	Scanning electron microscopy
EDS	Energy dispersive X-ray
FEG-SEM	Field emission gun scanning electron microscopy
SSD	Silicone drift detector
ICP-OES	Inductively coupled plasma optical emission spectroscopy
AAS	Atomic absorption spectroscopy
GC	Gas Chromatography
GC-MS	Gas chromatography-mass spectroscopy
RF	Radiofrequency
VU	Ultraviolet Spectroscopy
UV-Vis	Ultraviolet-visible spectroscopy
DMF	Dimethylformamid
PTFE	Polytetrafluoroethylene
HOPG	Highly ordered pyrolytic graphite

Chapter 1: Introduction and

Literature Review

1.1. Background of the study

The worldwide depletion in light crude oil (LCO) reserves and a declining availability of conventional crudes has resulted in a significant increase in the price for oil, especially in developing countries like Nigeria. LCO as used in this context, refers to oil that has a low viscosity compared to the heavier crude oil (HCO) with high viscosity. The HCO contains higher proportions of impurities such as metal cations, sulphur and asphaltenes which make the processing of these crude oils more difficult and hence the oil itself is less desirable[1, 2]. The impurities, in addition to polluting the crude oil, also present a disposal problem to the environment.

Current methods used for the removal of asphaltenes and their associated metal cations to upgrade and lighten the crude oil include; distillation, solvent refining and hydrotreating processes. The conventional hydrotreating processes use catalysts and hydrogen to facilitate the refining process and increase the value of the oil by reducing the viscosity and removing the impurities. The catalysts, which are the major active component of the process, can be poisoned by the nickel and vanadium cations that are released when the asphaltenes in the crude oil break down. The poisoning process is a result of the irreversible binding of the nickel and vanadium cations to the catalysts which gradually reduce their efficacy.

In order to prolong the life of the catalysts, removal of the metal ions from the crude oil is necessary before the ions come in contact with the active materials. The scale of the refining process means that this removal process has to be simple, cost effective and generate minimal waste during its operation. Common methods for the removal of metal ions from solution include complexation, adsorption, solvent extraction, reverse osmosis, ultrafiltration or ion exchange[3-5]. Of all these methods, metal ion exchange from aqueous solution with ionic species in a solid matrix is an attractive option due to the basic simplicity of the application. While numerous materials can be used for ion exchange on a small scale such as resins, the exchange of metal cations on an industrial scale is dominated by zeolites and clays. Zeolites and clays are cheap to purchase and are considered environmentally benign since they break down to natural materials such as quartz and feldspars on decomposition, and are easily

recycled for the target application by flooding with a solution concentrated in the original exchangeable cations (normally sodium). Many different natural and synthetic zeolitic materials have been used to remove species which are harmful or damaging to industrial processes such as the natural zeolite, clinoptilolite, in the SIXEP effluent plant in Sellafield or the synthetic zeolite, Linde 4A, in water softening[6-7]. This work is therefore focused on identifying suitable zeolitic materials for the removal of nickel and vanadium cations from crude oil before it is passed through to the downstream processes where the active catalysts can be contaminated and damaged by these species. However, the necessity to work in an aqueous environment where these processes are effective, is a challenge which must be addressed if the aqueous efficacy levels are to be replicated.

1.2. Statement of the research problem

Heavier crude oils are majorly composed of hydrocarbons along with much higher levels of contaminants than are present in the lighter crude oils. The predominant and most undesirable contaminants in crude oil are the metal cations, which not only act as environmental poisons on burning, but also have detrimental effects on the processing catalysts[8]. While significant effort has been made to investigate different ways to regenerate these materials, catalysts that are poisoned by metal cations are difficult and expensive to regenerate[9]. The most problematic metal ions in crude oil are nickel and vanadium, the amounts of which usually vary from a few ppm to more than 1000 ppm. Depending on the source of crude oil, the concentration of vanadium varies from as low as 0.1 ppm to as high as 1200 ppm, while that of nickel commonly varies from trace to 150 ppm[1]. Other metal cations found in crude oil include iron, sodium, potassium, lithium, calcium, strontium, copper, silver, manganese, tin, lead, cobalt, titanium, gold and chromium[10] with significant variation in the concentrations of the species depending on the local geology of the oil field.   The majority of these metal ions are removed during the processing of HCO into lighter, higher value oil. Unfortunately, the nickel and vanadium cations in the crude oil act as poisons to the catalysts used in the process thereby generating downtime costs as the catalyst is replaced. While other poisons such as coke can also render the hydrotreating catalysts

ineffective, their mechanism of catalyst poisoning differs; the poisoning by coke is quite rapid and reversible but that by the vanadyl cations is slow,cumulative and irreversible[11]. The irreversible poisoning of the catalysts then causes an increase in the processing costs as well as environmental problems in the disposal of waste catalysts.

1.3. Significance of the study

Much work has been devoted to understanding the poisoning effect of hydroprocessing catalysts by metal cations and coke, but only a few studies have really targeted the removal of these poisonous species from crude oil. Some of these studies include solvent extraction [12, 13], oxidation of metal contaminants[14], hydrodemetallization (HDM) and electrochemical techniques[15]. Alternative process technologies have recently been emerging; some of these emerging technologies include irradiation technology, membrane technology and bioconversion [16,17]. However, these technologies have major drawbacks of high cost and complexity of operation, which make them uneconomical. The metal ions exchange/adsorption with zeolites is a simpler, cheaper and more environmentally friendly compared to the other techniques. Precedence for the use of zeolites in the industry is also important, since the processing of oil is ubiquitous and making changes to processes is difficult; in addition to their ion exchange/adsorption properties, zeolites are also used in the petroleum industry for cracking.

1.4. Aim

The aim of this research is to explore the potential of synthethic zeolite materials for the selective removal of (catalytically) poisonous metal cations extracted from crude oil.

The first stage of the project was to identify a group of zeolitic materials with varying aluminium to silicon ratios and ring sizes to investigate the ability of zeolites to remove the nickel and vanadium cations, which are the most detrimental to the operation of the catalysts used in hydroprocessing, effectively from aqueous solution. A variety of materials were synthesised and characterised by powder X-ray diffraction, thermogravimetric analysis and infra-red spectroscopy. As well as varying the type of

framework (X, Y A and sodalites), the charge balancing extra framework sodium cations were also varied to examine whether potassium or lithium based materials were more proficient at ion exchange than the original sodium rich materials. The concentration of the nickel/vanadium in solution was also varied to mimic the wide variation observed in natural crude oil extracted from different areas of the world. Further work was carried out to surface modify zeolite frameworks with organic ligands to investigate any improvement in the uptake of the poisoning ions compared with the unmodified framework materials by using different chelating species on the organic ligand.

Porphyrins containing nickel cations were synthesised in order to mimic the breakdown of asphaltenes and the subsequent removal of the ions from the oil by solvent extraction. Hydrogen donor solvents were used to protonate the porphyrin and remove the species before using the zeolites to extract the ions from the resulting emulsions. These framework materials were employed with the aim of removing the metal ions (Ni^{2+} and V^{4+}) from crude oil in a hydroformulated state (emulsion) before they poison the catalysts in the proceeding hydrotreating processes. Research on crude oil emulsion forming and metal ion removal from emulsified and non- emulsified media shows that crude oil with high vanadium and nickel contents are capable of forming stable emulsions and the metal ion removal from the emulsified media found to be much higher than in the non-emulsified media[18-19]. Based on these studies and for the fact that crude oils contain significant quantities of water, it is believed that the metal ions in crude oil could be removed in an emulsified medium using framework materials. Thus, the efficacy of using the various framework materials for the removal of these metal ions was first evaluated using aqueous media and the most efficient materials used with the crude oil.

1.5. Crude oil

Crude oil, one of the fossil fuels, is formed over millions of years from the remains of aquatic plants and animals due to the combined effect of time and temperature. Petroleum products derived from crude oil are high value commodities, but the

unrefined crude oil itself, straight from the ground, has much lower value. Before crude oil became commonplace in 1859, crude oil had limited uses such as an adhesive in construction, water-proofing for ships, fuel for flaming projectiles and a base for a wide variety of ointments[20-23]. However, after 1859, petroleum became increasingly important to the World's economy. In 2014, 60% of the World's shipping , on a tonnage basis, is concerned with the movement of petroleum-based materials[22]. Most human activities in the 21st century would be significantly inhibited without crude oil despite environmental concerns regarding carbon based emissions.

Crude oil, based on their API (American Petroleum Institute) gravity, can be classified as light (API>31.1), medium (API between 22.3 and 31.1), heavy (API<22.3) and extra heavy (API<10) oils.

Heavy crude oils can be described as 'colloidal solutions consisting of three groups of materials namely: oils, resins and asphaltenes'. Resins and asphaltenes along with high proportions of metal ions, raise the viscosity of the oil as well as increase the cost of treatment thus making the oil less desirable[2, 24]. Asphaltenes, as the heaviest material, represent a group of large molecules, which can be separated from the crude oil by precipitation using paraffinic hydrocarbons such as pentane, hexane and heptane. They contain large proportions of metal ions particularly vanadium and nickel. Figure 1.1 shows the schematic structure of asphaltenes.
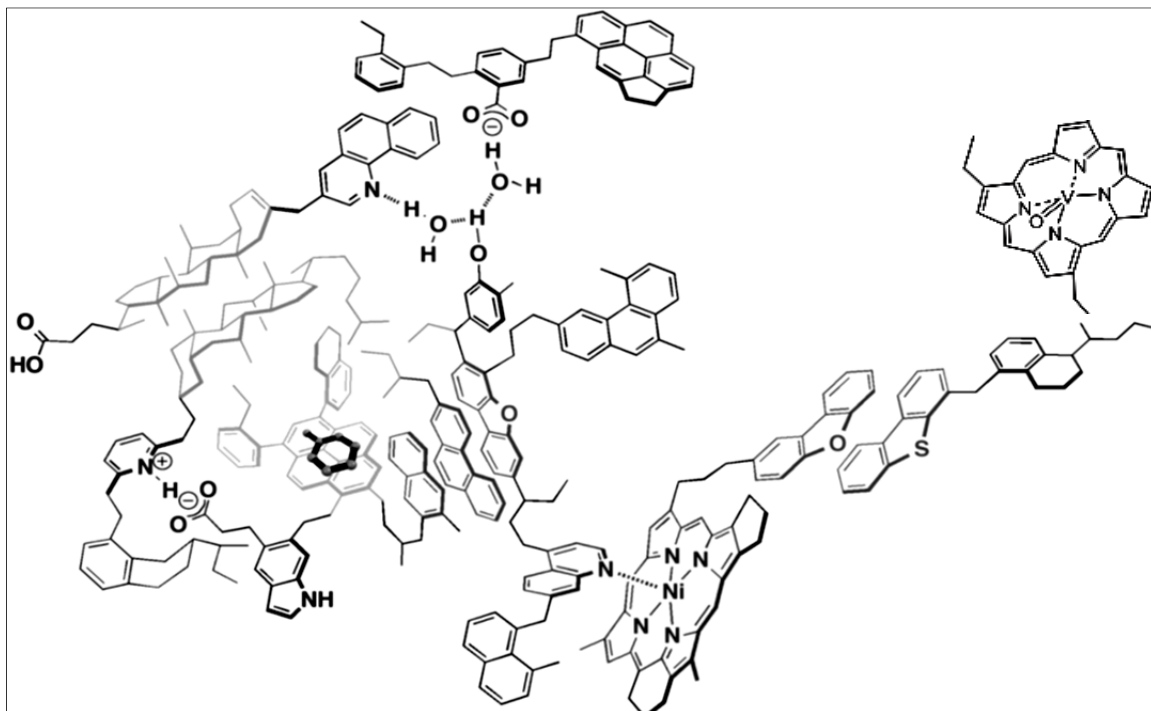
Figure 1.1: Representative asphaltenes molecules, also showing association between molecules.[25]

Resins, like asphaltenes, also represent a group of large molecules. The difference between the two lies in the fact that resins are less-polar than asphaltenes but more polar than oil. Resins act as dispersing agents for the polar asphaltenes, forming micelles (Figure 1.2) similar to that in surfactants (detergents) where the polar asphaltenes and non-polar oils are bound together via the intermediate polarity resin[26]. Micelles are aggregates of asphaltenes and resins held together by weak physical interactions. Asphaltenes occupy the core of the micelles with resins adsorbed on the external surface, thereby dispersing the asphaltenes in oil. This aggregation makes it possible for crude oil to form emulsions.
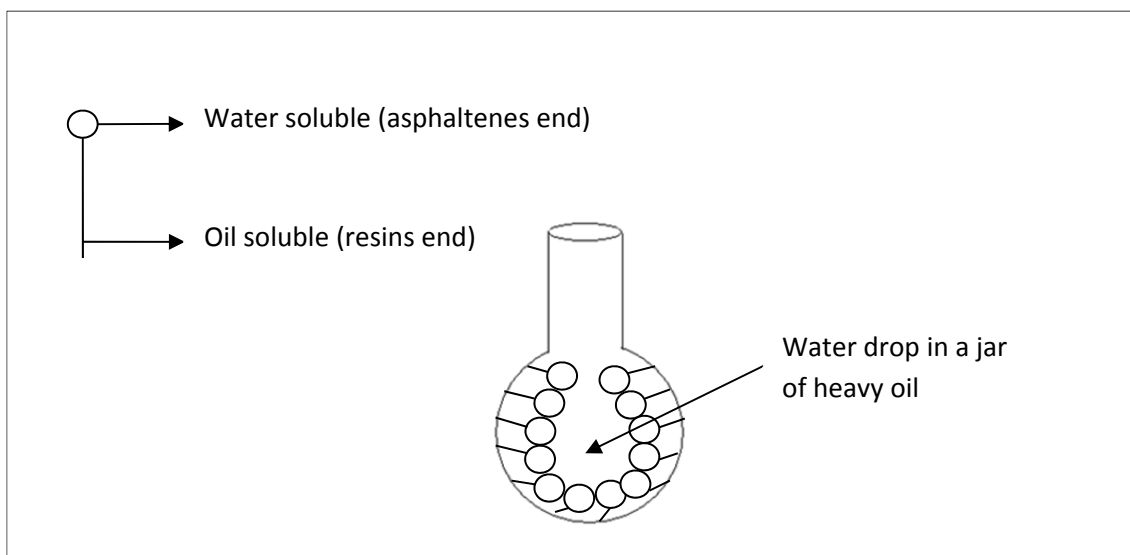
Figure 1.2: Indigenous surfactants in crude oil

Without the presence of the intermediate polarity resins, asphaltenes would coagulate and form sediments during storage and transportation of the heavier oils. It is therefore essential that during processing of the oil, resins are converted at a similar rate to asphaltenes. Otherwise, a much greater rate of the conversion of resins than that of asphaltenes would result in the incompatibility of the components of the colloidal system[25].

The large molecules in crude oil, resins and asphaltenes, are broken down into lighter, higher valued petroleum products through a series of hydrogen addition and carbon rejection processes during petroleum processing as described in section 1.6.

1.6. Petroleum processing

Modern day refineries are extremely complex, owing to their different histories, locations, and market drivers. Hence, no single refinery can be conveniently used to give a general description of an oil refinery. All the differences notwithstanding, almost all refineries perform some common basic operations namely: separation, which includes distillation and solvent refining, conversion which comprises carbon removal and hydrogen addition processes. Other common operations include reforming comprising both catalytic and steam reforming, rearrangement which are basically isomerization processes, combination which comprises the catalytic

polymerization and alkylation, treating, finishing or blending and finally waste treatment or recovery units[2]. The schematic illustration of the petroleum refinery processes is as presented in figure 1.3.
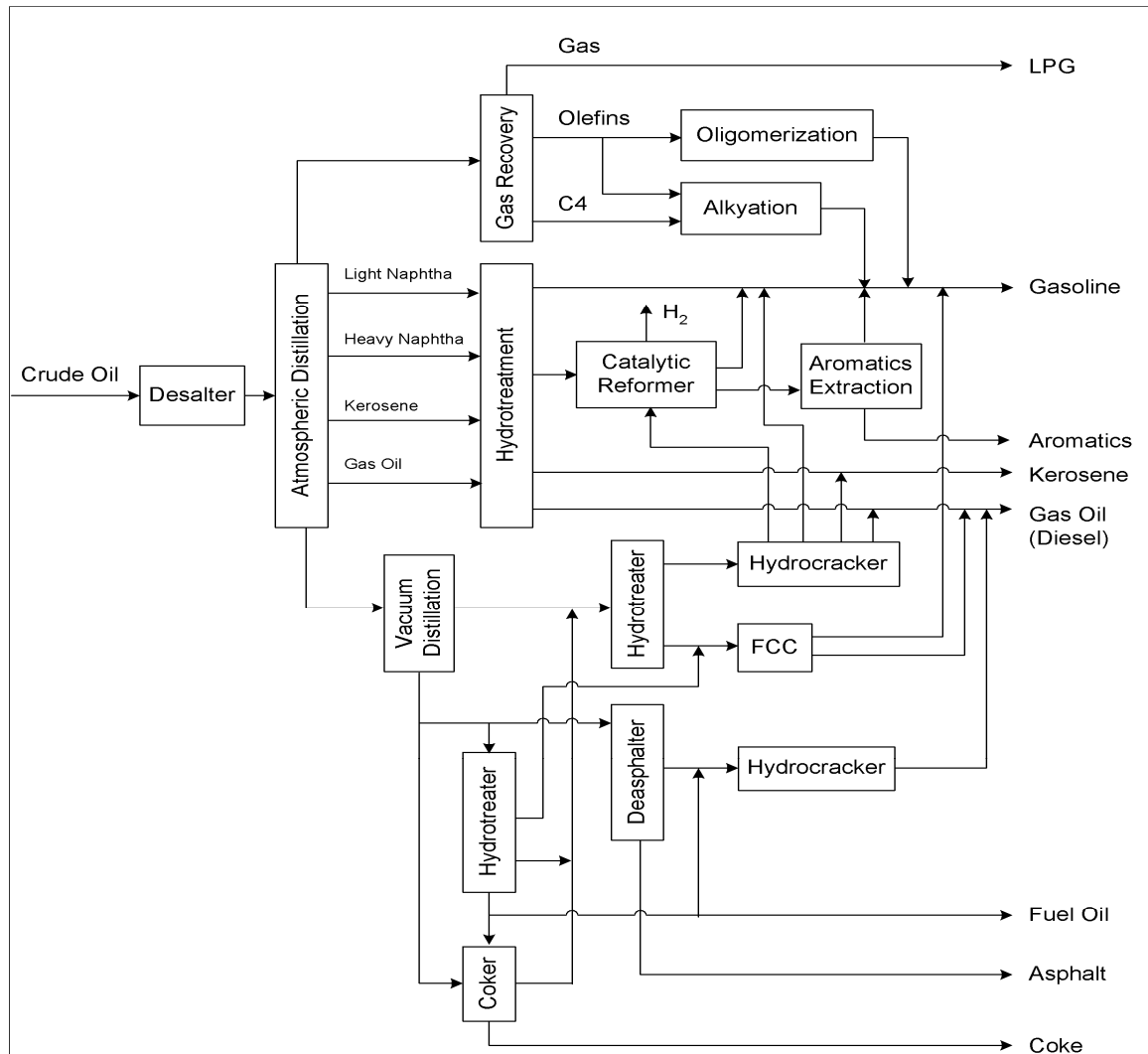
Figure 1.3: Schematic illustration of a petroleum refinery[2]

The various processes in the refinery are aimed at achieving an improved quantity of refined crude oil, improving the refined oil quality by removal of impurities like metal ions and sulphur as well as improving the quality of petroleum feedstock for downstream processes. A brief description of each of the key processes is given in the subsequent sections.

1.6.1. Distillation

Distillation is the process of separating crude oil fractions by the difference in their boiling points. Crude oil distillation unit is known to be the biggest unit in most plants in terms of throughput. Many downstream conversion units also use distillation for product separation. For example, in a coker, hydrocracker, or fluid catalyst cracking (FCC) unit, an atmospheric tower, a vacuum tower, and a multi-column gas plant may be required[27].

1.6.1.1. Atmospheric distillation

Crude oil distillation is a complicated process, majorly because of the impurities contained in crude. Some of these impurities include: water, salts, metals and suspended solids. These contaminants have to be removed from the crude in order to reduce corrosion, plugging, and fouling in crude oil heaters and towers as well as preventing the poisoning of catalysts in downstream units[27]. A desalting process is employed for the removal process. The two most common methods of crude oil desalting are chemical and electrostatic separation. Chemical desalting uses water and surfactants to dissolve salts and impurities from the crude oil at elevated temperature while electrostatic desalting makes use of a strong electrostatic charge to effect the separation of water from oil[27]. Figure 1.4 represents a schematic diagram of the crude oil distillation unit.
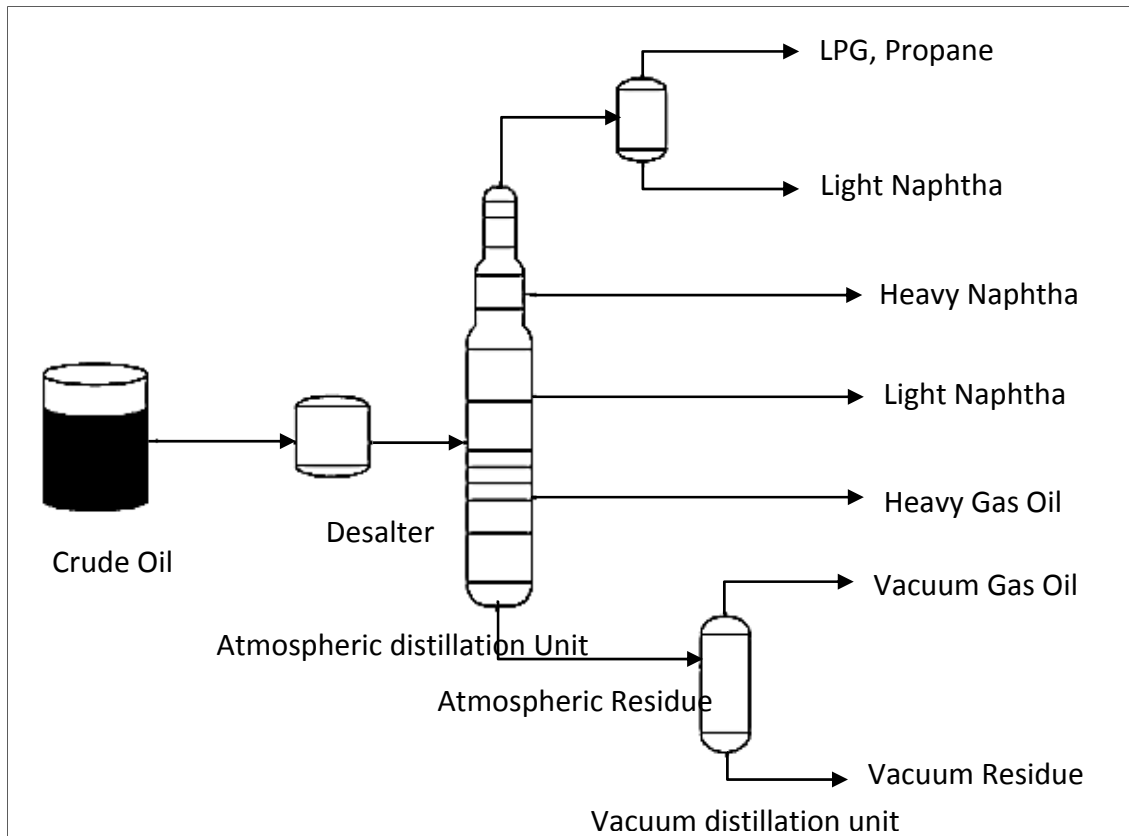
Figure 1.4: Crude distillation unit[2]

A modern crude oil distillation tower is able to process upto 200,000 barrels of oil per day. It may contain up to 40 fractionation trays, about 50m tall, spaced at regular intervals. Desalted oil is first sent through a network of pre-heat exchangers, then to a fired heater, where the oil is heated at 343°C before reaching the distillation towers. The temperature is maintained at 343°C so as to prevent the oil from cracking and depositing carbon inside the flow pipelines and equipment. Steam is added to the crude oil once it has entered the distillation tower to enhance separation by decreasing the vapour pressure in the column. When heated crude oil is fed into the lower part of the tower, the lighter oil fraction vaporise. Losing heat as they rise, they condense into liquids which flow downwards into the higher temperature and are again vaporised. A given molecule of oil evaporates and condenses many times before finally leaving the tower. The unvaporized heavy fuel oil and/or asphalt residue drops to the bottom of the tower, where it is drawn off[28].

1.6.1.2. Vacuum distillation

Vacuum distillation is carried out in a vacuum created by a vacuum pump, contrary to the atmospheric columns; the vacuum columns have larger diameters and a simpler interior. Vacuum distillation is used to recover additional light vacuum gas oils from the residue obtained from atmospheric distillation towers. The product here can be used as a lube base stock, heavy fuel oil, or as feed to a conversion unit[29].

1.6.2. Solvent refining

Solvent refining is a process used to segregate compounds with similar compound types, such as paraffins and aromatics. Three main types of solvent refining include; solvent deasphalting, solvent extraction, and solvent de-waxing[30].

1.6.2.1. Solvent deasphalting

Solvent deasphalting is a process used to precipitate aromatic compounds from crude oil. Propane deasphalting, for example, is used to precipitate asphaltenes from residual oils. The deasphalted oil (DAO) is then sent to downstream units like; hydrotreaters, FCC units, hydrocrackers, or fuel-oil blending for further processing. These are easier to process due to the low amounts of coke and catalyst poisons like nickel and vanadium. Solvent deasphalting of residual oil in propane is carried out between 65 to 120°C and 2514 to 4240 kPa while the separation occurs in a tower, which may have a rotating disc contactor[2]. Solvent deasphalting process will be discussed in more detail in section 1.6.3.1.1.

1.6.2.2. Solvent Extraction

Solvent extraction is used to remove aromatics and other impurities from lube and grease stocks. Here the crude stock is dried, then exposed to the solvent in a counter-current or rotating disk extraction unit. Heating, evaporation, or fractionation is used to recover the solvent from the extraction mixture[2].

1.6.2.3. Solvent De-waxing, Wax De-oiling

Solvent de-waxing is used to remove wax from deasphalted lube base stocks. It is a simple process which involves mixing the crude stock with the solvent, chilling the

mixture to crystallize wax, and recovering the solvent. Toluene and methyl ethyl ketone (MEK) are the most commonly used solvents[2].

1.6.3. Conversion

The rising demand for automotive gasoline has increased the demand to convert heavier crude oil fractions into petroleum which are lighter and contain higher hydrogen-to-carbon ratios (H/C). The H/C of commonly used crude oils ranges from 1.5 to 2.0, and the H/C for asphaltenes is 1.15.[2]

Most conversion processes like fluid catalytic cracking, thermal cracking, and deasphalting aim at increasing the H/C by rejecting carbon. Other processes like hydrocracking and hydrotreating, increases the H/C by adding hydrogen[31]. Carbon rejection here means that heavy molecules are cracked into a smaller molecule with a higher H/C and another smaller molecule with a lower H/C. The cracking process is therefore used to inter-convert crude oil products and thus maximise commercial value[31].

Refining processes can be classified into two broad groups; non-catalytic processes which include solvent deasphalting and thermal processes and the catalytic processes, which include residue fluid catalytic cracking and hydroprocessing[31].

Catalytic processes are common place in the industry due to their high yield of liquid products even though their costs of operations are high. Moreover, liquid products obtained from non-catalytic processes contain higher amounts of S, N and metals (V, Ni, etc.) that indeed need further purification[31].

1.6.3.1. Non Catalytic processes

1.6.3.1.1. Solvent Deasphalting: pros and cons

Solvent deasphalting, as mentioned earlier, is a physical method used to precipitate asphaltenes from crude oil[3]. It is a unique separation process in which residual oil is separated by molecular weight (density) rather than by difference in the boiling points. Residual oil is the low-grade oil after the distillation of petroleum. The residual oil and heavy crude oil contain high concentrations of metal-containing aromatic compounds

(asphaltenes)[32]. During the process of deasphalting of the crude oil, the lighter fractions of oil are physically separated from the heavier asphaltenes containing oil by simply mixing the heavy crude oil with a very low boiling solvent e.g. butane or propane. The deasphalting oil present in the heavy crude oil solubilises in the solvent while the insoluble precipitates separates out as asphaltenes. The separation into the two phases, that is, the deasphalted oil phase and the contaminant phase, is carried out using an extractor and or separating funnel[32]. The design of the extractor is such that it efficiently separates the two phases and minimizes contamination of the deasphalted oil phase. Parameters such as temperature and pressure affect the yield and quality of deasphalted oil produced. Lower extraction temperature increases the deasphalted yield but decreases the quality of the oil. Deasphalted oil (DAO) is said to be a good feedstock for fluid catalytic cracking (FCC) and hydrocracking since it contains low metal content[32]. Solvent deasphalting has the advantage of producing very low contaminated deasphalted oil as well as being a relatively low cost process that has flexibility to meet a wide range of DAO qualities[32].

When the metal content of the feedstock is low, it is possible to hydrotreat the residue at moderate residue conversion levels to reach high-asphaltenes conversion levels in catalytic fixed bed reactors. It is also possible to convert more difficult crude oil feedstock with higher conversion levels, but the high-metal content of the asphaltenes containing crude oil feeds necessitate the use of specific technologies for residue hydroconversion[3]. Indeed, metal ions such as nickel and vanadium are concentrated in residue feeds and will progressively deposit and concentrate on the hydroconversion catalyst. Catalyst addition is then required to maintain catalyst activity during operation. In addition to high-metal ions content, high conversion levels followed by subsequent hydrogenation, generates significant reaction heat that needs to be controlled by an adequate mixing in order to avoid large thermal gradients along the reactor[3].

1.6.3.1.2. Thermal processes: pros and cons

Thermal processes are simply based on the redistribution of hydrogen in the heavier fractions of petroleum oil to produce the lighter fractions containing more hydrogen.

Thermal processes results in the formation of liquids, gases and coke[33]. At moderate pressures, this process transfers hydrogen from the heavy molecules to the lighter molecules resulting in the production of carbon residues or coke. Thermal processes include processes like delayed coking, fluid coking and flexi coking, visbreaking and gasification.

The gasification process is used in the refinery to convert organic or fossil based carbonaceous material into carbon monoxide, hydrogen and carbon dioxide. This process involves total and complete cracking of heavier crude oil fractions at high temperatures (>700°C) to gaseous products[33].

Delayed coking is a semi-batch cracking process, which operates at temperatures between 487 and 520 ^{o}C where cracking takes place, generating coke and cracked vaporized products in a large coke drum. It is a good and commonly used process by refiners to convert low value residue to valuable products (naphtha and diesel) and gas oil due to its ability to handle any kind of heavy crude oil[34]. It is highly selective at a given temperature and pressure providing partial conversion of liquid products and complete rejection of metal ions and carbon. The process however, has the disadvantages of cost, high coke formation and low liquid product yield[34].

Fluid coking and flexi coking differ from the delayed coking by the use of higher operating temperature conditions. Although these processes have higher yield of product compared to delayed coking, they have a disadvantage of poor quality product yield[34].

Visbreaking is a mild form of thermal cracking used to convert atmospheric residue to gas oils and naphtha. This process in addition to the gas oil and naphtha produces a low-viscosity residual fuel. This process focuses on improving the viscosity of the heavy products and usually operates at very high temperatures (450-500 ^{o}C) and then cracking takes place either at long residence time (soaker visbreaking) or low specific residence time (short time visbreaking) to avoid coking reactions. This process is usually used to increase refinery distillate yield but costly due to the high temperature requirement[34].

1.6.3.2. Catalytic processes

Catalytic processes include: residue fluid catalytic cracking and hydroprocessing of crude oil feeds.

1.6.3.2.1. Residue fluid catalytic cracking: pros and cons

This process is very selective towards high petroleum products compared to hydroprocessing and thermal processes. However, it has a limitation of using only feedstocks of high quality. The catalyst used in this process is of acidic matrix. The process, due to its limitation, can only treat atmospheric residue (AR) which contains relatively low amounts of metals, sulphur and carbon. These feeds are, however, limited in refineries making the process less likely[24].

1.6.3.2.2. Hydroprocessing: pros and cons

Hydroprocessing, comprises hydrotreating processes; hydrodemetallization (HDM), hydrodesulphurization (HDS) and hydrodenitrogenation (HDN), etc. used for the removal of impurities such as metal cations, sulphur and nitrogen along with reduction of asphaltenes contents from petroleum oil, thereby providing additional quantity of better quality feedstock for selective processes like fluid catalytic cracking and residue catalytic cracking. The diversity in hydroprocessing is not only based on catalyst development, but also process technology which can be selectively based on the desired product yield[35]. Hydroprocessing of heavy oils is difficult because of the complex nature of the heteroatom bearing molecules. During hydroprocessing, some heteroatoms escape out from the systems as gaseous products and the more refractory compounds remain in the liquid products, while metals get irreversibly deposited on the catalysts causing permanent deactivation[36].

Hydroprocessing combines the principles of hydrotreating and hydrocracking processes where residue feedstock is treated at low temperature but at high hydrogen pressure with or without catalysts. For example, in hydrotreating process, there could be a large pore size cracking where a demetallization catalyst is used in the front end and a high activity hydrodesulphurization catalyst employed subsequently. Most of the processes utilise catalyst except a few like hydrovisbreaking. Catalyst used here are transition metal sulphides dispersed on high surface area support. Hydroprocessing

technologies have advantages of product selectivity and production of cleaner fuel; however, it also has a disadvantage of relatively high cost, due to high hydrogen requirement. Hence residue hydroprocessing combines the processes of catalyst development, process operation and the condition of operation[37].

1.6.4. Catalytic reforming

Catalytic reforming is a process used to convert low-octane heavy naphtha (valuable C5-plus molecules) into high octane product (light gases). This is done by blending of several different refinery streams like, butanes, straight-run gasoline, reformate, alkylate, isomerate, FCC, oxygenates, and others. High-octane product has a high content of benzene-toluene-xylene (BTX); thus it is used as source of aromatics for petrochemical plants. The hydrogen produced is also useful in hydrotreaters, hydrocrackers and other hydrogen addition processes[37]. Catalytic reforming catalysts contain highly dispersed platinum (Pt), rhenium (Re) and tin (Sn). The activity of these catalysts is inhibited by sulphur in the feedstock[37].

1.6.5. Isomerization

Almost all conversion processes have isomerization occurring as a side-reaction. However, in refining, isomerization processes are on-purpose reactions specifically setup to produce desired end products. Examples include; isomerization of n-butane, n-pentane, and n-hexane. The main purpose of n-paraffin isomerization is to produce isoparaffins with substantially higher octane numbers. The most common catalyst for isomerising n-butane is platinum (Pt) on alumina promoted by chloride[37].

1.6.6. Lubes, Waxes and Greases

The bottom fractions (atmospheric and vacuum residues) can be converted by the numerous conversion processes, or they can be used to make lubes, waxes and greases[37].

1.7. Nature of metal ions in crude oil

The metal cations which cause the poisoning of the catalyst during hydroprocessing are often associated with the asphaltene species (Figure 1.1). The nickel and vanadium ions usually exist in combination with naphthenic acid-like soap and

complex organometallic species such as metalloporphyrins which occur as part of the bulk asphaltene material. Vanadium and nickel in crude oil can be described in two broad forms; porphyrinic and non-porphyrinic, which is roughly split 50:50.[32] Several forms of vanadium and nickel containing porphyrins have been identified in heavy feeds (figure 1.5). Size exclusion chromatography has revealed the presence of both large and small vanadium containing molecules linked to these groups[38]. The latter disappear after hydroprocessing of the crude oil while the large molecules are more resistant. The large vanadium containing molecules were believed to be associated with asphaltenes, most likely in a porphyrin-like form. A confirmation study revealed that porphyrins may be occluded by a strong non-covalent interaction as part of the asphaltenes aggregates[39]. Once porphyrins were released from the aggregates, i.e., by an interaction with a solvent, a molecular weight typical of porphyrins was approached. Grigsby and Green also confirmed this observation[40]. Vanadium in crude oil exists predominantly as the vanadyl ion in chelates with porphyrins[41].
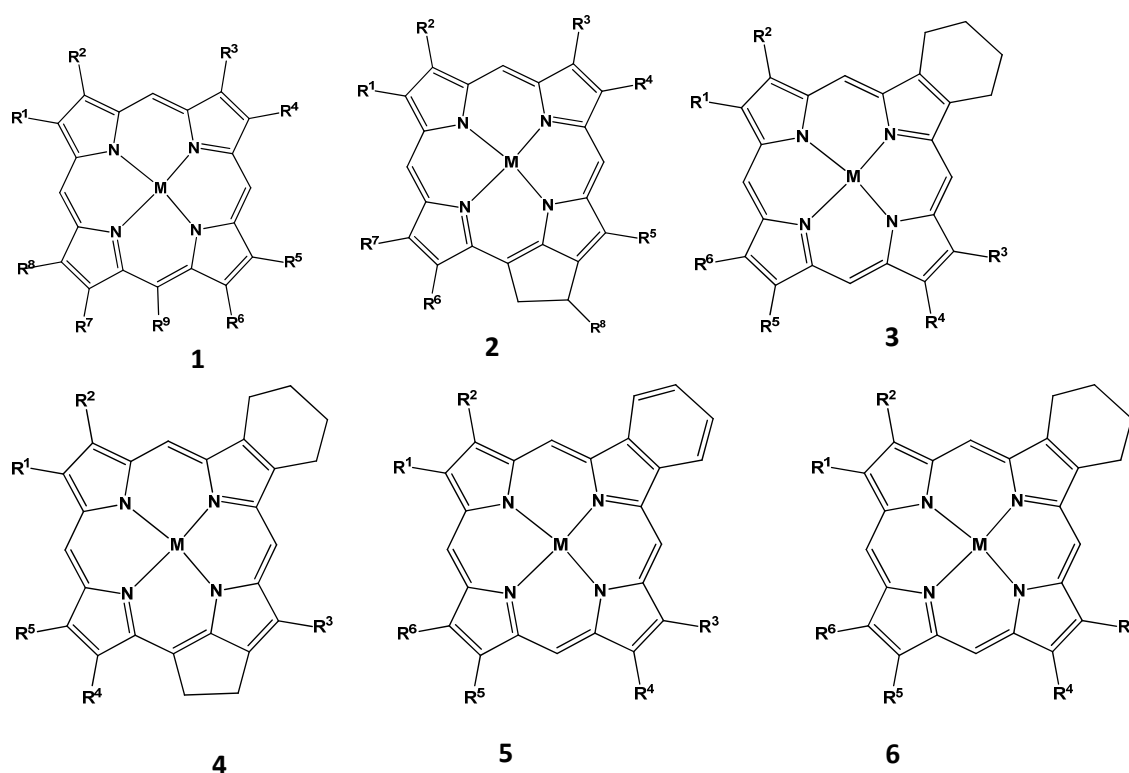
Figure 1.1: Major porphyrin structural types in heavy crude oil are; (1) etio, (2) Desoxophylloerythroetioporphyrin (DPEP), (3) benzoDPEP, (4) TetrahydrobenzoDPEP (THDPEP), (5) benzoetio, (6) tetrhydrobenzoetio[36]

The conventional hydrotreating and hydrocracking processes are used for the removal of metal ions from crude oil during refining. However, the catalysts used in the processes are easily deactivated by metals and coke. A brief description of the hydrotreating processes is given in section 1.8.

1.8. Hydrotreating processes

The processes used in petroleum refining can be grouped into; thermal, catalytic and hydroprocessing processes as earlier mentioned. The hydroprocessing comprise; hydrotreating, hydrocracking and hydrofinishing.

Hydrotreating does the hydrogenative heteroatom removal and hydrogenation while the hydrocracking performs hydrogenation and cracking successively and simultaneously. Hydrofinishing can be said to be another form of hydrotreating that is used to achieve the final specifications of fuels. Thus each of these processes are individually optimized according to the molecular composition and boiling range of the specific petroleum fraction being processed[42].

The primary objectives of hydrotreating includes; removal of impurities, such as heteroatom and metal-containing compounds from a feedstock, increasing the hydrogen content of the feedstock, and lowering the molecular weight without a substantial loss in liquid product yield.

Higher molecular weight feedstock, such as high vacuum distillates, atmospheric and vacuum residues, have impurities like; sulphur-containing compounds, nitrogen-containing compounds, oxygen-containing compounds, and polynuclear aromatic (PNA) compounds and in addition have significant concentrations of metal-containing compounds (M-compounds). V and Ni are the major metals in petroleum and mostly in the form of porphyrin complexes of $V^{4+}=O$ and Ni^{2+} [43].

Crude oils, in addition to the above impurities, often contain salts and naphthenates of some metals such as iron, magnesium and calcium. The metal salts can be removed rather easily by a desalting process before the distillation. However, small amounts of the metal compounds may be remaining in the feed, particularly Fe or its derived FeS,

which often cause operational problems. Naphthenates may dissolve iron from valves or the reactor and transfer lines, which can be included in the feeds to downstream processes. Iron dissolved by naphthenic acid in crude causes plugging by forming FeS in the catalyst bed or on the filter as well as promote coking reactions. Finely dispersed FeS may enhance coking reactions[44]. These impurities increase with increasing boiling point, thus, the hydrotreating process of choice depends majorly on the boiling range of the feedstock of interest and the product quality specification.

Oxygen-compounds are less problematic during crude oil processing in terms of catalysts poisoning. However, some oxygen compounds such as phenols and naphthenic acids lead to corrosion problems in the reactors and storage vessels.

Specific processes have however, been developed for the removal of sulphur-compounds, nitrogen-compounds and metal-containing compounds because of the problems they pose during crude oil processing. These processes are; hydrodesulphurization (HDS), hydrodenitrogenation (HDN) and hydrodemetallation (HDM) processes for the removal of sulphur, nitrogen and metal ions respectively. Metal-containing impurities are found particularly in high boiling fractions, such as atmospheric and vacuum residues. Thus, hydrodemetallation processes are geared towards the high boiling and more viscous feedstocks[45]. Nevertheless, trace amounts of metal-compounds in the light crude oil must not be overlooked since they cause problems in the long run. Brief discussion on these processes is given in sections 1.8.1 to 1.8.3.

1.8.1. Hydrodesulphurization

The current industrial method for removal of sulphur from fuel oil is hydrodesulphurization which requires high temperature and pressure, thereby making the process very expensive[32].

Desulphurization process can be grouped into two types; hydrodesulphurization (HDS) and non-hydrodesulphurization (non-HDS) depending on the role of hydrogen in removing sulphur[34]. In HDS, hydrogen is used to decompose organosulphur compounds thereby eliminating them from the refinery stream whereas non-HDS do

not require hydrogen. HDS is carried out at high temperatures and partial pressures converting organosulphur compounds to hydrogen sulphide and hydrocarbons. The conventional HDS process is usually carried out using sulphided $CoMo/Al_2O_3$ and $NiMo/Al_2O_3$ catalysts. The performance therefore is dependent on the catalyst properties, nature and concentration of sulphur present in the feed stream. The organosulphur compounds found in higher boiling crude oil fractions like heavy oils contain predominantly thiophenic rings which are more difficult to remove through hydrotreating compared to sulphides[46].

The HDS of heavy oils containing thiophenic compounds proceeds through two reaction pathways, the first pathway is the hydrogenolysis where the sulphur atom is directly removed from the molecule whereas in the second pathway, the aromatic ring is hydrogenated and sulphur removed subsequently[32]. For the non-HDS, the catalytic decomposition is done in the absence of hydrogen. Sulphur removal is achieved by adjusting the boiling point of the sulphur-containing compounds and separation done by extraction or adsorption and decomposition through selective oxidation[32].

1.8.2. Hydrodenitrogenation

Hydrodenitrogenation is a process used in the removal of nitrogen-containing compounds from crude oil. The nitrogenous compounds, like the metal and sulphur impurities, have adverse effects on the catalyst during various catalytic processes such as hydrotreating, catalytic reforming and catalytic cracking. Petroleum products with high amounts of nitrogen most times do not fit product specification[46]. This is because the nitrogenous compounds are very unstable, form deposits and cause coloration easily. Hydrodenitrogenation process is therefore used during product processing to improve the quality of product derived from high nitrogen-containing feedstock[46].

1.8.3. Hydrodemetallization

The hydrotreating process used in removing metal ions from crude oil is known as hydrodemetallisation. Nickel greatly increases the gas (H_2) and coke production of the catalyst, while vanadium reduces both catalyst activity and selectivity by destroying the catalysts structure and producing increased gas (H_2) and coke[47, 48]. Both nickel and

vanadium have the ability of undergoing dehydrogenation, hence their presence on the catalyst tends to promote dehydrogenation reaction during crude oil processing.

All the impurities in crude oil including metals, sulphur and nitrogen could be removed alongside asphaltenes during the deasphalting process since they exist as complexes with asphaltenes in the form of metalloporphyrins. However the process in addition to the removal of these impurities, remove large amounts of hydrocarbons that could be processed into valuable products. To overcome this limitation, other options have been investigated. These options include chemical treatment or solvent extraction, electrochemical treatment, hydrotreating etc. The process that proved to be most effective at reasonable removal of metals is the hydrotreating process. Hydrotreating may not be economical or practical for the processing of heavy crude oil with high metal contents due to catalyst deactivation. However, if these metals are removed prior to hydrotreatment, then the process would be more efficient[49].

1.9. Hydrotreating Catalysts

Catalysts used for hydrotreating are molybdenum and tungsten-based sulphides with promoters of nickel or cobalt sulphides supported on a high surface area alumina carrier. Alumina is said to be the best support in terms of its surface area (200 - 300 m^2/g), pore size control, affinity to sulphide for high dispersion, mechanical strength and cost. These catalysts are active in the sulphided state, being either pre-sulphided or sulphided on stream with a sulphur-containing feed[50].

About 15 - 20wt% molybdenum precursor is first impregnated so as to be highly dispersed onto alumina while the Co or Ni precursor (1 - 5wt%) is impregnated onto the Mo phase. The impregnated catalyst is carefully calcined and sulphided in the commercial application for the stable catalytic activity[50]. The active species is believed to be the Co/NiMoS phase. The Co/NiMoS phase consists of small layered crystals of S and Co/NiMo. The bottom of the Ni/CoMo layers, which contact the Al_2O_3 surface, is difficult to sulphide into the active form,[50] hence multi-layered stacks of these are believed to be more active on alumina supports. The edge and rim of the Co/NiMoS phases are believed to be particularly active for hydrotreating reactions. This is

because of the relatively small size of the slabs (10-50 Mo/slab); a good fraction of the terminal sulphur ions will be absent in order to maintain an approximate MoS_2 stoichiometry. These coordinative unsaturated sites (CUS) or sulphur anion vacancies are located at the edges of the slabs and have Lewis acid character. These sites can adsorb molecules with unpaired electrons, e.g., NO, pyridine, and are believed to be the sites for catalytic reactions. Because of the high concentration of vacancies (about 1 vacancy/edge Mo atom), double and even multiple vacancy centres can be present. Microscopic analyses like; TEM and STM have been used to understand the morphology of Co (Ni) MoS phase crystals on alumina and shows the crystal size of this phase in commercial catalysts is very small[51]. Characterization studies of these catalysts have been reviewed by a number of authors[52,53]. These studies have shown that sulphided catalysts containing Mo consist of essentially monolayer slabs or clusters of slabs of MoS_2 partially covering the alumina surface (Figure 1.6). Reports have shown that the presence of Co or Ni does not affect the basic slab size of the MoS_2, being located at the edge sites of the slabs[53]. The Co or Ni does not appear to appreciably increase the number of vacancies, but the vacancies associated with the Co or Ni are considerably more active than those associated with the Mo, leading to the increased 'promotional' activity of the catalyst. The vacancy concentration under hydroprocessing conditions is thought to be a function of the H_2 and H_2S concentrations[53]. The implication of this to deactivation is obvious that, any strongly adsorbed species, for example, metal deposit, N-compound, coke molecule, which occupies (poisons) an active vacancy site, will cause a loss in catalytic activity. This could affect the Mo vacancies, and more importantly, the more active Co or Ni sites. Since most reactants will most likely require multi vacancy site centres for adsorption, it may not even be necessary to poison all the sites of the active centres to cause deactivation, i.e., one poison molecule could conceivably poison the entire centre for reaction[53].
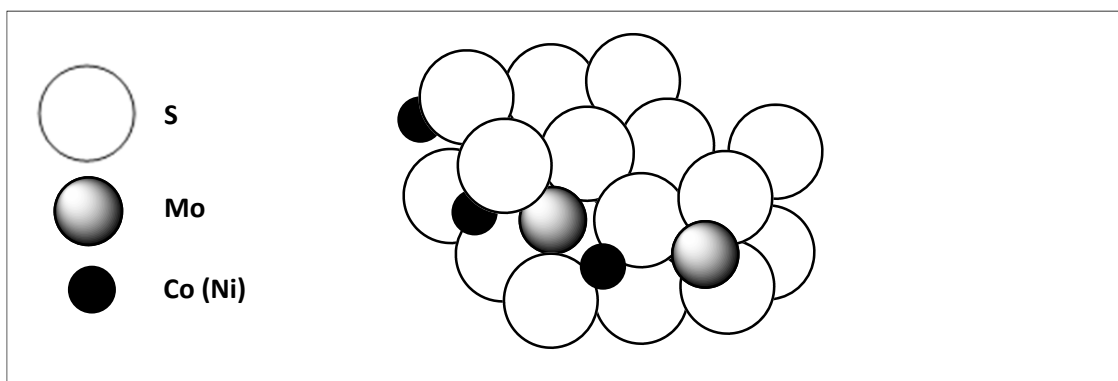
Figure 1.2: Model of MoS_2 slab[49]

1.10. Deactivation of hydrotreating catalysts

Hydroprocessing reactions occur on the active sites of the catalysts. A suitable pore size distribution is required to ensure the access of reactant molecules to the active sites. Hydrotreating catalysts lose their activity in several ways, some of these include: sintering of the active phase into large crystal units, covering of the active sites by reactants and/or products including coke and degradation of the active phase, including degradation of sulphided forms. Blocking of pore mouths, of course, render active sites unavailable to reactants, while pore mouth restriction could increase diffusional limitations on reaction rates. Irreversible site poisoning would reduce the number of sites available for reaction, and may be more severe on promotional sites. Sintering of the active slabs, which comprise a plane of Mo or W atoms sandwiched between the two hexagonal planes of sulphur atoms, would reduce the total number of surface vacancies. Also, rearrangement of the structure might disproportionally reduce certain site centre configurations more than others, affecting catalyst selectivity as well as activity[54].

The catalysts deactivation usually occurs in three steps: initial rapid deactivation, intermediate slow but steady deactivation and rapid deactivation at the end of the cycle. The initial rapid deactivation phase is said to be due to rapid coking on active sites having very high acidity. The slow but steady deactivation is believed to be associated with metal deposition, sintering and/or coking during the course of the process cycle. The final, catastrophic loss in activity is attributed to pore constriction and ultimate pore blockage[54].

For hydroprocessing of relatively light feeds, deactivation of the catalyst is minimal and the process can operate for long periods of time before replacement of the catalyst. However, for heavy crudes, catalyst deactivation can be serious, having an important commercial economic implication with respect to catalyst lifetime[54].

A number of studies have been performed to understand the underlying phenomena leading to deactivation in order to develop longer life catalysts[54-57]. These studies have however identified various factors responsible for deactivation of hydroprocessing catalysts, thereby making difficult assessment of the individual factors responsible. A few reviews published on deactivation of hydroprocessing catalysts also point to the same conclusion[53,58,59]. Catalyst deactivation by coke and metal deposits occurs simultaneously for metal containing feed. As indicated previously, species which poison active sites on the catalyst contribute to the overall deactivation, as well as changes in the catalyst structure which may occur during the operation. It is not easy to distinguish quantitatively between the contributions of all these causes to deactivation. However, as shown in figure 1.7, there is a significant difference between the deposition patterns of coke and metals.
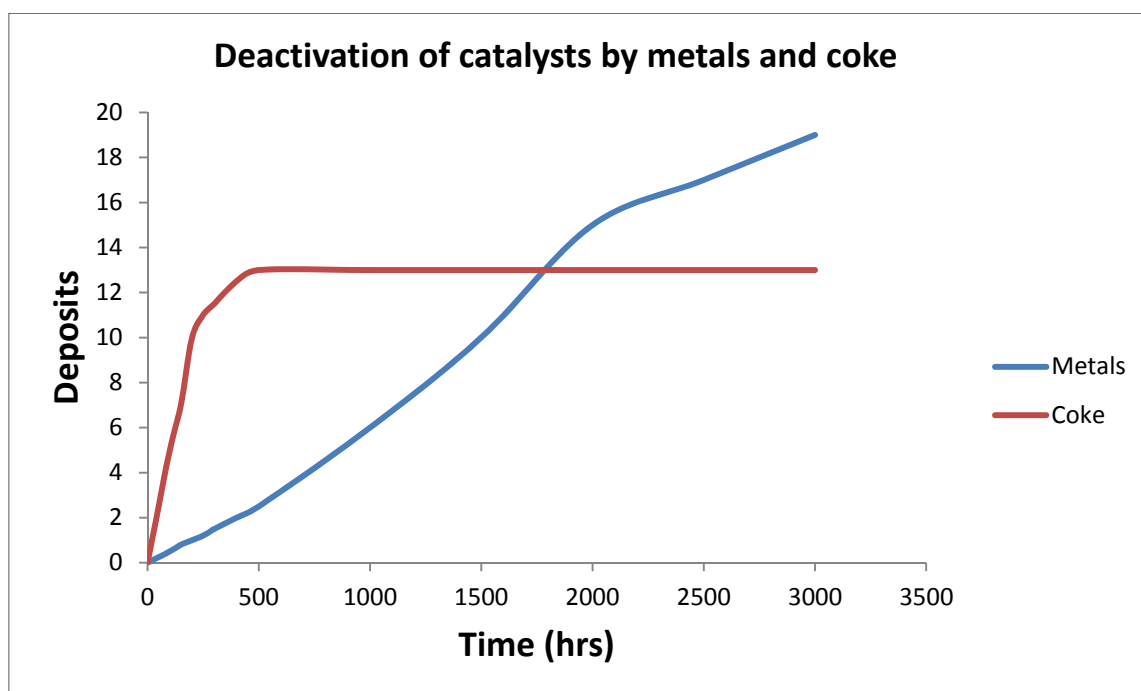
Figure 1.3: Metals and coke deposits as a function of time[36]

The former (coke) deposits rapidly during the initial stages before attaining a steady-state, while metals exhibit more or less linear deposition patterns with time. The coke and metal build up depend on the properties of the feed and hydroprocessing conditions[36].
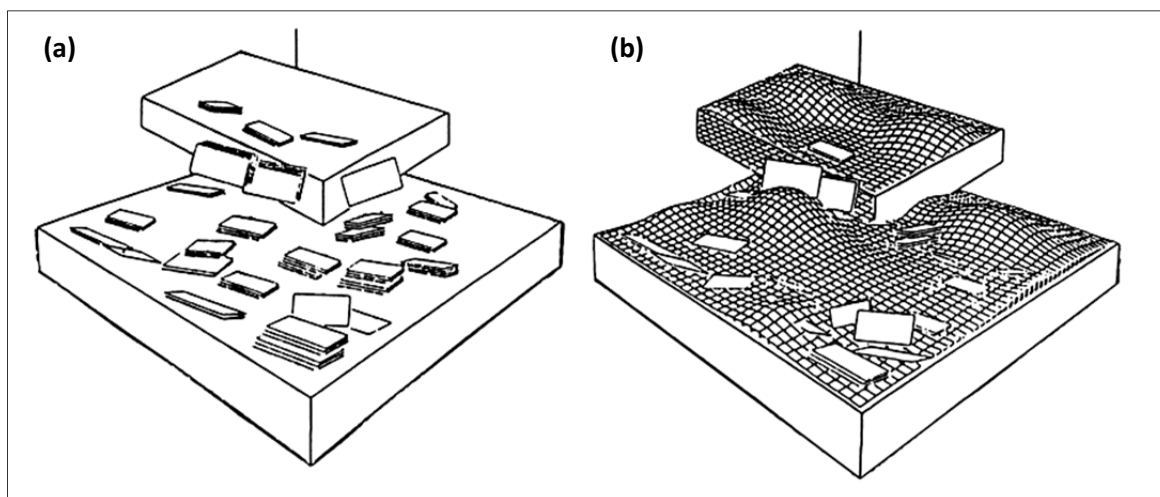
Figure 1.4: Model of fresh (a) and deactivated (b) catalysts[36]

During hydroprocessing, some of the metals present in the feed along with coke formed will deposit on the catalyst surface and cause deactivation (figure 1.8). As earlier mentioned, it is again emphasized that the deactivation by metals always occurs simultaneously along with that by coke and it is irreversible. Kinetic data have shown that the rate of metal deposition varies from metal to metal. For example, in the case of V and Ni, the initial deposition occurs at much higher rate for V than for Ni, and increases with increasing pore diameter[60]. Cross-sectional profiles show that some metals tend to deposit on the external surface of the catalyst particles, whereas others are more evenly distributed. This leads to diffusion limitations which affect access to the active sites in the particle interior. It is evident that coke and metals plug the pores and eventually may lead to a complete loss of the activity[61,62]. At the end of the run, a complete loss of activity is generally not observed, end run however occurs when either the temperature to maintain the activity is too high for reactor design or the loss of active sites by pore plugging is too large to maintain design activity by raising the temperature.

Understanding the hydrometallization (HDM) mechanism is important to explain catalyst deactivation as well as catalysts preparation. All evidence suggests that the presence of H_2 and catalyst is essential for the HDM of porphyrins to occur. Otherwise, their conversion will be very low. The detailed mechanism of HDM has been investigated and results showed the presence of the intermediates proposed by other researchers, as well as new intermediates not identified and/or proposed previously (figure 1.9)[63]. In this case, M represents either Ni or V=O, as it was assumed that the different metal species should have little influence on the mechanism. In the first step, the tetraphenylporphyrin (M-TPP) is converted to chlorin (M-TPC), in agreement with other researchers[64-66]. In the next step, the M-TPC is converted to tetrahydroporhyrin and/or isobacteriochlorine (M-TPiB). The formation of bacteriochlorin is less likely but cannot be ruled out completely. In the next step, the M-TPiB is hydrogenated to hexahydroporphyrin (M-TPHP). The octahydrogenated species arising from the hydrogenation of M-TPHP was not confirmed, but assumed to be part of the mechanism. Nevertheless, there are indications that the non-porphyrin type of the metal containing compounds may account for more metals than the porphyrins[63].

Figure 1.5: Schematic representation of the mechanism for hydrodemetallisation (HDM) of metalloporphyrins (M=Ni or V=O)[61]

In summary, the high levels of metal ions in crude oils presents an additional cost to the refineries for the processing of the heavy crude oil, either by high cost of hydrogen addition or yield loss by carbon rejection and catalysts deactivation, all of which necessitate a pre-treatment process step to reduce the metal contents of the crude oil feeds prior to getting into the processing stream. If a pre-treatment step is developed

to remove/reduce the metal ions concentration before the crude oil enters the processing stream, then the conventional processing methods could be more efficient with significant savings in time and costs. There is currently no known metal extraction step prior to the hydroprocessing stages that is effective, economical, and able to address the problems associated with the deactivation of catalysts and environmental issues. Synthetic zeolites are a class of framework materials that may help to achieve a reduction in the metal content of crude oil prior to the hydroprocessing stages.

1.11. Zeolites

Zeolites are crystalline, hydrated aluminosilicates of alkali and alkaline earth cations, consisting of three dimensional frameworks of SiO_4^{4-} and AlO_4^{5-} tetrahedra linked through the shared oxygen atoms. They are porous materials, characterized by the ability to adsorb molecules of appropriate cross-sectional diameter (adsorption property, or acting as molecular sieves) and to exchange their constituent cations without major change of their structure (ion-exchange property)[6]. Due to their shape selectivity and, the remarkable ion exchange properties, zeolites have found wide industrial applications, including the oil industries.

1.11.1. Background History of Zeolites

Zeolites can be natural or synthetic with more than 150 zeolite types synthesized and 40 naturally occurring zeolites known[67]. Natural zeolites are formed from volcanic ash whilst synthetic zeolites are synthesised from a Si and Al source normally in alkaline solution. The history of zeolites dates back to the 18th century with the discovery of the mineral stilbite by a Swedish mineralogist, A.F. Cronstedt, who named it from two Greek words for 'boiling stone' ('zein' – boiling and 'lithos' – stone)[68]. Following their discovery, zeolites were found to possess the following properties: catalytic properties; high hydration propensity; stable crystal structure when dehydrated; low density and high void volume when dehydrated; cation exchange and sorption properties[6]. A number of works were carried out to further investigate these properties. The results showed that zeolites could be reversibly dehydrated with no apparent change in their transparency or crystal morphology. The reversibility of ion

exchange on zeolite minerals was first reported by Eichhorn[69]. Friedel and Bull, later proposed that, the structure of dehydrated zeolites consists of open porous frameworks[67]. This proposal was further confirmed by occlusion of liquids, such as alcohol, benzene and chloroform, by dehydrated zeolites. The first molecular sieve effect was observed when dehydrated chabazite crystals rapidly absorbed water, methyl alcohol, ethyl alcohol and formic acid, but essentially excluded acetone, ether or benzene. The first hydro-thermally synthesized zeolite, levynite was reported by St. Claire Deville[6]. Syntheses of more zeolites was reported after levynite; however the unavailability of reliable characterisation techniques made it impossible to verify such materials, until 1930, with the development of X-ray diffraction technique, that the zeolites structures were properly identified.

1.11.2. Molecular sieves

The discovery of zeolite materials led to the synthesis of other materials which were not core aluminosilicates, these materials were found to be very much related to zeolites. A new term "molecular sieves" was then introduced to include this class of materials that exhibited selective adsorption properties. These materials may contain other elements in place of silicon and aluminium. Different classes of molecular sieves, which includes; silicates, metallosilicates, metalloaluminates, $AlPO_4S$ and silico- and metalloaluminophosphates, as well as zeolites have now been discovered[67]. However, poor thermal and hydrothermal stability of their metal-substituted analogues has hindered their commercial application. Toxicological studies on natural zeolites have shown that zeolites are inert, non-toxic and safe to use medicinally[67].

1.11.3. Classification and Nomenclature of Zeolites

Zeolites and zeolite related materials in addition to their chemical composition are classified according to their framework structure. Each framework type can be described by their secondary building units, framework density, channel system, crystal symmetry and unit cell constant[70]. Three classification schemes are available for classifying zeolite structures. These classifications are based upon defined aspects of crystal structure as well as historical basis placing zeolites with similar properties such as morphology into the same group. The first structural classification of zeolites is

based on the frameworks topology, with distinct framework receiving a three-letter code. The second structural method for the classification of zeolites is based on a concept termed "secondary building units" (SBU) which is the geometric arrangements of tetrahedra[67,70]. In most cases the SBUs tend to control the morphology of the zeolites. The third broad classification scheme is similar to the SBU classification, except that it includes some historical concepts of how the zeolites were discovered and named. This scheme uses a combination of zeolite group names which have specific SBUs and is widely used by geologists[67].

The structure commission of the International Zeolites Association (IZA) is responsible for approving proposed zeolite nomenclature. There is no systematic way of naming zeolites, once approval is given by the commission, it is assigned three-letter code e.g. FAU for faujasite and zeolite X and Y, L TA for zeolite A, MFI for zeolite ZSM-5 etc.

1.11.4. Structures of Zeolites

Zeolites are crystalline alumino-silicates whose framework structures consist of cavities or pores that are occupied by cations and/or water molecules[71]. The fundamental building block of all zeolites is a silicon or aluminium tetrahedron (AlO_4 or SiO_4 tetrahedra).

The silica tetrahedra is electronically neutral with its +4 charge balanced by the four tetrahedral oxygen anions. On the other hand, each alumina tetrahedron has an excess charge of -1 since it is trivalent and is bonded to four oxygen anions (Figure 1.10). Hence each alumina tetrahedron requires a +1 charge from a cation (e.g. sodium) in the structure to be electronically neutral.
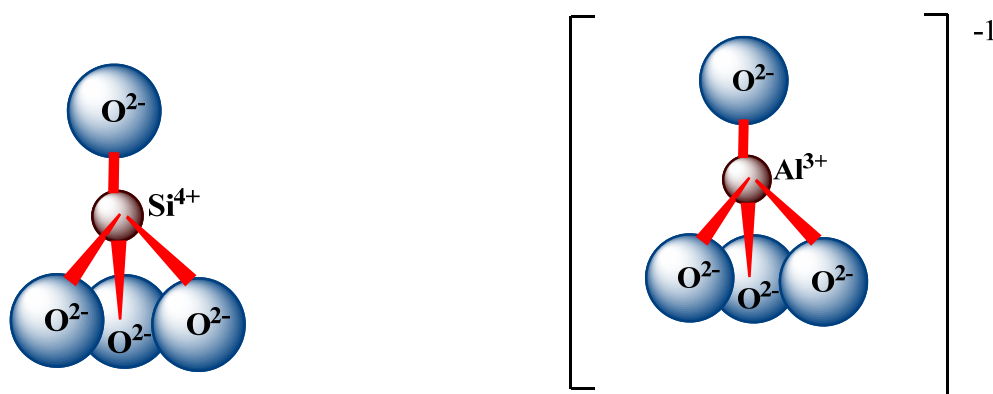
Figure 1.6: Silica tetrahedron (left) and alumina tetrahedron (right)

This then forms a 3-dimensional framework with linked systems and well defined pores. The tetrahedra are arranged in such a way that each of the oxygen anions is shared with another silica or alumina tetrahedron[67].

Zeolites have a molecular sieve action due to their open channel network; hence they are able to allow some ions to pass through while blocking others. Both the cation and the water molecule have considerable freedom of movement and this permits ion exchange and reversible dehydration. Exchangeable cations include; sodium, lithium, cadmium, lead, zinc, copper, ammonia, silver and protons among others. The zeolite channels or pores are microscopically small, and have molecular size dimensions. A representative empirical formula for a zeolite proposed by Barrer is as shown below.

$M_{2/n}O:Al_2O_3:xSiO_2;yH_2O$
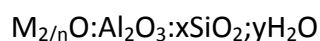
Where M represents the charge-balance cation, n the charge of the cation, x is generally $\geq$ 2, and y the water contained in the voids of the zeolite. According to Demsey's rule, no two AlO_4 can be linked directly by sharing their corners in the zeolite framework. One most striking feature of the porous structure is that the pore openings are of molecular dimensions, [72] another fascinating feature is the versatility of the structures themselves. Zeolite structures can be modified during synthesis to incorporate catalytically active metals or elements to suit a particular application of interest.

1.11.4.1. Zeolites Building units

The individual tetrahedra (AlO_4 or SiO_4) represent primary building units. The alumina and silica tetrahedra are combined into more complicated secondary units which form the building block of the zeolite crystal structure. The majority of zeolites are formed from the secondary building units. Secondary building units (SBUs) consist of selected geometric groupings of those tetrahedra. Such building units can be used to describe all the known zeolite structures. Some of the building units recognized in zeolites framework are as shown in figure 1.11. These include 4, 6 and 8-member single rings, 4-4, 6-6, and 8-8-member double rings, and 4-1, 5-1, and 4-4-1 branched rings[67]. Most zeolite frameworks are derived from several different SBUs. Similarities and differences in structures of zeolites require a building unit that takes into account the arrangement of these SBUs in space. There is more than one possibility of joining for example a 4-ring unit hence linking of each ring results in what is called extended chain building unit. An alternative method of describing extended zeolite structures is to visualize zeolites in two-dimensional sheet units. The framework structure is generated by attaching layers to form a complex structure. These planar projections provide information on the relative orientation of the 8, 10 and 12 ring pore openings of the different structures. They also help in understanding the area of crystal purity.
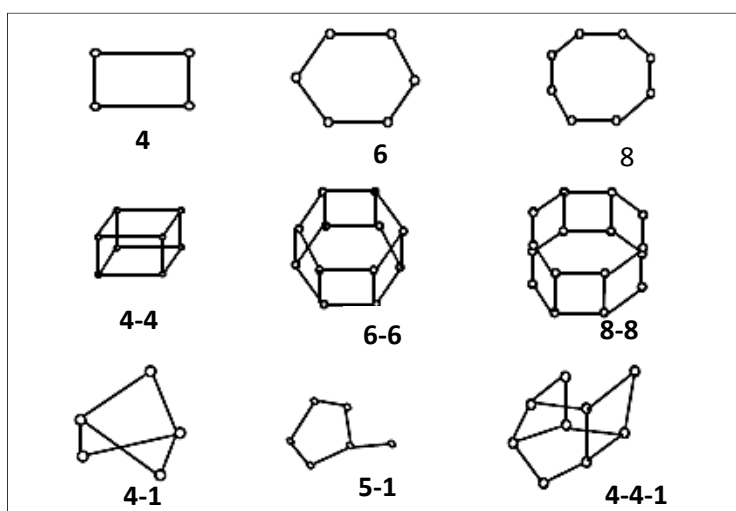
Figure 1.7: Some secondary building units in zeolites[67]

1.11.4.2. Pores and Channel openings in Zeolites

The structures of zeolites are often described according to their framework type in terms of size of pore openings and the dimensions of their channel system[73]. These pore openings are characterized by the size of the ring that defines a pore. This is designated as n-ring, where n is the number of T (= Al or Si tetrahedral) atoms in a ring. Different pore openings are assigned for different ring sizes. Hence zeolites with ring size 8, 10 and 12 are termed small pore, medium pore and large pore zeolites respectively[74]. A number of methods have been proposed to examine pore size; the commonly used involves selecting the proper molecular probes and examining the ability of the zeolite to adsorb these probes. Such probes include; methane, n-hexane, 2-methylpentane, cyclohexane, oxylene, and mesitylene commonly applied for determining pore size. Erionite, chabazite, and type A (Ca^{2+} exchanged form) 8-ring zeolites adsorb methane, but not cyclohexane. ZSM-5, ZSM-11, EU-1, and theta-1 (10-ring zeolites) all adsorb methane, n-hexane, and alkanes readily, while adsorbing cyclohexane slowly. These 10-member ring zeolites will not adsorb mesitylene. Finally, 12-member ring zeolites such as Type-Y, Mordenite (synthetic), ZSM-12, and zeolite Beta readily adsorb all the probe molecules.

The size and shape of the pore opening depends on; the configuration of the T and O atoms relative to each other, the Si/Al ratio, the size of the cation, the location of the cation, temperature[67]. Some zeolites and their micropore diameter are as shown in Figure 1.12.
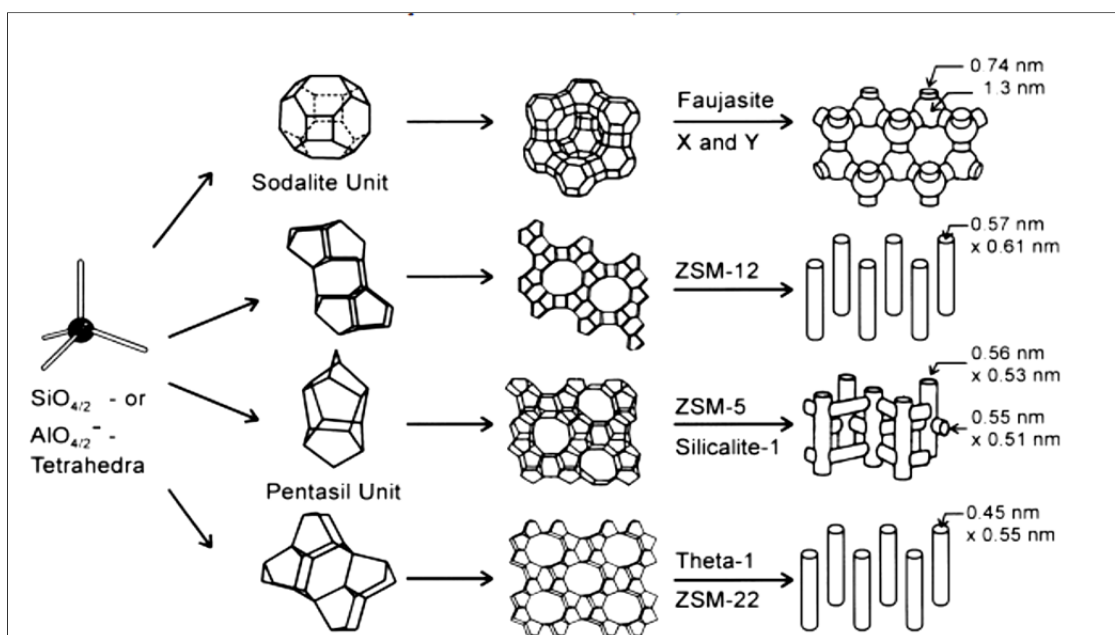
Figure 1.8: Structure of four selected zeolites (from top to bottom: faujasite or zeolites X, Y; zeolite ZSM-12; zeolite ZSM-5 or silicalite -1; zeolite Theta-1 or ZSM-22) and their micropore systems and dimensions[70]

1.11.5. Properties and applications of zeolites

Synthetic and natural zeolites have become increasingly important due to the wide range of their chemical and physical properties. There are three main applications of zeolites: adsorption, catalysis and ion exchange. These enable zeolites to be used for example as molecular sieves and separation membranes, absorbents for organic vapours, ion exchangers for water purification, and catalysts for petrochemical industry. A few of the applications are discussed below;

1.11.5.1. Ion exchange for removal of heavy metal ions from wastewater

The existence of a negative charge due to aluminium in a tetrahedron coordinated silicon framework structure of zeolites has to be compensated by mobile cations. The presence of these free mobile cations in the structure is therefore responsible for the ion exchange capacity of zeolites. This property of zeolites has given rise to a number of applications. For example, zeolites synthesised from fly ash were found to be efficient for chromium III immobilization from aqueous solution compared to other sorbents used for immobilization of metal ions[75]. This mechanism of chromium

removal involves ion exchange and precipitation as chromium hydroxide. A similar work was also carried out which shows the effectiveness of synthesised zeolites for metal ions removal from water[76]. From the result, it was observed that, among the metal ions targeted (cadmium and lead); the removal efficiency for cadmium was higher compared to lead, this could be explained based on the difference in size between the two metals. Nickel and copper removal from aqueous solution by batch ion exchange with solid lithium-, sodium-, potassium-, rubidium- and caesium-based Y zeolites have also been studied under competitive and non-competitive conditions[77]. The extent of transition metal (TM) removal was found to be strongly dependent on the nature of the out-going alkali metal (AM) cation with the overall preference of the zeolite for exchange with both metals increasing in the order CsY<RbY<NaY<LiY. Earlier work done by Keane revealed that alkali metal ion exchange of NaY and KY at a total normality of 0.1 mol., in the temperature range 298-373 K proceeds with negligible hydronium ion exchange to completion in the case of Li^+, Na^+ and K^+ exchange whereas Rb^+ and Cs^+ exchange terminates at 69% and 76% of the total capacity of NaY and KY, respectively[78]. The use of coal fly ash, natural clinker and synthetic zeolites for the removal of heavy metals from acid mine drainage has also been investigated[79]. This investigation shows that, faujasites have a higher efficiency at removing the metal ions from solution compared to Na-phillipsite, thus the materials has the potential to provide methods for the treatment of AMD. The removal efficiency of clinoptilolite and sepiolite from lead containing aqueous solution was investigated[80] . The results of the investigation revealed that the removal of lead ion both by clinoptilolite and sepiolite involves the contribution of both adsorptions by ion exchange and precipitation. The ion exchange capacity of clinoptilolite for lead removal showed good performance.

1.11.5.2. Adsorption of organic pollutants from industrial effluent

Zeolites as adsorbents have been used extensively as an alternative to other adsorbents like, activated carbon, silica gel, alumina etc. This property has made it possible for the removal of coloured substances from wastewaters as well as the removal of metals when combined with its ion exchange capacity. For example, zeolite

ZSM-5 is reported to be efficient in the removal of printing ink[81]. In the study, it was found that the combined flocculation/zeolite process for printing ink removal from simulated wastewater showed higher removal efficiency (95%) compared to removal by single flocculation step. ZSM-5 and Beta zeolites both in NH_4-form were found to be the most efficient in enhancing total organic carbon (TOC) removal. It was also shown that zeolite MCM-22 is effective in the removal of dye from wastewater. The adsorption kinetics was reported to follow the pseudo-second-order model with the external diffusion as the control process[82].

1.11.5.3. Molecular sieve or separation membrane

Due to the sieving property of zeolites, they can be used as filters or separation membranes to selectively separate mixtures based on size. This application has been used in a number works, B-ZSM-5 zeolite membranes for example were used to selectively separate n-C_4H_{10} from i-C_4H_{10} and n-hexane from 2, 2-dimethylbutane at 298 - 473K. Continuous X-type zeolite membranes of high quality synthesis were also reported to effectively separate 1, 3-propanediol from glycerol in aqueous mixture by pervaporation[83]. The separation mixture was found to be highly selective which was due to preferential adsorption of 1, 3-propanediol.

1.11.5.4. Gas sensing

Zeolites due to their, inherent ability to absorb polar compounds can be used as excellent materials for gas separation and purification[84]. Their absorptivity, high surface area and presence of mobile ions and catalytic activity make them attractive as chemical sensors. Zeolites in gas sensors could play two possible roles; they could either act as the main functional element or auxiliary elements.

1.11.6. Ion exchange with Zeolites

Ion exchange is an intrinsic property of zeolites which allows the replacement of cations held in their aluminosilicate anion framework by ions present in the external solution or melts[85]. In an ion exchange system, two phases are majorly involved; the exchanger and the external solution, although a third phase (vapour) could also be involved. With respect to this property of zeolites, a number of research works have

been carried out mostly in the modification of zeolites whereby cations are introduced into the zeolite frameworks to modify the catalytic or molecular sieving actions of the parent zeolites. However, not all zeolites are capable of undergoing this cation replacement. Zeolites with condensed frameworks (high density and low porosity), for example analcine and natrolite have limited and slow exchange properties.

The ion exchange reaction between cation A_S^{Za}, initially in solution and B_Z^{Zb}, initially in a zeolite is represented as thus:

$$Z_b A_S^{Za} + Z_a B_Z^{Zb} \longleftrightarrow Z_b A_Z^{Za} + Z_a B_S^{Zb}$$ Equation 1.1

B_Z^{Zb} & A_Z^{Za} are the cations inside the zeolite crystal; Z_a & Z_b are the valences of these ions; A_S^{Za} & B_S^{Zb} are cations in solution.

The cation exchange capacity of a zeolite is a result of the degree of substitution of Al for Si in the framework. Thus the greater the degree of substitution of Al for Si, the greater the number of cations required to maintain electronic neutrality in the zeolites[86]. These charge balancing cations are capable of exchanging with external cations from solution, and the channel structure of zeolites is responsible for their function as a "molecular sieve". The channels and cages of a particular zeolite are clearly defined by their shape and dimensions. The open channels thereby allow free passage of ions through the framework structure. Again it is possible for ions to exchange only partially, because the volume of the ions is such that these completely fill the intra-crystalline space in the channels before 100 % exchange is attained[87]. The selectivity of zeolites for different ions depends on: the nature, size and charge of the cationic species, temperature and the concentration of the cationic species in the solution, the anion associated with the cation in solution, the state of solvation and the structural characteristics of the particular zeolite. A particular ion can therefore be excluded from the exchanger because of its size. Apart from the size of zeolite pores, the hydrophilic or hydrophobic character of zeolite greatly influences ion-sieving selectivity. For example, zeolite Y with a lower anionic charge (Si/Al ~ 1.5-3) takes up preferentially larger cations while the highly negatively charged framework of zeolite X

(Si/Al ~ 1-1.5) prefers smaller cations. Thus the ion exchange selectivity of zeolites is dependent on the anionic strength of the zeolites, so that siliceous zeolites with low field strength prefer larger cations, e.g. Cs^+, characterized by a lower charge density, whereas aluminous zeolites are more selective for cations with a higher charge density[88]. The ion or molecular selectivity/seiving of the zeolites gives their catalytic property that can be employed in petroleum refining during the hydrocracking process.

1.11.7. Zeolites studied

1.11.7.1. Zeolite A

Zeolite A exhibits the LTA (Linde Type A) structure (Figure 1.13). It has a 3-dimensional pore structure with pores running perpendicular to each other in the x, y, and z planes, and is made of secondary building units 4, 6, 8, and 4-4[89]. The pore diameter is defined by an 8- membered oxygen ring and is small at 4.2 Å leading to a larger cavity of minimum free diameter 11.4 Å.[90] The cavity is surrounded by 8 sodalite cages connected by their square faces in a cubic structure. The unit cell is face centered cubic ($a = b = c$ 24.55 Å) with Fm-3c symmetry. The Si/Al ratio as determined by SEM-EDS is 0.96. It is stable at temperatures up to 700 ^{o}C after which it decomposes[91]. Powder X-ray diffraction of the sample matched with the ICDD database with anhydrous composition ($Na_{12}Al_{12}Si_{12}O_{48}$)$NaAlO_2$.

(a)   (b)
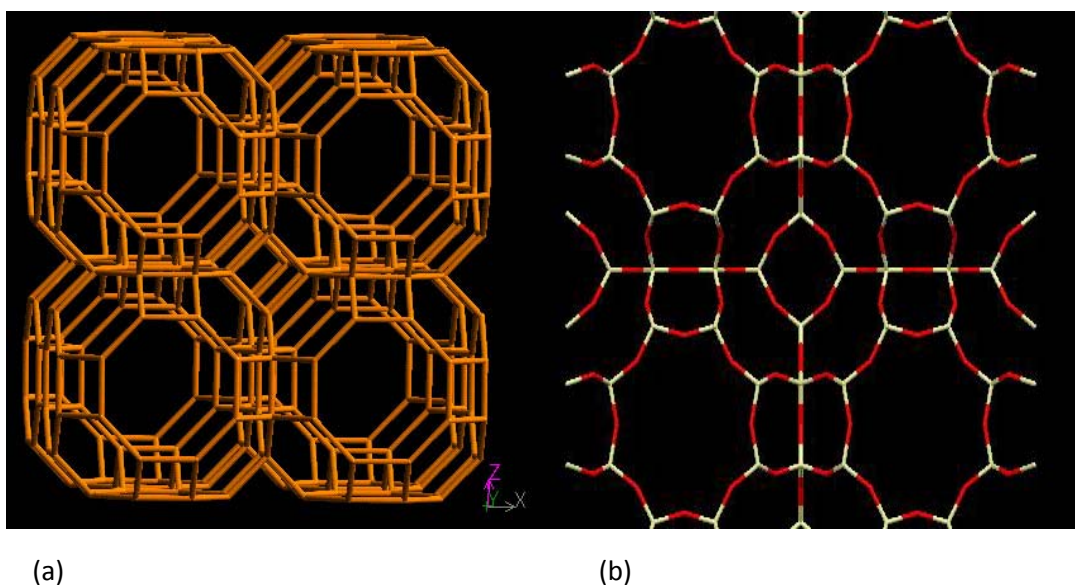
Figure 1.9: 3-dimensinonal framework structure of zeolite A[92](a), Projection of framework structure of zeolite A down *b* axis, adapted from reference 92 using Atoms crystal structure drawing package (b)

1.11.7.2. Zeolites X and Y

Zeolites X and Y are synthetic forms of the naturally occurring mineral known as faujasite. They have identical structural framework, which differs only by their framework charges[6, 67]. This difference is created by the relative amounts of aluminium substituted for silicon in the aluminosilicate framework such that zeolite Y had a higher Si/Al ratio than zeolite X. These zeolites have a three-dimensional channel system consisting of cavities separated by 12-membered oxygen rings with a structural diameter of about 7 Å. The zeolites have nearly 50% of the volume of the crystal available for absorption. They also contain smaller cavities known as sodalite cages connected to the supercages by the 4- and 6- memebered tetrahedra rings [67]. The unit cell is face-centered cubic with symmetry of Fd-3. Their Si/Al ratios as determined by SEM-EDS are 1.3 and 2.7 for X and Y respectively. Powder X-ray diffraction of the samples of zeolite X and Y matched with the ICDD database with anhydrous compositions $Na_{88}Al_{88}Si_{104}O_{384}$ and $Na_{54.91}Al_{56}Si_{136}O_{384}$ for the X and Y zeolites respectively. The rare earth exchanged Y zeolite has been reported to show improved catalytic properties on the cracking reactions especially in respect to thermal stability.

They are also good adsorbent for removal of organic pollutants[93]. The structure of faujasites is as shown in figure 1.14.

(a)   (b)
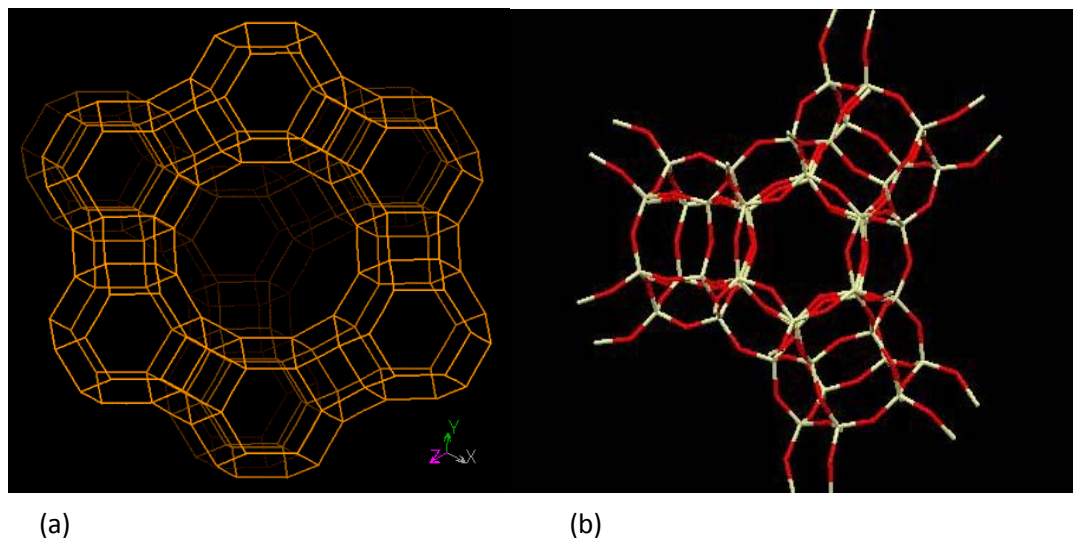
Figure 1.10: 3-dimensional framework structure of faujasites (X, Y)[93] (a), framework structure of faujasites, adapted from reference 92 using Atoms crystal structure drawing package (b)

1.11.7.3. Sodalites

Sodalite is a well-known class of anion-containing framework constructed from vertex-linking TO_4 tetrahedron (T= Si or Al) into 4- and 6- member rings to form a cage structure (figure 1.15)[94]. The unit cell of sodalites is made up of cages, each containing two cationic exchange sites.
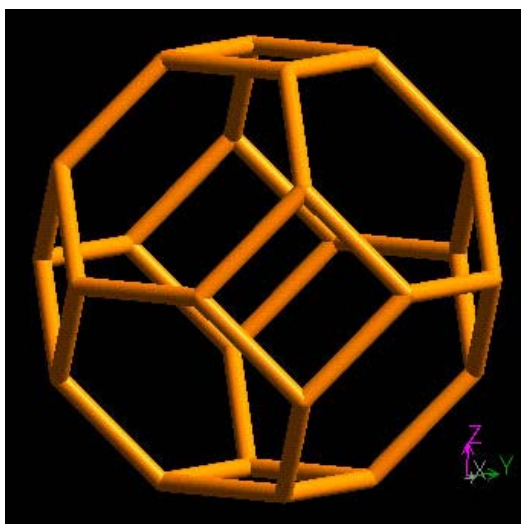
Figure 1.11: Sodalite framework structure[95]

The cage structure (β- cage) is the building block of many zeolites, for example zeolite A and zeolite X. Its largest pore size is about 2.4 Å the smallest among all zeolites. The sodalite framework exhibits a cubic symmetry, formed by a strictly alternating connection of corner sharing SiO_4 and AlO_4 tetrahedra that is highly flexible and can accommodate its degree of expansion by cooperative tetrahedron tilt to accommodate guest species of different sizes. Sodalites have a general structural formula of Na_8 $[AlSiO_4]_6$ X_2 [95]. It is important to mention here that sodalite has about 212 different forms, the sodalite Na_8 $[AlSiO_4]_6$ X_2 (X= Cl^- , OH^- or both) and hydrosodalite (Na_6 $[AlSiO_4]_6$ $6H_2O$) were used in this work since their structure is similar to that incorporated in the larger frameworks of the other zeolites A, X and Y.

The main zeolites of study in this research work are zeolite A, zeolite X and zeolite Y. Sodalites and hydrosodalites are only studied to investigate the metal uptake behaviour by these zeolites since they all have sodalite units (β-cages) as part of their framework structure. The sodalites will therefore not be studied in depth compared to the target zeolites A, X and Y.

The 3-dimensional framework structures of the zeolites studied and their maximum pore size dimensions are as shown in figure 1.16.
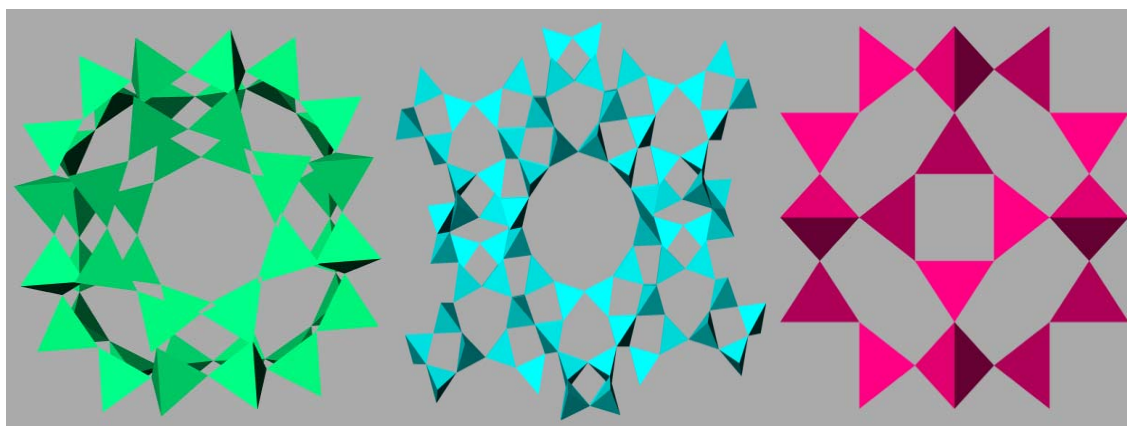
Figure 1.12: 3-Dimensional framework structures of zeolites a (left, pore size=4.1 Å); Zeolite X,Y (middle, pore size = 7.3 Å);Sodalite (right, pore size =2.3 Å), showing their channel and pore size

1.12. Conclusion

The background of the study, statement of the research problem, significance of work, aims and objectives have shown the importance of this research work to the petroleum industry. The literature review on crude oil and zeolites is aimed at giving a further deeper and wider understanding of the problem and the use of zeolites materials as the possible solution to the problem.

References

1. C.S. Hsu and P. R. Robinson, Practical advances in petroleum processing, Springer science + Business Media, Inc., New York NY, 2006.

2. M.S. Rana, V. Sámano, J. Ancheyta and J. A. I. Diaz, Fuel, 2007, 86, 1216-1231.

3. R.D. Griffin, Principles of Hazardous Materials Management, Lewis, Ann Arbor, 1988.

4. M.L. Davis, D.A. Cornwell, Introduction to Environmental Engineering, McGraw-Hill, New York, 2nd edition,1991.

5. J.E. Fergusson, The Heavy Elements: Chemistry, Environmental Impact and Health Effects, Pergamon, Oxford, 1990

6. D.W. Breck, Zeolite Molecular Sieves, Structure, Chemistry and Use, Wiley, New York, 1974.

7. A. Dyer, H. Enamy, R.P. Townsend, Sep. Sci. Technol., 1981, 16, 173.

8. M.F. Ali and S. Abbas, Technol., 2006, 86, 573-584.

9. D.S. Thakur, M.G. Thomas, Appl. Catal.,1985, 15, 197.

10. C. Dekker, J. Oil Gas, 1999, 97, 44.

11. M. Marafi, A. Stanislaus, Resour. Conserv. Recy., 1990, 53(1-2), 1-26.

12. B.R. Utz, H.R. Appell, B.D. Blaustein, Fuel, 1986, 65, 1085.

13. R.E. Overfield and N. J. Washington, Method for extracting nickel and vanadiumm compounds from oils, 1985.

14. S. Garcia-Segura, J. Keller, E. Brillas, J. Radjenovic, J. Hazard. Mat., 2015, 283, 551-557.

15. D. Acavedo, L. F. D'Elia Camacho, J, Moncada, Z. Puentes, Fuel, 2012,92, 264-270.

16. K. Welter, E. Salazar, Y. Balladores, O. P. Marquez, J. Marquez and Y. Martinez, Fuel Process Technol., 2009, 90, 212-221.

17. H. Kalipcilar, S. K. Gade, R. D. Noble and J. L. Falconer, J. Membr. Sci., 2002, 210, 113.

18. A. Filippidis, A. Godelitsas, D. Charistos, P. Misaelides and A. Kassoli-Fournaraki, Appl. Clay Sci. , 1996, 11, 199.

19. G.P.Canevari and R.J.Fiocco, International oil spill conference, 1997, 309-314.

20. Energy in the United States, 1635-2000, Energy Information Administration, U.S. Department of Energy: Washington, D.C., 2003.

21. B.Moldauer (ed.) All About Petroleum, American Petroleum Institute: Washington, D.C., 1998.

22. K. Weinkauf "The Many Uses of Petroleum from Discovery to Present," Desk and Derrick Club of Tulsa: Tulsa, Oklahoma, 2003.

23. Significant Events in the History of Energy, Energy Information Administration, U.S. Department of Energy: Washington, D.C., 2003.

24. M.S. Rana, V. Sámano, J. Ancheyta and J. A. I. Diaz, Fuel, 2007, 86, 1216-1231.

25. F. Mostowfi, K. Indo, O.C. Mullins, & R. McFarlane, Energy Fuels, 2009, 23, 1194-1200.

26. M.F. Ali and M.H. Alquam, Fuel, 2000, 79, 1309-1316.

27. J. G. Speight, Baki Özüm, 2002, Petroleum refining processes, New York, Marcel Dekker, pg 312-439.

28. J.G. Speight, Petroleum Chemistry and Refining, Taylor & Francis, USA, 1998.

29. J.G. Speight, The Chemistry and Technology of Petroleum, 2nd Edition, Marcel Dekker Inc., New York.

30. R.E. Overfield, E.Y. Sheu, S.K. Sinha and K. S. Liang, Fuel Sc. Technol.Int., 1989,7,611.

31. M. S. Rana, V. Sámano, J. Ancheyta and J. A. I. Diaz, Fuel, 2007, 86, 1216-1231.

32. J. Ancheyta, M. Rana and E. Furimsky, Catalysis Today, 2005, 109, 3.

33. T. Gentzis, P. Rahimi, R. Malhotra and A. S. Hirschon, Fuel Process Technol., 2001, 69, 191-203.

34. J. Ancheyta, F. Trejo and G. Centeno, Fuel, 2004, 83, 2169-2175.

35. P.C.H. Mitchell, Catal. Today, 1990, 7, 439.

36. E. Furimsky, F.E. Massoth, Catal. Today, 1999, 52, 381- 495.

37. S. Matar, L.F. Hatch, Chemistry of Petrochemical processes, Gulf Publishing Company, Texas, 1994.

38. E. L. Sughrue, D. W. Hausler, P. C. Liao and D. J. Strope, Ind. Eng. Chem. Res., 1988, 27, 397.

39. K. Sakanishi, N. Yamashita, D. D. Witehurst and I. Mochida, Am. Chem. Soc., 1997, 42, 373.

40. R.D. Grigsby and J. B. Green, Energy Fuels, 1997, 11, 602.

41. I.V. Babich and A. Moulijn, Fuel, 2003, 82, 607-631.

42. H. Topsoe, B. S. Clausen, F. E. Massoth, Hydrotreating Catalysis, Springer: Berlin,1996.

43. T. Takatsuka, Hydrotreatment - Science & Technology, Kabe, T. (Ed.), IPC: Tokyo, 2000.

44. J. Wei, Catalyst Design - Progress and Perspective, Hegedus, L. L. (Ed.), John Wiley & Sons: New York, 1987.

45. M. N. Siddiqui, M. F. Ali, A. Al-Malki, B. El-Ali and G. Martinie, Fuel, 2006, 85, 1354-1363.

46. W. Wu and Chen.J., J.Petrol. Sci. and Eng., 1999, 22, 25-30.

47. R.F. Wormsbecher et al, Vanadium Poisoning of Cracking Catalysts: Mechanism of Poisoning and Design of Vanadium Tolerant Catalyst System, Davison Chemical Division, W. R. Grace and Company, 7379 Route 32, Columbia, Maryland 21044.

48. J.J. Mcketta, 1991, Petroleum processing handbook, New York, Marcel Dekker, pg 683.

49. N. Márquez, F. Ysambertt and C. De La Cruz, Analytica Chimica Acta, 1999, 395, 343-349.

50. D.D.Whitehurst, T. Isoda, I. Mochida, Adv. Catal., 1998, 42, 345.

51. J.V. Lauritsen, M. Nyberg, R. T. Vang, M. V. Bollinger, B. S. Clausen, H.Topsøe, K. W. Jacobson, E. Lagsgaard, J. K. Norskov, F. Besenbacher, Nanotechnol., 2003, 14, 385.

52. R.L. Dickenson, F.E. Biasca, B.L. Schulman and H.E. Johnson, Hyd. Proc. 2,1997, 57

53. F.E. Massoth, G. Muralidhar, in: H.F. Barry, P.C. Mitchell (Eds.), Fourth Climax Int. Conf. Chemistry and Uses of Molybdenum, Climax Molybdenum Co., Ann Arbor, MI, 1982, 343.

54. H. Topsoe, B.S. Clausen, F.E. Massoth, in: J. Anderson, M. Boudart (Eds.), Catalysis, Science and Technology, Vol. 11, Springer, 1996.

55. D.S. Thakur, M.G. Thomas, Ind. Eng. Chem. Prod. Res. Dev., 1984, 23, 349.

56. M. Absi-Halabi, A. Stanislaus, D.L. Trimm, Appl. Catal., 1991, 72, 193.

57. J. Wei, in: C.H. Bartholomew, J.B. Butt (Eds.), Catalyst Deactivation, Elsevier, Amsterdam, 1991.

58. C.H. Bartholomew, in: M.C. Oballa, S.S. Shih (Eds.), Catalytic Hydroprocessing of Petroleum and Distillates, Marcel Dekker, New York, 1994

59. C.H. Bartholomew, Chem. Eng., 1984, 12, 96.

60. A. Fonseca, P. Zeuthen, J. B. Nagy, Fuel, 1996, 75, 1363.

61. S. Kobayashi, S. Kushiyama, R. Aizawa, Y. Koinuma, K. Imoue, Y. Shimizu, K. Egi, Ind. Eng. Chem. Res., 1987, 26, 2245.

62. E. Newson, Ind. Eng. Chem. Proc. Des. Dev., 1975, 14, 27.

63. A.C. Jacobsen, B.H. Cooper, P.N. Hannerup, in: 12th Petrol World Congr, vol. 4, 1987, 97.

64. J.P. Janssens, G. Elst, E.G. Schrikkema, A.D. van Langeveld, S.T. Sie, J.A. Moulijn, Recl. Trav. Chim. Pays Bas, 1996, 115, 465.

65. H.J. Chen, F.E. Massoth, Ind. Eng. Chem. Res., 1988, 27, 1629.

66. Y. Kamiya, S. Nagae, Fuel, 1985, 64, 1242.

67. R. Szostak, Molecular sieves, Principles of Synthesis and Identification, Van Nostrand Reinold, New York, 1989.

68. F.A. Mumpton, L.B. Sand and F.A. Mumpton, A new industrial mineral commodity. Natural Zeolites: Occurrence, Properties, Use, Pergamon Press, New York, USA., 1978.

69. H. Van Bekkum, E.M. Flanigen, P.A. Jacobs and J.C. Jansen, Introduction to zeolite science and practice. Studies in Surface Science and Catalysis, Elsevier Science Publishers, Amsterdam, 2001.

70. J.B. Nagy, P. Bodart, I. Hannus and I. Kiricsi, Synthesis, Characterization and use of zeolitic microporous materials., DecaGen publishers Ltd, Szeged, Hungary, 1998.

71. F.R. Ribeiro, F. Alvarez, F. Henriques, F. Lemos, J.M. Lopes and M. F. Ribeiro, J. mol. Catal. A Chemical, 1995, 96, 245.

72. K. Sahner, G. Hagen, D. Schönauer, S. Reiß and R. Moos, Solid State Ionics, 2008, 179, 2416.

73. X. Querol, N. Moreno, J. C. Umana, A. Alastuey and E. Hernandez, Int. J. Coal Geol., 2002, 50, 413.

74. J. Weitkamp, Solid State Ionics, 2000, 131, 175.

75. D. Wu, Y. Sui, S. He, X. Wang, C. Li and H. Kong, J.Hazard. Mat., 2008, 155, 415.

76. R. Shawabkeh, A. Al-Harahsheh, M. Hami and A. Khlaifat, Fuel, 2004, 83, 981.

77. M.A. Keane, colloids and surfaces A: Physicochemical engineering aspects, 1998, 138, 11.

78. M.A. Keane, Micropor. Mat., 1994, 3, 93.

79. C.A. Ríos, C. D. Williams, C.L. Roberts, J. Hazard. Mater., 2008,156, (1-3), 23-35.

80. M. Turan, U. Mart, B. Yüksel and M. S. Çelik, Chemosphere, 2005, 60, 1487.

81. P.J. Mead and Weller M.T., Micropor. Mat., 1994, 3, 281.

82. S. Wang and Z. H. Zhu, J. Hazard. Mat., 2006, 136, 946.

83. S. Li, V. A. Tuan, J. L. Falconer and Noble R.D., Micropor. Mesopor. Mat., 2002, 53, 59.

84. M.W. Ackley, S. U. Rege and H. Saxena, Micropor. Mesopor. Mat., 2003, 61, 25.

85. A. Dyer, An Introduction to Zeolite Molecular Sieves, John Wiley & Sons, Chichester, 1988.

86. R.A. Sheppard and J. G. Arthur, Mineralogy, Chemistry, Gas Adsorption, and NH^{4+} - Exchanged capacity for selected zeolitic tuffs from the western United States., U.S. Geological Survey Open-File Report, 1982.

87. R.P. Townsend, The Am. Min., 1984, 17, 128.

88. M. Adabbo, D. Caputo and C. Colella, Micropor. Mesopor. Mat., 1998, 28, 315.

89. E. N. Coker, A.G. Dixon, R.W. Thompson and A.J. Sacco, Micopor. Mat., 1995, 3, 637.

90. R. Grizzetti and G. Artioli, Micropor. Mesopor. Mat., 2002, 54, 105.

91. A. Pillay and M. Peisach, J.Radioanal. Nucl. Chem., 1990, 153, 75.

92. R.P. Penilla, A. Guerrero Bustos and S. Goñi Elizalde, Fuel, 2005, 85, 823.

93. W.T. Tsai, K.J. Hsien and H.C. Hsu, J. Hazard. Mater., 2009, 166, 635.

94. A.V. Borhade, S.G. Wakchaure and A.G. Dholi, Indian J. Phys., 2010, 84, 133.

95. A. Filippidis, A. Godelitsas, D. Charistos, P. Misaelides and A. Kassoli-Fournaraki, Appl. Clay Sci. , 1996, 11, 199.

Chapter 2: Characterisation Methods

2.0: Introduction

The characterisation of a new synthetic material is an important part of any research programme. It is important to investigate the structural properties of the material as well as the physical and chemical properties, since the structure of a solid material often governs its observed properties.[1]

The characterisation of samples within this thesis was carried out using a combination of techniques that fall under the categories; X-ray (diffraction and fluorescence), vibrational spectroscopy, thermal analysis and solution analysis. Brief descriptions of the techniques used are discussed in the following chapter, including the experimental parameters used.

2.1. X ray techniques

X-ray photons are a type of electromagnetic radiation that is produced as the result of the ejection of an inner orbital electron followed by the transition of an electron in an atomic orbital from a higher to a lower energy state.

Three basic phenomena occur when a monochromatic beam of X-ray photons falls on a given sample, namely; absorption, scattering and fluorescence[2]. These three phenomena form the basis of three very useful X-ray techniques; radiographic analysis using the absorption effect, X-ray diffraction using the scattering effect and X-ray fluorescence, which can be used for elemental identification, by analysing the fluorescent spectrum generated from surface of a material.

X-ray methods used in characterizing the solid state materials prepared in this work were; powder X-ray diffraction (PXRD), X-ray fluorescence spectroscopy (XRF) and Energy Dispersive X-ray-Spectroscopy Scanning electron microscopy (EDS-SEM).

2.1.1. The Generation of X-rays

X-rays are produced from an X- ray tube source containing a tungsten filament (figure 2.1). When the tungsten filament is heated, electrons are produced and accelerated by a high voltage towards the anode where the metal target is situated. The energetic electrons strike the metal target resulting in the ejection of 1s electron from the

metal, leaving the orbitals vacant in a quantised amount. These vacancies are then filled with electrons from higher energy orbitals with the difference in energy between the lower and higher energy orbitals being emitted as an X-ray of precise energy.

The emitted X-ray then leaves the X-ray tube through a beryllium window which is transparent to X-rays due to the low atomic number of beryllium.   The type of X-ray emitted can be determined according to the spin state and vacancy filled.   The different types of X-ray emitted include; $K_{\alpha1}$, $K_{\alpha2}$, $K_{\beta1}$ and $K_{\beta2}$ (figure 2.2). $K_{\alpha1}$ for example is a transition of 2p electrons to 1s electron shell which gives a weighted wavelength of 1.5418 Å (typical of a copper source). This 2p to 1s transition gives a doublet ($K_{\alpha1}$ and $K_{\alpha2}$) corresponding to the wavelengths, 1.5406 Å and 1.5444 Å, resulting from the two different spin states of the electron[3].
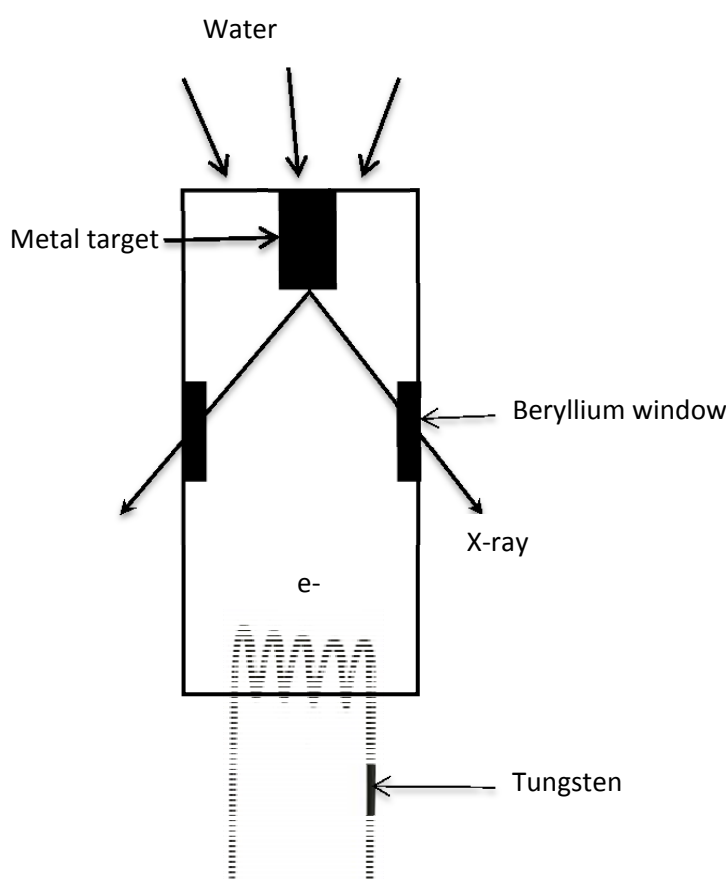
Figure 2.1: Schematic diagram of an X-ray tube.[1]
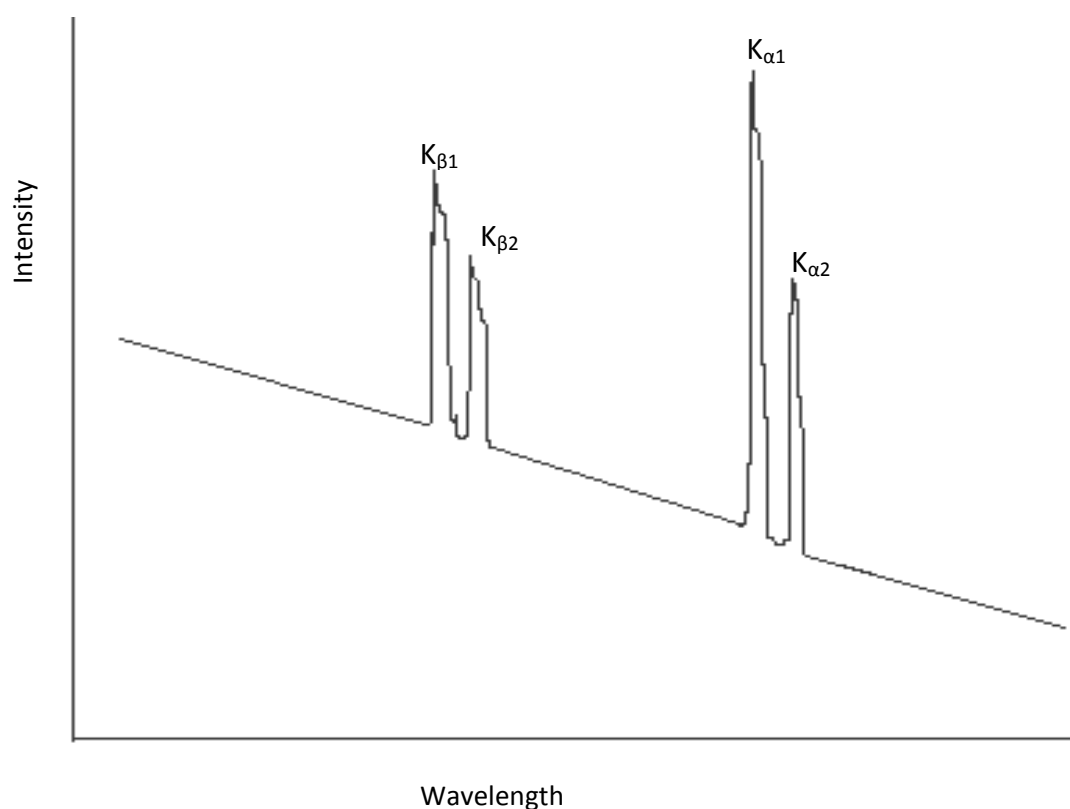
Figure 2.2: Schematic diagram of the output from the X-ray tube

The generated X-rays then pass through a monochromator which blocks the $K_{\alpha 2}$, $K_{\beta 1}$ and $K_{\beta 2}$ radiation (Bremsstrahlung radiation) while allowing only the $K_{\alpha 1}$ X-rays through. These $K_{\alpha 1}$ X-rays are then passed through a collimator through a series of slits to concentrate the beam into a single direction and destination. The X-ray tube can incorporate a different metal target depending on the requirements of the user and the samples being analyzed.

2.1.2. Unit cells and crystal systems
A unit cell is the smallest repeating unit of a structure which shows the full symmetry of the crystal structure. The unit cell axes are defined as a, b and c and unit cell angles as α, β and γ.
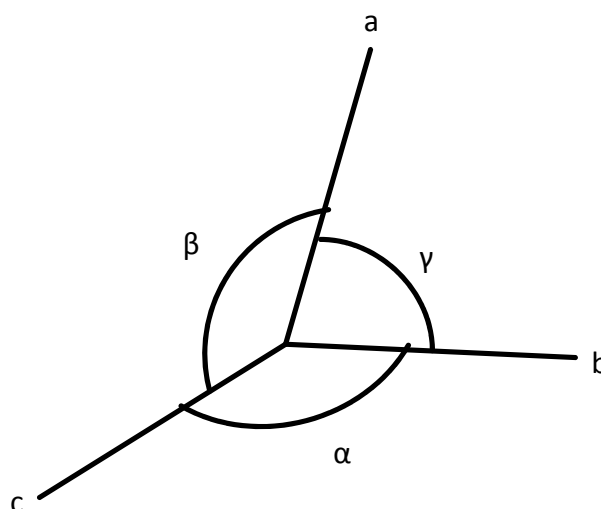
Figure 2.3: Schematic diagram showing the unit cell axes as defined by *a*, *b* and *c* and angles *α*, *β* and *γ*

There are seven possible unit cell shapes in 3-dimensional crystal structures known as crystal systems and they show the way in which atoms, ions and molecules can be effectively packed together to form a space filling lattice.[4] Unit cells in 3-dimensional repeating structures have different shapes based upon the symmetry of the structure. In all cases, the unit cells are parallelepipeds, the different shapes however, arise depending on restrictions placed on the lengths of the three edges (*a*, *b*, and *c*) and the values of the three angles (*α*, *β*, and *γ*). The seven different unit cell shapes or the so-called seven crystal systems that result from these restrictions are listed below in Table 2.1.

Table 2.1: The seven crystal systems and their unit cell edges and angles are shown in table below

Crystal System	Unit cell shape (Unit cell edges: a b c ; Unit cell angles: α β γ)
Cubic	$a = b = c,$ $\alpha = \beta = \gamma = 90°$
Tetragonal	$a = b \neq c,$ $\alpha = \beta = \gamma = 90°$
Orthorhombic	$a \neq b \neq c,$ $\alpha = \beta = \gamma = 90°$
Monoclinic	$a \neq b \neq c,$ $\alpha = \gamma = 90°; \beta \neq 90°$
Triclinic	$a \neq b \neq c,$ $\alpha \neq \beta \neq \gamma \neq 90°$
Hexagonal	$a = b \neq c,$ $\alpha = \beta = 90°; \gamma = 120°$
Trigonal*	$a = b \neq c,$ $\alpha = \beta = 90°; \gamma = 120°$

Within a unit cell, symmetry related points on face or body centres can also exist. These extra lattice points are combined with the seven basic crystal systems to give fourteen Bravais lattices (Figure 2.4).

Primitive Cubic (p)   **Body-centred Cubic (I)**   **Face-centred Cubic (F)**

Primitive tetragonal (p)   **Body-centred tetragonal (f)**   **Primitive orthorhombic (p)**   **Body-centred orthorhombic (f)**

Base-centred orthorhombic (C)   **Face-centred orthorhombic (F)**   **Rhombohedra (R)**   **Hexagonal (p)**

Primitive monoclinic (p)   **Base-centred monoclinic (C)**   **Triclinic (p)**
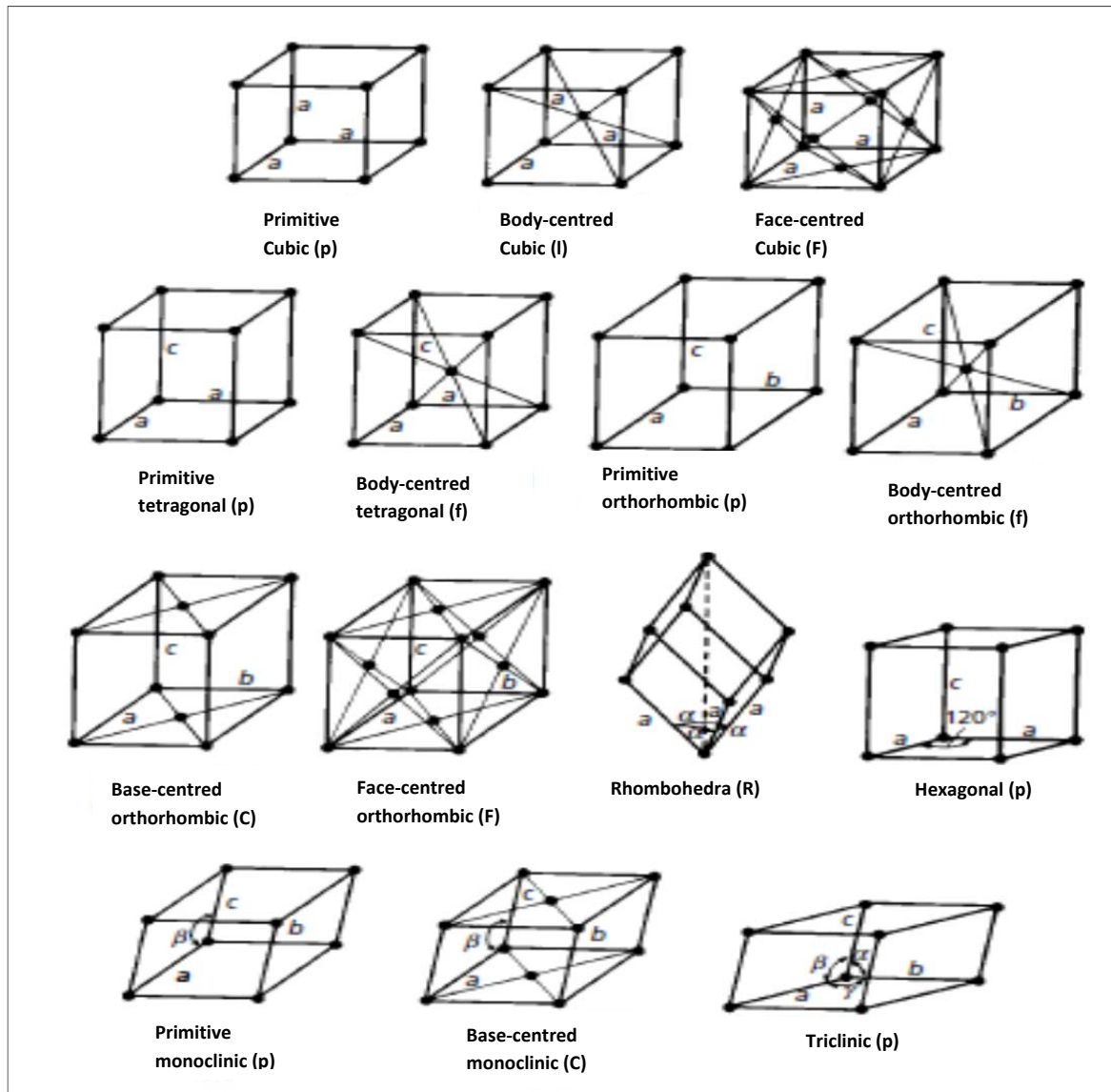
Figure 2.4: The fourteen Bravais lattices.[4]

All materials crystallise with structures which fall into one of these groups; however the unit cell can be of different sizes and can have different aspect ratios within the constraints of symmetry. The full symmetry of a crystal lattice is described by the space group and this relates the symmetry of a unit cell to those around it.

2.1.3. Lattice Plane and Miller Indices

The lattice plane is a concept introduced by Bragg's law and it is defined by the shape and dimensions of the unit cell. A crystal consists of unit cells packed together to form an infinite, regular array structure and within this structure there are planes of atoms,

called lattice planes. X-rays interacts with these planes of atoms in the three-dimensional lattices. Each plane represents a member of a parallel set of planes where each lattice point lie on one of the planes. The spacing between these lattice planes is called the d-spacing (d_{hkl}) measured in Angstroms.

The d-spacing can thus be defined as the perpendicular distance between any pair of adjacent planes whereby one passes through the origin[5].

The Miller indices are a set of numbers used to label the lattice planes in a crystal system (Figure 2.5).
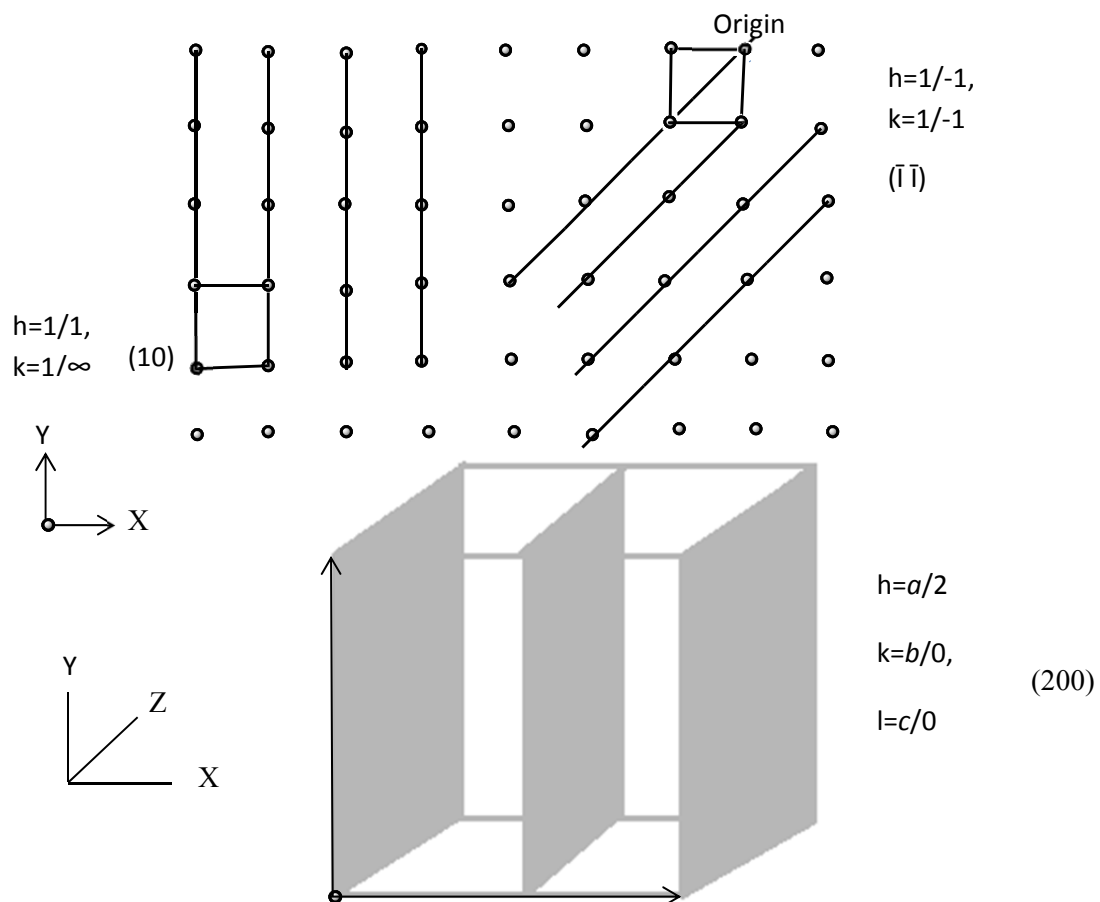
Figure 2.5: Crystal planes in 2-dimensional (upper) and 3-dimensional (lower) with Miller indices indicated by the numbers in brackets

The Miller indices (hkl) are used to indicate the point at which a plane in the crystal intercepts with the axes of the unit cell. These indices (hkl) correspond to the unit cell parameters *a*, *b* and *c* and are used to describe the location of a plane in a unit cell structure (except for hexagonal systems that use four co-ordinates). These hkl values

represent the reciprocal values of where a plane intercepts the *a*, *b* and *c* axes of the unit cell with 0 as the origin and 1 as a whole unit cell length. A zero in the Miller indices indicates that the plane runs parallel to that axis and never intercepts with it. The (200) Miller indices shown in figure 2.5 (lower) for example, indicates a plane that cuts ½ way along the a axis (h) but runs parallel to both *b* and *c* axes where there is no intercept.

2.1.4. Bragg's law

When X-rays of a fixed wavelength strike a crystalline material at certain incident angles, intense reflected X-rays are produced when the waves of the scattered X-rays interfere constructively. In order for constructive interference to occur, the differences in the distances between the atoms must be equal to an integral number of wavelengths (Figure 2.6). The general relationship between the wavelengths of the incident X-rays, angle of incidence and spacing between the crystal lattice planes of atoms is known as Bragg's law:

Equation 2.1: Bragg's law

$$n\lambda = 2d.\sin\theta \hspace{4cm} \text{Equation 2.1}$$

Where n = "order" of reflection, λ = wavelength of the incident X-rays (Å), d = inter-planar spacing of the crystal (Å) and θ= angle of incidence (^{o})
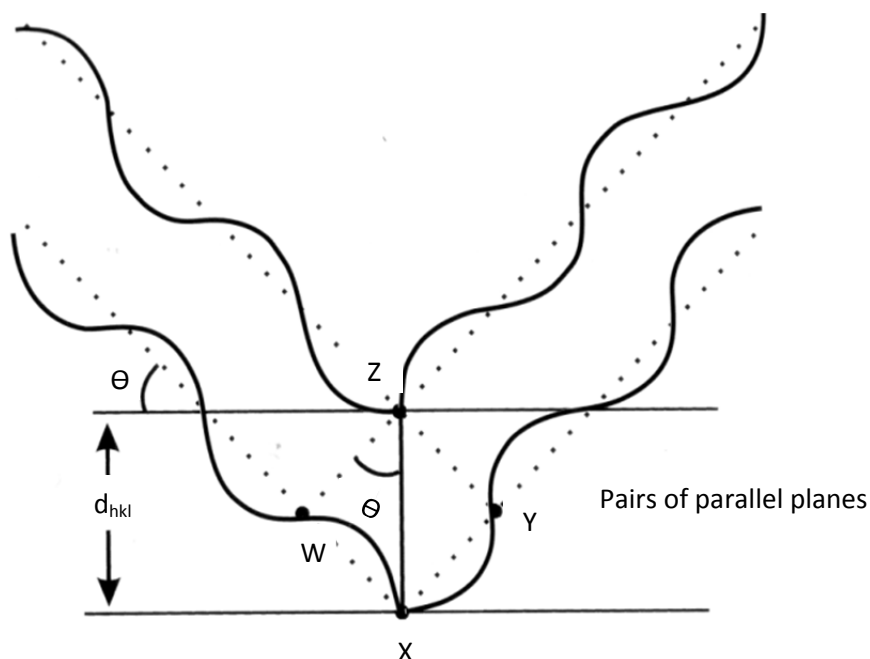
Figure 2.6: Illustrations for the Bragg's law/equation.[1]

The wavelength of the X-ray beam (λ) must be comparable to that of the periodic spacings within a crystal structure in order for scattering to occur. There are two ways of using Bragg's law in X-ray experiments; the first is used in laboratory X-ray diffraction and involves using radiation of a fixed wavelength and altering the angle of incidence, θ.   Whereas the second method, where the angle is fixed and the wavelength varied, is more often used in neutron diffraction experiments where time of flight measurements are made. During an XRD experiment in reflection geometry, the Bragg angle, θ, is measured at a fixed wavelength of radiation to collect scattered intensity as a function of the 2θ angle. By using X-rays of a known wavelength, λ, the d-spacing of the Bragg reflections can be calculated.

2.1.5. Powder X-ray diffraction

X-ray diffraction is one of the most widely and least ambiguous, non-destructive analytical techniques used to determine the position of atoms in molecules and solids. It information on the crystal structure of compounds by measuring the crystal diffraction peaks due to individual chemical compounds in a sample, how the atoms

are arranged in space, texture, lattice parameters and crystal phase, bonding within and between molecules.

Relative to other methods of X-ray analysis, powder X-ray diffraction allows for rapid, non-destructive analysis of multi-component solid mixtures without the need for extensive sample preparation.

Powder X-ray diffraction allows characterization of unknown materials in solid state/materials chemistry. Identification of unknown sample is based on comparison of the diffraction pattern to a database such as the International Centre for Diffraction Data's powder diffraction file (ICDD-PDF) or the Cambridge Structural Database (CSD), or by indexing the crystal diffraction peaks.

2.1.5.1. The PXRD experiment

X-ray diffraction involves the interaction of matter with an X-ray beam resulting in scattering. This scattering is used to generate diffraction data in the form of an X-ray pattern (plot of intensity vs. 2 θ), with the aid of a detector.

The scattering in PXRD occurs as a result of the diffraction of X-ray photons by an atom within an ordered, long range crystal structure. This involves the interaction of the X-ray photons with electron clouds of the atoms of a sample. Thus the degree of scattering is dependent on the number of electrons in an element in a particular plane. This gives the basis for sample identification in PXRD.

Basically three components are required for a successful diffraction experiment, these are; X-ray source, sample compartment and a detector for data collection (figure 2. 7)
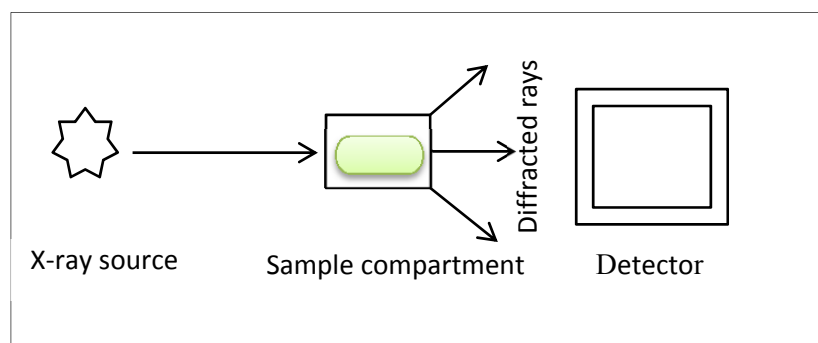

Figure 2.7: Setup for an X-ray diffraction experiment

In reality, the PXRD experiment is far more complicated (figure 2.8) than that presented here, however, for ease of understanding; the simplified setup (figure 2.7) can be adopted.
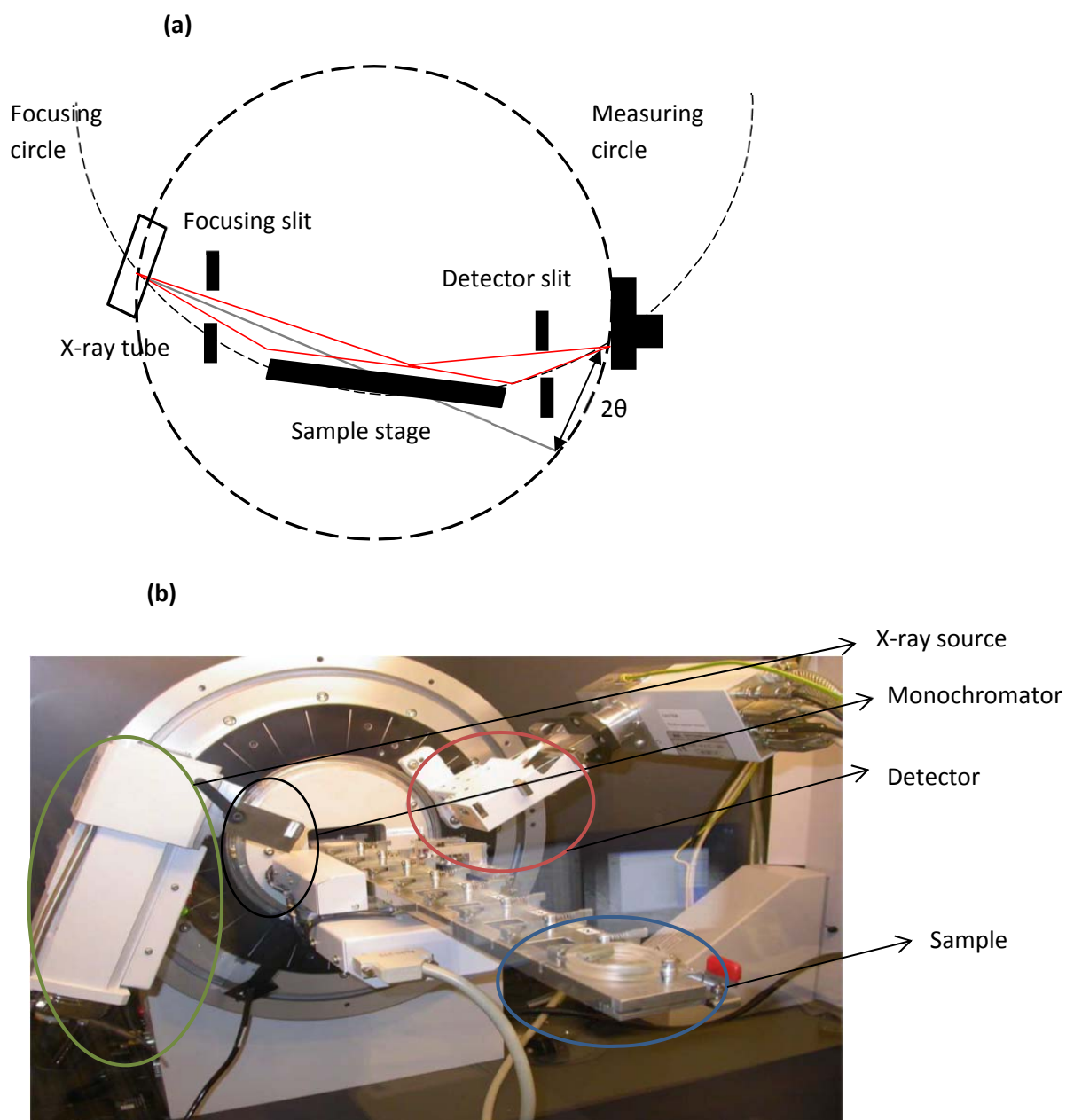

Figure 2.8: Schematic diagram of X-ray diffractometer (a) and Bruker D8 Advance powder diffractometer (b)

2.1.5.2. PXRD experimental parameters

The instrument used in these experiments was a Bruker D8 Advance diffractometer (figure 2.8b) operating with a copper X-ray tube, a monochromator with a Linx Eye detector. The PXRD data were collected using Cu Kα_1 (1.5406Å) radiation, over the 2θ range between 5 - 60° using a step size of 0.022° for 43 minutes.

The D8 is a fixed wavelength diffractometer and works by rotating the detector through a range to include all angles of incidence (2θ) that can be set to the users specification. In PXRD, a pattern of reflections indicating 2θ values versus intensity is produced.

2.1.6. X-ray fluorescence (XRF)

XRF like PXRD is a non-destructive X-ray technique used for elemental analysis. Unlike other techniques that analyse for metals (ICP and AAS), XRF technique does not require time-consuming, expensive and hazardous sample preparation techniques. This technique allows both the qualitative and quantitative identification of elements to be made due to the relationship between emission wavelength and atomic number, leading to the isolation of individual characteristic lines.

2.1.6.1. Principle of X-ray fluorescence

X-ray fluorescence involves the interaction of matter with X-ray beam similar to that in X-ray diffraction, the difference however lies in the fact that instead of resulting in elastic scattering, it results in fluorescence (inelastic).

In XRF, the electron transition takes place only between the inner shells of the atom, which are not involved in chemical bonding. Thus the independency of chemical bonding, allows the technique to analyse samples directly without advanced sample preparation. This makes XRF the best method for elemental analysis.

The term fluorescence is applied to this technique because the absorption of radiation of a specific energy results in the re-emission of radiation of a different energy (generally lower).

Bromine atom
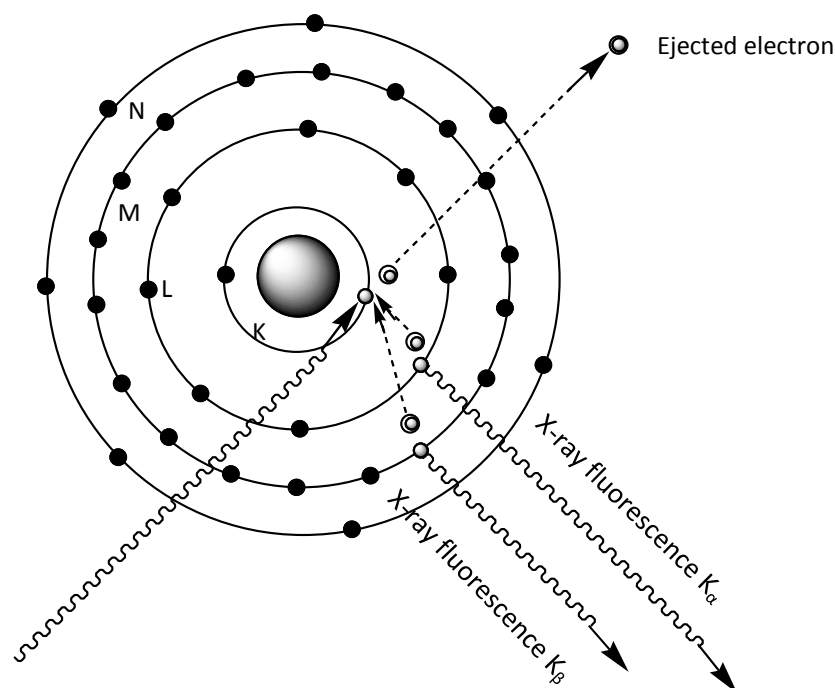
Figure 2.9: Schematic of an XRF experiment

2.1.6.2. XRF experimental parameters

The samples were prepared as pellets (discs) and run on a Spectro Xepos instrument with a 50mW palladium X-ray tube, under a helium gas atmosphere in 32mm sample cups and a peltier cooled solid state detector. Three scans were obtained from the run; the first to analyse for heavy elements (Z = 92 and higher) had a tube voltage of 45 kW, a current of 0.55 mA and a scan time of 100 s. The 2nd scan had tube voltage 48kW, current 0.5mA, scan time 100s, analyses for medium elements (Z > 18 < 92) and 3rd scan had tube voltage 25kW, current 1mA, and scan time 120s, analyses for light elements (Z < 18). The first scan used secondary Compton scattering and a molybdenum target, second scan used Barkla scattering and aluminium oxide target and the third scan used Barkla scattering and HOPG target.

The different targets are therefore needed to be able to analyse for the different group of elements (heavy, medium and light elements).

2.1.7. Scanning electron microscopy /Energy dispersive X-ray Spectroscopy (SEM-EDS)

SEM-EDS is used to measure the elemental composition as well as the surface observation of samples (sample imaging). The technique allows both the qualitative, quantitative and surface imaging of samples by the interaction of incident electron beam with the sample. This interaction induces X-ray fluorescence in the sample which is detected using a cooled semiconductor detector. The spectral lines specific for each element are then used to generate the elemental composition of the sample. SEM could also be used to form 3-dimentional images of sample surfaces on the nanometre to micrometre scale using electrons instead of photons[6]. This technique, despite its numerous advantages, has limitations in detecting elements below atomic number 4 [7] and the masking of elements that are in small amounts by those with very high amounts.

2.1.7.1. The principle of SEM-EDS

The principle of operation for SEM-EDS involves, focussing electron beam on the sample by either scanning across the surface of the sample or focusing on a particular point. The electron beam is generated using an electron gun and lenses used to focus the beam usually to a spot size of less than 10nm[6]. The energy of the X-rays generated by the atoms of the sample during interactions with electron beam is detected by the detector. These are then used to generate the elemental composition as well as an image of the sample. It is important for the sample chamber to be under vacuum since electrons are involved. Another requirement is that the sample should be able to avoid charging by being conductive. This is usually achieved with the use of gold coating especially for non-conducting samples.

2.1.7.2. SEM-EDS experimental parameters

The EDS spectra and SEM micrographs were produced on an EDAX Pheonix, EDX with a Carl Zeiss 1530 VP Field Emission Gun Scanning Electron Microscope (FEG-SEM) microanalysis system. The samples were sprinkled onto 12mm aluminium stubs using ''carbon sticky tabs''. These were then gold coated using an Emitech SC 7640 gold/palladium sputter coater to reduce the static charges during the analysis.

2.2. Vibrational spectroscopy techniques

IR and Raman spectroscopy can be grouped under vibrational spectroscopy, since both are capable of investigating the vibrational modes of the functional groups in materials.

The selection rule for IR activity involves a change of dipole moment during the vibration while that for Raman active is a change of polarisability[7]. Thus the techniques are used in a complementary manner.

2.2.1. FTIR spectroscopy

2.2.1.1. FTIR Theory

FTIR spectroscopy makes use of the infrared region of the electromagnetic spectrum which ranges between $14000-10 cm^{-1}$. This region is further divided into; near ($14000-4000 cm^{-1}$), mid ($4000-400 cm^{-1}$) and far ($400-10 cm^{-1}$) infrared regions. IR spectroscopy data are obtained, when the frequency of incident radiation is varied and the quantity of radiation absorbed or transmitted measured.

Atoms in a solid vibrate continuously at frequencies of $10^{12}-10^{14}$ Hz. When a molecule adsorbs energy it becomes excited, however this can only occur at a certain quanta of energy depending on the nature of the bonds and functional groups present in a sample, hence the need to scan at several frequencies. When a bond in a molecule absorbs energy it becomes excited and vibrates. There are different types of vibrations that could occur in a molecule; the most common ones are the stretching and bending vibrations. Each bond in a molecule has unique stretching and bending frequencies e.g. XY_2 Compounds.
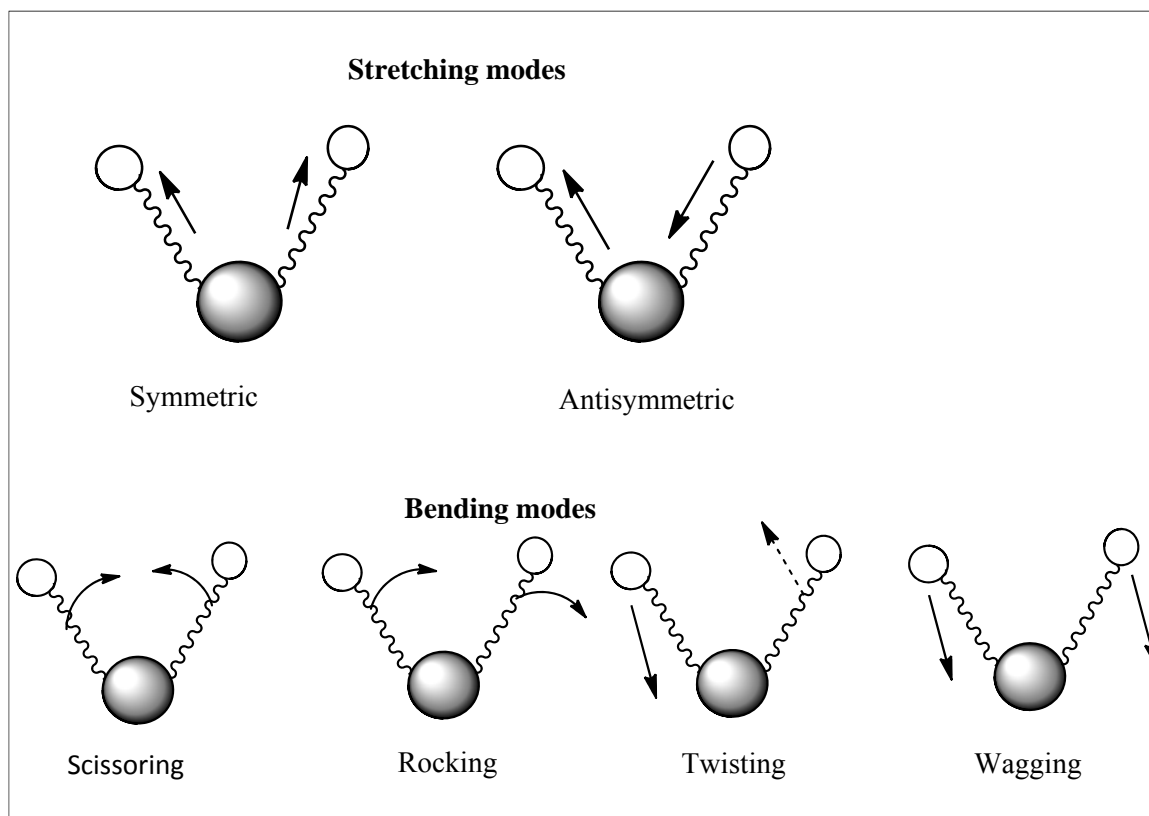
Figure 2.10: Vibrational modes for XY_2 compounds

The vibrations are due to a change in bond angle and bond lengths and using Hooke's law it is possible to estimate the amount of vibration based on the size of the atoms surrounding a bond (Equation 2.2). Hooke's law treats a bond like a "spring" and when a mass (atom) is added to the end of this spring, the bond oscillates harmonically. This in turn can be used to analyze which vibrations in a spectrum are due to which bond or functional group[8].

Equation2.2: Hooke's law

V = 1/ (2πc) √F/m   Equation 2.2

Where V = frequency, c = the speed of light (constant), F = the strength of a bond and m = mass of an atom

From the equation 2, it is shown that the heavier the atoms surrounding a bond, the lower the frequency and the stronger the bond between atoms, the lower the frequency.

2.2.1.2. FTIR experiment

In an FTIR experiment, light from a laser source travels through a monochromatic prism, an interferometer containing several mirrors and a beam splitter and then the sample. A second beam with a longer wavelength then combines with the first to form a complex interference pattern at the detector (Figure 2.11). Computer software then analyzes the complex interference patterns to produce an IR spectrum of a sample. The whole process from start to the appearance of an IR spectrum on a computer screen is rapid (less than a minute) and gives greater sensitivity and better resolution than more traditional direct plot IR systems.
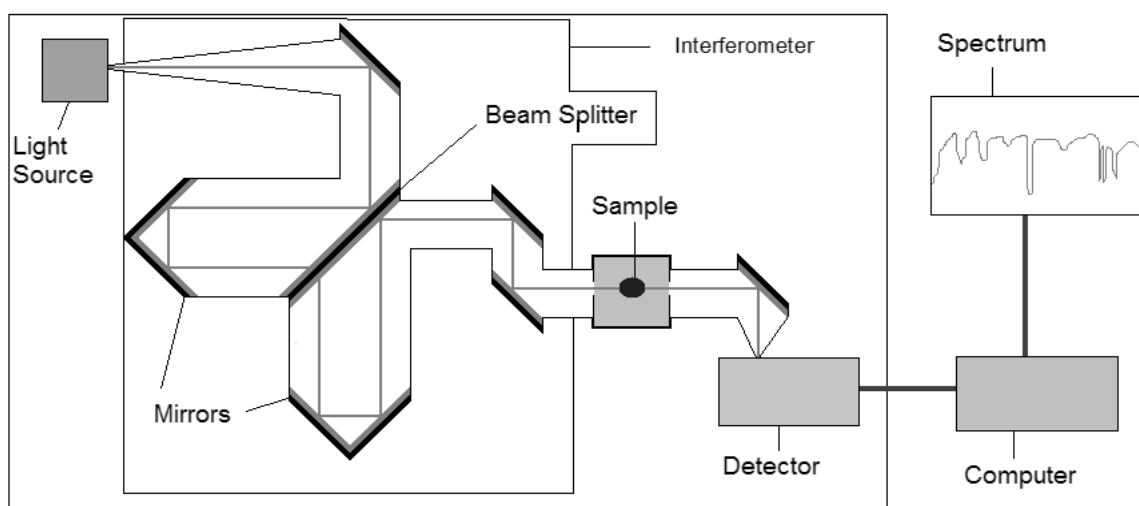
Figure 2.11: A Schematic Diagram of an FT-IR Experiment

2.2.1.3. FTIR experimental parameters

The Perkin-Elmer Paragon 1000 FT-IR spectrophotometer was used in this experiment to collect FT-IR data for the samples. Samples were prepared by making discs of a small amount of the sample (~3mg) in KBr and measurements were carried out over the IR region of 1200-400cm^{-1} for parent zeolites and 4000-1000 cm^{-1} for the ligand attached zeolites. A background spectrum was measured before every sample to compensate for atmospheric conditions around the FT-IR instrument.

2.2.2. Raman spectroscopy

2.2.2.1. Raman spectroscopy theory

Raman is an optical technique that is similar to FT-IR spectroscopy in that it detects vibrations produced by bending/stretching frequencies of bonds within a molecule.

2.2.2.2. Raman Experiment

When light passes through a material, some of the light is absorbed and some scattered. Nearly all of the scattered light has the same frequency as the incident light; this is called elastic scattering or Rayleigh scattering. However, a little fraction of the scattered light is shifted in frequency; this process is called Raman scattering and the associated frequency shift is called the Raman shift[9].

Raman scattering is caused by the light interacting with some kind of oscillation inside the material, and the Raman shift measures the frequency of the oscillation involved. Many kinds of oscillations produce Raman shifts, e.g. molecular vibrations and rotations, lattice vibrations etc.; a complex structure like an organic compound can oscillate in many ways and can therefore produce a complicated Raman spectrum[9].

Two types of Raman scattering are possible depending on the manner in which the incident photon interacts with the electron clouds of the sample matter (figure 2.12). If an electron in the ground state interacts with the incident photon, it will be excited to a virtual energy level and will remain in a higher energy level on relaxation. This type of Raman scattering is known as Stokes Raman scattering and results in loss of energy of the incident photon. On the other hand, if the interaction occurs with an electron already in an excited state, the electron will be excited to a virtual state but will relax to a ground state. This Raman scattering is known as Anti-Stokes Raman scattering which results in a gain in energy of incident photon [10]. The scattering is dependent on the vibration of molecules thus, spectrum similar to that in IR can be generated complementary to IR data.
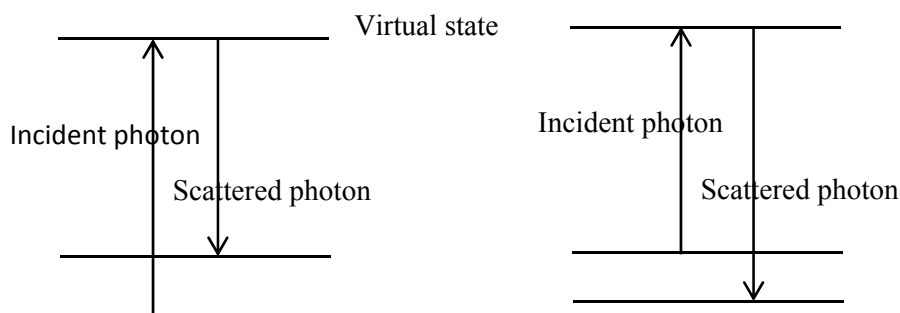
Figure 2.12: Photon scattering in Raman Spectroscopy

Selection rules for Raman spectroscopy dictate that vibrations of molecules must generate a detectable change in polarisability or anisotropic polarisability (figure 2.13). This is because Raman is a weak effect. This means intense monochromatic light source (lasers) is used for successful Raman spectroscopic analysis.
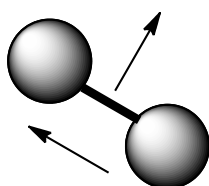
Figure 2.13: Anisotropic polarisation of a homonuclear diatomic molecule

Raman spectroscopy is not regularly used in zeolite characterisation since it is difficult to obtain highly quality spectra due to fluorescence. In addition, the low polarisability of the framework bonds leads to very weak signals whereas the same bonds are highly polarised and give good IR spectra. However, Raman spectroscopy can be useful for characterising complex ions within zeolites or species grafted to zeolites since the framework itself is less Raman active, the grafted species and occluded ions are easily evidenced. Recently UV-Raman spectroscopy spectroscopy has been shown to be very sensitive in characterising zeolites structures without any fluorescence interference from the zeolites[11].

2.2.2.3 Raman experimental parameters

For Raman spectroscopy, the Jobin-Yvon Labram HR, was used to run the samples. Samples are placed under the instrument's microscope and illuminated by a focused laser beam. Back-scattered light is collected and analysed using a diffraction grating and CCD. A useful spectrum from a single spot on the sample can be produced in seconds. The automated scanning stage and temperature controller permit fine scanning in 3 spatial coordinates and temperature. Wavelengths: 633 nm (red), 514 nm (green) and 488 nm (blue); Raman shifts: 100 cm^{-1} up to 3000 cm^{-1} and more.; resolution down to 0.35 cm^{-1} (for the 1800 mm^{-1} grating and red light); scannable temperature range: -200 ^{o}C to 600 ^{o}C; automated XYZ mapping stage (0.1 μm steps in X and Y).

2.3. Thermal Analysis

Thermal analysis involves the measurement of the changes in the physical properties of a substance as function of temperature under a controlled temperature programme[12]. Processes under thermal analysis include; thermogravimetric analysis (TGA), differential thermal analysis (DTA) and differential scanning calorimetry (DSC)[13]. However, the DSC will not be discussed since it was not used in this study.

2.3.1. Thermo gravimetric Analysis

Thermo gravimetric analysis (TGA) is a destructive technique used for measuring the change in mass of a sample as a function of temperature. A plot of temperature against mass gives the thermogravimetric curve. TGA is often used as a comparative technique for groups of samples. The data obtained gives information such as the moisture content of a sample. The temperature programme selected is both sample and property dependent. Different factors can be determined depending on the temperature programme selected; isothermal experiments can study factors such as decomposition, phase transitions, oxidation of a sample as a function of time, whereas non-isothermal experiments can study the same factors as a function of temperature.

2.3.2. Differential thermal analysis (DTA)

DTA measures the temperature difference of a sample as compared to an inert reference (alumina) under identical conditions. The temperature difference is then plotted against time to give a DTA curve.

2.3.3. Experimental parameter for TGA and DTA

The thermal analysis (TGA and DTA) of the zeolites were carried out under the flow of nitrogen while monitoring the weight loss on a Q600 SDT v20.9 Build 20, to ascertain the actual amount of water contained in the zeolites. A small amount of sample is used (ca. 10 mg) for the analysis; however calibration of the instrument is vital before each analysis, therefore a standard of indium or zinc is used for calibration.

2.4. Solid State Nuclear Magnetic Resonance

Solid State Nuclear Magnetic Resonance (SSNMR) is a type of NMR spectroscopy, characterized by the presence of directionally dependent (anisotropic) interactions.

2.4.1. SSNMR theory

NMR is based on the concept that some nuclei within a molecule have a magnetic moment (spin). The spatial proximity and or chemical bond between two atoms can result in interactions between these nuclei, these interactions are orientation dependent.

Two directionally dependent interactions mostly observed in SSNMR are; chemical shift anisotropy (CSA) and the internuclear dipolar coupling. Others include; anisotropic J-coupling in NMR and g-tensor in electron spin resonance.

Spin systems also interacts with an applied magnetic field. When a magnetic moment (spin) is subjected to a magnetic field, a net magnetisation occurs (Figure 2.14), the individual magnetic moment is observed to preferentially align to the applied field[14]. This net magnetisation is measured as a spectrum using an alternating radiofrequency.
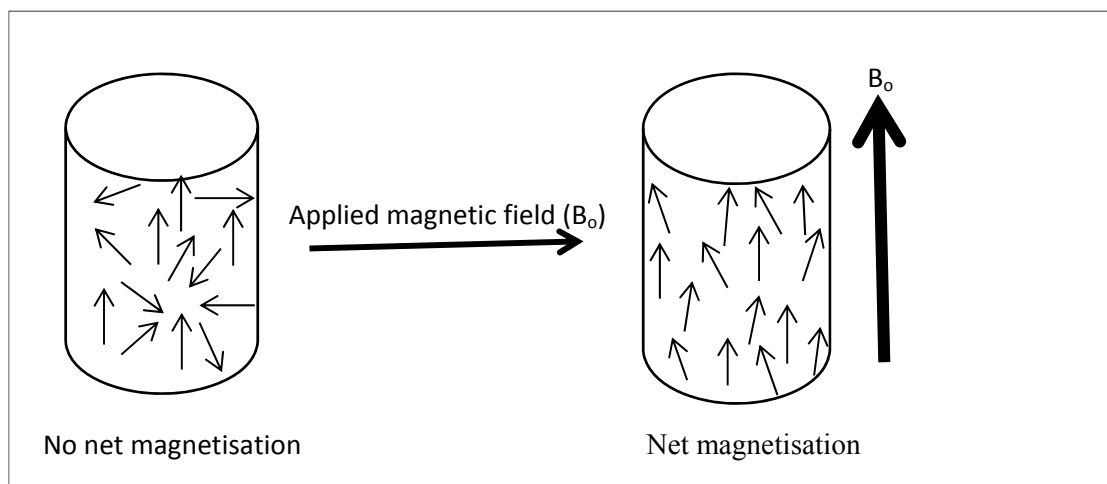
Figure 2.14: Schematic representation of spin interaction with a magnetic field (B_o)

Solution NMR spectra consist of a series of very sharp transitions, due to the averaging of the anisotropic NMR interactions by rapid random tumbling (Brownian motion). Unlike the solution NMR, solid state NMR (e.g. powder, crystal) spectra are very broad, as the full effects of anisotropic interactions are observed in the spectrum.

High resolution SSNMR spectra can give data similar to that obtained from solution NMR spectra but some special techniques are required, these includes; magic angle spinning (MAS), cross polarisation (CP) etc.

As problematic as anisotropic effects can be in NMR, there is a range of situations where the broad NMR lines in SSNMR provides much information on chemistry and dynamics in the solid state.

2.4.1.1. Magic angle spinning

Solid State NMR is prone to anisotropic interactions. This is because the 'tumbling' found in liquid NMR is not possible in solid state samples, dipole-dipole couplings thus dominates the NMR. For example, protons can couple with themselves in the same molecule as well as neighbouring molecules in a crystal lattice through hydrogen bonding.

Magic angle spinning is one of the techniques employed to suppress the effects of these interactions in SSNMR. [15, 16] Chemical shielding and dipolar interactions are both

governed by the $(3\cos^2\theta-1)$ terms. Other factors governing dipolar interactions include; $(D \alpha 1/r^3)$ and $(D \alpha \gamma A-\gamma B)$. However, the first term is more easily employed in removing dipolar couplings and other anisotropic interactions. For solution NMR, rapid isotropic tumbling averages the $(3\cos^2\theta-1)$ term to zero.

The magic angle spinning introduces an artificial motion similar to that in solution NMR by placing the axis of the sample rotor at an angle (54.74 °) known as magic angle with respect to the applied magnetic field B_o (figure 2.15). At this angle, the term $(3\cos\theta-1)=1$, however the rate of the magic angle spinning (MAS) must be greater than or equal to the magnitude of the anisotropic interactions for the component $(3\cos^2\theta-1)$ to equal zero. Powdered samples are tightly packed into rotors and spun at rates from 1-35 KHz depending on the experimental requirements. If on the other hand the sample is spun at rate less than the magnitude of the anisotropic interactions, spinning sidebands (SSB) becomes visible which can be separated by rate of spinning.
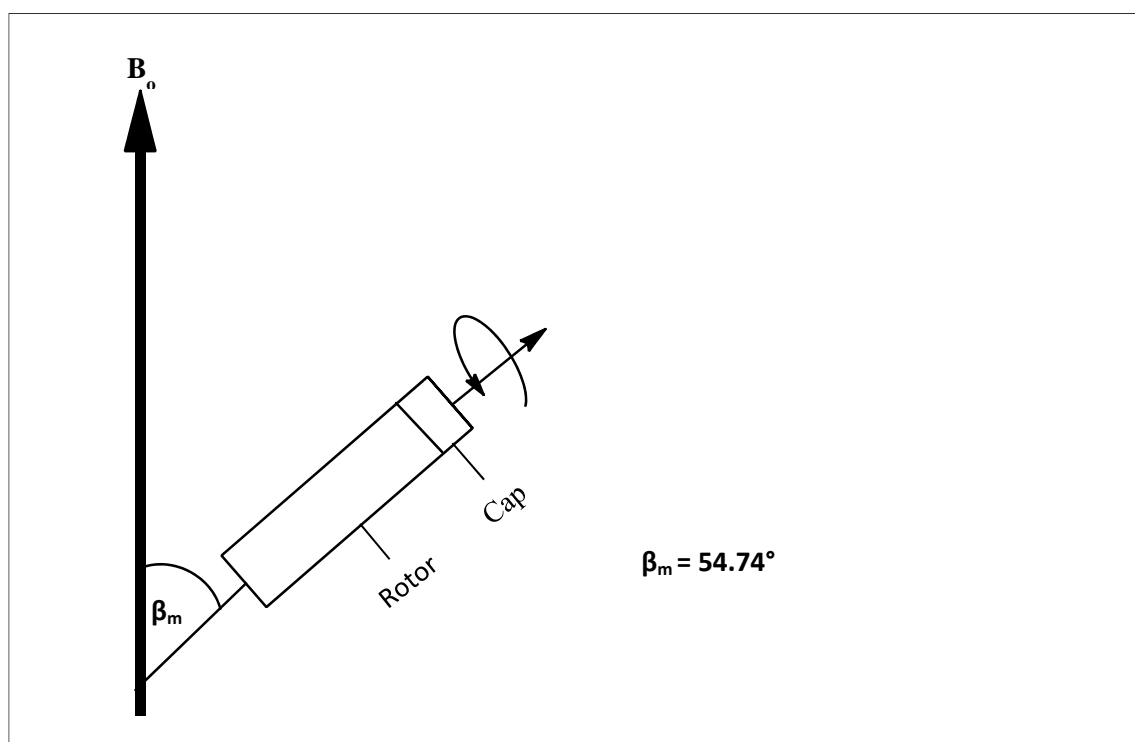

Figure 2.15: Magic Angle Spinning

For polycrystalline powders containing multiple NMR active nuclei within the molecule, it is not certain that all the nuclei will be oriented with the magic angle. A vast majority of the nuclei may rather align closer to the applied magnetic field. However, at sufficiently high spinning rates (>10KHz), the non-oriented spin pairs will be forced to be oriented with the magic angle by what is known as effective MAS, hence effectively removing the anisotropic effects from spectra data collected. In cases where this cannot be achieved by high speed spinning, spinning sidebands (SSB) suppression pulse programs may be used.

2.4.1.2. Cross polarization

Cross polarization is another useful technique in solid state NMR. This technique utilizes the polarization from abundant spins like ^{1}H and ^{19}F. The polarization from these spins is transferred to low abundant spins like ^{13}C and ^{15}N.

The overall effect of cross polarization is to enhance the signal-to-noise ratio by enhancing the signal from low abundant spins as well as subjecting the abundant spins to large fluctuating magnetic field resulting from motion. The abundant nuclei to this effect are induced to have rapid relaxation delay. The relaxation delay between each scan is important as; too short relaxation delay results to magnetization being saturated (no signal) and too long delay times on the other hand results in a waste of the instrument time.

Solid organic crystalline materials have relaxation delay time of 10-300 s for ^{1}H and 60-3000 s for ^{13}C. Amorphous or poorly crystalline materials have delay times as low as 1-30 s for ^{1}H and 2-60 s for ^{13}C. Thus observing for example ^{13}C via the abundant ^{1}H spins, will result in shorter relaxation times compared to direct observation of ^{13}C. Cross polarization (CP) experiment is as described in figure 2.16.
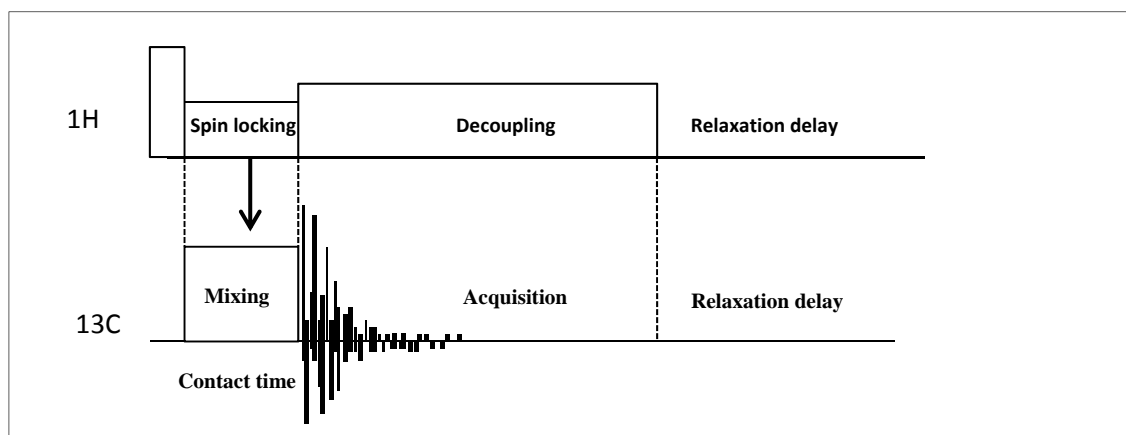
Figure 2.16: Schematic representation of a cross polarization experiment

CP requires that nuclei are dipolar coupled to one another. It occurs after a 90 ^{o}C pulse is applied to the magnetization of 1H. The resultant effect is to magnetize ^{13}C, during this last process, two activities occur simultaneously; proton decoupling and collection of the free inductive decay (FID). The proton decoupling is such that the remaining dipolar coupling interaction with the ^{13}C is removed.

2.4.2. Solid State NMR experimental parameters

Solid-state NMR spectra were recorded on Bruker Avance 500MHz NMR spectrometer, equipped with a 4mm MAS HX probe, 100W proton amplifier and 500W X amplifier. Cross-polarization used a 1H pulse of 2 us (at −5.5 dB), a ramped proton CP pulse of 2ms (at −4.0 dB) and a carbon CP pulse of 2ms (at −3.1 dB). 1H →29 Si and 13C cross-polarization (CP)/MAS NMR experiments were carried out to selectively enhance the signals of Si and C atoms strongly when interacted with hydroxyl groups. TPPM15 proton decoupling was applied during the 30 ms acquisition time. FIDs contain 3k data points which were Fourier transformed into 16k data points; an exponential function of 20 Hz was applied to the FID using Bruker TOPSPIN (1.3) software. Spectra were referenced to external TMS (1H, 13C, 29Si) and the magic angle was set up using KBr. Magic angle spinning of 10kHz was used. CP-MAS 29Si used a relaxation delay of 5 s between each scan; DP-MAS 29Si used a relaxation of 10 s. Direct polarization was used for 1H and 27Al spectra (4us at 1dB).

2.5. Elemental and Solution based analysis

Elemental and Solution based analysis as grouped in this research work include techniques used to determine the elemental composition of samples as well as those analysis carried out in the liquid state. Techniques grouped under the solution based analysis include; inductively coupled plasma optical emission spectroscopy (ICP-OES), atomic absorption spectroscopy (AAS), gas chromatography (GC) and ultraviolet spectroscopy (UV) while the techniques for the determination of the elemental composition of samples include; Elemental Analysis (CHN), ICP-OES and AAS.

2.5.1. Elemental Analysis

Elemental analysis is a destructive analytical technique used to quantitatively determine elements in a sample. The most common form of elemental analysis, CHNX analysis, is accomplished by combustion analysis. In this technique, a small sample (ca. 5 mg) is burned in an excess of oxygen, and various traps collect the combustion products, including carbon dioxide, water, and nitric oxide. The weights of these combustion products can be used to calculate the composition of a sample in terms of % weights of carbon (C), nitrogen (N), oxygen (O) and any other heteroatom's (X). In this research an Exeter analytical ink (EAI) CE-440 elemental analysis machine was used.

2.5.2. ICP-OES

ICP-OES is an analytical technique used for the determination of trace elements; mainly heavy metals. It measures about 70 elements in aqueous solutions. However, it cannot measure H, N, O, C, He, F, Ne, Cl and a few other elements. The optimum working range for element concentration is 0.5-100ppm.

2.5.2.1. Principle of operation of ICP-OES

The technique is based on the principle of spontaneous emission of photons from atoms and ions that have been excited in a radiofrequency (RF) discharge. Gaseous and liquid samples may be introduced directly into the instrument but solid samples may need to be extracted or acid digested for the analyte to be present in solution. The sample introduced into the instrument usually in the aqueous state is converted

into micro-droplets (aerosol) by use of the nebulizer into the plasma. In the core of the plasma, the ICP holds a temperature of 10,000K [17] therefore the micro-droplets quickly vaporizes and gets excited, converting atoms to ions. The excited state species (atoms and ions) relaxes to the ground state releasing photons of light. The emitted light has a wavelength that is specific for each element. Thus the wavelength can be used to identify the elements from which they originate using a solid state detector.

2.5.2.2. ICP-OES experimental parameters

The ICP-OES data of the samples in this work were collected on a thermo scientific iCAP 6000 series spectrophotometer. The data were collected on both the standard of known analyte concentration and aqueous sample solutions of unknown concentration, over a span time of 2 min per sample.

2.5.3. Atomic absorption spectroscopy

Atomic absorption spectroscopy is a technique used in determining the concentration of an analyte in a sample solution to be analyzed. It is employed for the quantitative and qualitative determination of chemical elements using the absorption of radiation by atoms in the gaseous state.

2.5.3.1. Principle of operation of AAS

This technique relies on the Beer-Lambert Law to determine the unknown concentration of an element in a sample using absorption spectrometry. Standards of known analyte concentration are required to establish a relationship between the analyte concentration and the measured absorbance. Electrons from the atoms using the atomizer are promoted to higher energy levels by absorbing a defined quantity of energy (wavelength). This energy is specific to a particular element that is to say that each wavelength corresponds to only one element giving the technique its elemental selectivity.

2.5.3.2. AAS experimental parameters

The AAS data of the samples were collected on an iCE 3000 series AA spectrophotometer. The spectrophotometer has a serial number of ITL294S/NC083300024 and solar software for data collection. The data were collected

on both the standards of known analyte concentrations and aqueous sample solutions of unknown concentration, over a span time of 2min per sample.

2.5.4. Gas chromatography (GC)

GC is an analytical technique used for separating and analysing compounds without decomposition. Typical uses of GC include; purity testing of substances, separating different components of a mixture as well as identifying a compound. For this research work, this technique is used as a fingerprint in identifying the different crude oil samples used in the analysis.

2.5.4.1. Principle of operation of GC

GC like any other forms of chromatography relies on the use of a stationary phase and a mobile phase for the separation of compounds in a mixture. For a GC, the process is between a liquid stationary phase and a gas mobile phase at a controlled gas temperature. The mobile phase is a carrier gas (inert gas) and the stationary phase is a column, containing a microscopic layer of liquid/polymer on an inert support. The gaseous compounds interacts with the walls of the stationary phase (inner coated column), causing each of the compounds to elute at a different time known as retention time of the compound. This retention time is compared to produce the GC data.

2.5.4.2. GC experimental parameters

The crude oil samples were subjected to GC-MS analysis. This was done using GC 8000 series MD 800 and column of 30m DB5MS. 1µL sample was injected into the column at a temperature of 250 ^{o}. The gas interference temperature was also kept at 250 ^{o}. The samples were initially heated at 35 ^{o} for 10 min then at the rate of 10 ^{o} C/min to 300 ^{o} C for 10 min. The acquisition type was full scan between 50-500 amu.

2.5.5. UV-Vis spectroscopy

UV-Vis spectroscopy is a technique that utilises light in the visible and adjacent (near – UV and near infrared) regions of the electromagnetic spectrum to measure the electronic transitions of molecules from the ground state to excited state.

2.5.5.1. Principle of operation of UV-VIS spectroscopy

The UV-VIS spectroscopy is also based on the principle of the Beer's law which states that the absorbance is directly proportional to the path length b, and the concentration of the absorbing species.

A = Ɛbc

The absorption of UV or visible radiation corresponds to the excitation of outer electrons. Three types of electronic transitions are known, these are; transition involving; π, σ and n electrons, transitions involving charge transfer electrons and finally, transition involving d and f electrons.

Electrons are promoted from their ground state to an excited state when an atom or molecule absorbs energy, resulting to rotation and vibration with respect to each other. These vibrations and rotations also have packed discrete energy levels (figure 2.17).

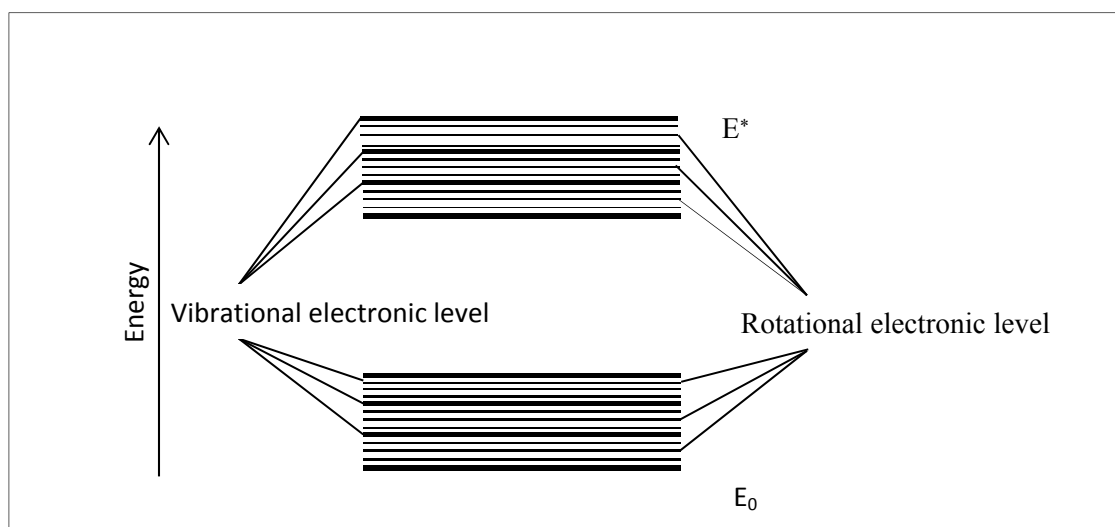Figure 2.17: Schematic of packed discreet energy levels

Molecules containing bonding pi (π) electrons or non-bonding (n) electrons can absorb the energy in the form of ultraviolent/visible light to excite these electrons to higher anti-bonding molecular orbitals (figure 2.18). This is because the absorption peaks for these transitions fall within the convenient region of the spectrum (200 - 700 nm).

These transitions need an unsaturated group in the molecule to provide the p electrons.
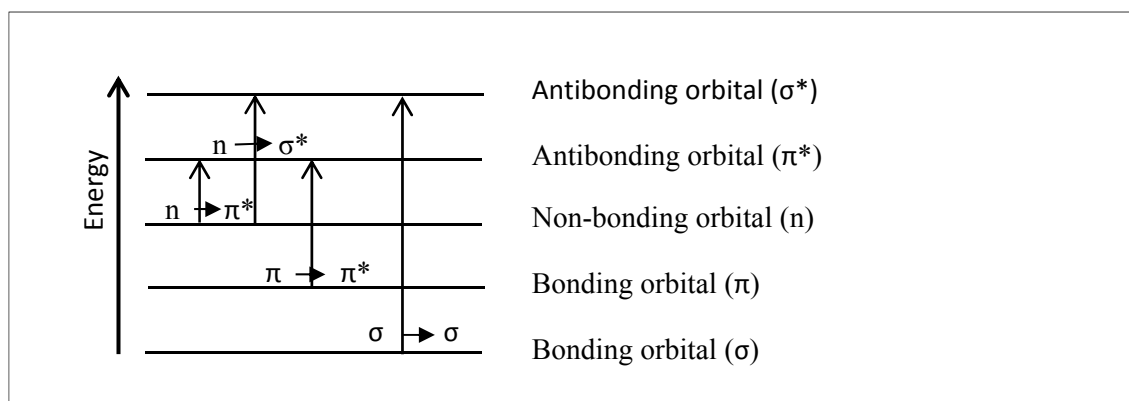

Figure 2.18: Types of electronic transition

The absorption of ultraviolet/visible radiation by molecules is restricted to certain functional groups known as chromophores which contain valence electrons of low excitation energy. Chromophore-containing molecules usually give a complex spectrum, due to the superposition of vibrational and rotational transitions on the electronic transitions resulting in overlapping lines which appears as a continuous absorption band.

The absorbing species are typically dissolved in a solvent. This solvent also has effects on the spectrum of the species. These effects could either be a shift to shorter wavelengths (blue shift) with increasing solvent polarity (n $\longrightarrow \pi^*$) or $\pi \longrightarrow \pi^*$ (blue shift) which is caused by the attractive polarization forces between the solvent and the absorber thus lowering the energy levels of the excited and unexcited states.

A number of inorganic species show charge-transfer absorption (charge-transfer complexes). However, these complexes can only demonstrate charge-transfer behaviour, if one of its components must have electron donating properties and another component an electron acceptor.

2.5.5.2. UV-Vis spectroscopy experimental parameters

The UV data of the samples were collected on a UV-1650PC UV-VIS spectrophotometer. The spectrophotometer has a serial number of ITL9001S/NA10774430138, UV-probe 2.42 and a window 7 platform. The samples were diluted in dimethylformamide (DMF) to measure the visible spectrum.

2.6. Conclusion

Analytical techniques described in this chapter; PXRD, FTIR, Raman, SSNMR, TGA, SEM-EDS, CHN, ICP-OES, AAS, UV-vis and gas chromatography, were used for the characterisation of the zeolites prepared as well as the exchanging metal ions solution and crude oil. PXRD was used as the main technique for phase identification alongside SSNMR. FTIR and Raman were also used for identification but in a complementary manner. Thermal analyses were used to determine the phase changes as well as weight losses due to zeolitic water. Solution based analysis were used for metal determination as well as fingerprint technique.

References

1. S.E. Dann, Reactions and Characterisation of Solids, Royal Society of Chemistry, UK, 2000.

2. R. Jenkins, X-ray techniques: overview, Encyclopaedia of Analytical Chemistry, R.A. Meyer (ed), John Wiley and Sons Ltd, Chichester, 2000.

3. A.R. West, Chapter 3. Crystallography and diffraction techniques, Basic solid state chemistry, second edition, John Wiley and Sons Ltd., Chichester, 1999.

4. C. Hammond, The Basics of Crystallography and Diffraction, Oxford University press Inc., New York, 2009.

5. C. Kirk, Inorganic Structure Determination PXRD lecture notes 1, crystallography, 17-20, 2012.

6. J.I. Goldstein, C.E. Lyman, D.E. Newbury, E. Lifshin, P. Echlin, L. Sawyer, et al., Scanning Electron Microscopy and X-ray Microanalysis, third edition, Plenum publishers, London,2003.

7. B.H Stuart, Infrared spectroscopy: fundamentals and applications, analytical techniques in the sciences, John Wiley and Sons Ltd, Chichester, 2004.

8. R.L. Carter, Molecular Symmetry and Group Theory, John Wiley & Sons, New York, 1998.

9. Y. Yu, G. Xiong, C. Li and F. Xiao, Micropor. Mesopor. Mat., 2001, 46, 23-24.

10. T.R. Gilson, P.J. Hendra, Laser Raman spectroscopy, John Wiley and sons Ltd, London,1970.

11. G.D. Knowlton and T. R. White, Clays and Clay Minerals, 1981, 29, 403-411.

12. M.E. Brown, Introduction to Thermal Analysis. Techniques and applications, Chapman and Hall, London, 1988.

13. G.W.H. Höhne, W.F. Hemminger, H.J. Flammersheim, Differential scanning calorimetry, second edition, Springer, London, 2003.

14. M.J. Duer, Solid-state NMR spectroscopy, principles and applications, Blackwell Science Ltd, Oxford, 2002.

15. E.R. Andrew, A. Jasinski. Nuclear magnetic resonance spectra of rapidly-rotated solids containing reorienting molecular groups, J. Phys. Part C Solid, 1971, 4, 391.

16. E.R. Andrew, A. Bradbury, R.G Eades. Nuclear magnetic resonance spectra from a crystal rotated at high speed, Nature, 1958, 182, 1659-1659.

17. X. Hou, B.T. Jones, Inductively Coupled Plasma/Optical Emission spectrometry, Encyclopaedia of Analytical Chemistry, R.A. Meyer (ed), John Wiley and Sons Ltd, Chichester, 2000.

Chapter 3: Syntheses of Zeolites

3.0: Introduction

The history of zeolites synthesis dates back to the 18th century with the preparation of levynite by St. Clair Deville as the first hydrothermally synthesised zeolite [1].

Syntheses of more zeolites were reported after levynite; however, the paucity of reliable characterisation techniques made it impossible to verify the early materials. With the development of the X-ray diffraction technique in 1930, it became possible to characterize zeolitic structures and properly identify them. The use of X-ray diffraction for identification purposes of minerals was first described by Leonard in 1927 [2]. However, the definitive synthesis of zeolites, including the preparation of the analogue of mordenite, was first reported by Barrer in 1948 [3]. Inspired by Barrer's work, studies were carried out on zeolite synthesis by both individuals such as Milton or Breck, as well as industries such as Union Carbide or Mobil Oil in search of new approaches for separation and air purification. Between 1949-1954, Milton and Breck discovered several zeolite types, some of which included zeolites A, X and Y [1]. Based on the properties of synthetic zeolites; Union Carbide commercialized them as a new class of industrial material for separation and purification in 1954 [1]. Since then these zeolites have been applied in wastewater treatment, including the removal of metal ions from solution [4-7].

Zeolites synthesis is normally carried out under hydrothermal conditions [8, 9]. A silicate solution is mixed with an aluminate solution to give a gel-like alkaline suspension. Depending on the type of zeolite to be targeted, various cations or anions may be added to the synthesis mixture. The synthesis proceeds at high temperature (90 – 200 $^{\circ}$C) in sealed high pressure vessels thus crystallising the target zeolite.

The zeolite synthesis involves two important steps; cell nucleation and crystallisation. Nucleation, as the name implies, is a process whereby aggregates of precursors assemble to form nuclei which grow with time. The zeolite is finally formed during the process of crystallisation. A schematic of zeolite synthesis is as presented in figure 3.1.
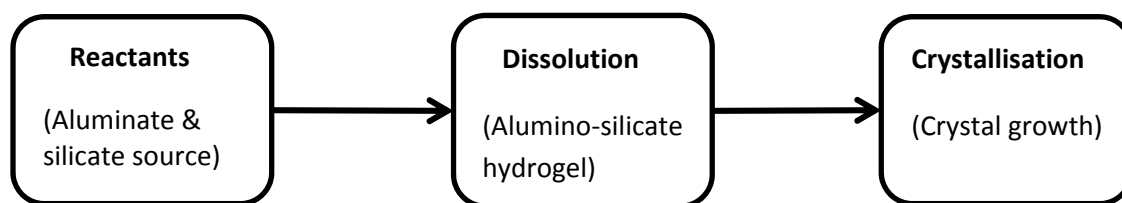
Figure 3.1: Schematic of zeolite synthesis

In this section, the syntheses of zeolite materials as the starting materials for the ion exchange reactions are reported. Synthetic zeolites that were targeted were zeolite A ($Na_{12}Al_{12}Si_{12}O_{48}.24.2H_2O$), zeolite X ($Na_{88}Al_{88}Si_{104}O_{384}.238.8H_2O$), zeolite Y ($Na_{54.91}Al_{56}Si_{136}O_{384}.246.5H_2O$), sodalite ($Na_8$ $(AlSiO_4)_6Cl_2$) and hydrosodalite (Na_6 $(AlSiO_4)_6.6H_2O$).

As earlier mentioned in chapter 1, the sodalites and hydrosodalites were synthesised to compare the ion exchange behaviour in zeolite A, zeolite X and zeolite Y which are the main target zeolites in this research work, as these zeolites are made up of sodalite units. Thus the sodalites and hydrosodalites may not be discussed in as much detail as the main target zeolites.

Since the literature suggests that the ion exchange properties of zeolites can be significantly influenced by the counter-cation type [4, 6]; lithium and potassium analogues of the parent sodium materials were also prepared by solution based ion exchange to examine the effect on nickel/vanadium exchange behaviour.

3.1. Experimental

3.1.1. Syntheses

3.1.1.1. Zeolite A

Zeolite A was synthesized following the method described by Thompson and Huber (1982) [10]. The batch composition for the synthesis is given by:

$3.165Na_2O:Al_2O_3:1.926SiO_2:128H_2O$
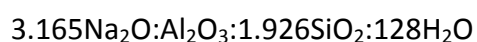
80 mL distilled water was added to 0.72 g sodium hydroxide and mixed until dissolved. The solution was then divided into two equal volumes; one half of the solution was added to 8.26 g sodium aluminate and mixed gently while the second half was added to 15.48 g sodium silicate solution and also mixed gently until solution became clear. The two solutions were then mixed together quickly until homogenized. The combined solutions were then transferred into a 200 mL Parr digestion bomb and crystallised at 100 ^{o}C for 3 h. The product was then filtered under vacuum using a Buchner funnel and a Whatman filter paper. The product was further washed trice with 50 mL distilled water for each wash. The product (87% yield) was dried at 80 ^{o}C overnight in an oven.
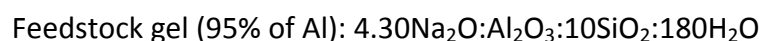
3.1.1.2. Synthesis of Zeolite X

Zeolite X was synthesised following the method described by Lechert and Kacirek [11, 12]. The batch composition for the synthesis is given by:

$NaAlO_2:4SiO_2:16NaOH:325H_2O$
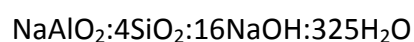
100 g of water was added to 100 g of NaOH and stirred until dissolved. The solution was then added to 97.5 g of aluminium hydroxide and stirred until dissolved and 202.5 g of water added to it. 100 g portion of the above solution was measured into beaker containing 612 g water and 59.12 g NaOH and mixed until dissolved. 219.7 g sodium silicate solution, 612 g water and 59.12 g NaOH were separately prepared by mixing the weighed samples until dissolved. The two solutions were quickly added and stirred for 30 min. The gel from the batch preparation was transferred into a Parr digestion bombs and crystallised at 90 ^{o}C for 8 h, 12 h and 24 h respectively. The precipitate was filtered and washed to pH less than 10 after crystallization. The product obtained was dried at 100 ^{o}C overnight and characterized.

3.1.1.3. Synthesis of Zeolite Y

Zeolite Y was synthesised following the method described by Ginter, Bell and Radke [13]. The batch compositions for the synthesis are given by:

Seed gel (5% of Al): $10.67 Na_2O:Al_2O_3:10SiO_2:180H_2O$

Feedstock gel (95% of Al): $4.30Na_2O:Al_2O_3:10SiO_2:180H_2O$

Overall gel: 4.62 $Na_2O:Al_2O_3:10SiO_2:180H_2O$

Preparation of seed gel: 19.95 g of water, 4.07 g NaOH and 2.09 g of sodium aluminate were added, stirred in 50 mL conical flask until dissolved. The solution was added to 22.72 g sodium silicate solution, stirred for 10 min and allowed to age at room temperature for a day.

Preparation of Feedstock gel: 130.97 g water, 0.14 g NaOH and 13.09 g sodium aluminate solution were added and stirred in a 500 mL beaker until dissolved. The solution was then added to 142.43 g sodium silicate solution and stirred vigorously until the gel appeared smooth.

Overall: The seed gel prepared was slowly added to the feedstock under vigorous stirring for 20 min.

Crystallization: The mixture was then transferred into a 200 mL capacity Parr digestion bomb and crystallised at 100 ^{o}C for 7 h. The wet solid product was filtered under vacuum, washed with deionised water until the pH of filtrate was below 9 and dried at 100 ^{o}C overnight. The product was then characterised.

3.1.1.4. Synthesis of Sodalites

Sodalite was synthesised using the Hund Method [14]. 0.73 g of aluminium powder was dissolved in aqueous NaOH solution (12 M, 80 mL prepared by dissolving 480 g of NaOH in 1000 mL water); 30 g of sodium chloride was then added to the solution. This mixture was heated to 120 ^{o}C in a round bottom flask and a solution of sodium silicate in aqueous sodium hydroxide (12 M, 15 mL) added drop wise over 30 min. The reaction mixture was then refluxed at 120 ^{o}C for 24 h and the resultant white powder product filtered off, washed with distilled water (200 mL), dried at 130 ^{o}C and characterised.

3.1.1.5. Synthesis of hydrosodalite

Hydrosodalite was synthesised as reported in literature [15]. The precursor of hydrosodalite, hydroxysodalite, was synthesised by digesting kaolin with 16 M NaOH in a Parr digestion bomb at 220 ^{o}C for 24 h. The hydroxysodalite was refluxed in water

for 48 h at 110 $^{\circ}$C to produce hydrosodalite. The product was filtered, washed and dried at 80 $^{\circ}$C overnight and characterised.

3.1.1.6. Synthesis of K- and Li-zeolites

Potassium zeolite A (KZA) and lithium zeolite A (LiZA) were prepared by exchanging 1 g of zeolite A with 50 mL portions of 0.1 M solutions of the appropriate metal nitrate (KNO$_3$, LiNO$_3$) in a 250 mL flask fitted with a stirrer, condenser and thermocoupled well. The suspension was then immersed in a thermostatically controlled oil bath and refluxed at 110 $^{\circ}$C under agitation for 24 h. After equilibration for 24 h, the product was filtered, washed briefly with deionised water, dried and kept under saturated NaCl solution in the desiccator to equilibrate. Both the solid product and supernatant liquid were analysed for the different alkali metal ions using atomic absorption spectroscopy. A similar procedure was carried out for zeolite X, zeolite Y and sodalite using the same solutions and timings but substituting the different zeolites.

3.1.2. Characterization of the synthesized zeolites

The synthesised zeolites were characterised using; power X-ray diffraction (PXRD), Fourier transformed infrared spectroscopy (FTIR), Raman spectroscopy, Thermogravimetric analysis (TGA) and gravimetric determination of chlorides in sodalites.

3.1.2.1. Powder X-ray diffraction (PXRD)

PXRD was used to characterise the phases present in the zeolites. The technique was used to provide information such as; the types and nature of crystalline phases present, structural make-up of phases, degree of crystallinity and size of crystallites.The intenisty of the peaks, the 2θ positions of the peaks as well as the width of the peaks, give some information on the degree of crystallinity, crystalline phases present and crystallites size respectively. The data were used for the identification of the unknown samples by comparing with the standard references from the ICDD database.

The PXRD data compared against the standard references from the ICDD database for the theoretical phases showed the targeted zeolite framework structures were

formed, thus presenting the as-synthesised zeolites as the targeted zeolites. The PXRD patterns for the zeolites suggest that all of the materials crystallise as a single crystalline phase with high degree of crystallinity as shown by the excellent match between the ICDD database and the patterns observed (figures 3.2-3.6). However, the exact aluminium to silicon ratio, and hence the counter-cation content is more challenging to determine since the cell parameters of the zeolites vary to a very small degree over the compositional range of Al:Si; although it should be noted that due to Lowenstein's rule the maximum Al:Si ratio under these conditions is 1:1. An example, is that both zeolite X and zeolite Y crystallise with the same faujasite (FAU) framework structure; but have different Al:Si ratios. The patterns reported as matching the figures are based on best fit with the ICDD database, the original target material described by the literature, supported by elemental analysis.

Zeolite A, X, sodalities and hydrosodalites were successfully synthesised at once, however, Zeolite Y was only successfully synthesised after several attempts. Zeolite X syntheses was optimised with varying crystallization times (8 h, 24 h and 48 h). There were no significant differences observed at the different times. However, the crystallization time of 8 h seemed to be the optimum time for zeolite X giving a high crystallinity in a relatively shorter crystallization time as indicated by the better to signal to noise for the data compared to the 24 h and 48 h time of crystallization (figure 3.3, insertion).
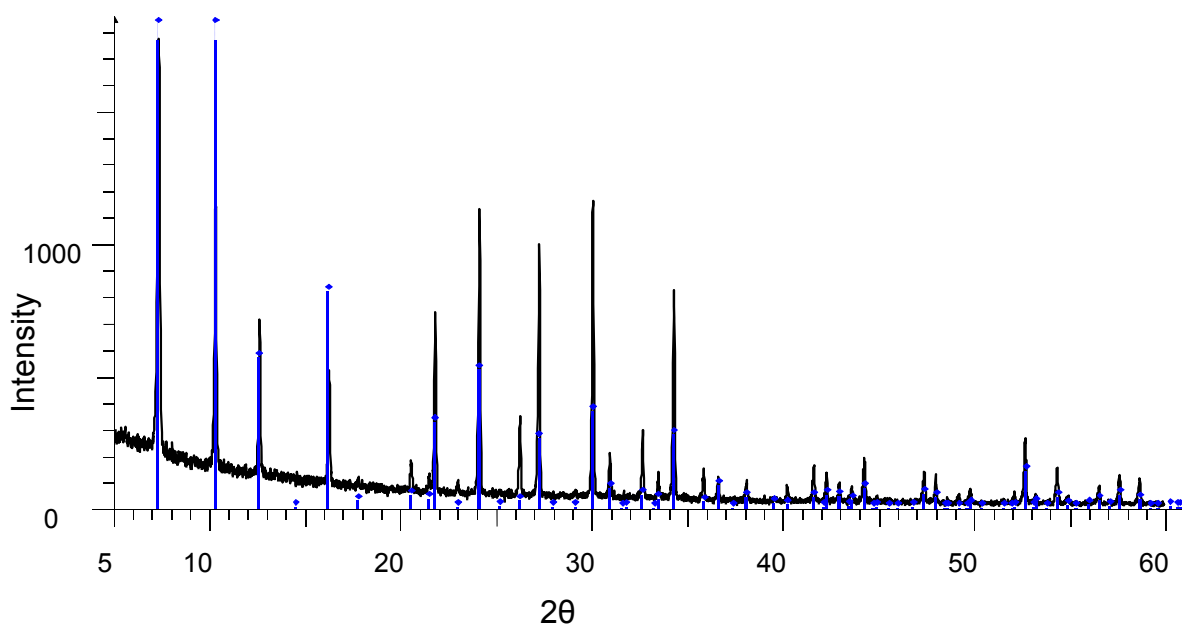
Figure 3.2: PXRD pattern for zeolite A (experimental pattern) matched with the reference pattern 01-089-3859 (vertical tick marks), anhydrous formula $(Na_{12}Al_{12}Si_{12}O_{48})NaAlO_2$ [10].
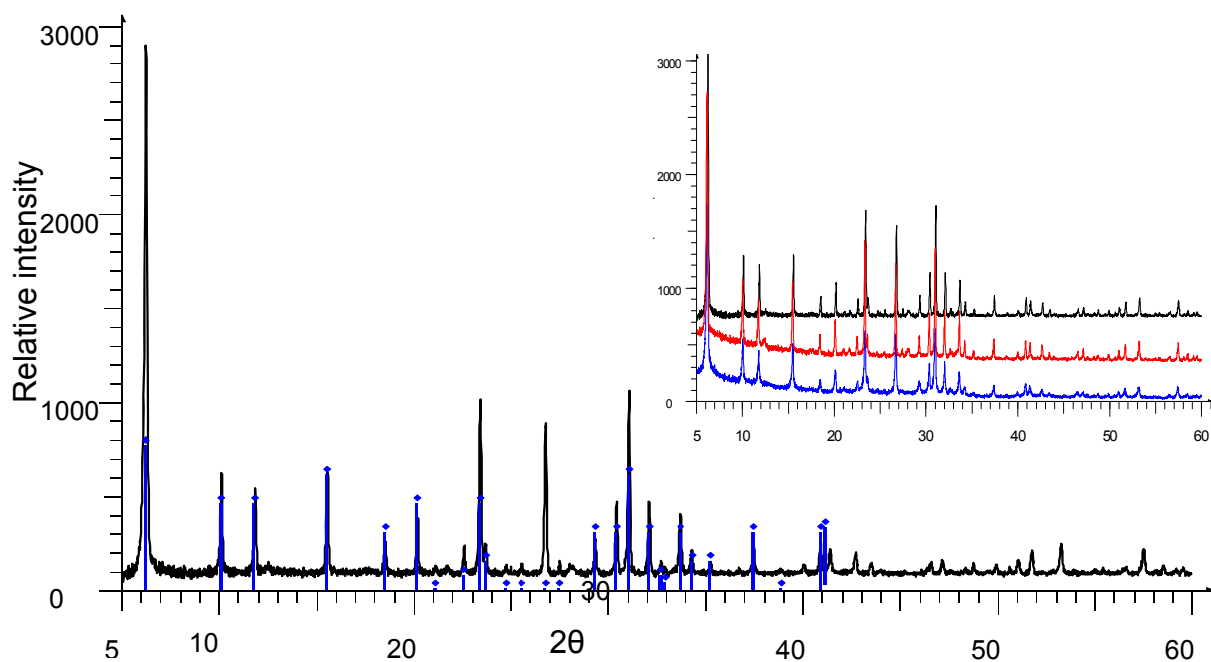

Figure 3.3: PXRD pattern for zeolite X (experimental pattern) matched with the reference pattern 01-070-2168 (vertical tick marks) at different crystallization times 8 h (upper), 12h (middle) & 24h (lower) , anhydrous formula $(Na_{88}Al_{88}Si_{104}O_{384})$ [11, 12].
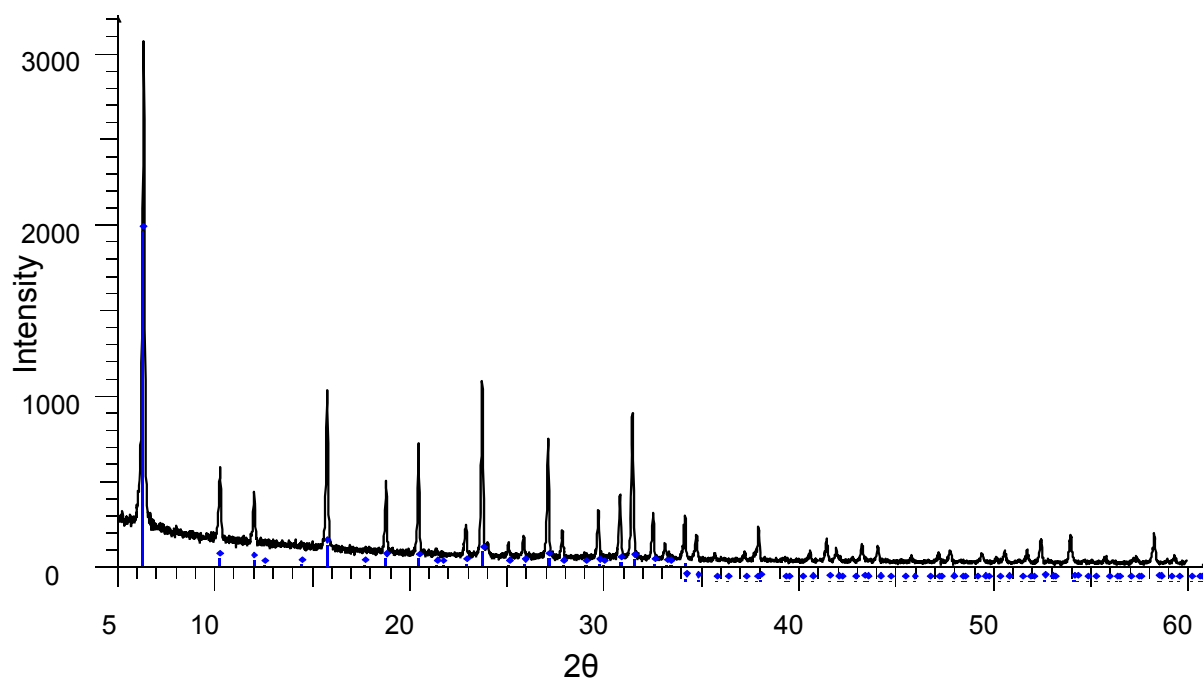
Figure 3.4: PXRD pattern for zeolite Y (experimental pattern) matched with the reference pattern 01-070-4285 (vertical tick marks), anhydrous formula $(Na_{54.91}Al_{56}Si_{136}O_{384})$[13].
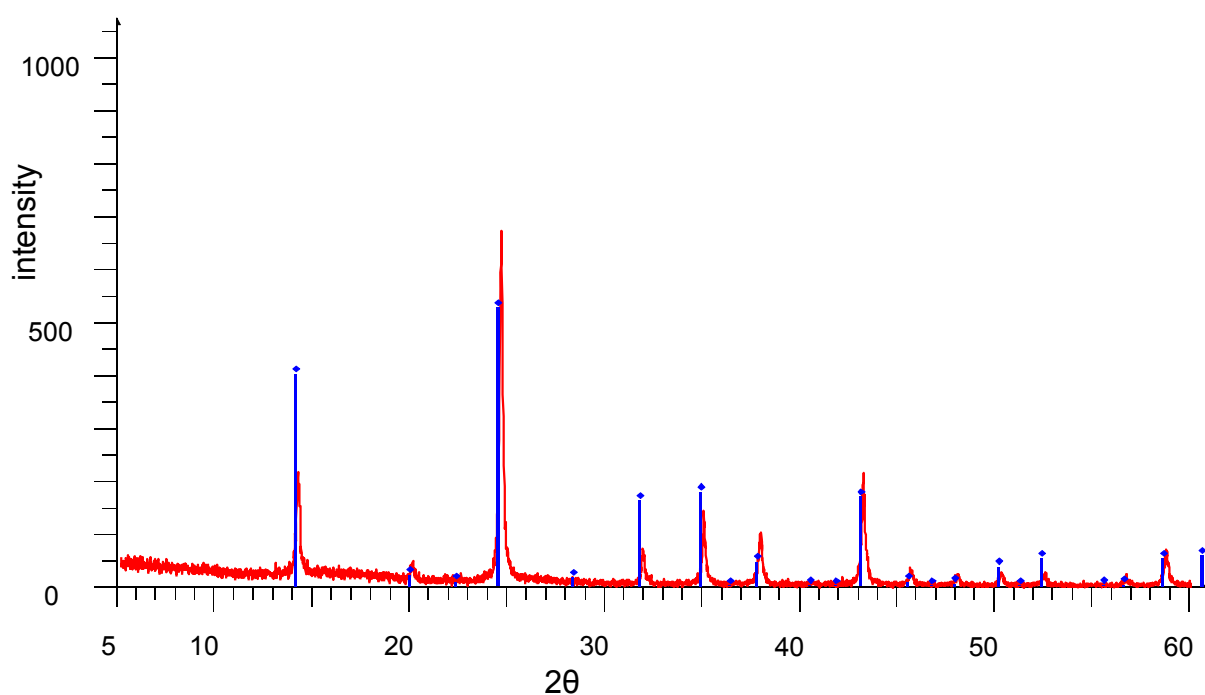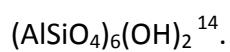

Figure 3.5: PXRD pattern for sodalite (experimental pattern) matched with the reference pattern 01-076-1639 (vertical tick marks), anhydrous formula Na_8
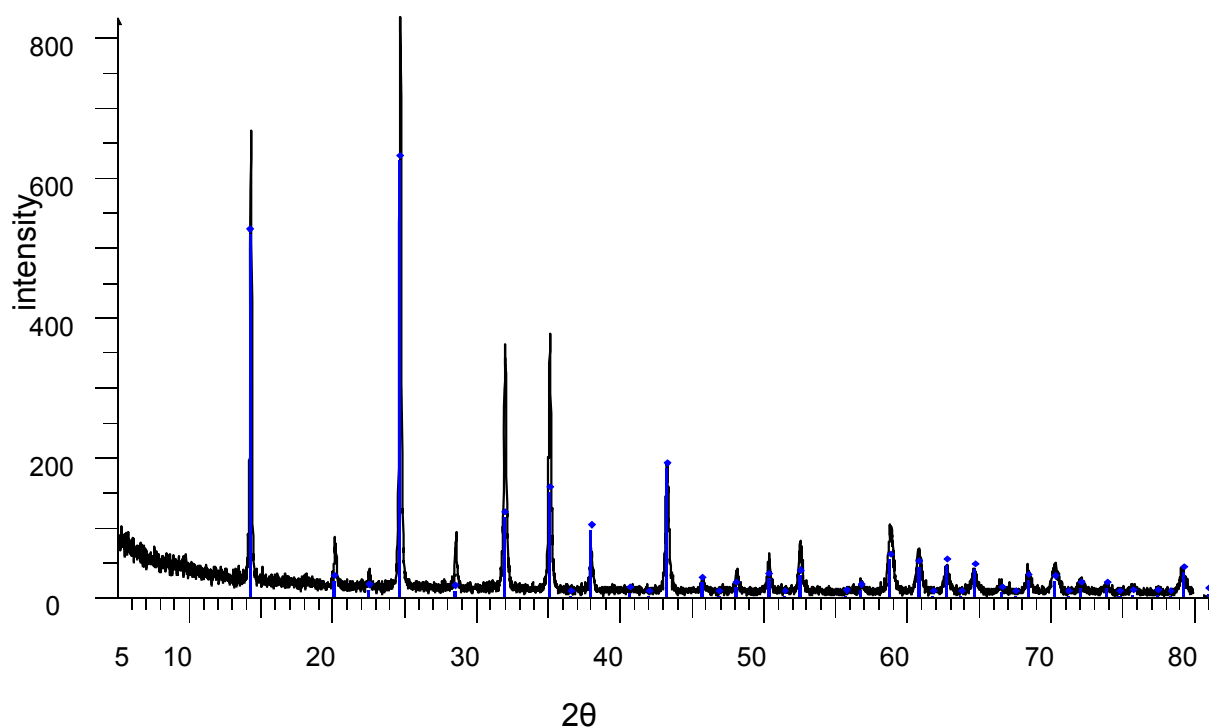
$(AlSiO_4)_6(OH)_2$[14].

Figure 3.6: PXRD pattern for hydrosodalite (experimental pattern) matched with the reference 00-040-0702 (vertical tick marks), anhydrous formula $Na_6 [AlSiO_4]_6$[15].

The PXRD of zeolite A have shown occlusion of some $NaAlO_2$ as indicated by the formula of the matched pattern, resulting to a Si/Al ratio slightly lower than 1. This has been earlier postulated as reported by Barrer[3]. However, for subsequent ion exchange reactions, the anhydrous formula $Na_{12}Al_{12}Si_{12}O_{48}$ as obtained from the literature followed would be used.

The PXRD of sodalite prepared matched a reference pattern with anhydrous formula $Na_8 (AlSiO_4)_6(OH)_2$. This is because sodalites can crystallize as Cl^-, OH^- or mixture of both on the anion site in the cage. In order to ascertain the amount of chloride in the sodalite, gravimetric determination of chloride was carried out. This method of chloride determination involves precipitation of chloride from the sodalite sample using silver nitrate, isolation of the silver chloride precipitate by filtration, determining its mass and using the stoichiometry to calculate the percent chloride in the sodalite.

0.6g of the sodalite material was dissolved in concentrated nitric acid and made up with distilled water. The nitric acid breaks down the sodalite framework structure thus exposing the chloride which then reacts with the $AgNO_3$ according to equation 3.6.

$$Ag^+ (aq) + Cl^- (aq) \longrightarrow AgCl (s) \hspace{4cm} \text{Equation 3.2}$$

The experimental mass of AgCl generated, gave a calculated Cl % = 9.8% as compared to the expected Cl % = 7.3% for a sodalite sample with the formula $Na_8 [AlSiO_4]_6Cl_2$. The excess of chloride ions might be due to insufficient washing of the sodalite sample after synthesis which could result in residual chloride ions being present in the product or it could be due to the poor solubility of the silicate/aluminate species in the solution resulting in precipitate being measured as chloride.

3.1.2.2. Fourier Transform Infrared Spectroscopy (FTIR)

Infrared spectroscopy was used to investigate the key functional groups in zeolites samples. This gives information on two classes of vibrations; internal stretching of the framework tetrahedra and those due to external linkages between tetrahedra.

FTIR results for the synthesised zeolites further confirmed, in agreement with the PXRD, that the syntheses formed the target zeolites. The infrared spectra for the main zeolites of study are as presented in fig. 3.7. The band assignments for all the zeolites compared with literature data [16-17] is summarised in Table 3.1.
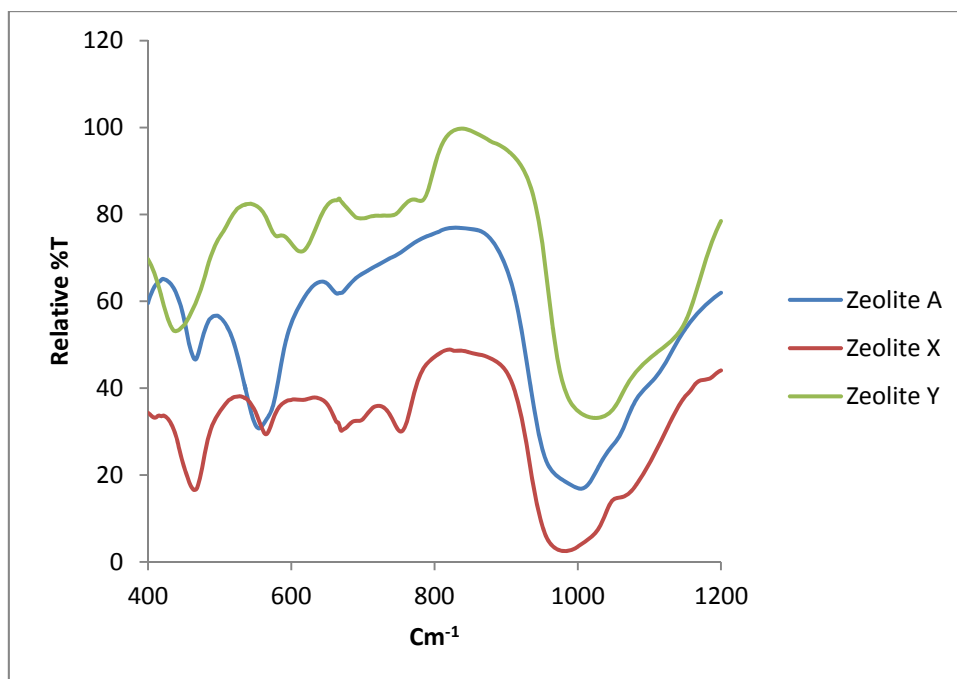
Figure 3.7: FTIR spectra of the targeted zeolites A, X and Y

A broad band was observed in the region 950-1050 cm^{-1} for all the zeolites which can be attributed to the asymmetric vibrations of Si-O bridging and Si-O non bridging bonds. The band in the range 650-750 cm^{-1} is due to the symmetric stretching of internal vibrations while that around 670-720 cm^{-1} is assigned to the symmetric stretching of external T-O linkages in the zeolites. Vibrations of the double six rings (D6R) connecting the sodalite cages occurred between 550-650 cm^{-1} while the internal vibrations due to the bending of the T-O tetrahedra occurred between 450- 480 cm^{-1} for all the zeolites [18].

Table 3.1: Infrared bonds for the synthesised zeolites compared with documented standards [16-18].

	Reference Band assignment (cm^{-1})	Band assignment for synthesised zeolites (cm^{-1})				
Intra-tetrahedra linkages (Internal Vibrations)						
		Zeolite A	Zeolite X	Zeolite Y	Sodalite	Hydro-sodalite
Asymmetric stretch	1250-950	1004	979	1019	979	980
Symmetric stretch	720-650	664	750	717	736	734
T – O bending	500-420	466	463	459	467	461
Inter-tetrahedra linkages (External T – O linkages)						
Double ring	650-500	555	563	579	668	
Pore opening	420-300	379	408, 368	384	436	282
Symmetric stretch	750-820	-	671	666	711	
Asymmetric stretch	1150-1050	-	-	1150	-	

3.1.2.3. Raman spectroscopy

As previously described in Chapter 2, Raman spectroscopy provides information which complements the spectroscopic information derived from Infrared data, since the two techniques have different selection rules. Raman spectroscopy is particularly useful in the investigation of occluded species within the zeolite framework as most of the framework vibrations are not Raman active. In addition, Raman allows the lower frequency framework modes to be examined. In this section, data were collected to confirm the identification of the zeolite frameworks in complementary to the Infrared data.

Zeolite A (figure 3.8) and sodalite (figure 3.9) displayed features in the 950-1200 cm^{-1} range which can be attributed to the zeolite -Si-O-Al- chain asymmetric stretching modes. These data were in good agreement with the literature for the target material [19, 20]. A strong band at 490 cm^{-1} and four other weak bands at 280 cm^{-1}, 340 cm^{-1}, 410 cm^{-1} and 700 cm^{-1} were reported by Angell [19] while a similar strong band at 492 cm^{-1}

and weak bands at 281 cm^{-1}, 347 cm^{-1}, 405 cm^{-1} and 714 cm^{-1} were also reported by Roozeboom and Robson [20].

The corresponding band frequencies observed in this work were; a strong band at 492 cm^{-1} and weak bands at 287 cm^{-1}, 342 cm^{-1}, 408 cm^{-1} and 699 cm^{-1}. An additional band was also observed at 1044 cm^{-1}. There was no significant shift in bands positions compared with the literature data for zeolite A.
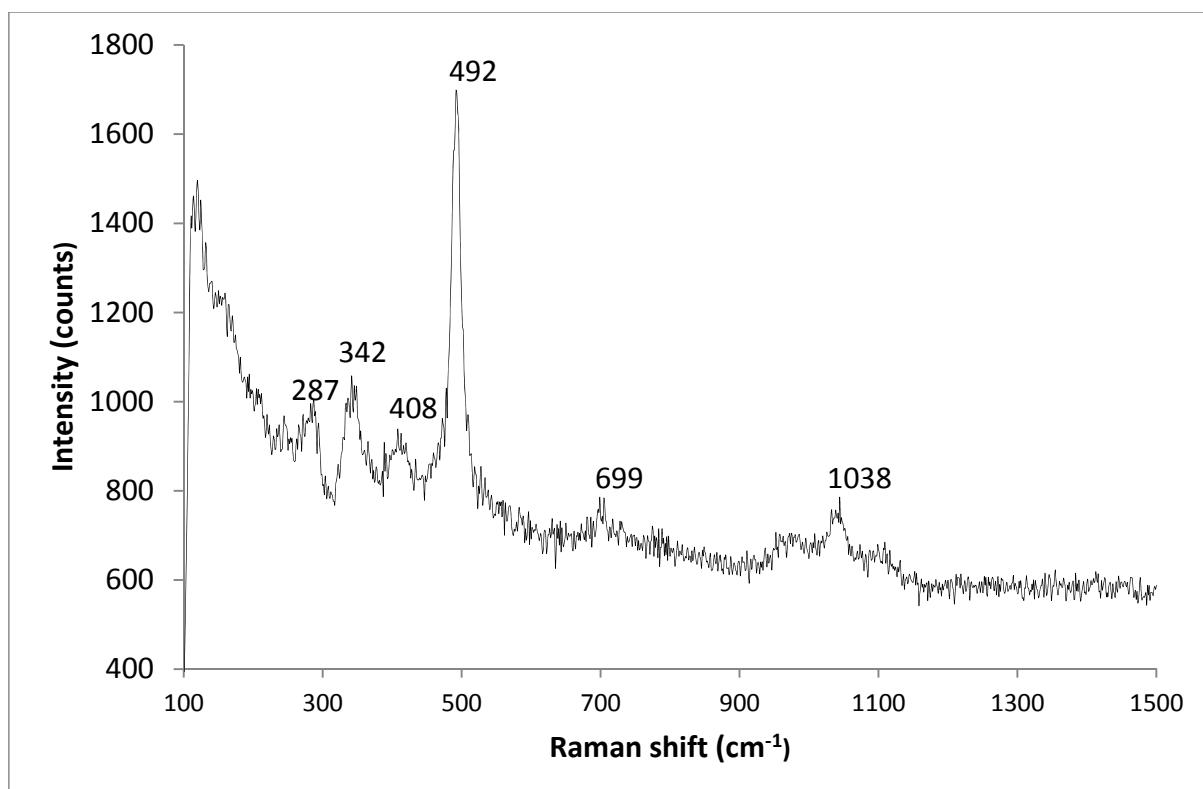

Figure 3.8: Raman spectrum of zeolite A, anhydrous formula ($Na_{12}Al_{12}Si_{12}O_{48}$) ($NaAlO_2$)
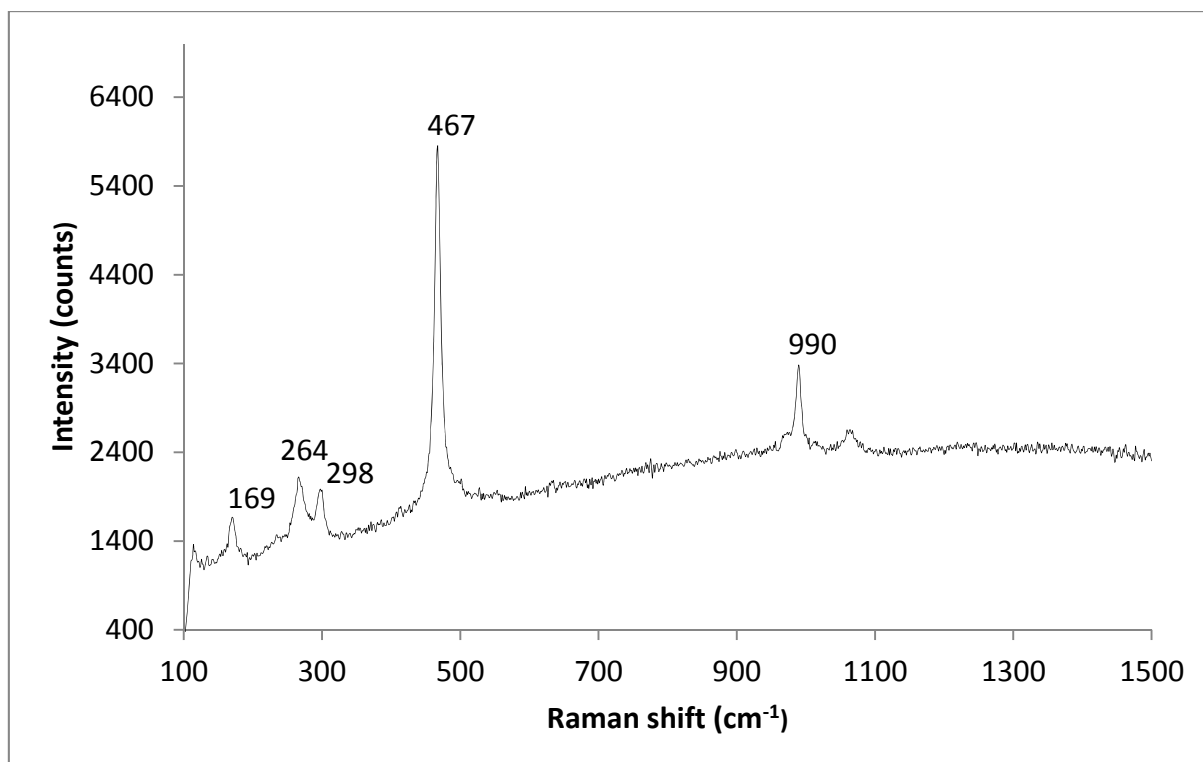
Figure 3.9: Raman spectrum of sodalite, $Na_8(AlSiO_4)_6Cl_2$

Zeolite X and Y both crystallise with the faujasite (FAU) structure where the key structural features are double six-membered rings (D6R) linked by single four-rings (S4R) of tetrahedra. These features can be identified by a broad band in the range of 470-510 cm^{-1} in the Raman spectra of these materials which has previously been assigned to the 6-fold and 4-fold ring stretches[21]. The expected Raman absorptions for zeolite X from the literature were observed at 505 cm^{-1}, 375 cm^{-1} and 282 cm^{-1} [19]; 512 cm^{-1}, 376 cm^{-1} and 291cm^{-1} [20] which are in good agreement with 517 cm^{-1}, 384 cm^{-1} and 293 cm^{-1} (figure 3.10) in this work. Corresponding data for zeolite Y has absorptions at 503 cm^{-1}, 350 cm^{-1} and 300 cm^{-1} [19]; 511 cm^{-1}, 369 cm^{-1} and 298 cm^{-1} [20]. The analogous data collected from the zeolite Y prepared in this work are; 504 cm^{-1}, 312 cm^{-1} and 362 cm^{-1} (figure 3.11).
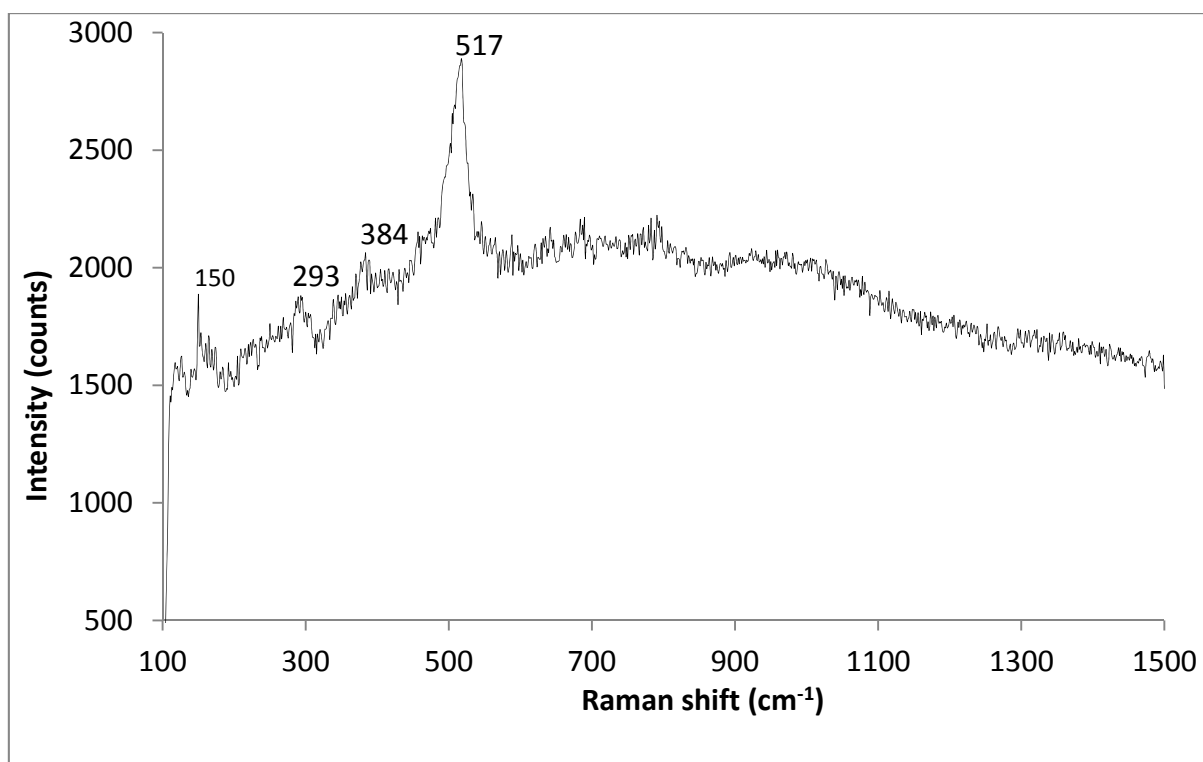
Figure 3.10: Raman spectrum of zeolite X, anhydrous formula ($Na_{88}Al_{88}Si_{104}O_{384}$)

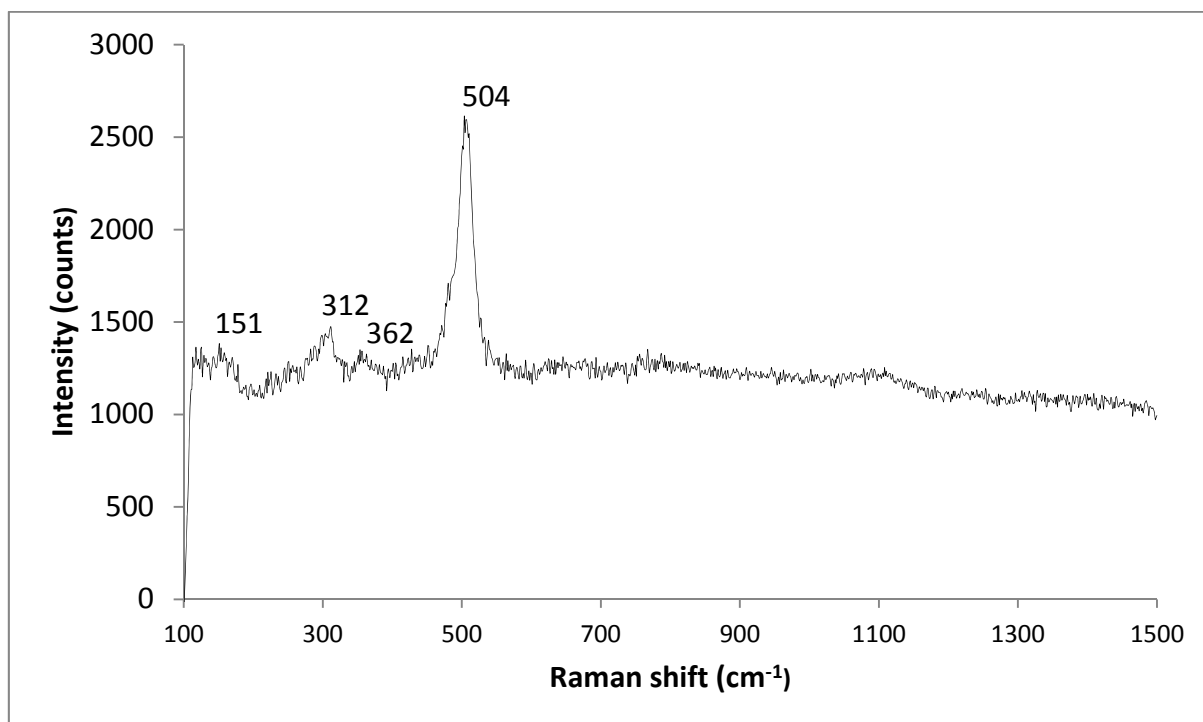
Figure 3.11: Raman spectrum of zeolite Y, anhydrous formula ($Na_{54.91}Al_{56}Si_{136}O_{384}$)

Raman spectra for the synthesised zeolites compared with documented standard samples [19-21] is summarised in Table 3.2 .

Table 3.2: Raman spectra for the synthesised zeolites compared with documented standard [19-21]

Bending vibration					
	Reference Band assignment (cm^{-1})	Band assignment for synthesised zeolites (cm^{-1})			
		Zeolite A	Zeolite X	Zeolite Y	Sodalite
Si-O-Al 4-membered ring	510-450	492	517	504	467
Si-O-Al 6-membered ring	450-300	342, 408	293, 384	312, 362	298
Si-O-Al 8-membered ring	280 - 300	287	-	-	264
External T – O linkages					
Symmetric stretch	700	699	-	-	
Asymmetric stretch	950-1250	974,1044	-	-	990

3.1.2.4. Thermogravimetric analysis (TGA)

The thermogravimetric analysis data for zeolite A, zeolite X and zeolite Y are summarised in Table 3.3. The percentage weight loss for the parent zeolites by thermogravimetric analysis reveals the loss of water in a single temperature range (20 – 400 ^{o}C) for all the zeolites considered (figure 3.12). The low intensity exothermic peaks at 850 - 1000 ^{o}C for zeolites A and X corresponds to the temperatures for structural collapse for the zeolites, zeolite Y however, maintained it's framework structure even upto about 1000 ^{o}C (figure 3.13-3.15).

Table 3.3: Thermal analysis for zeolite A, X & Y

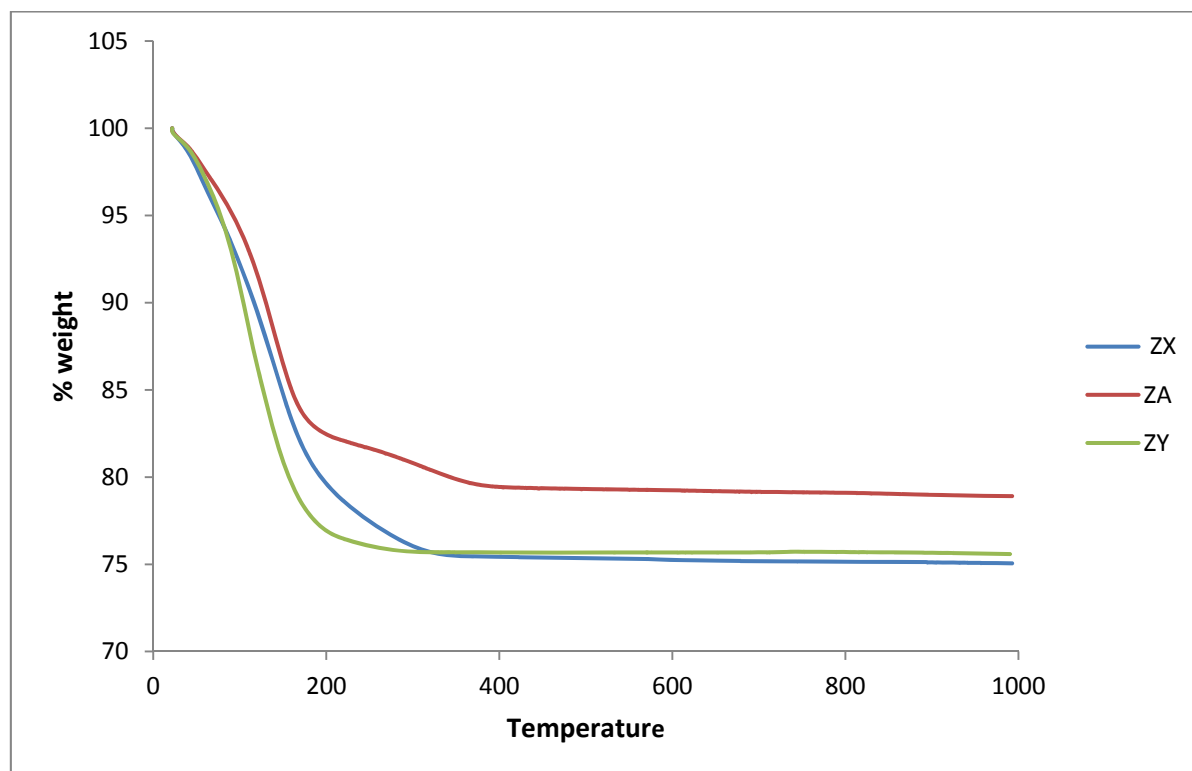| Sample	Water desorption		
	Weight loss (%)	Temperature range for weight loss (^{o}C)	structural collapse temperature (^{o}C)
Zeolite A ($Na_{12}Al_{12}Si_{12}O_{48}.24.2H_2O$)	21	20 - 400	850 - 900
Zeolite X ($Na_{88}Al_{88}Si_{104}O_{384}.238.8$)	25	20 - 400	850 - 950
Zeolite Y ($Na_{54.91}Al_{56}Si_{136}O_{384}.246.5$)	25	20 - 300	Upto 1000

Figure 3.12: Thermogravimetric analysis of the zeolites Y, X and A under the flow of nitrogen
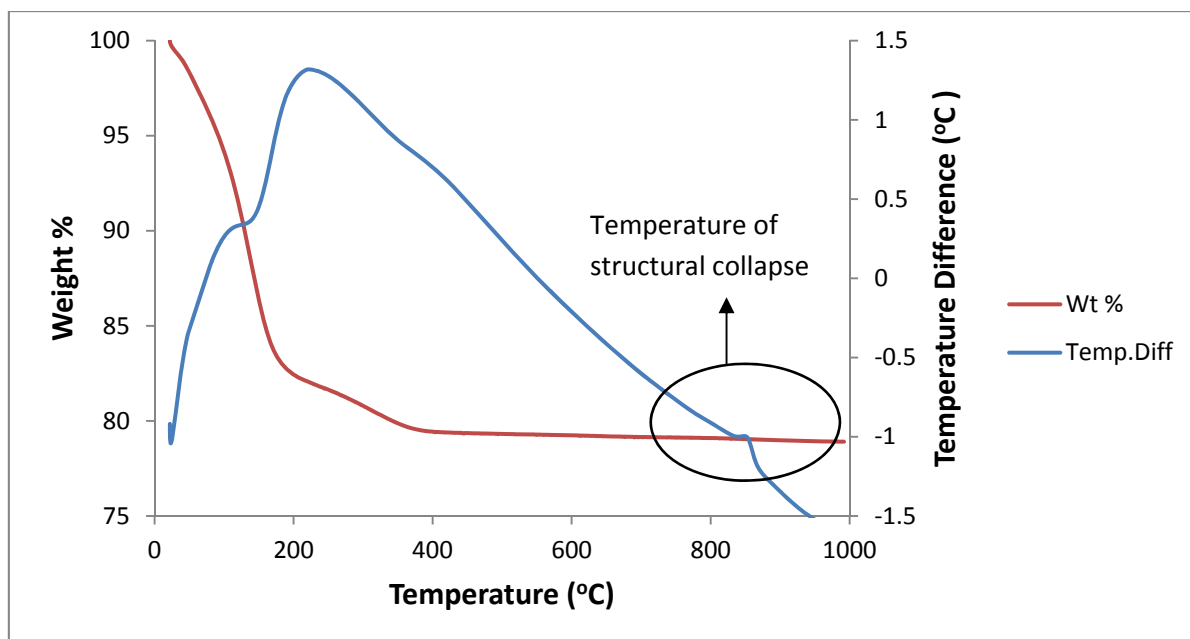
Figure 3.13: TGA and DTA showing the weight loss and thermal behaviour of zeolite A
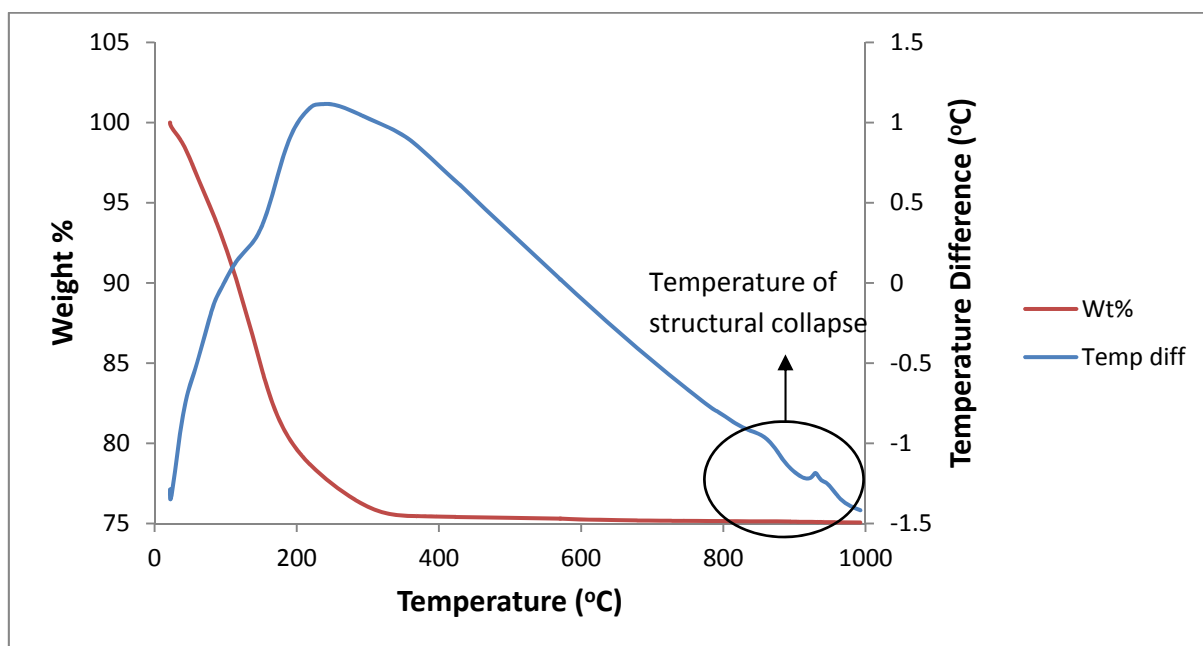
Figure 3.14: TGA and DTA showing the weight loss and thermal behaviour of zeolite X
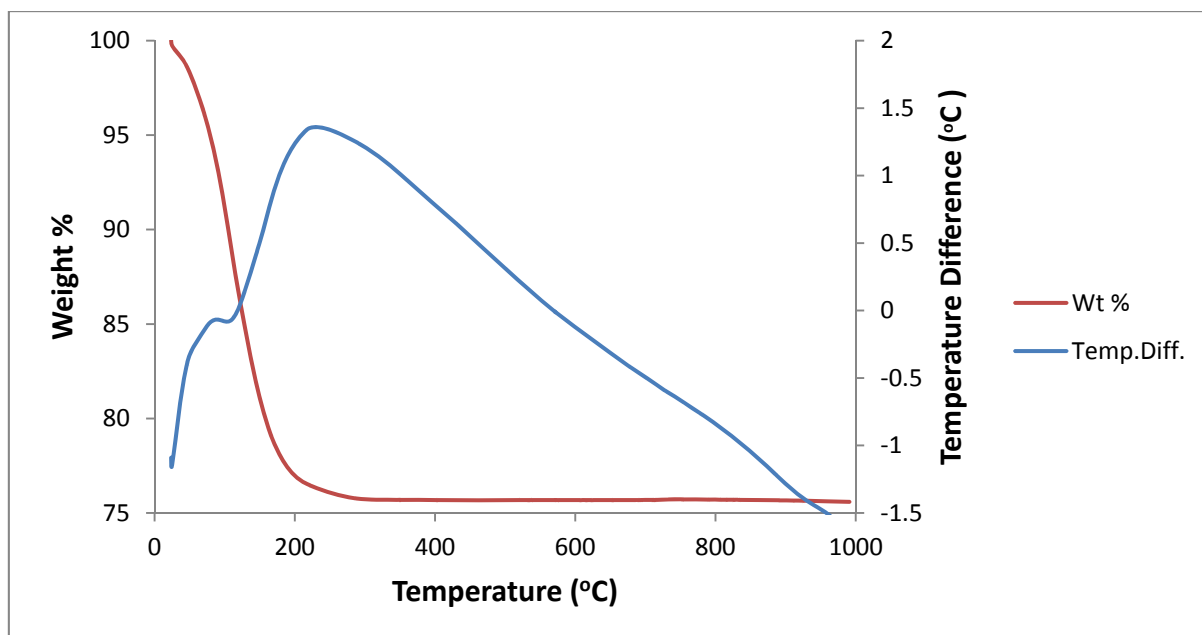
Figure 3.15: TGA and DTA thermograms showing the weight loss and thermal behaviour of zeolite Y

The weight loss at 20 - 400 ^{o}C for zeolite A is 21 % and the loss on ignition as determined by TGA is ~23 %. Zeolites are hydrophilic materials which readily absorb water leading to their widespread industrial and domestic application as sorbents. The weight loss on ignition is in good agreement with the theoretical water content of hydrated zeolite A (often referred to as zeolite 4A) which corresponds to the removal of the water molecules in the unit cell that comprise a theoretical water content of 22 % [22].

Similar thermogravimetric experiments for zeolite X and zeolite Y at 20 – 400 ^{o}C and 20 - 300 ^{o}C respectively generated calculated weight losses of ~ 25 % and 26 % in good agreement with the theoretical values.

The percentage weight loss as determined by the TGA for the parent hydrosodalite indicates that six molecules of water per unit cell were lost at temperature range of 150-300 ^{o}C as shown by the thermogram in figure 3.16.
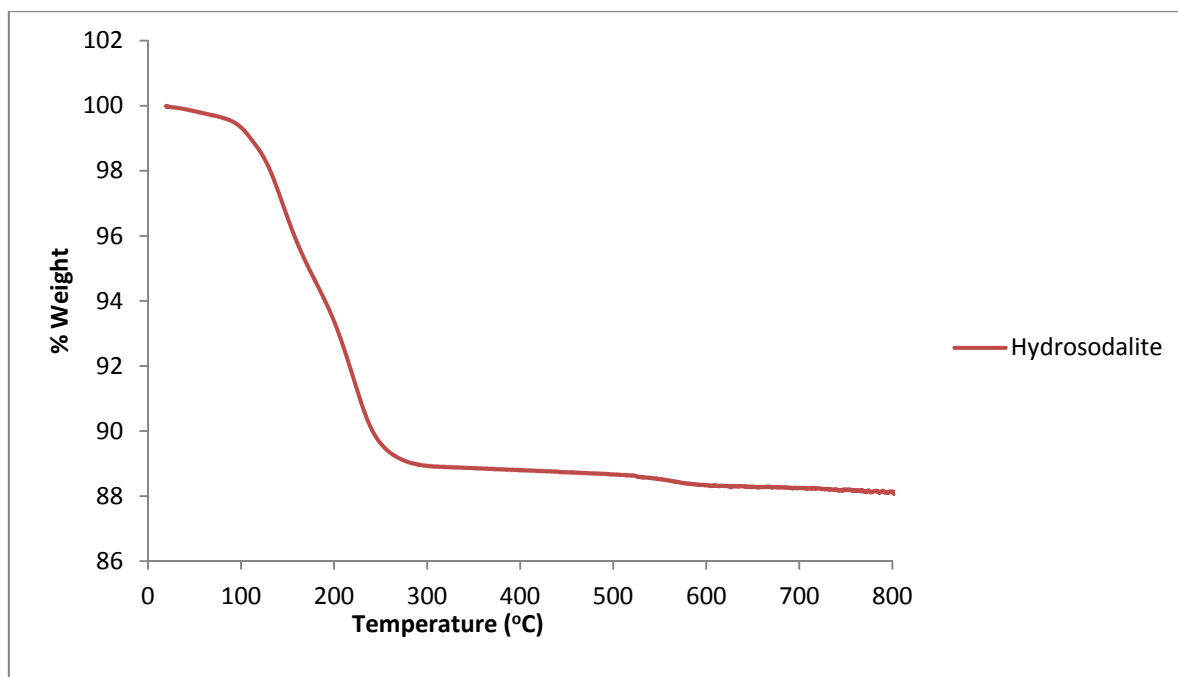
Figure 3.16: TGA showing the weight loss and thermal behaviour of hydrosodalite

3.1.2.5. SEM-EDS

SEM-EDS analysis of the parent zeolites was carried out to determine the elemental composition of the zeolites. From the elemental composition, the Si/Al ratios of the zeolites can be calculated. Table 3.4 shows the elemental composition as determined by the SEM-EDS and the Si/Al ratios of the zeolites.

Table 3.4:Elemental composition before and after nickel ion exchange

Elements	% weight		
	Zeolite A	Zeolite X	Zeolite Y
O	48.0±0.02	45.0±0.4	48.7±0.07
Na	15.7±0.04	15.4±0.9	9.2±0.04
Al	18.5±0.02	16.5±0.5	11.5±0.0
Si	17.8±0.01	22.0±0.8	30.7±0.1
Si/Al	0.96	1.3	2.7

The Si/Al ratios of zeolites A, X and Y as calculated from the elemental composition were; 0.96, 1.3 and 2.7 respectively, having good agreement with the matched patterns of ICDD database.

3.1.3. Results and characterization of Potassium and lithium zeolites

Results of the potassium and lithium exchanged zeolite A, zeolite X, zeolite Y and sodalites are as presented in appendix 1

The ion exchange of the zeolites with alkali metals (lithium and potassium) was successful for all the zeolites as presented in Table 3.4; it is observed that the zeolites had a higher affinity for potassium compared to lithium ions (Figure 3.17).
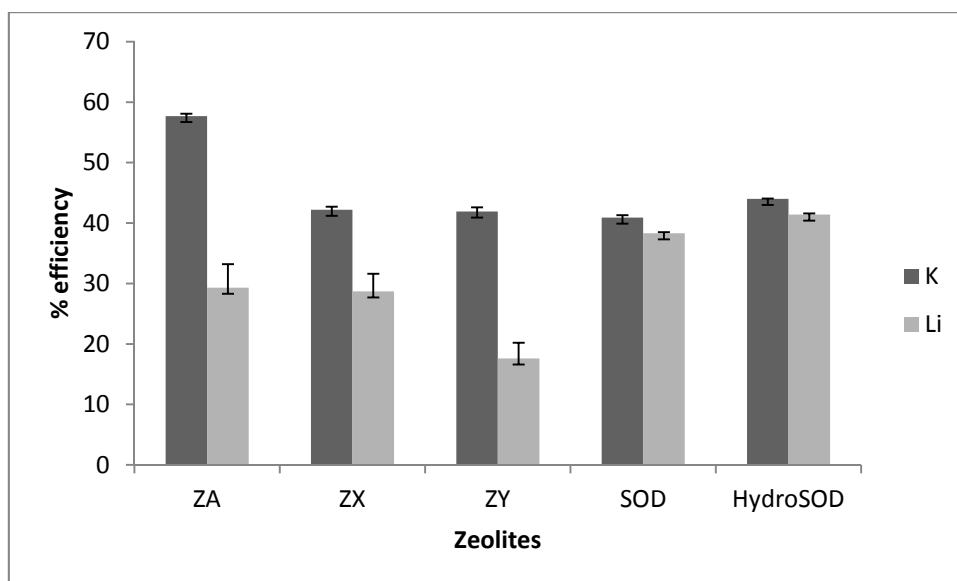
Figure 3.17: Efficiency of K^+ and Li^+ uptake by zeolites

This behaviour can be explained based on the Si/Al ratio as well as the differing pore/ring sizes of the zeolites. Zeolite Y with a higher Si/Al ratio (lower anion framework charge) is observed to prefer alkali metals in order of increasing size compared to zeolite A and zeolite X with high anion framework charge (lower Si/Al ratio). This observation is in line with the conclusions made by earlier studies [8]. The conclusions were; (1) zeolites with high anion framework charge (Si/Al = 1-1.5) prefer monovalent alkali metals in the order of decreasing size and (2) Zeolites with high anion framework charge (Si/Al = 3) prefer univalent alkali metals in the order of increasing size.

The behaviour can also be based on the decreasing hydrated ionic radius of the alkali metals down the group from Li^+ – K^+ (Table 3.5). In their hydrated states, K^+ would be preffered to Li^+.

Table 3.5: Ionic and Hydrated radius of alkali metal ions

Ions	Ionic Radius (Å)	Hydrated Radius (Å)
K^+	1.33	3.31
Na^+	0.95	3.58
Li^+	0.60	3.82

Potassium and lithium ion exchange with Na_8 $[AlSiO_4]_6Cl_2$ and Na_6 $[AlSiO_4]_6.6H_2O$ at higher concentration of the metal nitrate solution (2 M), gave a significantly higher exchange of the alkali metals compared to the exchange at lower concentration of metal ions. Previous work on alkali metal exchanged hydrosodalite showed that the exchange proceeds to almost completion [15]. This is expected as sodalites have a simple, less complicated framework structure and should have a good exchange capacity for the K^+ and Li^+ cations. Varying the experimental conditions like temperature could improve the exchange of the cations.

Generally, the selective affinity of the targeted zeolites for the family of alkali metals investigated is shown to follow the order: K^+ > Na^+ > Li^+, which is similar to earlier work carried out where the sequence was reported to be Cs^+ > Rb^+ > K^+ > Na^+ > Li^+ for zeolite Y, zeolite X and zeolite A [4].

3.1.3.1. PXRD of K- and Li-zeolites

The K- and Li-zeolites were characterised using PXRD and the patterns compared with those of the parent zeolites. The PXRD data for the zeolites shows alkali metal (K, Li) exchange had occurred.

In case of potassium-zeolites, the PXRD showed a shift in reflections to the left, which indicates an increase in the unit cell lattice parameter, possibly as a result of a change

in position between cations of different sizes assuming a constant water of hydration. Thus when K^+ takes the place of Na^+, the lattice parameters will increase. This shift was observed for all the zeolites exchanged with potassium (figure 3.18a-e) hence suggesting potassium ion exchange occurred for all the zeolites.

PXRD data for lithium-zeolites also showed a shift in the reflections, this shift however is to the right indicating that a smaller ion (Li) has taken the place of a bigger ion leading to a decrease in unit cell parameters of the zeolite framework. This shift is again seen to be consistent for all the zeolites (figure 3.19a-e) suggesting lithium ion exchange occurred for all the zeolites. An internal standard (silicon standard) was used each time to check the alignment of the reflection peaks.
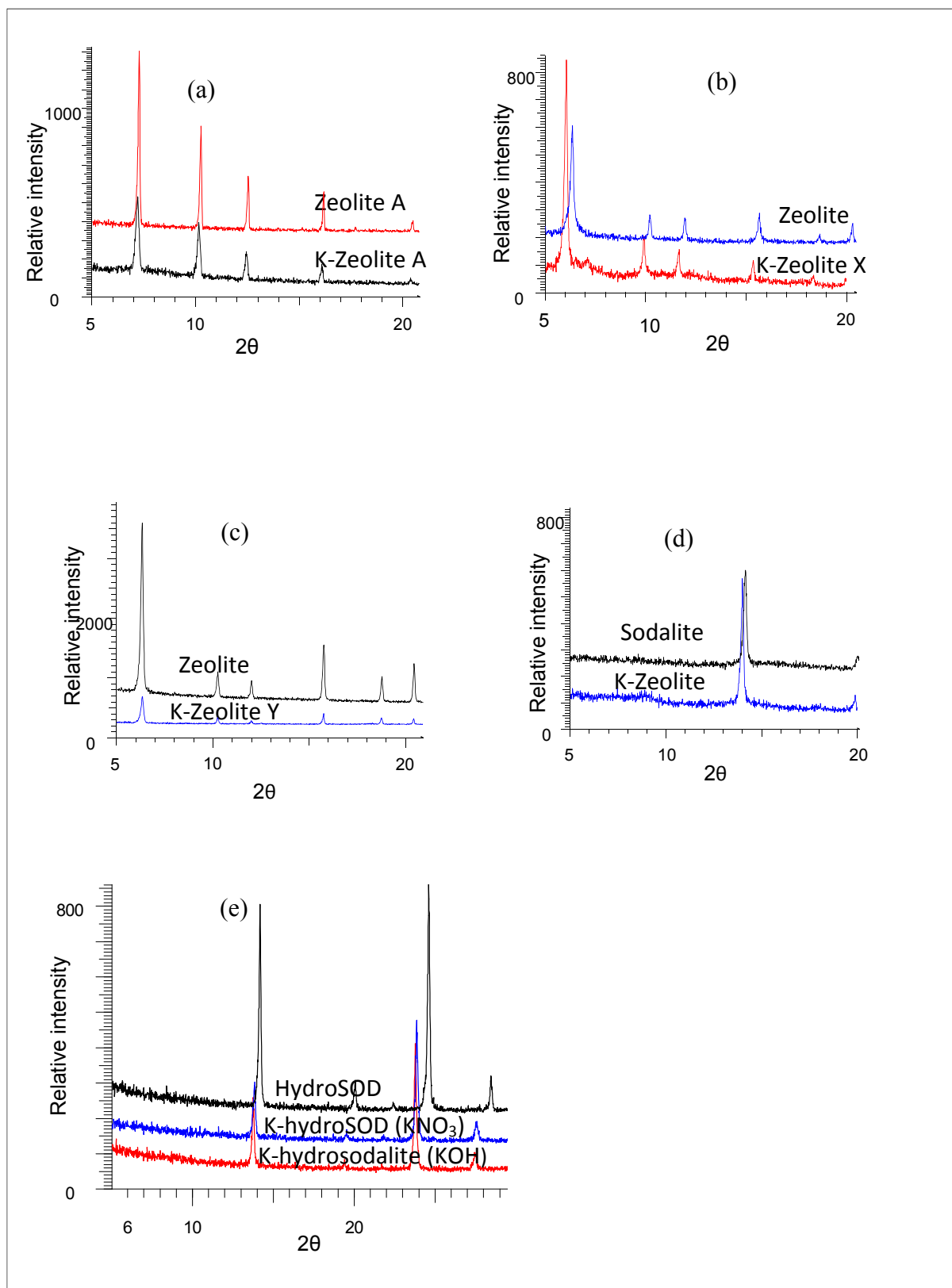
Figure 3.18: PXRD pattern for potassium zeolites (a) A (b) X (c) Y (d) sodalite (e) hydrosodalite compared with their parent zeolites respectively
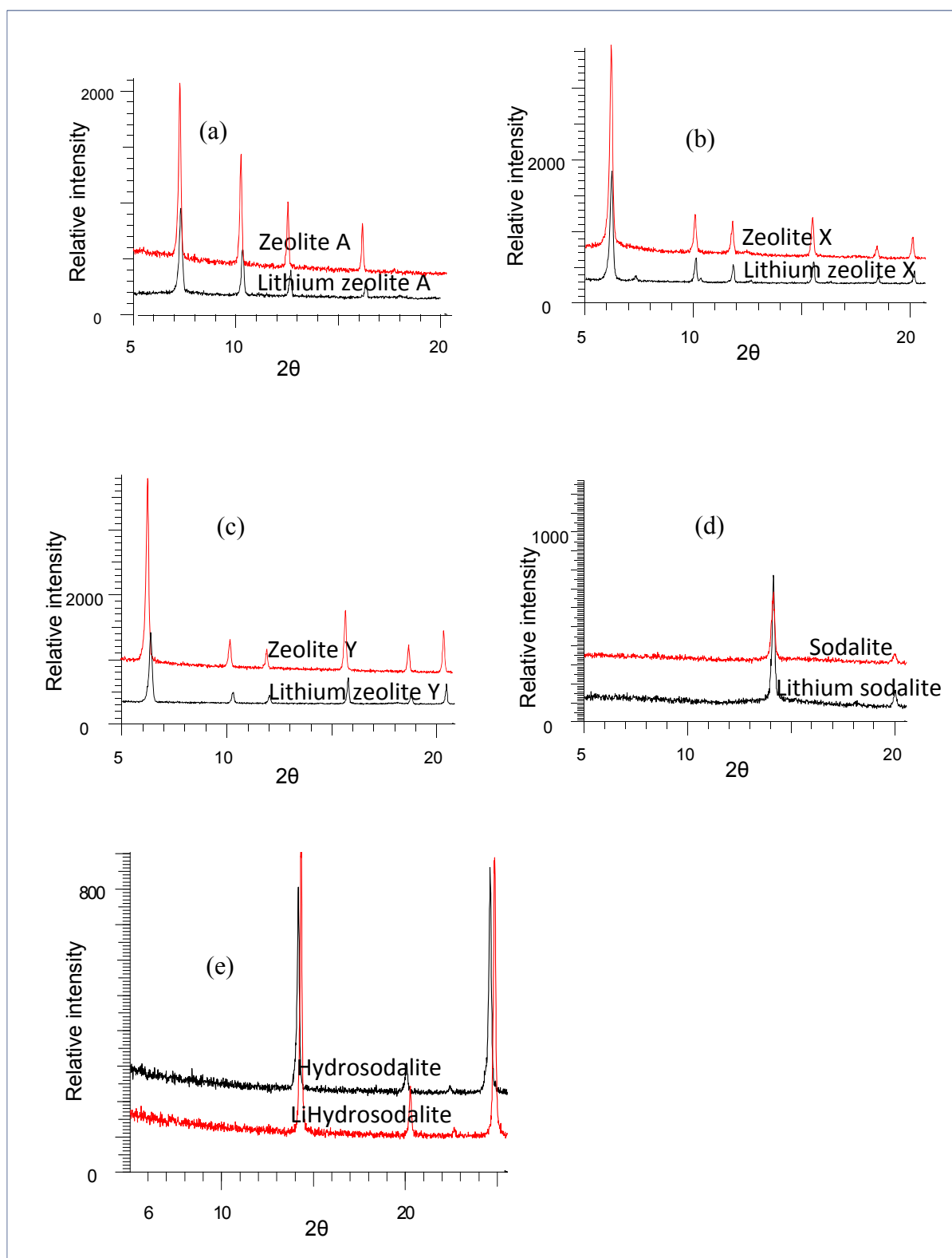
Figure 3.19: PXRD pattern for lithium zeolites (a) A (b) X (c) Y (d) sodalite (e) hydrosodalite compared with their parent zeolites respectively.

3.1.3.2. TGA for K- and Li-zeolites

The thermal analysis was carried out only on the target zeolites A, X and Y. From the weight loss profiles, the K- and Li- zeolites had water contents, as presented in Table 3.5.

Table 3.5: Thermal analysis of zeolites before and after alkali metal exchange

Sample	Water desorption							
	Weight loss before K and Li cations exchange		Weight loss after K-zeolite exchange		Weight loss after Li-zeolite exchange		Temp. range for 1st weight loss	Temp. range for 2nd weight loss
	(%)	(Moles)	(%)	(Moles)	(%)	(Moles)	(^{o}C)	(^{o}C)
Zeolite A	21	24.2	21	24.8	24	29.7	20-400	525-850
Zeolite X	25	238.8	23	211.3	27	263.2	20-350	525-600
Zeolite Y	25	246.5	23	215.8	28	284.6	20-300	500-600
HydroSOD		6.0		6.0		7.0	50-400	500-800

The thermal analysis (TGA) on the zeolite materials before and after alkali metal exchange showed that all the zeolites lost water in two distinct temperature ranges (Table 3.5). Two factors are presumed to affect the loss of water from the zeolite structures; polarisability and size of the metal cation. Lithium being a smaller, highly polarised cation is most stable when fully hydrated, hence may not be willing to give up its water of hydration easily. The total water loss for the lithium exchanged zeolites is found to be higher than that for the parent zeolites. This behaviour is expected due to the small size of lithium and consequent increase in the charge density on the ion. The thermal behaviour of the potassium-zeolites may also be explained based on the size of metal cation, it is possible that as the size of the metal cation that is

accommodated in the six-membered ring β-cage of zeolite structures increases from lithium to potassium, it blocks the path of the contained water molecules, leading to a water loss in two steps at higher temperature ranges. The total water loss is less in the case of potassium, because of its increased size and lower charge density.

The thermal behaviour of the alkali metal exchanged hydrosodalites is similar to that observed for zeolites A, X and Y; the water loss for lithium-hydrosodalite is higher (seven moles) than that for potassium-hydrosodalite (six moles). The alkali exchanged hydrosodalites; particularly the potassium hydrosodalite had their initial weight loss at a much lower temperature range (50-100 ^{o}C). This could be due to drying of the samples after the alkali metal ion exchange where a small amount of water was lost before the TGA analysis. The weight loss observed for the alkali metal hydrosodalites was largely dependent on the alkali metal exchanged. The TGA for the alkali metal hydrosodalites indicates that as the ionic radii increase, the cell parameters increase and the initial weight loss occurs at a lower temperature while the second weight loss occur at higher temperature. Thus for Lihydrosodalite with a smaller unit cell,the two weight loss regions 'pulled' together resulting in the weight loss at a single temperature range of 50-400 ^{o}C (figure 3.20). These results are in good agreement with earlier studies on hydrosodalite [15]. Unlike the Lihydrosodalite, the percentage weight loss for Khydrosodalite was not smooth even though there were no defined weight loss regions (figure 3.21).
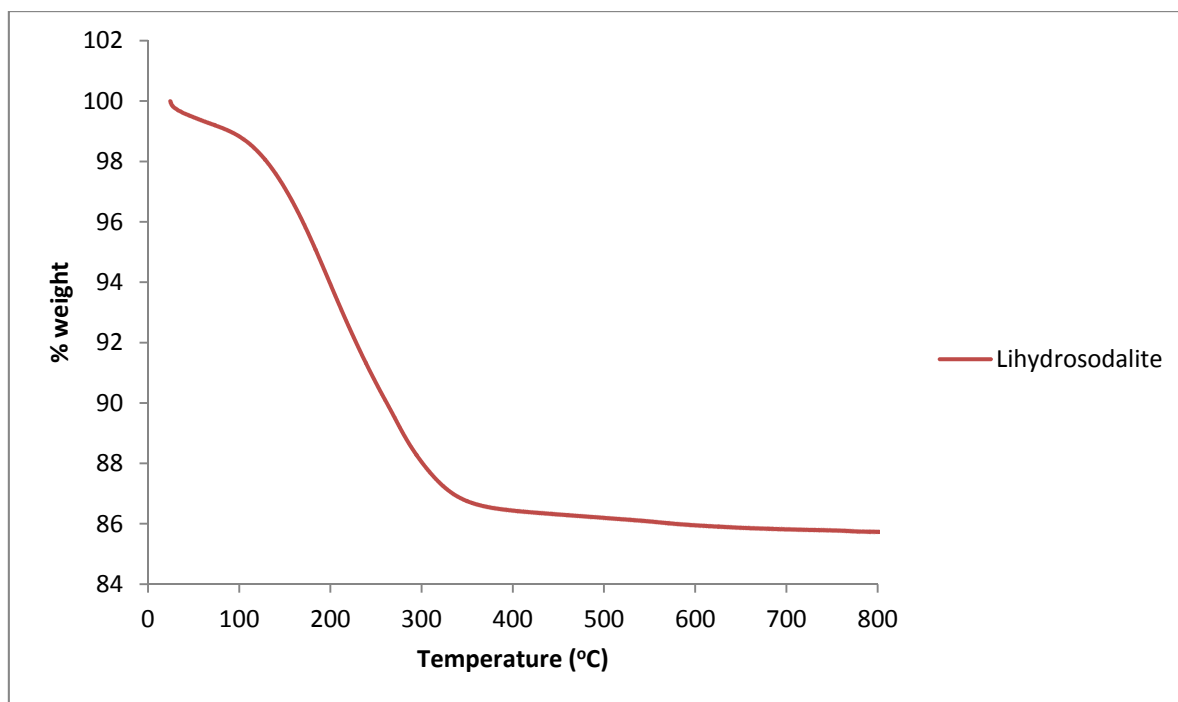
Figure 3.20: TGA showing the weight loss and thermal behaviour of Lihydrosodalite
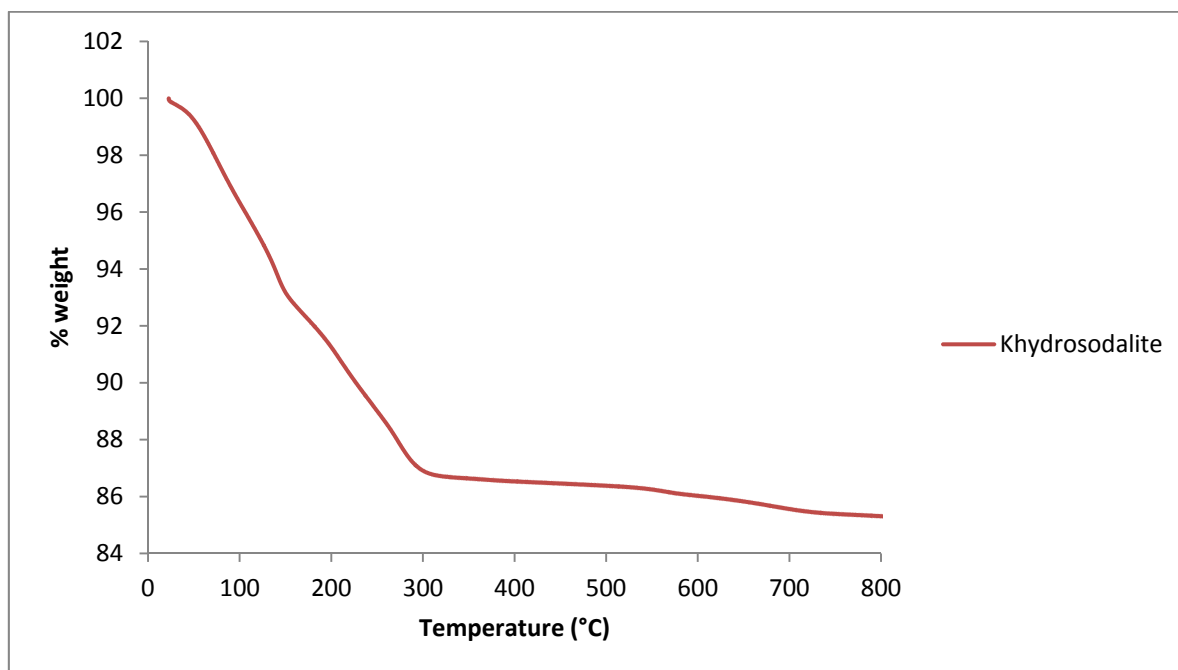
Figure 3.21: TGA showing the weight loss and thermal behaviour of Khydrosodalite
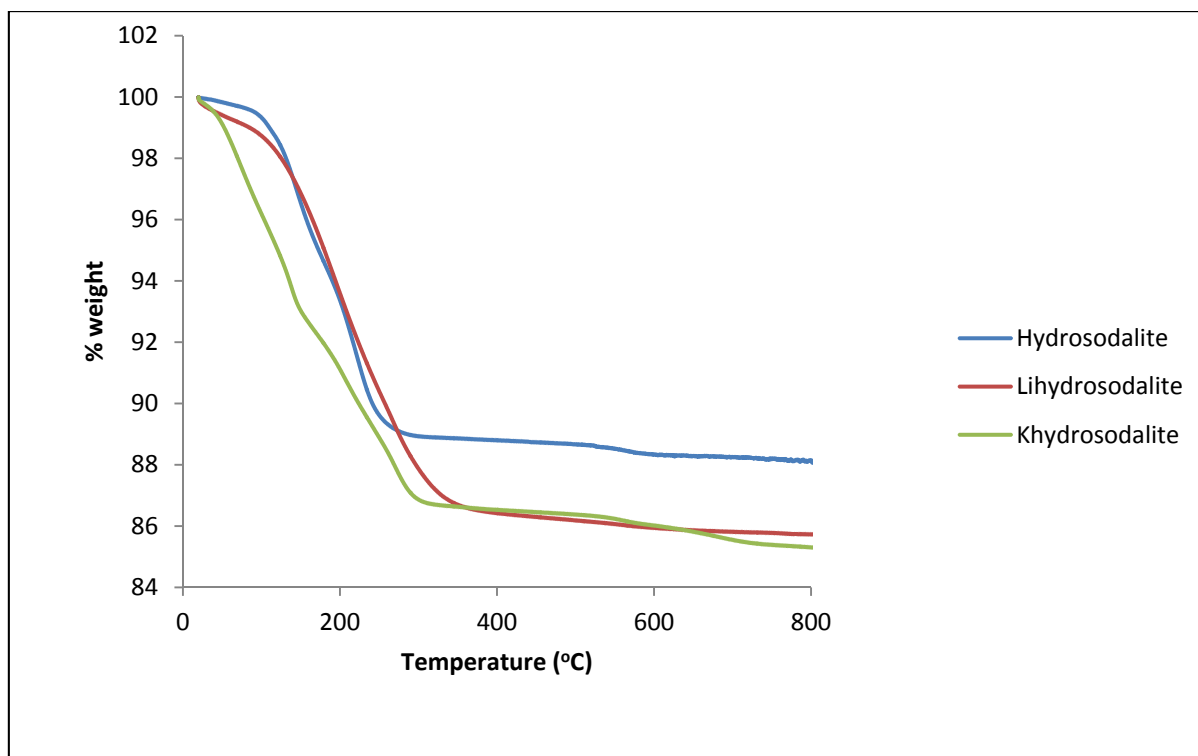
Figure 3.22: Combined TGA showing the weight loss and thermal behaviour of hydrosodalite, Li-hydrosodalite and K-hydrosodalite

3.4. Conclusion

Zeolites A, X, Y, sodalite (Na_8 [$AlSiO_4$]$_6Cl_2$) hydrosodalite (Na_6 [$AlSiO_4$]$_6$.$6H_2O$), potasium and lithium zeolites were synthesised and characterised. Characterization of the zeolite materials using multi-analytical techniques such as PXRD, FTIR, Raman and TGA showed that the zeolites were of a single phase and contained 24.2 moles, 238.8 moles and 246.5 moles water of crystallisation for zeolite A, zeolite X and zeolite Y respectively as determined by the TGA. The Si/Al ratios of 0.96. 1.3 and 2.7 for zeolites A, X and Y were calculated from the elemental composition determind from SEM-EDS analysis.

References

1. D.W. Breck, Zeolite Molecular Sieves, Structure Chemistry and Use, Wiley, New York, 1974.

2. M.I. Occelli and H. Kessler, Synthesis of Porous Materials: Zeolites, Clays and Nanostructures, CRC Press, New York, 1997.

3. R. M. Barrer, Hydrothermal Chemistry of Zeolites, Academic Press, New York, 1982.

4. M.A. Keane, Colloids Surf. A: Physicochem. Eng. Aspects, 1998, 138, 11-20.

5. M.A.S.D. Barros, P.A. Arroyo, E. Sousa-Aguiar, C.R.G. Tavares, Adsorption, 2004, 10, 227–235.

6. J.S. Kim, M.A. Keane, J. Chem. Technol. Biotechnol., 2002, 77, 633-640.

7. I.C. Ostroski, C.E. Borba, E.A. Silva, P.A. Arroyo, R. Guirardello, M.A.S.D. Barros, J. Chem. Eng. Data, 2011, 56, 375-382.

8. A. Dyer, An Introduction to Zeolite Molecular Sieves, John Wiley & Sons, Chichester, 1988.

9. R. Szostak, Molecular Sieves, Science and Technology, J. J. Weitkamp (Ed). Springer, Berlin, 1989.

10. R.W. Thompson, M. J. Huber, J. Cryst. Gr., 56 (1982) 711

11. H. Lechert and H. Kacirek, Zeolites 11 (1991) 720.

12. H. Lechert and H. Kacirek, Zeolites 13 (1992) 192.

13. D. M. Ginter, A. T. Bell, C. J. Radke, in Synthesis of Microporous Materials, Vol. 1, Molecular Sieves, M. L Occelli, H. E Robson (eds.), Van Nostrand Reinhold, New York, 1992, 6.

14. F. Hund, Z. Anorg. Allg. Chem, 1984, 511, 225.

15. E. Kendrick and S. Dann, J. Solid State Chem., 2004, 177, 1513-1519.

16. C. M. B. Henderson and D. Taylor, spectrochimica Acta, 1977, 33A, 283-290.

17. E.M. Flanigen, R.L. Parton and W.P. Katonah, Silica polymorph and process for preparing same, 1978, C01B 33/12. 4073865.

18. W. Mozgawa. J. Mol. Struct., 2001, 596 129 – 137.

19. C. L. Angell, J. Phys. Chem., 1973, 77, 222.

20. F. Roozeboom and H. E.Robson, Zeolites, 1983, 3, 321-328.

21. C.L. Knight, M. A. Williamson and R. J. Bodnar, Raman spectroscopy of zeolites: characterization of natural zeolites with the laser Raman microprobe, P.E. Russell (Ed). San Francisco press, Inc., San Francisco, 1989.

22. P. Sidheswaran and A. N. Bhat, Thermochimica Acta, 1997, 298, 55-58.

Chapter 4: Exchange of nickel and vanadium ions from aqueous solution using zeolitic media.

4.0: Introduction

A number of technologies/techniques have been developed for the removal of metal ions from liquids, such as electro-flotation, reverse osmosis, adsorption, chemical oxidation and ion exchange [1-5]. Among these technologies, ion exchange and adsorption are the most utilised because of their relatively low costs and simplicity of application [6, 7].

Ion exchange can be broadly defined as the transfer of ions across a boundary; this definition thus includes transfer of ions from one liquid phase to another [8]. However, for the purpose of this work, the focus is on those exchanges of ions that occur between a liquid phase and a solid phase (inorganic), which is insoluble in the liquid. The ion exchange between a monovalent cation in solution and that in the solid phase, is presented in the stoichiometric equation (1).

$$M^-Na^+_{solid} + K^+_{solution} \rightleftharpoons M^-K^+_{solid} + Na^+_{solution}$$ Equation 4.1
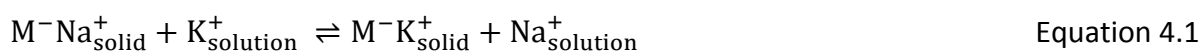
M^- represents a fixed solid anion while Na^+ and K^+ refers to exchanging cations moving reversibly between solid and liquid phases. A similar stoichiometric equation can be written for anions where the solid anion becomes solid cation and Na^+ and K^+ replaced by anions.

To fit the strict definition of ion exchange, the process must be completely reversible [8]. However, in practice interferences from other non-reversible reactions like salt imbibition, precipitation, surface sorption and chelating effects, may be observed [8].

The extent to which an ion-exchanger takes up ions is known as its capacity. For an ion exchanger to be effective at exchanging ions it must have; high exchange capacity, regular and reproducible composition and structure, thermal and chemical stability and resistance to poisoning, mechanical strength stability and attrition resistance as well as consistency in particle size [8]. An ion-exchanger is said to exhibit selectivity for a particular ion when it preferentially takes up the ion from a solution/liquid containing two or more counter ions. The selectivity is quantified using an ion exchange isotherm. At fixed temperature, solutions/liquids containing counter ions of varying amounts of Na^+ and K^+ are equilibrated with known, equal, weights of the exchanger. At equilibrium, the solids and liquids are

separated and both phases analysed for the counter ions or one phase analysed and the other determined by difference.

Ion exchangers can be both organic and inorganic. Some ion exchange materials include resins, clay, natural and synthetic zeolites. Zeolites have been known for their adsorption and ion exchange properties [9-13]. They are characterised by high porous structural frameworks that are made up of TO_4 tetrahedra, where T = Si or Al. These tetrahedra are joined between their oxygen atoms to form sub-units. The sub-units join to form lattices by repeating identical building blocks [14-15]. The Si/Al ratio has a large effect on the ion exchange capacity of a given zeolite. If no Al is present in the framework, the framework will be neutral. Thus the lower the Si/Al ratio, the higher the charge imbalance on the framework and the more M^+ counter ions must be available to counter balance the excess charge on the framework. The negative charge is compensated by the cations present during synthesis and held in the interstices of the structure on crystallization[8]. This arises from the isomorphous substitution of Al^{3+} for Si^{4+} on the oxygen framework. The maximum number of Al^{3+} substituted is governed by the Lowenstein rule; for a given substitution of Al^{3+} for Si^{4+}, it is impossible to achieve another substitution in the first silicon shell around the aluminium atom[9]. Thus, in theory, a large factor of the effectiveness of a zeolite as an ion exchanger is a low Si/Al ratio. Both natural and synthetic zeolites have proven to be effective selective cation exchangers [16-32]. They have been successfully used as ion-exchangers, where the indigenous (typically sodium) charge balancing cations are easily exchanged with cations in aqueous solutions [33, 14, 34-36].

A number of studies have been reviewed on the impact of certain parameters on ion exchange process[37]. Results of these analyses show that the adsorbate type, solution pH, metal concentration and ionic strength are usually the most influential parameters[37]. The solution temperature, size of crystallites and agitation could also influence the process[37]. The presence of other ions in solution is shown to have significant effect on the ion exchange process[37]. The chemical and /or thermal modification of the natural materials could also increase the efficiency of the exchange process.

Previous work on Ni^{2+} exchange from aqueous solution with Na^+ in zeolite X (Na_{87} $(AlO_2)_{87}(SiO_2)_{105}$ nH_2O), have shown that at initial nickel (II) concentration of 0.05M, 40 % of

the Na^+ were displaced by Ni (II) from solution[38]. The concentration of exchange sites were found to decrease with increasing degree of the Ni (II) exchange[38]. The study by Bae and Seff shows that nickel ion exchange of zeolite X of composition $Na_{92}Si_{100}Al_{92}O_{384}$ per unit cell increased up to about 48 %. After the exchange, a total of 45 Ni (II) ions were found per unit cell at four crystallographic sites. 30 of the cations were said to be distributed at 2 different sites III' positions, 2 at sites I, 8 at sites I' and 5 at sites II [39].

The ion exchange of amino- and aqua- complexes of nickel and cobalt from residual ammoniacal liquors of the nickel hydrometallurgical industry using ammonium-clinoptilolite suggests an increase in the interaction between the metal-cation (Ni^{2+} and Co^{3+}) and the ligand (H_2O and NH_3) affect the complex-cation exchange [40]. The ion exchange kinetic between the NH_4^+ and the complex cation is favoured in the order [Ni $(H_2O)_6]^{2+}$ > [Ni $(NH_3)_6]^{2+}$ > [Co $(NH_3)_6]^{3+}$. Temperature was shown to have a significant effect on the exchange of the metal ions especially Ni^{2+} due to the increasing accessibility of ion exchange site's compared with exchange at low temperature [40].

Other studies on the removal of Ni (II) from aqueous solution by natural clinoptilolite show an increase in its sorption with increasing temperature [41]. The Ni (II) cations were almost uniformly distributed inside the clinoptilolite indicating that the removal of Ni (II) from solution is mainly by ion exchange [41].

Solid state ion exchange of nickel into zeolites (mordenite, Y, L and mazzite) using DRS technique shows that, in the dehydrated mordenite and zeolite Y, Ni (II) were present in both regular tetrahedral and distorted tetrahedral symmetries [42]. The relative amount of tetrahedral and distorted tetrahedral nickel species are related to the heating temperature and heating time used for calcination. For the dehydrated zeolite L and mazzite, the Ni (II) cations were shown to be mainly in distorted octahedral symmetry [42].

Other materials like clay minerals and resins have also been extensively used to investigate the removal of Ni (II) from solution. Nickel ion exchange has been used to study the location of Ni (II) in Ni-intercalated vermiculites [43]. The study suggests the entry of Ni^{2+} into two positions of the structure; the interlayer space and the octahedral layer [43].

Resins have also been used in the removal of Ni (II) from solution. The nickel ion exchange by Lewatit cation-exchange resin showed the optimum pH for the exchange process to be 6. At the optimum condition, the Ni (II) uptake by the resin decreases with increasing initial metal concentration [44]. This indicates the effect of the resin dosage on the amount of Ni (II) removed from solution. Similar optimum pH values were obtained for other types of resins such as the use of acidic cation resin in a fixed bed column [45] and Dowex HCR S/S cation exchange resin [46].

Literature on the removal of V (IV) from solution is limited compared to V (V) oxidation state. Few papers on the subject of V (IV) removal from solutions have been published. Some of these include; the removal of V (IV) ion from aqueous solution by commercial calcium hydroxyl apatite [47], sorption of V (IV) using chitosan [48] and the adsorption of V (IV) on alumina and anatase [49]. The uptake of V (IV) by these adsorbents was shown to increase as the pH increases from 2-4 and reaches a maximum adsorption in the pH range 3-3.5. These investigations agree with the fact that the speciation of vanadium in water is dependent on the pH condition and the concentration of the system[50]. Research suggests 12 species of vanadium co-existing in solution, these can be; cationic, anionic or neutral[50]. Speciation diagrams for vanadium by Baes and Mesmer and Peacock and Sherman suggests that the cationic forms of vanadium (VO^{2+}) exists below pH 3; anionic forms exists in the pH range 4-11 while at pH 2, more V^{5+} are found in solution[51-52].

The present chapter, reports the exchange of nickel and vanadium ions from aqueous solution using zeolitic media.

4.1. Experimental

4.1.1. Zeolitic exchange
The zeolitic ion exchange was carried out with aqueous solutions of Ni (II) and V (IV) at concentration range of 0.01 M - 0.1 M which covers the maximum concentrations of the species expected from crude oil analysis. The nickel and vanadium solutions were made with Ni $(NO_3)_2.6H_2O$ and $VOSO_4.4H_2O$ respectively. Once the solutions were made, their pH was tested using an electronic pH meter before the ion exchange.

4.1.2. Zeolitic exchange with nickel (II)

Nickel ion exchange was carried out with the materials prepared in chapter 3 using a roller mixer. 0.5 g zeolite samples were added to 300 mL of (0.01 M, 0.025 M, 0.05 M, 0.075 M, and 0.1 M) solutions of nickel in polyethylene bottles and left to equilibrate on the roller mixer for 24 h. After equilibration, the samples were removed, filtered by gravity through fluted filter paper and the mixing bottles washed twice with 50 mL distilled water through the filter. The zeolite residue left on the filter paper was then dried overnight at 80 ^{o}C and characterized PXRD, FTIR and TGA. The supernatant solution was also analysed using ICP-OES following the necessary dilutions.

4.1.3. Nickel exchange with K- and Li-zeolites

The nickel ion exchange with K- and Li-zeolites was carried out using similar procedure to that described for the parent zeolites. 300 mL of 0.1 M and 0.01 M solutions of nickel ions into polyethylene bottles containing 0.5 g each of the exchanged zeolites and left to equilibrate on the roller mixer for 24 h. This was carried out in triplicates. The mixture was filtered after equilibration for 24 h, washed and dried overnight at 80 ^{o}C. Characterization of the solid product was done using PXRD, FTIR and TGA while the exchanged and the starting solutions where analysed for the exchanging ions using atomic absorption spectroscopy.

4.1.4. Zeolitic exchange with vanadium (IV)

Vanadium ion exchange was carried out with zeolite A, zeolite X and zeolite Y, using a roller mixer. 300 mL (0.01 M, 0.025 M, 0.05 M, 0.075 M, and 0.1 M) of $VOSO_4.4H_2O$ solutions prepared were measured into polyethylene bottles and placed on a roller mixer for 24 h. Varying concentrations were used to compare the effect of concentration on the vanadium-zeolite exchange.   The mixture was filtered, washed with distilled water and dried at 80 ^{o}C overnight. The solid product was characterized using PXRD and FTIR while the supernatant solution was analysed using atomic ICP-OES following the necessary dilutions

4.1.5. Selective removal of metal ions from a mix metal solution

A solution containing a mixture of five metal cations (Ni(II), V(IV), Zn(II), Fe(II) and Cu(II)), with each metal ion concentration of 0.05 M was prepared and ion exchange carried out with the parent zeolite A and Zeolite X. 10 mL of 0.05 M solutions each of Ni(II), V(IV), Zn(II),

Fe(II) and Cu(II) were measured into polyethylene bottles containing 0.5 g each of the parent zeolites and left to equilibrate on the roller mixer for 24 h. This was again done in triplicate. The mixture was filtered after equilibration for 24 h, briefly washed and dried overnight at 80 $^{\circ}$C. Characterization of the solid product was carried out using PXRD while the cations content were determined using ICP-OES.

4.1.6. Equilibrium and adsorption studies

The batch experiments were carried out with 50 mL (0.01-0.1 M) Ni (II) solution. 0.5 g of the zeolite material was added to the solution and the Ni (II) ion uptake by the zeolite determined. The polypropylene bottles containing the adsorbate and adsorbent were placed in a thermostatic orbital shaker and were shaken for 24 h at a constant speed of 200 rpm and constant temperature of 18 $^{\circ}$C. After 24 h, the samples were filtered and the filtrates analysed. Similar experiment was carried out with 50 mL (0.05 M) Ni(II) but at varying zeolite dosages. The kinetic studies were carried out in a similar manner. 0.5 g of the adsorbent was added to 50 mL of 0.05 M Ni (II) solutions into polypropylene bottles. The sample bottles were withdrawn from the shaker at regular time intervals and the samples filtered. The supernatant solution was analysed using an ICP-OES. The Ni (II) uptake by the zeolites was calculated using the following equations:

% removal = $(C_o-C_e)/C_o$ x100   Equation 4.1

$q_{e} = [(C_o-C_e) V]/M$ Equation 4.2

Where q_e is the amount of metal ion exchanged (mol/g); C_o and C_e are the initial and equilibrium concentrations of the metal ion (mol/L), V is the volume (L) and m is the mass of adsorbent (g). The same procedure was repeated for V (IV) solution.

4.2. Results and discussions

4.2.1. Zeolitic exchange with nickel

The zeolitic ion exchange was carried out in such a way as to obtain equilibrium; this was done by ensuring the moles of nickel ions were in excess (300 mL) of the moles of cations (Na$^+$) in the zeolite material. For a given zeolite, the amount of water contained in each of the zeolites, as determined by thermal analysis was used to calculate the formula for the

zeolites (Table 4.1). For example, TGA studies of zeolite A, with the formula $(Na_{12}Al_{12}Si_{12}O_{48})$ .XH_2O, showed X = 24.2 hence the moles of Na in zeolite was calculated thus;

$$\text{mass of Na in zeolite} = \frac{\text{molar mass of Na}}{\text{FW of zeolite}} \text{ x sample size (g)} \qquad \text{Equation 4.3}$$

So that for zeolite A,

$$\frac{275.88}{2140.58} \text{ x } 0.5 = 0.0644 \text{ g of Na}$$

$$\text{Moles of Na in zeolite A} = \frac{\text{mass of Na}}{\text{molar mass of Na}} = 2.803 \text{ x } 10^{-3} \qquad \text{Equation 4.4}$$

Table 4.1: Amount of Na in 0.5 g zeolite sample

| zeolites	Zeolitic water (moles)	Zeolitic Formula	Mass Na in 0.5g sample (g)	Moles Na in 0.5g sample (moles)
Zeolite A	24.2	$(Na_{12}Al_{12}Si_{12}O_{48}).24.2H_2O$	0.0644	$2.803 \text{ x } 10^{-3}$
Zeolite X	238.8	$Na_{88}Al_{88}Si_{104}O_{384}.238.8 \text{ } H_2O$	0.0558	$2.427 \text{ x}10^{-3}$
Zeolite Y	246.5	$Na_{54.91}Al_{56}Si_{136}O_{384}.246.5H_2O$	0.0374	$1.627 \text{ x } 10^{-3}$

Table 4.2, presents the pH of the nickel starting solutions before ion exchange while the result for the nickel ion exchange with zeolites A, X and Y is presented in Appendix 2.

Table 4.2: pH of nickel solutions before treatment with zeolites

Concentration (M)	pH
0.010	5.32
0.025	5.29
0.050	5.15
0.075	4.97
0.100	4.91

The chemical formula of the zeolites after nickel ion exchange (appendix 2) were calculated considering the fact that for every nickel ion replaced; two sodium ions are displaced so as to balance the charge.

The results for the nickel ion exchange with the zeolites, Ni (II) exchange with Na^+ in the zeolites had occurred for all the zeolites considered. The extent of the nickel ion exchange with the framework Na^+ however, varied for the different zeolites. Zeolite X is the most effective at the metal ions exchange with a 38 % exchage, followed fairly closely by zeolite A with 28 % exchange while the exchange for zeolite Y was to a far lesser extent (Figure 4.1).
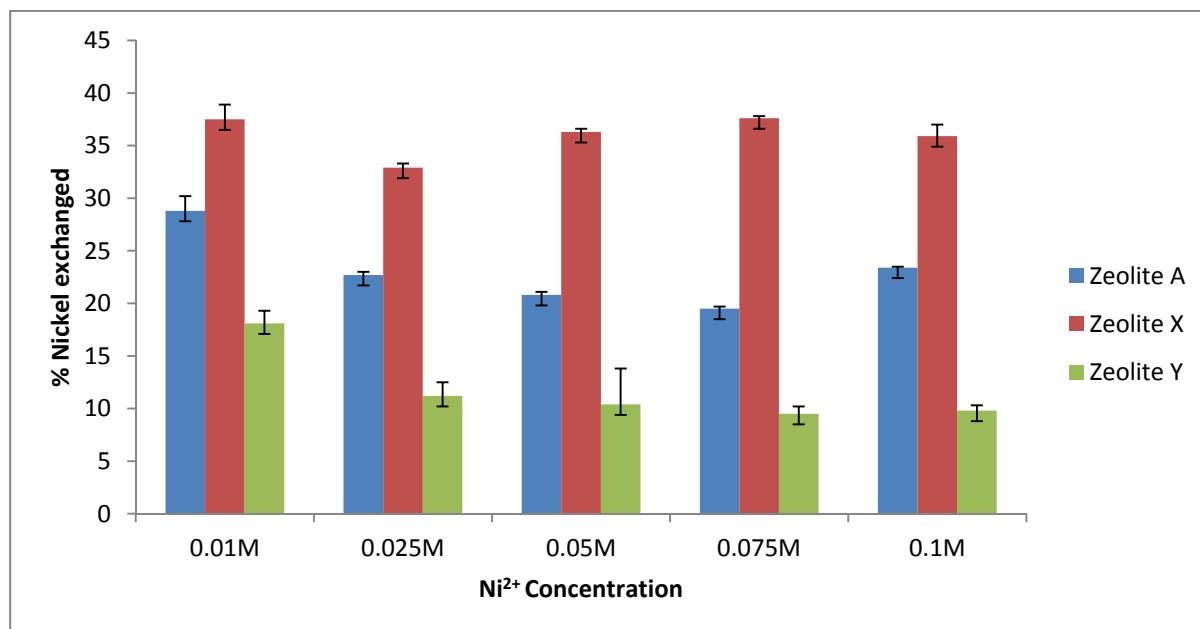
Figure 4.1: Efficiency of Ni^{2+} uptake by zeolites A,X and Y at varying concentrations

The percent nickel ion uptake by the zeolites decreases with increasing initial concentration. This could be attributed to the fact that at lower concentration, all the Ni (II) were exchanged at the accessible exchange sites and further increase in the initial concentration led to the saturation of the zeolites surfaces due to unavailability of exchange sites to accommodate any more Ni (II) from solution. A similar observation was made by Keane, 1998 where it was observed that an increase in solution transition metal concentration lowers the affinity of the zeolite for the in-coming transition metal cation [32].

The ion exchange behaviour of the zeolites may be explained based on their Si/Al ratios. This ratio indicates the amount of counter ions present in a zeolite due to the charge on the zeolite framework structure. Zeolite X, with low Si/Al ratio has high charge on the framework, due to the isomorphous substitution of Si^{4+} with Al^{3+}, thus the high charge imbalance attracts more cations (Na^+) which can in turn exchange with the Ni (II). Another factor that may be responsible for the ion exchange of zeolites is the different pore size or diameters of the zeolites. Zeolite X with largest effective window diameter of about 7.4 Å and an inner diameter of 12 Å will allow exchange of metal cations with greater ease compared to zeolite A which have the largest pore cavity of 11.7 Å and limiting diameter of 4.1 Å [53]. Zeolite X and Y however, are both faujasites with pore diameter of 7.4 Å and an inner diameter of 12 Å, formed by 12-membered ring. They differ only in their Si/Al ratio (X=1-2, Y=3). Thus the main factor determining the ion exchange activity between zeolite X and Y would be the Si/Al ratios.

Again from literature, the ion exchange behaviour of these zeolites can be explained based on the fact that, sodium cations in the unit cells of faujasites are located in three different kinds of crystallographic sites; sites I (16 cations), sites II (32 cations), and sites III (remaining cations) [54], each exhibiting different preferences for in-coming metal ions. As shown figure 4.2, sites I are located in the hexagonal prisms that connect cavities or sodalite cages; sites II are at the hexagonal faces near the centre of 6-membered rings which are windows between the supercages and sodalites; and sites III are in the large cavities, near the four-membered rings of the sodalite cavity [54]. Previous studies on the monovalent ion exchange in synthetic zeolite X with crystal formula Na_{85} [$(AlO_2)_{85}(SiO_2)_{107}$], showed that 16 of the 85 sodium cations in the unit cell, are located either in the hexagonal prisms (1 in each of the

16 prism per unit cell) or sodalite cages (2 on each of 8 sodalite cages). These cations form ion pairs with the fixed negative charges of the aluminosilicate framework. 32 of the 85 sodium cations are found in the large cages near the centre of the 6-membered ring tetrahedra which are windows between the super cages and sodalite cages and are tightly bound to the fixed negative charge of the aluminosilicate framework. The remaining 37 cations are either in constant motion within the large cavities or other crystallographic sites that could not be detected [55]. Reports shows that ion exchange occurs first at sites III, then at sites II, and finally at sites I. The selectivity for exchange at site III in zeolite X was observed below 40 % while that for II corresponds to around 50 % of all existing sites [54]. The selectivity for site I could not be explained on the basis of equilibrium, however the selectivity is limited for steric reasons.

The composition of the synthetic zeolite X used for this study is given by the anhydrous formula $Na_{88} Al_{88} Si_{104} O_{384}$. In agreement with the work by Sherry [55], it can be said that of the 88 Na^+ in the unit cell, 16 of the cations are located in sites I, 32 located in sites II and the remaining 40 in sites III. Sites III which does not bind tightly to counter ions probably in hydrated state should prefer Ni (II) ions due to its hydrated ionic radius (4.04 Å) and the electrostatic (coulombic) interactions between the hydrated counter ions and anionic sites [55]. Thus the selectivity of the Ni (II) for the site is observed up to 40 % exchange.

The degree of Ni (II) exchange of approximately 38 % was observed for zeolite X, indicating that up to this concentration; only the most accessible Na^+ ions in sites III and II may have been exchanged.

A similar explanation is considered for zeolite A. Zeolite A with anhydrous composition ($Na_{12}Al_{12}Si_{12}O_{48}$), has 12 or 13 Na^+ per unit cell, 8 cations are located in the centre of 6-membered rings formed from tetrahedral on the 3-fold axis inside the α-cage. This position refered to as site 1. Thus about 30 % of the exchange corresponds to cations in the large cages (sites III). 28 % exchange was observed for zeolite A in this study, indicating that only the Ni (II) in the most accessible site (III), most have been exchanged. For zeolite Y, there are 16 cations in the small cages similar to zeolite X; however, the majority of the cations in the large cavities are most likely completely hydrated[55]. It is worth mentioning here that zeolite X had three times more type III sites than the zeolite Y, thus there is a simultaneous

exchange in sites II and III of the zeolite X which could bring about competition between the exchange sites, while for zeolite Y competition between these sites do is less[54].
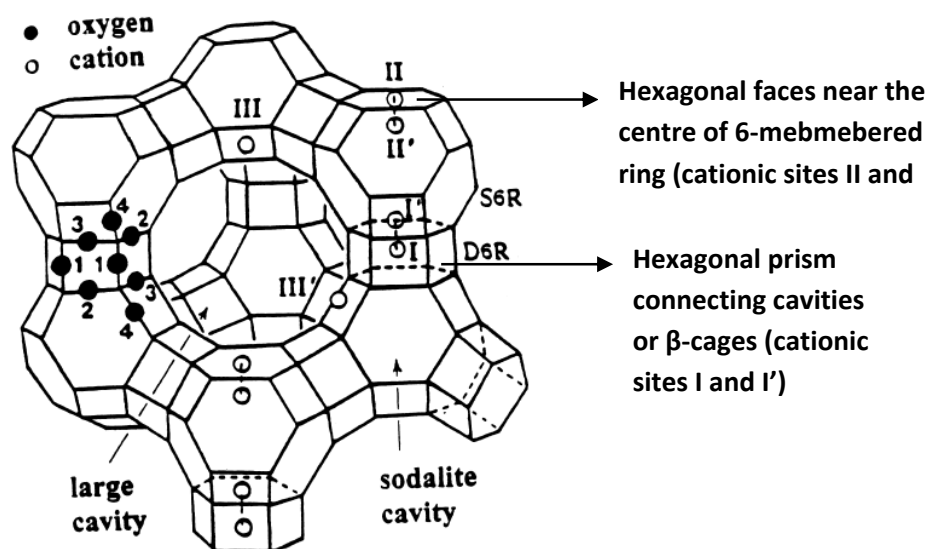

Figure 4.2: Faujasite crystal structure indicating site locations[54]

The last factor that might be responsible for the ion exchange behaviour of zeolites A, X and Y is the fact that these zeolites basically have sodalite cages as their building block and their ion exchange might be related to that of the sodalites and hydrosodalites. The metal ion exchange behaviour of hydrosodalite considered in this work gave a good % exchange, especially for the K- and Li-hydrosodalites which attests to the fact that the ion exchange behaviour in these zeolites is influenced by the β-cages. However, compared to zeolite X and zeolite A there are fewer cationic sites in sodalities (2 per cage) than are there in the zeolites (about 96 for the faujasites), thus exchange should be lower for the sodalites compared to zeolites A and X.

4.2.1.1. PXRD

The PXRD data for the zeolite X after exchange showed that ion exchange had occurred as shown by an observed shift in reflections (figure 4.3). An internal standard (silicon standard) was added to allow the calibration of data. It was observed that the magnitude of the shift increases as the concentration of nickel in solution increases. This shift indicates a change in the lattice parameter due to increase in 2θ, thus suggesting the possibility of an ion

exchange. Ionic radii (Shannon and Prewitt) for 6-coodinate Ni (II) ion (69pm) compared with that of Na$^+$ in same coordination state (102pm), clearly shows that Ni (II) is significantly smaller than Na$^+$ and much smaller considering the fact that, for every Ni (II) replaced, two Na$^+$ are displaced. Hence the exchange of Na$^+$ for Ni (II) gave a shift in reflections to the right.
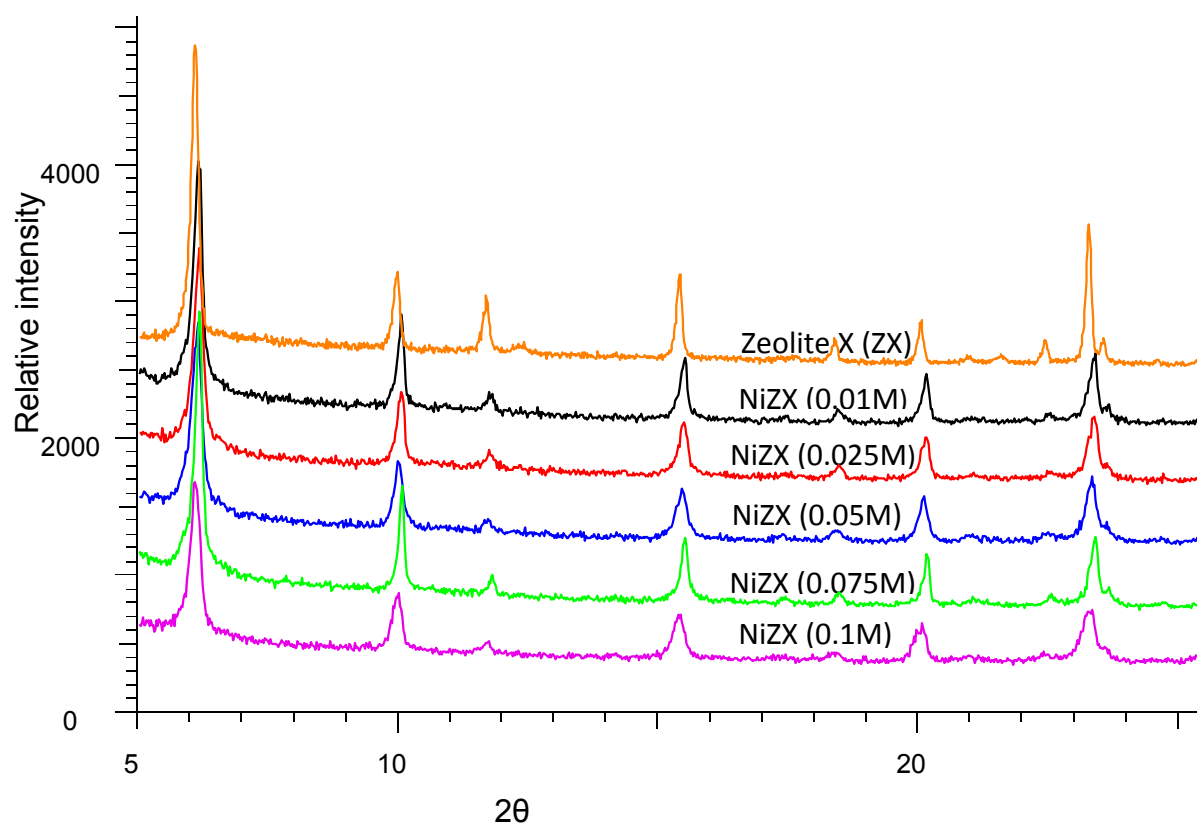

Figure 4.3: PXRD pattern for zeolite X after nickel exchange

Zeolite A did not show a significant shift in the reflections after nickel (II) exchange however, there was an observed increase in peak intensity at 2θ position around 18 ^{o} (figure 4.4). This change in peak intensity was proposed to be an allowed reflection for the structure which could be particularly observed by placing Ni (II) on a certain site. Refined crystal data of a matched pattern to that of the zeolite A used in this study, was used to check if the peak intensity change was due to the replacement of Na$^+$ by Ni (II) at specific exchange sites. This was done by replacing Na$^+$ with Ni (II) for each of the 3 Na$^+$ sites, one after the other using

'ATOMS'. Exchange at sites I and II did not give significant increase in the peak intensity at 2θ position 17.8349^o, however, at site III, a significant increase in the peak intensity was observed (figure 4.5) indicating the increase in the intensity was due to exchange of Na$^+$ for Ni^{2+} at site III. This is clearly seen by the decrease in the peak intensity at 2θ position 16.3112^o and a simultaneous increase in the peak intensity at 17.8349 ^{o}.
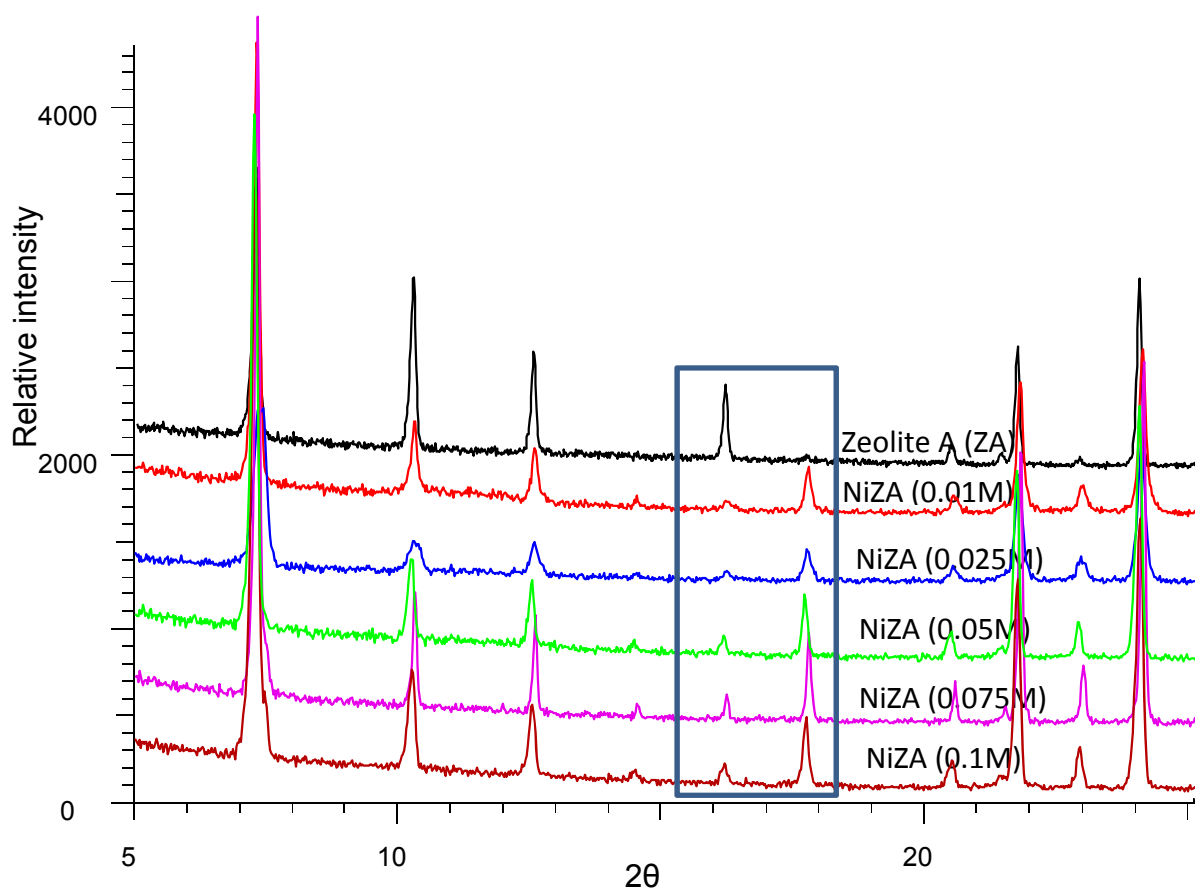

Figure 4.4: PXRD pattern for zeolite A after nickel exchange
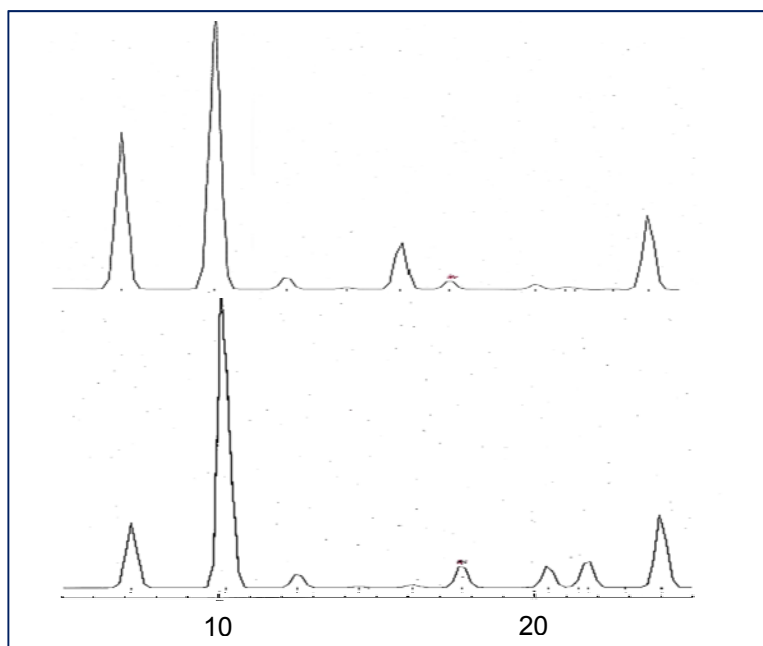
Figure 4.5: Effect of metal ion exchange on peak intensity for zeolite A without (upper) and with (lower) nickel exchange at site III.

No significant change was observed from PXRD data for zeolite Y after the nickel (II) exchange as compared with the parent zeolite Y (figure 4.6). This is in agreement with the data from the ICP-OES showing little nickel (II) exchange occurred. As noted earlier, this behaviour is presumed to be largely due to the Si/Al ratio rather than the pore size of the zeolite.

Figure 4.6: PXRD pattern for zeolite Y after nickel exchange

4.2.1.2 FTIR

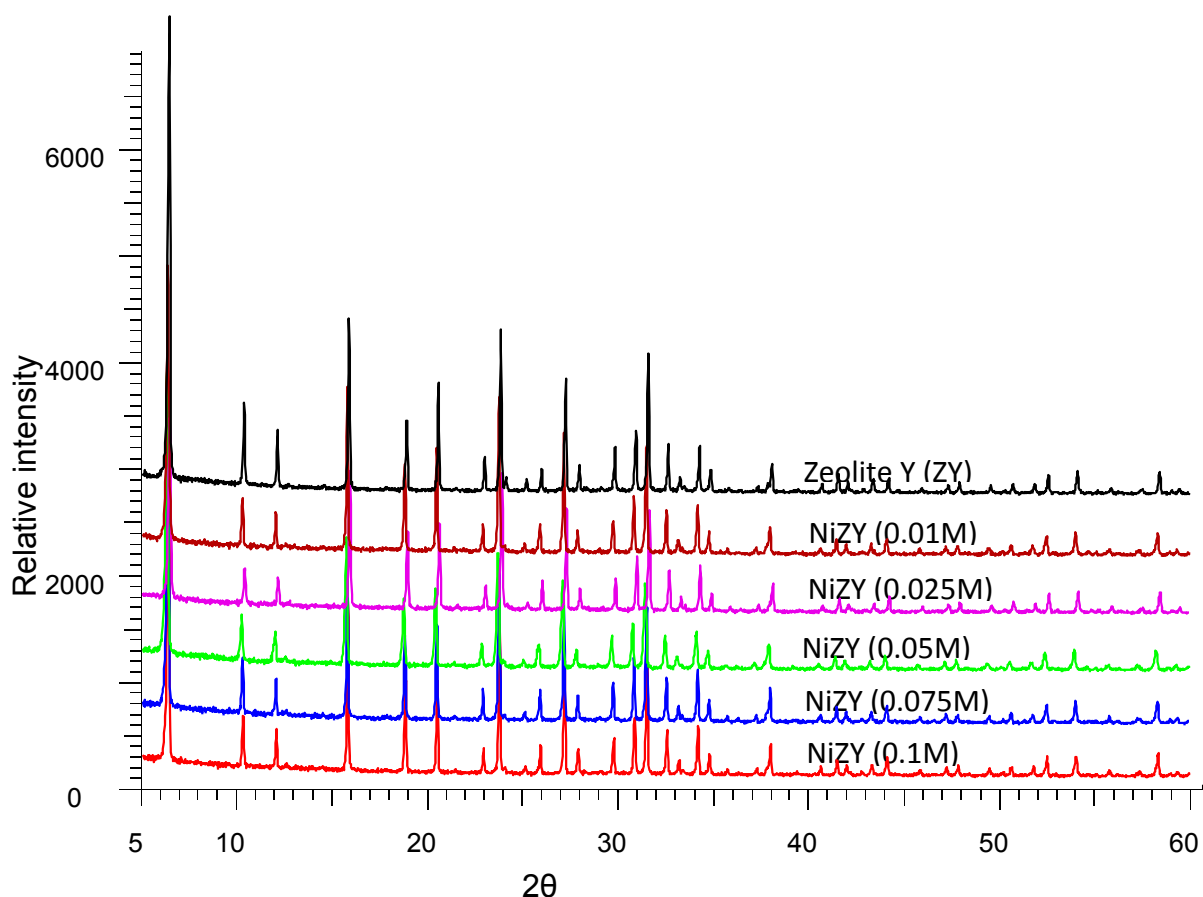Zeolite X was considered for the FTIR analysis since it is more efficient at the nickel (II) uptake. The infrared data for the nickel exchanged zeolites also supports the fact that nickel (II) exchange had occurred. This is clearly seen for zeolite X as indicated by absorption at 912cm^{-3}, a shoulder on a broad band centered at 978 cm^{-3} (arrow). This result is in agreement with earlier observations that the spectra of all transition metal-exchanged zeolites show a shoulder at about 915cm^{-1} on a broad band centred around 980cm^{-1} and increase with increasing ion exchange for hydrated zeolites[56]. Figure 4.7 presents the FTIR spectra for zeolite X after nickel ion exchange at varying concentrations as compared with that for parent zeolite X.
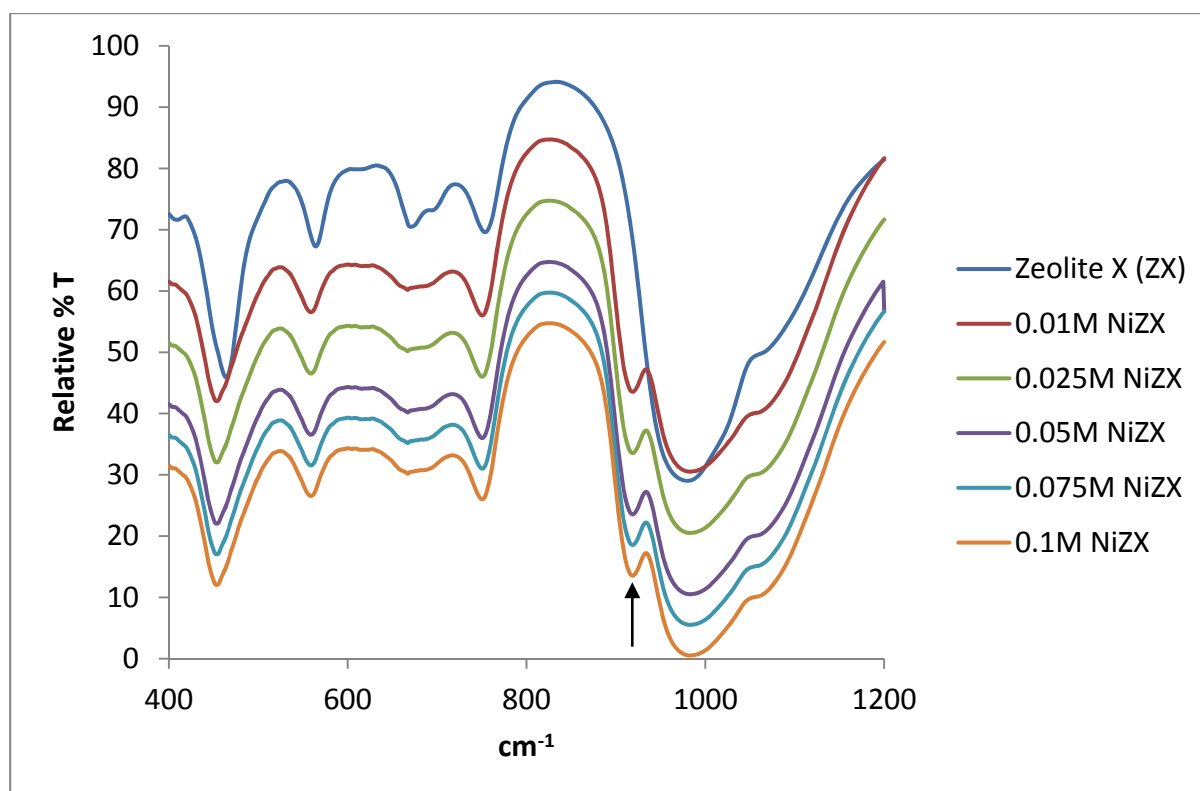
Figure 4.7: The FTIR spectra for nickel ion exchange with the zeolites

4.2.1.3. SEM-EDS

Zeolite X was considered for SEM-EDS analysis because it gave the highest nickel uptake of all the zeolites considered. EDS spectra for zeolite X before and after nickel exchange, detected nickel ions in the zeolite framework after the nickel loading (figure 4.8). The spectra also detected gold peaks which were due to the gold coating during the sample preparation. The EDS also quantified the amount of Ni (II) retained within the zeolite framework as well as giving the elemental composition of zeolite X with and without nickel ions (Table 4.4). The elemental composition data obtained showed a sharp decrease in the weight % of Na$^+$ of about 73 % after nickel ion exchange while the amount of Ni (II) increased from 0 to range up to 24.9 %. There was an observed framework silicon leaching but the decrease in aluminium was relatively low. This result indicates that the ion exchange of Na$^+$ by Ni (II) is most likely to have been at the exchange sites within the zeolites. The data obtained also showed a fairly consistent mole ratio of 2 Na$^+$ to 1 Ni^{2+} in support of the fact that most of the exchange was at the exchange sites of the zeolite.
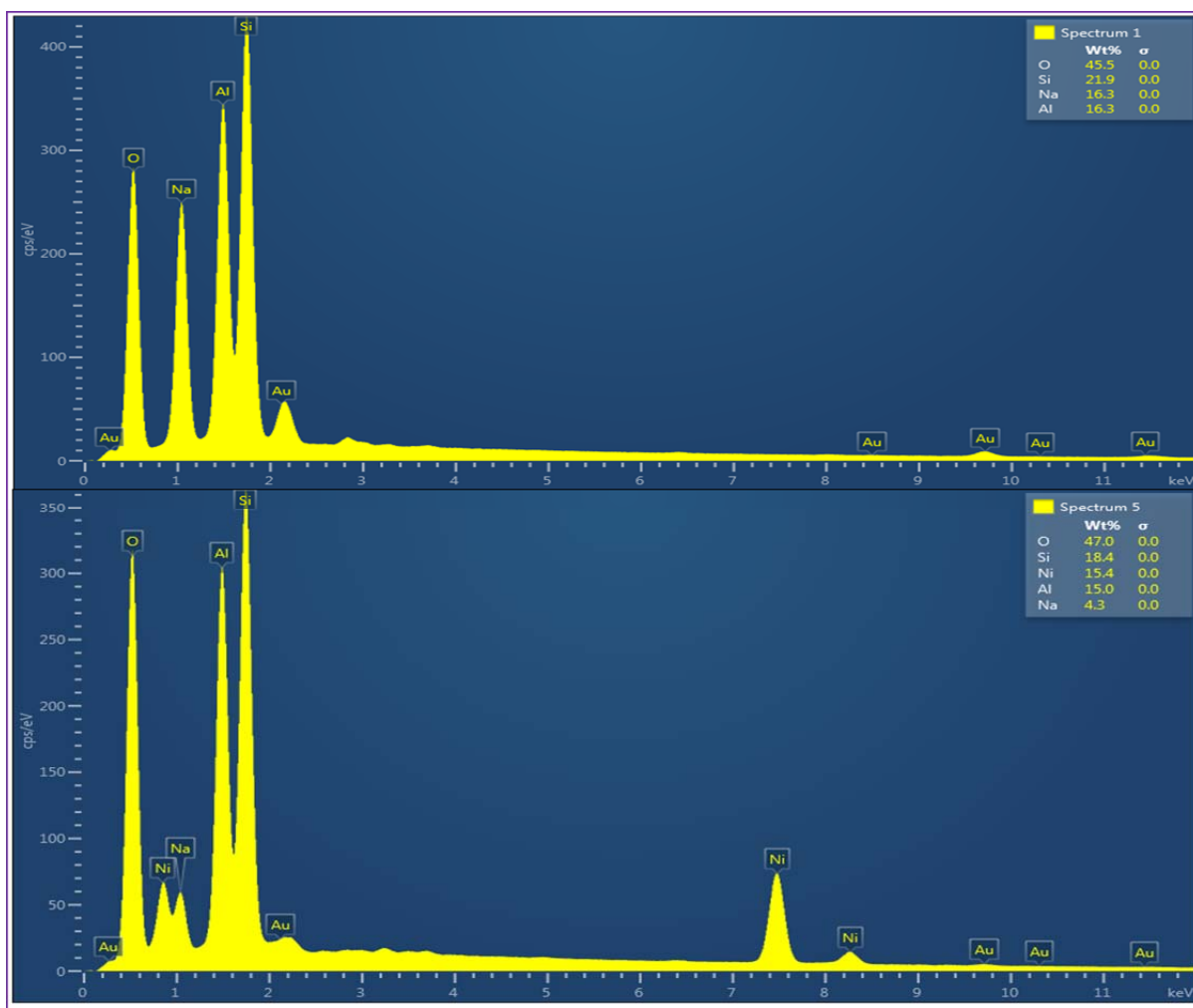
Figure 4.8: EDS spectra of zeolite X with (lower) and without (upper) nickel ion exchange at (0.01M) concentration

Table 4.4: Elemental composition before and after nickel (II) exchange

Element	Elemental composition (Wt. %)					
	Before exchange	After exchange				
		0.01M	0.025M	0.05M	0.075M	0.1M
O	45.5±0.4	47.0±2.9	51.2±0.4	51.3±5.4	45.0±0.7	45.1±1.4
Na	16.3±0.9	4.3±0.08	3.7±0.1	4.3±0.2	4.0±0.2	4.3±0.08
Al	16.3±0.5	13.0±0.2	13.5±0.0	13.7±0.3	15.0±0.03	14.6±0.7
Si	21.9±0.8	18.4±0.4	16.6±0.2	17.5±0.1	19.0±0.05	18.5±0.14
Ni	0.0±0.0	15.4±2.3	15.8±2	13.3±5.2	16.9±0.6	17.5±3
Na/Ni	0.0	2.00	2.04	2.26	1.89	1.73

The SEM micrographs of zeolite X before and after nickel exchange showed that the particles were closely similar in size and appearance suggesting that the exchange of Na^+ for Ni (II) had little or no effect on the zeolite framework. The particle size for both the nickel exchanged and as synthesised zeolites was measured to be ~2μm. Similar SEM micrographs were obtained for all the nickel (II) concentrations used (appendix 4). SEM micrographs of zeolite A before and after the nickel (II) exchange also showed the little or no damage to the framework structure of zeolite A (figure 4.10).
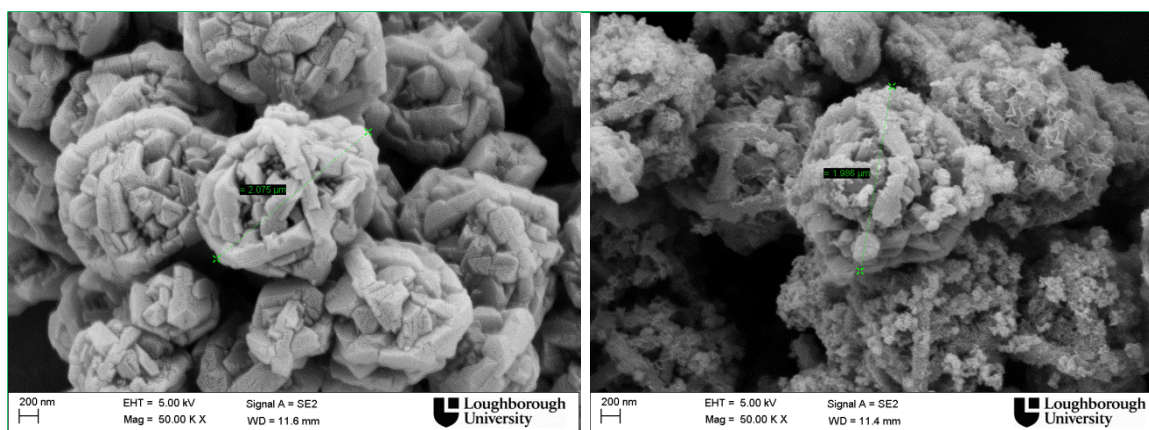

Figure 4.9: SEM micrographs of as synthesised zeolite X and nickel exchanged zeolite X
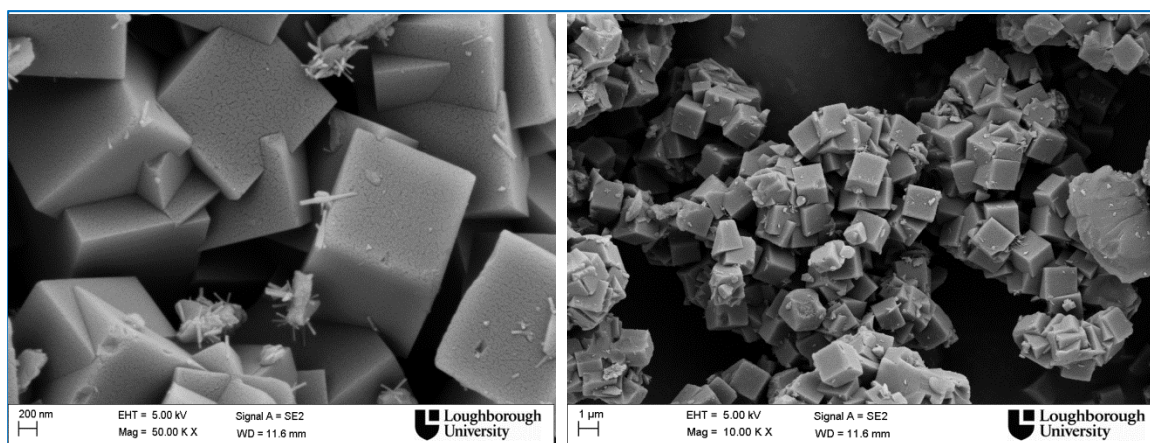
Figure 4.10: SEM micrographs of as synthesised zeolite A and nickel exchanged zeolite A

4.2.1.4. TGA

Zeolite X, which has consistently shown higher nickel removal efficiency is used to show the trend in the weight loss of the nickel exchanged zeolites compared to the as synthesised zeolite X. The % weight loss for Ni-zeolite X is found to be higher than that for parent zeolite X. This behaviour is expected based on the ionic radii of Ni (II) compared to Na^+ as explained in section 4.2.1.1. Ni (II) due its smaller size will have higher water of hydration than Na^+ which is reflected in the % weight loss. The different Ni^{2+} concentrations did not have any significant effect on the zeolitic water contents of the Ni-zeolite X.

Table 4.5: Thermal analysis of zeolite X before and after nickel (0.01M) exchange

Zeolites	Wt. loss (%)	Temp. range for wt. loss
Zeolite X	25	20-600
Ni-zeolite X	26	20-600

4.2.2. Nickel exchange with K- and Li-zeolites

The data for nickel ion exchange with K- and Li-zeolites compared with the parent zeolites (Figure 4.11 and 4.12) shows that nickel ion exchange had occurred. There was no significant increase in the nickel ion exchange activity of the alkali metal zeolites compared to the parent zeolites at higher concentrations (0.1M) of the nickel solutions (Figure 4.11).

However, at lower concentrations (0.01 M) there was a marked increase in the nickel exchange by the zeolites modified with alkali metals particularly zeolites A, X and Y (Figure 4.12).
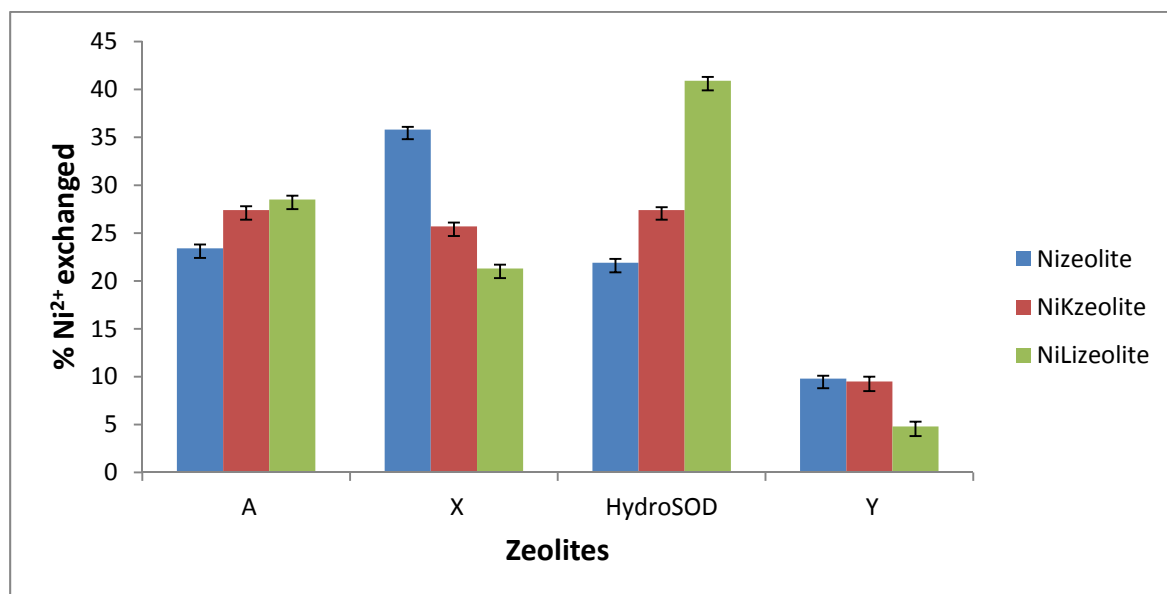

Figure 4.11: Comparative efficiency of nickel ion (0. 1M) exchange with parent zeolites and K- and Li-zeolites
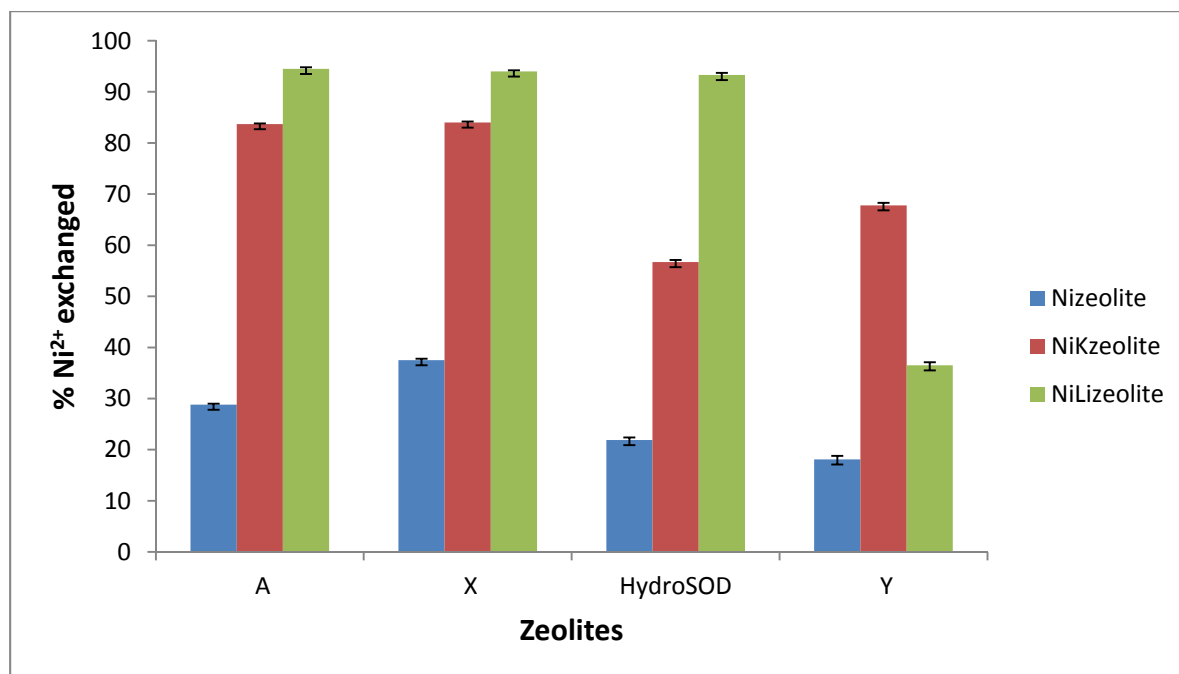

Figure 4.12: Comparative efficiency of nickel ion (0.01M) exchange with parent zeolites and K- and Li-zeolites.

This again indicates the effect of concentration on the nickel removal by these zeolites as noted previously. As the concentration (thus pH) increases, nickel ion exchange by the K- and Lizeolites decreases. Thus at concentration of nickel = 0.01M, alkali metal zeolites can be used to remove nickel ions from solution at higher efficiency compared to the parent zeolite.

The result obtained for the nickel (II) exchange with K- and Lizeolites follow a similar trend to that obtained for the parent zeolites. Zeolite X is found to have the highest uptake for nickel (II), closely followed by zeolite A. The nickel uptake by the hydrosodalite is significantly high too. However, compared to zeolites X and zeolite A, their Ni (II) uptake is lower. There are fewer cationic sites in sodalities (2 per cage) than are there in the zeolites (about 96 for the faujasites), thus the reason for lower Ni (II) exchange in hydrosodalites compared to zeolites A and X.

 The ion exchange behaviour of the K- and Li-zeolites, like the parent zeolites, can be explained based on the Si/Al ratios of the zeolites and the size of the K and Li metals. The higher the amount of Al in a zeolite, the better its ion exchange properties. Zeolite A and Zeolite X with a Si/Al ratio of 1 and 1-1.5 respectively will have higher ion exchange capacity compared to zeolite Y with Si / Al of ~3. The size of the K and Li ions plays another major role in the ion exchange reaction. If cations from the zeolite (Li^+ and K^+) are hydrated in solution, their hydration radius decreases down the group from Li^+ to K^+ (Table 3.5). As mentioned earlier in chapter 3, K^+ would be preferred to Li^+ in their hydrated state.

4.2.2.1. PXRD of nickel-K- and Li-zeolites and sodalites

The PXRD data for the nickel K- and Li-zeolites shows nickel ion exchange occurred. Earlier PXRD data for the K- and Li-zeolites showed shift in reflections, indicating an exchange of metal ions of different sizes. For the nickel- K- and Li-zeolites, there was no significant shift in the reflections compared to the parent zeolite (Figure 4.13). This could be due to the difference in ionic radii of nickel ions compared to that of the alkali metal ions.

The reflections for the Ni-K- and Li-hydrosodalites phases showed no noticeable shift in the patterns, however, the reflections showed low intensity compared to the parent and K and Li-hydrosodalite (Figure 4.14). This may be evidence of nickel (II) exchange by the zeolites or

reduction in crystallinity since the solution is slightly acidic and sodalite containing zeolites are particularly acid sensitive [8]
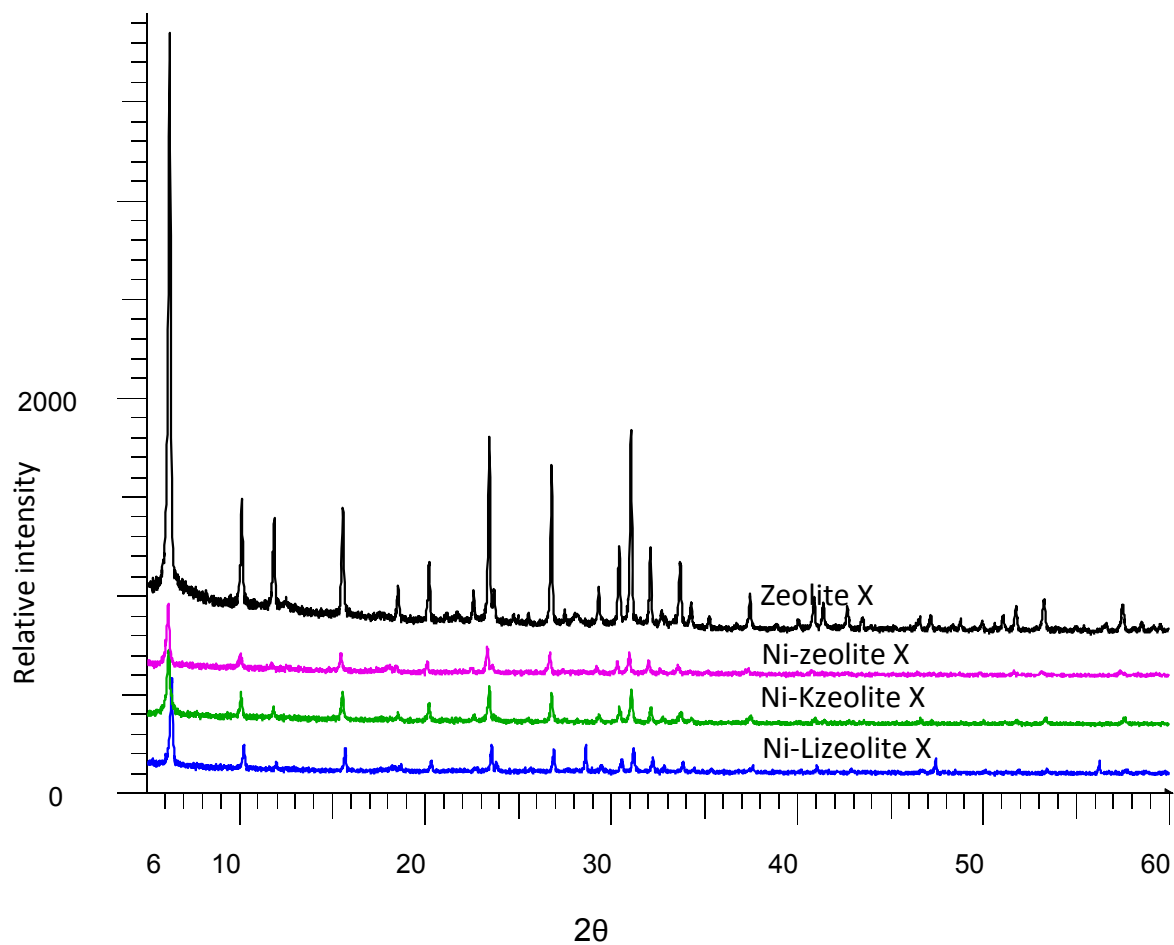
Figure 4.13: PXRD pattern for alkali metal-zeolite X after nickel exchange
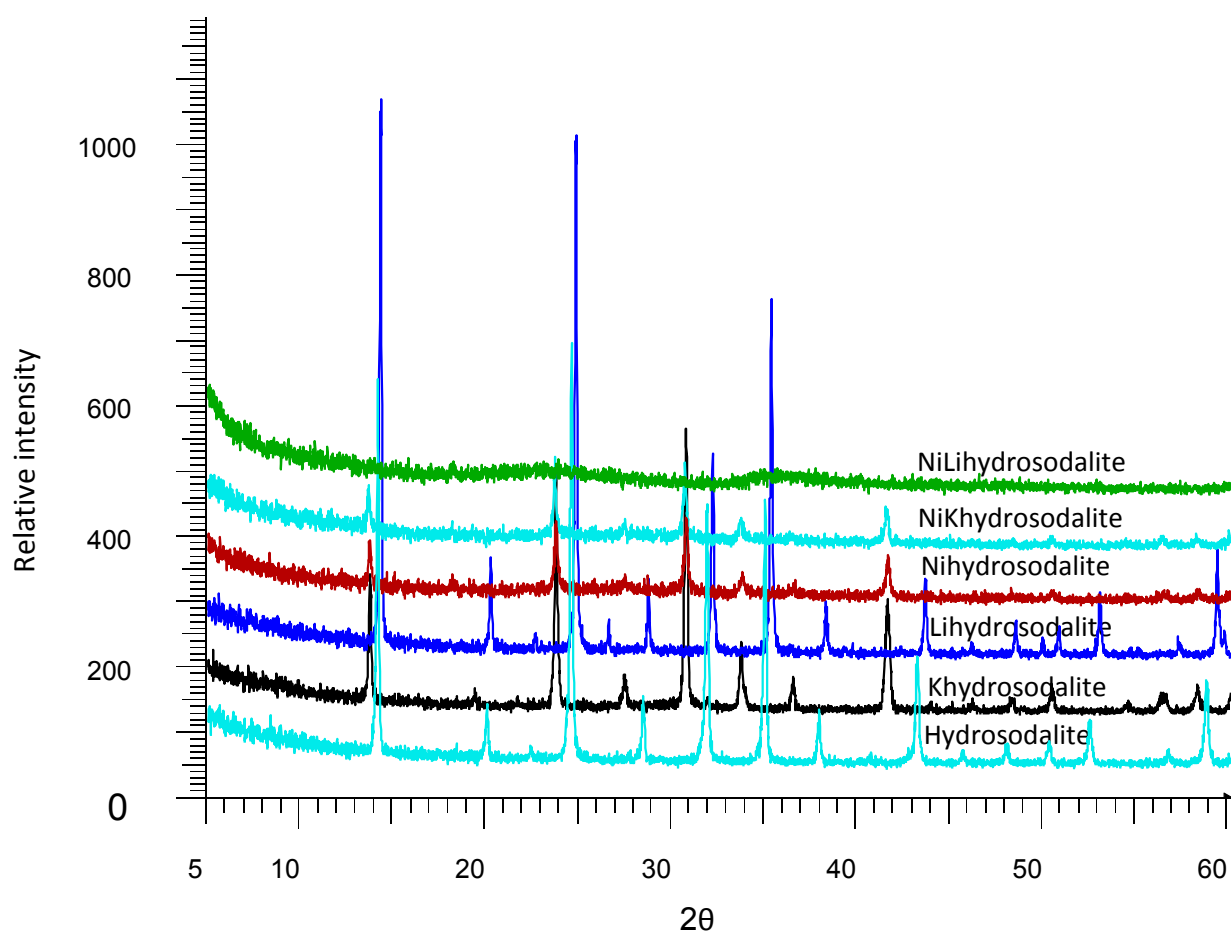
Figure 4.14: PXRD pattern for K- and Li-hydrosodalite before and after K- and Li- and nickel exchange

4.2.2.2. FTIR for Ni-K- and Li-zeolites

FTIR spectra for the Ni-K- and Li-zeolites showed a similar trend as that observed for the nickel-zeolites with absorption at $912cm^{-1}$ (arrow) which is a shoulder on a broad band centered at around $978cm^{-1}$ (figure 4.15). This is an indication that nickel ion exchange had occurred as earlier explained in section 4. 2.1.2.
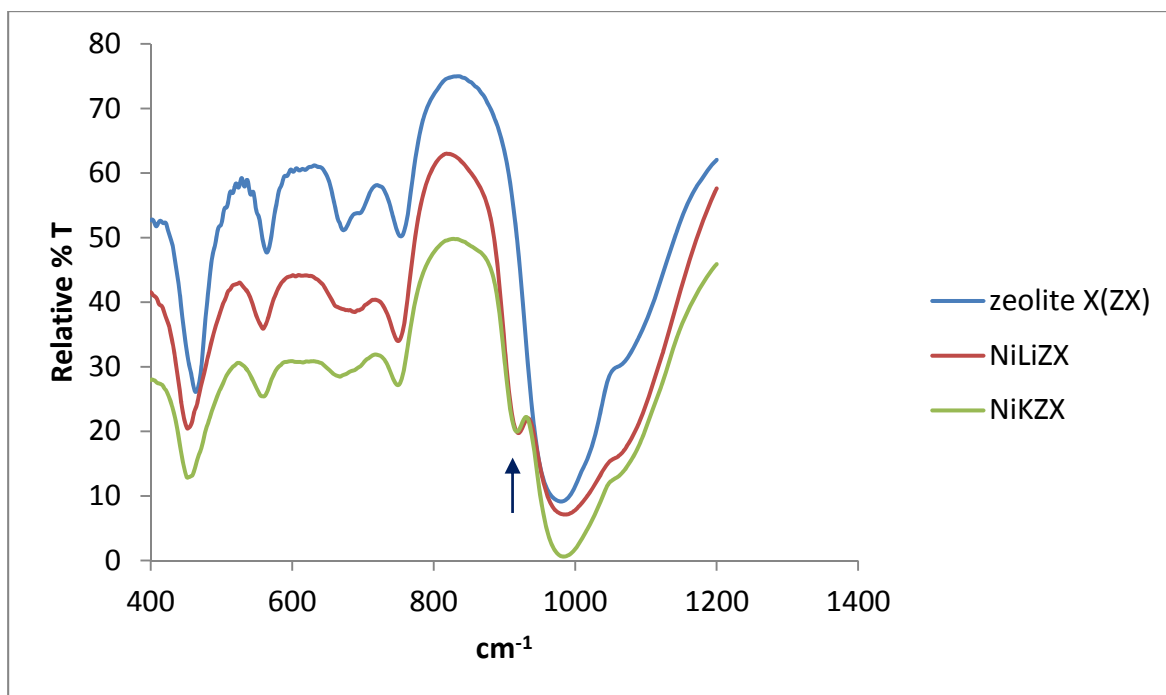
Figure 4.15: The FTIR spectra for nickel ion exchange with K- and Lizeolites

4.2.2.3. TGA for Ni-k- and Li-zeolites

The trend in weight loss for Ni-k- and Li-zeolites is similar to that observed for K- and Li-zeolites, zeolite X which has consistently shown higher nickel removal efficiency is used to show the trend in the weight loss (Table 4.7). Two distinct weight losses due to water were observed at temperature ranges 20-600. The % loss for Ni-Kzeolite X is observed to be lower than that for Ni-Li-zeolite X. The overall behaviour could thus be explained in similar manner as that for K- and Li-zeolites.

Table 4.7: Percent weight loss for the alkali metal zeolite X before and after nickel exchange

Zeolites	Wt. loss (%)	Temp. range for wt. loss
K-zeolite X	23	20-600
Ni-K-zeolite X	25	20-600
Li-zeolite X	27	20-600
Ni-Li-zeolite X	26	20-600

4.2.3. Factors affecting Ni (II) uptake by zeolites

4.2.3.1. Effect of time on Ni (II) ion exchange

The rate of Ni (II) removal by zeolite A and zeolite X from solution are shown in Figure 4.16 and 4.17. The results show that initial exchange was rapid due to the exchange of Ni (II) with sodium cations from the exterior surface after which, the metal ions entered into the pores (interior surface), at relatively slower rate. The rapid initial uptake rate could also be explained by the available exchange sites on the zeolite framework and the high concentration, thus the decrease of exchange sites reduces the uptake rate. The Ni (II) uptake reached equilibrium at 24 h of contact time, after which the rate of removal of the Ni (II) gradually decreased. The Ni (II) removal efficiency for zeolite A and zeolite X at equilibrium was 24 % and 39 % respectively. Therefore, considering technical and economic aspects, a contact time of 24 h was chosen for nickel ion removal from aqueous solution using zeolite A and zeolite X.
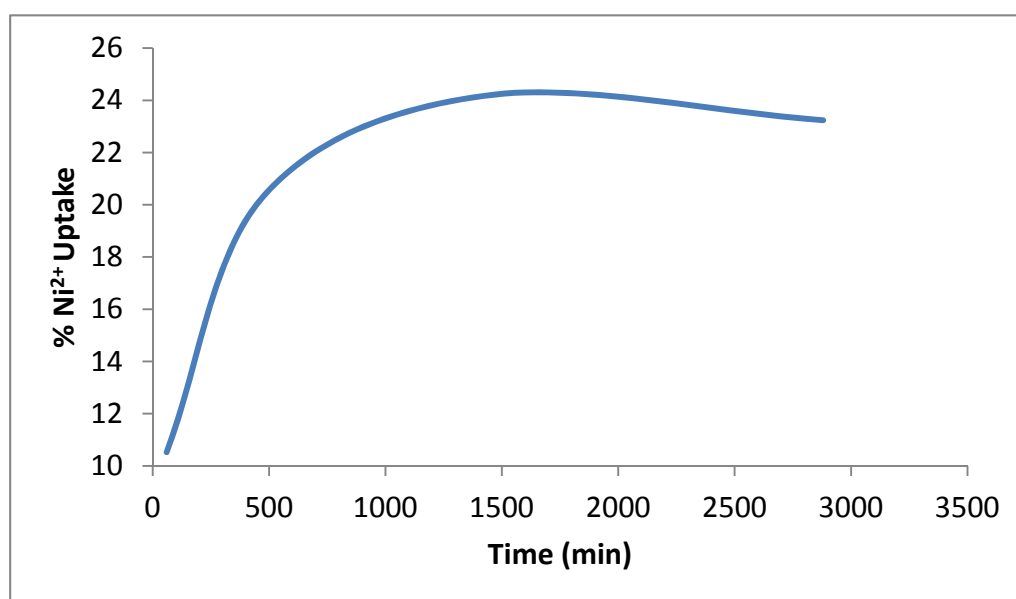
Figure 4.16: Effect of time on the adsorption of Ni (II) on zeolite A
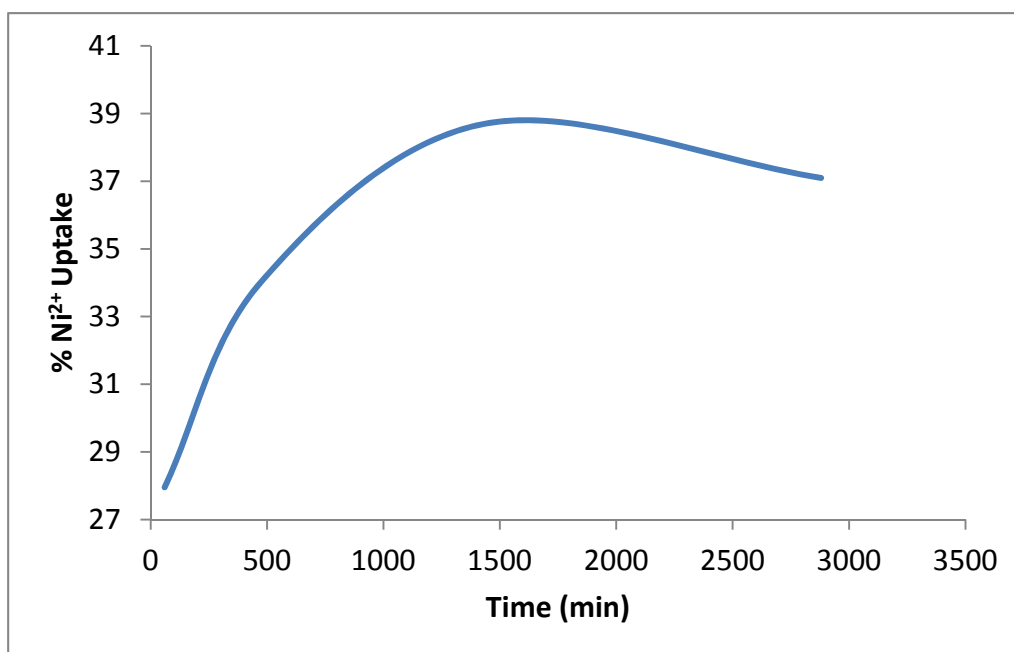
 Figure 4.17: Effect of time on the adsorption of Ni (II) on zeolite X

4.2.3.2. Effect of zeolite dose

The effect of zeolite dosage on the removal of Ni (II) (Figures 4.18 and 4.19), clearly shows an increase in the percentage removal of nickel ions with increasing weight of the zeolite material. This is an expected result because, as the amount of zeolite increased, the available surface area increased, thereby exposing more active sites for the metal ions to exchange. At zeolite dose beyond 0.5 g, the percent removal of Ni^{2+} gradually decreased, which could be as a result of insufficient agitation of the zeolites at zeolite dosage greater than 0.5 g.
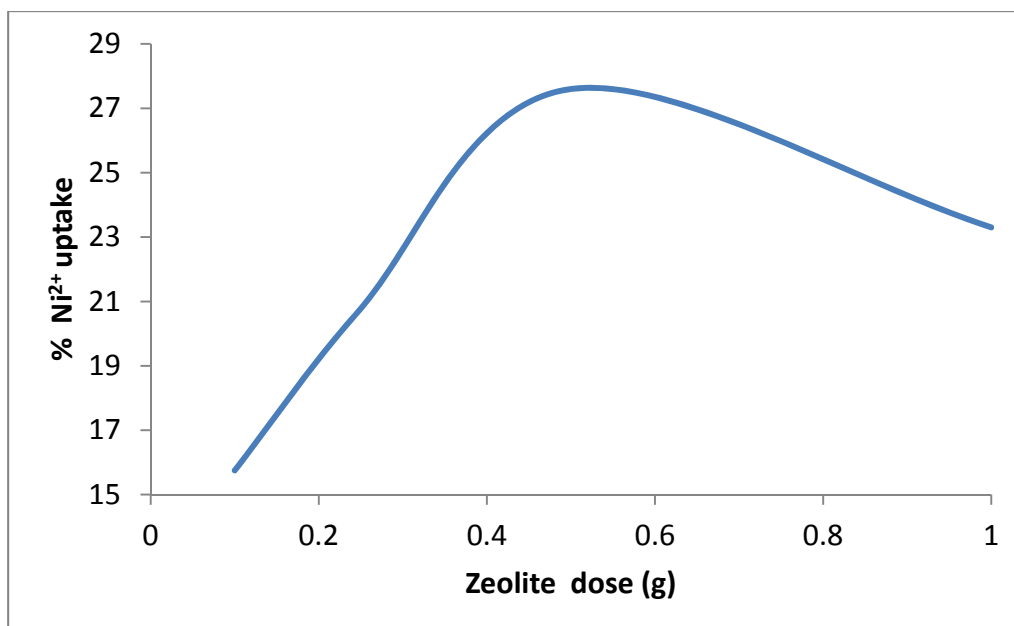
Figure 4.18: Effect of zeolite dose on the adsorption of Ni^{2+} on zeolite A
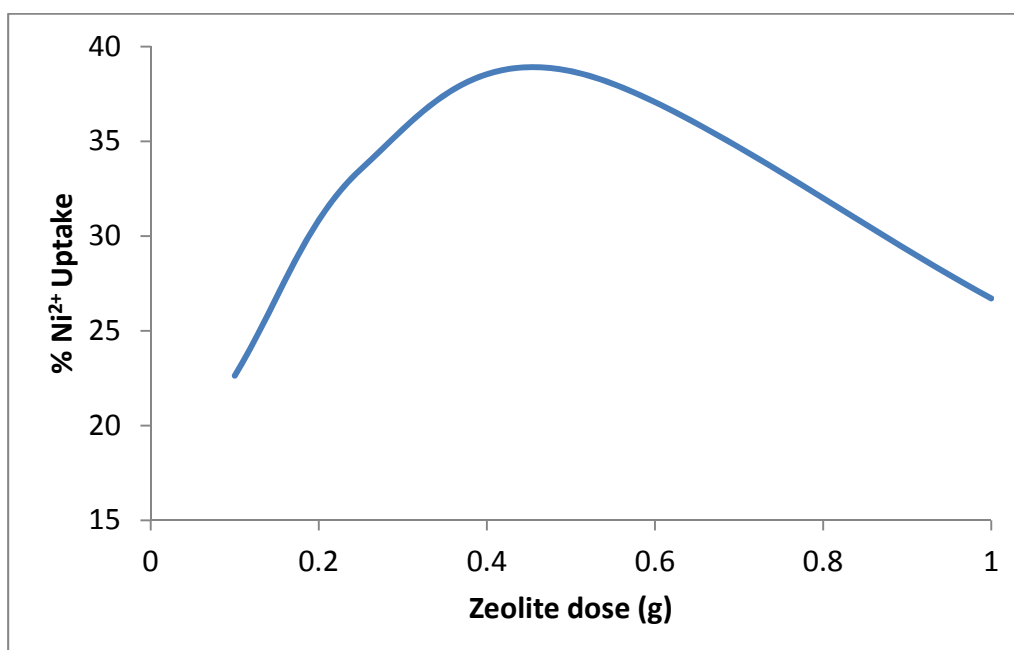
Figure 4.19: Effect of adsorbent dose on the adsorption of Ni (II) on zeolite X

4.2.3.3. Effect of initial concentration

The effect of initial concentration was investigated on the exchange process at a fixed temperature (18 ^{o}C). The experiments were performed at the initial concentrations (0.01 M, 0.05 M and 0.1 M) Ni (II) for both zeolite A and zeolite X. The Ni (II) ion uptake increases

with increasing initial metal ion concentration for both zeolite X and zeolite A. This could be as a result of the increase in concentration gradient which can be said be the driving force. The percent Ni (II) removal on the other hand, decreased with increasing initial metal ion concentration (Figures 4.20 and 4.21). This suggest that at lower concentration, Ni (II) was exchanged very quickly at the exchange sites and further increase in the metal ion concentration only led to the saturation of the zeolite surface since there were no more exchange sites available for the exchange reaction.
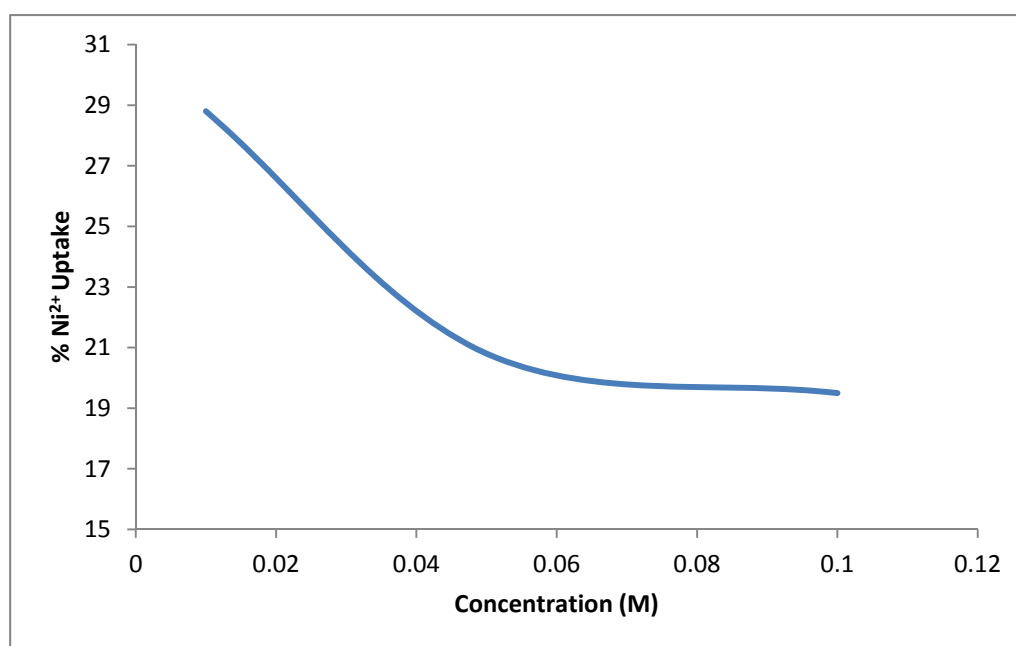
Figure 4.20: Effect of concentration on the adsorption of Ni (II) on zeolite A
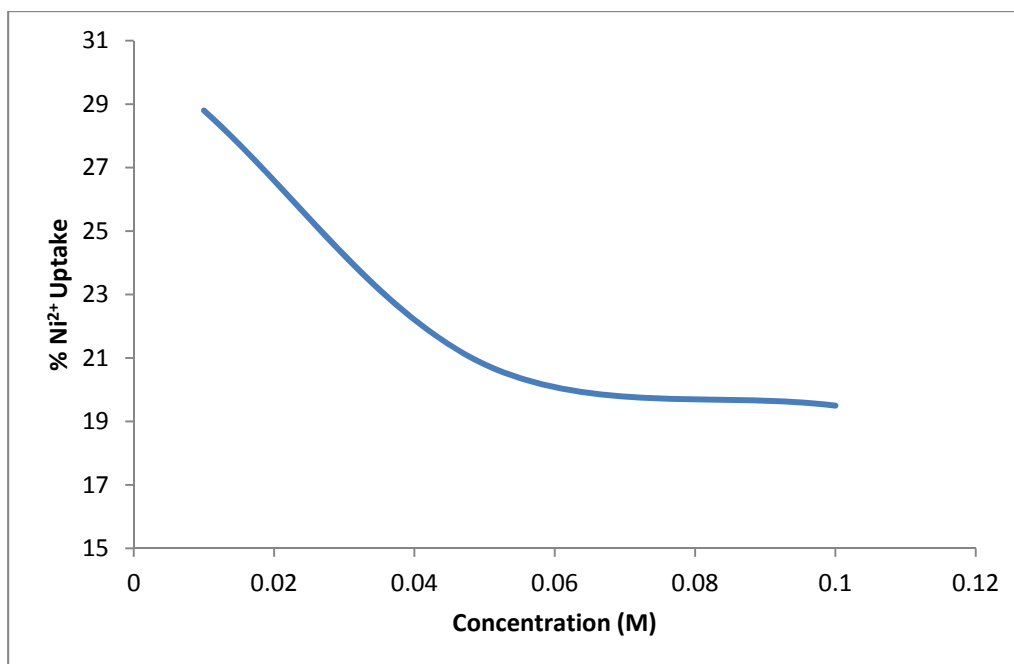
Figure 4.21: Effect of concentration on the adsorption of Ni (II) on zeolite X

4.2.4. Zeolitic exchange with vanadium

The vanadium (IV) solutions just like the nickel (II) solutions were tested for pH before contact with the different zeolites (Table 4.8). The result for the vanadium (IV) exchange with zeolites is as presented in appendix 3.

Table 4.8: pH of vanadium solutions before treatment with zeolites

Concentration (M)	pH
0.010	3.78
0.025	3.57
0.050	3.05
0.075	2.80
0.100	2.64

The highest vanadium (IV) removal was found for zeolite A with % removal of 84 % (appendix 3). Zeolite X also gave good exchange with % removal of over 60 % while zeolite Y was the least efficient at vanadium ion uptake. The vanadium exchange behaviour of these zeolites might also be explained based on their Si/Al ratios and pore sizes. However, considering the size of the vanadium ion (V^{4+}), the most important factor for the high vanadium exchange would be the Si/Al ratio. Hence the high charge imbalance due to a low Si/Al ratio of these zeolites could be responsible for their high activity. The type of vanadium ion present in a solution is very complicated and varies with the pH of the solution from +5 to +2. However for the $VOSO_4.4H_2O$ containing V (IV) it is assumed the oxidation state of V (IV) in the solution was maintained throughout the ion exchange process based on the colour of the (IV) solution (blue).

Concentration was observed to have an effect on the activity of the zeolites. For zeolite A, the activity increases as the concentration increases from 0.01 M to 0.05 M and then decreases as concentration goes higher to 0.1 M. This is an indication that the optimum pH for vanadium (IV) exchange is between pH 3 – 3.7. The result of this study is in agreement with other investigations on vanadium uptake using different exchange materials [48-52]. The uptake of vanadium by these materials were shown to increase with increasing pH and reaches maximum adsorption in the pH range 3-3.5.

The vanadium (IV) ion exchange however, was more challenging compared to that of nickel (II). The vanadium (IV) exchange even though seem to give high percent uptake by the zeolites, had issues associated with it. It was observed that the vanadium (IV) concentrations within the zeolites were more than the metal cations that were needed to balance the anionic charge of the zeolitic framework. This effect known as ''over ion exchange'', could be due to different factors, some of which include; ion exchange with cations other than Na^+ at the exchange sites, hydrolysis of the metal cation etc. The V (IV) due to its charge and small size could easily exchange with the silicon cations that form the framework structure of zeolites or can be hydrolysed leading to an increase in H^+ concentration in solution as presented in equation 4.2.

$$xVO^{2+} +\ \ yH_2O\ \rightleftharpoons (VO)_x\,(OH)_y^{2x-y}\ + xH^+ \hspace{3cm} \text{Equation 4.2}$$
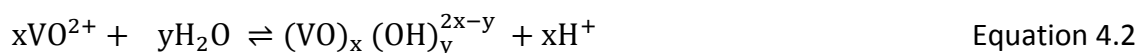
Where, y and x are positive integer numbers. Data analysis in the range 0.001-0.05M concentration of V (IV) suggest the species $(VO)_2\,(OH)_2^{2+}$, with x=2 and y=2 to be the predominant hydrolysis product of VO^{2+} [56]. Other hydrolysis products of VO^{2+} include, $VOOH^+$, $VO(OH)_2$ or $VO_2.H_2O$. The hydrolysed metal cations may have been taken up by the zeolites thus adding up to give the overall metal concentration in the zeolites.

4.2.4.1. PXRD of the vanadium exchanged zeolites

The ICP-OES data for the vanadium (IV) exchange with the zeolites showed a good vanadium uptake > 80 %, the PXRD spectra of the vanadium-zeolites however, showed a structural collapse for the most efficient exchanger (zeolite A and zeolite X) as shown in figures 4.22 and 4.23. The less efficient exchanger (zeolite Y) on the other hand retained its structure. This behaviour might either be because the vanadium in addition to exchanging with Na$^+$ within the zeolite framework also exchanged with silicon species that make up the framework of the zeolites, or it could be due to the high acidity of the vanadium solutions since most zeolites are not stable in acidic conditions[8]. The ability of zeolite Y to retain its structure shows its more stable/resistant to attack compared to zeolites A and X.
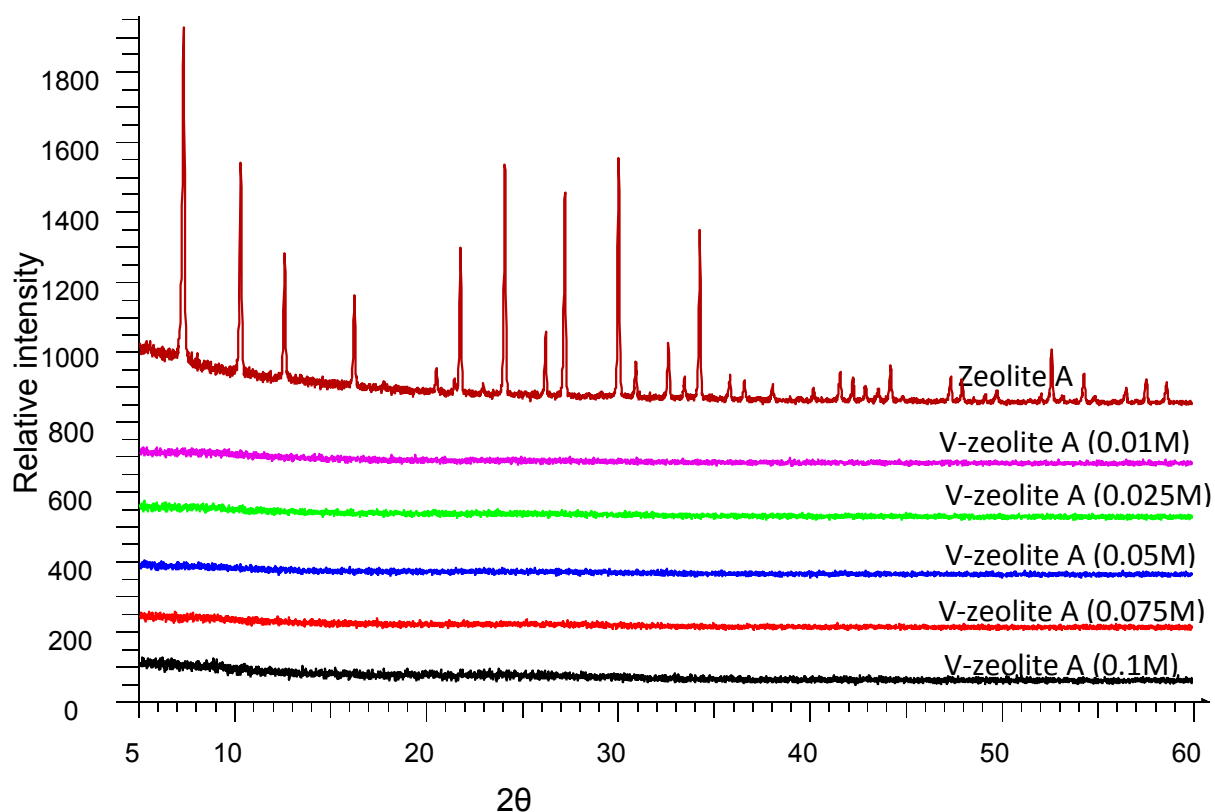
Figure 4.22: PXRD pattern for zeolite A after vanadium ion exchange
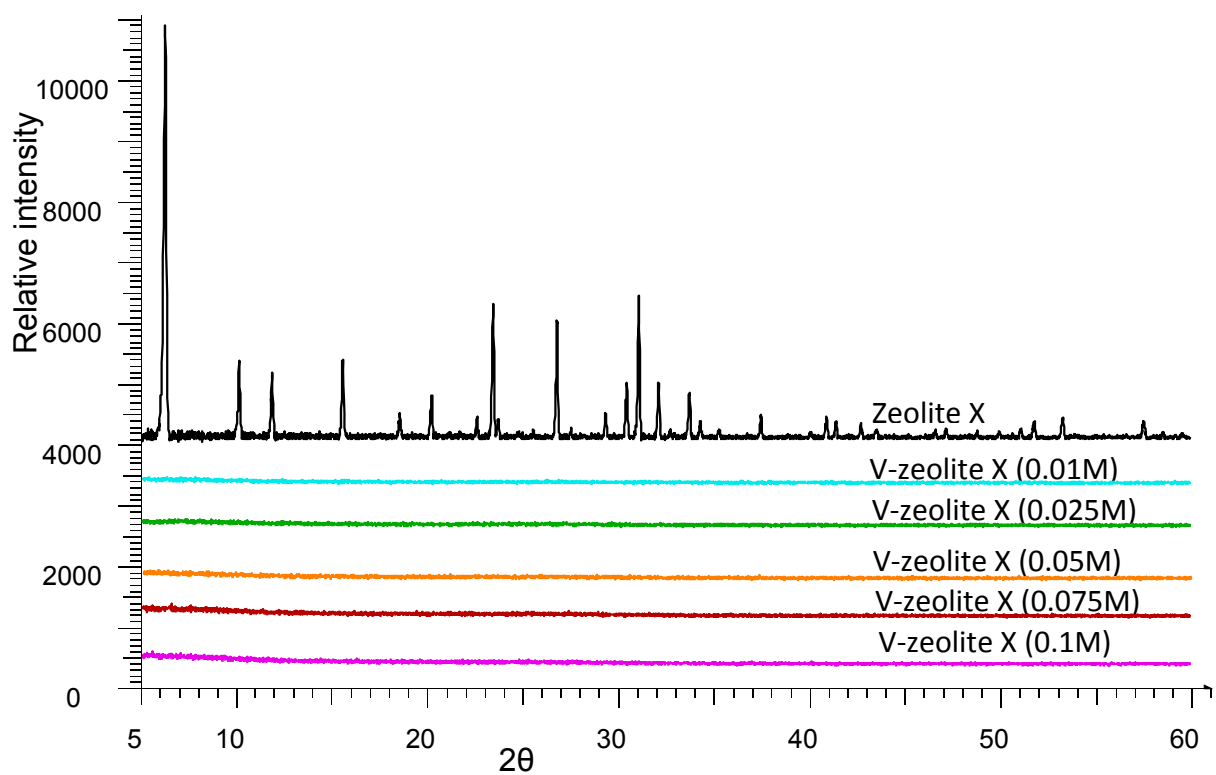
Figure 4.23: PXRD pattern for zeolite X after vanadium ion exchange

4.2.4.2. FTIR

The FTIR spectra of the vanadium exchanged zeolites further shows that the vanadium (IV) exchange had a significant effect on the zeolite framework (figure 4.24). The collapse of absorption bands from the spectra of the vanadium exchanged zeolites as compared to the as synthesised zeolite A clearly shows the destructive effect of vanadium loading on the zeolite.
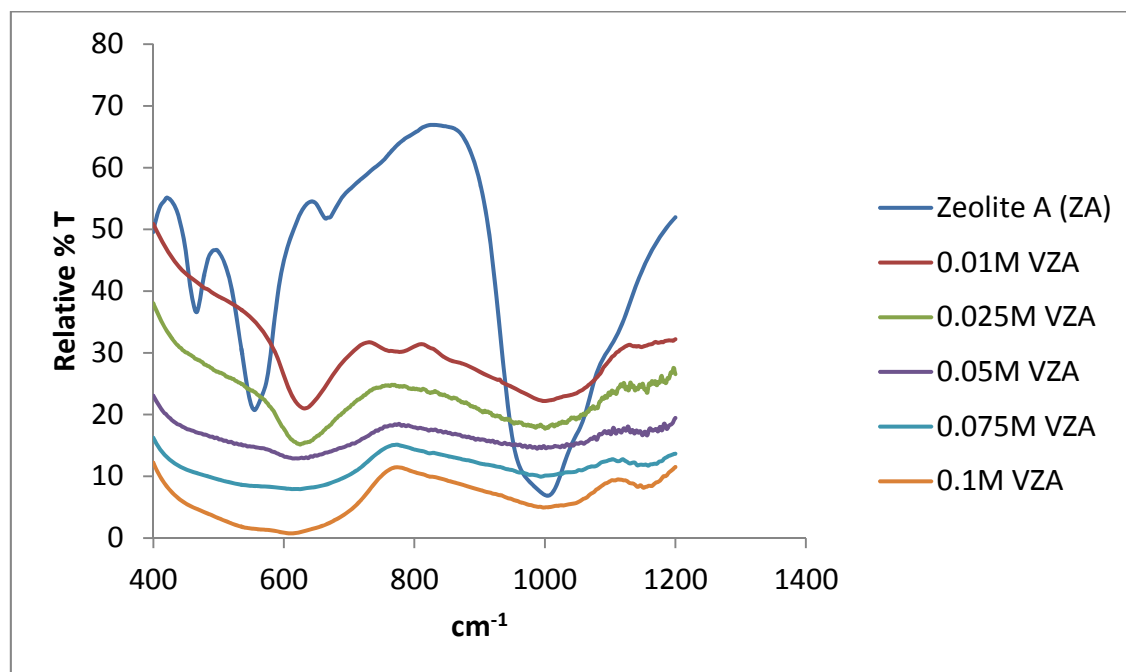
Figure 4.24: The FTIR spectra for vanadium (IV) exchanged zeolites compared to as synthesised zeolite A

4.2.4.3. SEM-SEM

Zeolite A was considered for SEM-EDS analysis since it gave the highest vanadium ion uptake. The SEM-EDS analysis was used to further investigate the effect of ''over ion exchange'' and the possible reasons for the zeolites structural collapse.

The SEM micrograph of zeolite A before and after V^{4+} (0.1 M) exchange showed that the particles differ in size and shape after the exchange (figure 4.25), suggesting that the vanadium ion exchange had a significant effect on the structural framework of the zeolite. Varying the concentration of the vanadium (IV) solution did not show any

significant change in the effect of the metal cation on the zeolite materials (appendix 5).
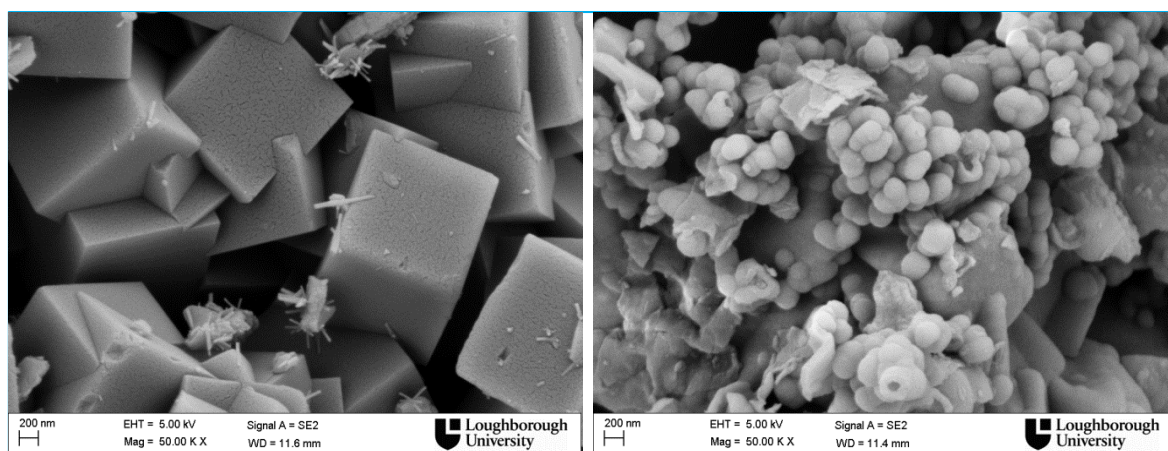
Figure 4.25: SEM micrographs of as synthesised zeolite A and vanadium (IV) exchanged zeolite A

The EDS spectra for zeolite A before and after vanadium (IV) exchange detected vanadium ions in the zeolite (figure 4.26). In addition, the EDS quantified the amount of vanadium (IV) as well as the elemental composition of the zeolite before and after vanadium (IV) exchange (Table 4.10). The elemental composition shows that all the Na^+ within the zeolite were exchanged and in addition, a significant amount of framework silicon ions (77.4 %) were also exchanged by the vanadium ions while the amount of Al ions remained fairly constant. This clearly explains the effect of ''over ion exchange'' and zeolite structural collapse observed for the zeolites after vanadium ion exchange.

Unlike the nickel (II) ion exchange, the data obtained for the V (IV) ion exchange did not show a consistent mole ratio of 4 Na^+ to 1 V (IV) to support the fact that the exchange occurs mostly at the exchange sites of the zeolite.
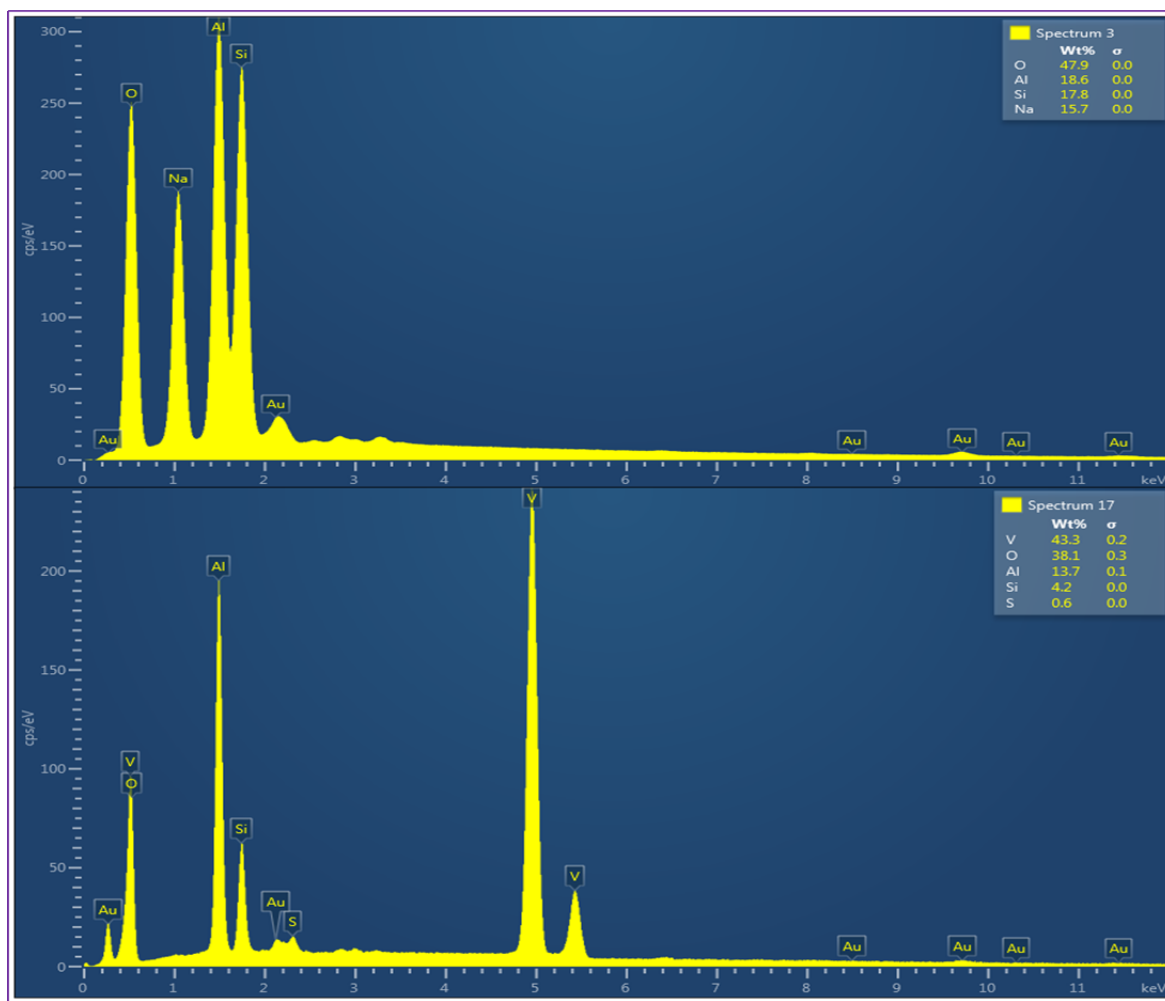
Figure 4.26: EDS spectra of zeolite X with (lower) and without (upper) vanadium ion exchange at (0.01M) concentration

Table 4.4: Elemental composition before and after vanadium ion exchange

Element	Elemental composition (Wt. %)					
	Before V^{4+} exchange	After V^{4+} exchange				
		0.01M	0.025M	0.05M	0.075M	0.1M
O	47.9±0.4	38.1±0.7	45.1±1.5	43.8±1.5	45.0±3	46.5±0.4
Na	17.8±0.9	0.0±0.0	0.0±0.0	0.0±0.0	0.0±0.0	0.0±0.0
Al	15.7±0.5	13.7±1.4	15.0±0.2	14.1±0.1	14.8±0.2	14.1±0.08
Si	18.6±0.8	4.2±0.5	9.1±0.08	11.9±0.2	15.2±0.2	14.7±0.2
V	0.0±0.0	43.3±0.01	29.8±1.3	29.1±1.9	23.8±2.7	23.1±0.7
Na/V	0.0	0.91	1.35	1.35	1.64	1.71

4.2.5. Factors affecting V (IV) uptake by zeolites

4.2.5.1. Effect of time on V (IV) adsorption

The result of the effect of time on V (IV) removal by zeolite A is similar to that observed for the removal of Ni (II) by zeolite A. The initial uptake of V (IV) was rapid and reached equilibrium at contact time of 24 h, after which the rate of V (IV) removal gradually decreased. The uptake of V (IV) for zeolite A at equilibrium was 89 %. Therefore, considering technical and economic aspects, a contact time of 24 h is the best time for the removal of V (IV) from aqueous solution by zeolite A.
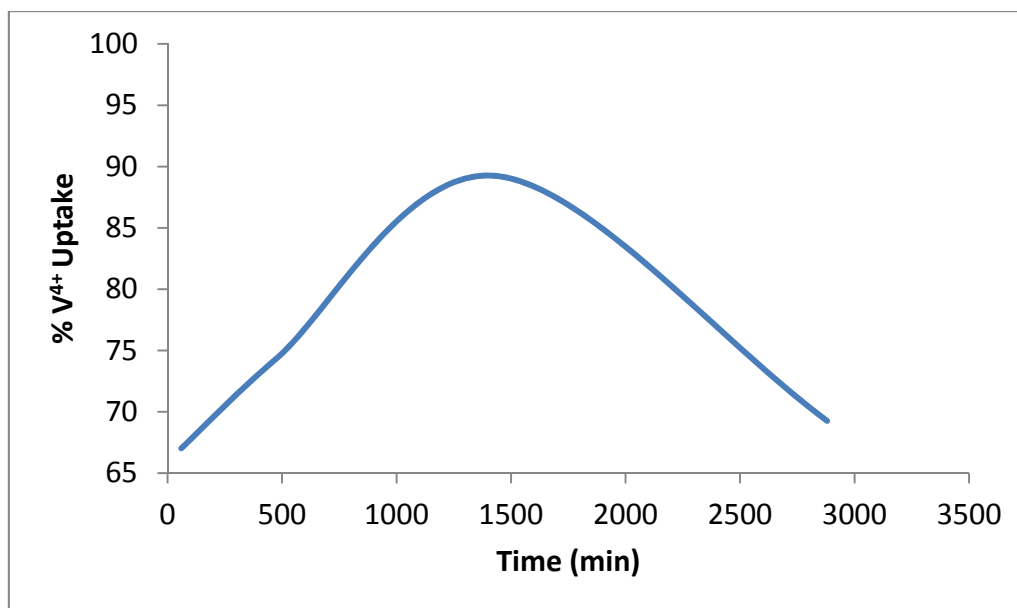
Figure 4.27: Effect of contact time on the adsorption of V (IV) on zeolite A

4.2.5.2. Effect of zeolite dose on V (IV) adsorption

The effect of zeolite dosage on the removal of V (IV) shows that the percentage removal of V (IV) increased with increasing weight of the zeolite (Figure 4.28). This is similar to the result obtained for Ni (II) and can be explained by the increased surface area available, thereby exposing more exchange sites for the vanadium (IV) exchange.
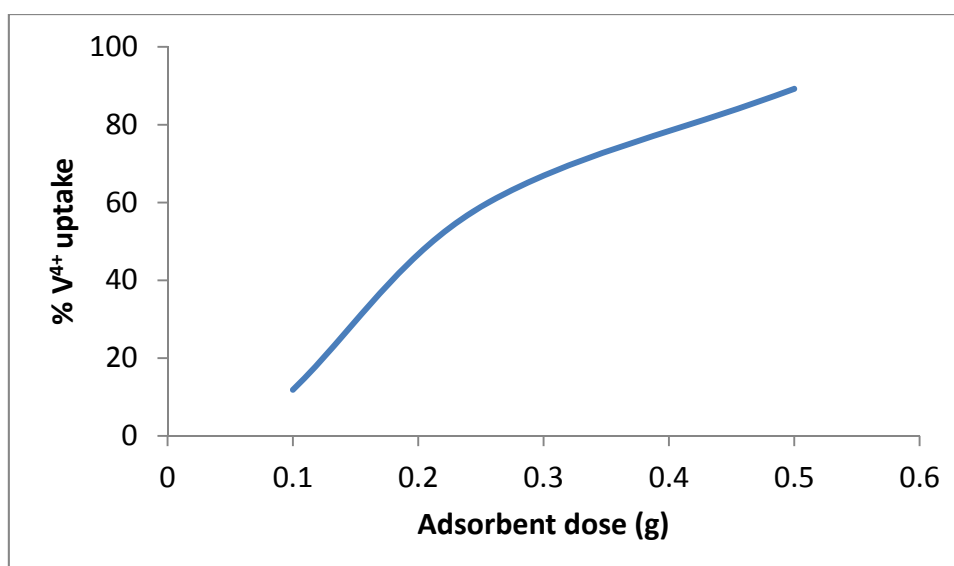
Figure 4.28: Effect of zeolite dose on the adsorption of V (IV) on zeolite A

4.2.5.3. Effect of initial concentration on V (IV) adsorption

The effect of initial concentration was investigated on the sorption process at a fixed temperature (18°C). The experiments were performed at the initial concentrations of 0.01 M, 0.05 M and 0.1 M V (IV) at 18°C for zeolite A. The initial uptake of the V (IV) ions increased and then decreased sharply as the concentration increased for zeolite A (Figure 4.29). The results for the effect of initial concentration for V (IV) ions shows that beyond the concentration of 0.05 M, the amount of V (IV) ions removed, decreases indicating a depletion of active sites available for ion exchange.
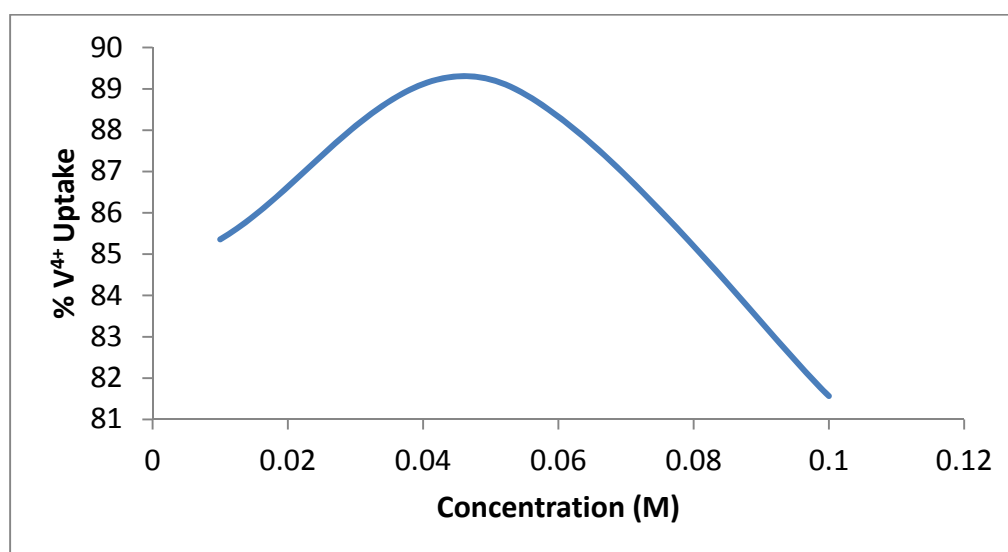
Figure 4.29: Effect of concentration on the adsorption of V (IV) on zeolite A

4.2.6. Selective removal of metal ions from mix metal solution

The selectivity of the zeolites for the different metal ions was investigated from a mix metal solution containing five different metal cations (Ni (II), V (IV), Zn (II), Fe (II) and Cu (II)). The selective metal removal studies shows a good uptake of the all the metal cations by the zeolites (Figure 4.30). The V (IV) and Fe (II) removal were observed to be higher than Ni (II) and Cu (II) while that for Zn (II) was much lower. This result suggest that Fe (II) could be a competing ion in the selective zeolitic removal of the Ni (II) and V(IV) from solution and hence from crude oil. It was however, observed that the metal cations within the zeolites is more than that needed to balance the anionic charge on the zeolitic framework.
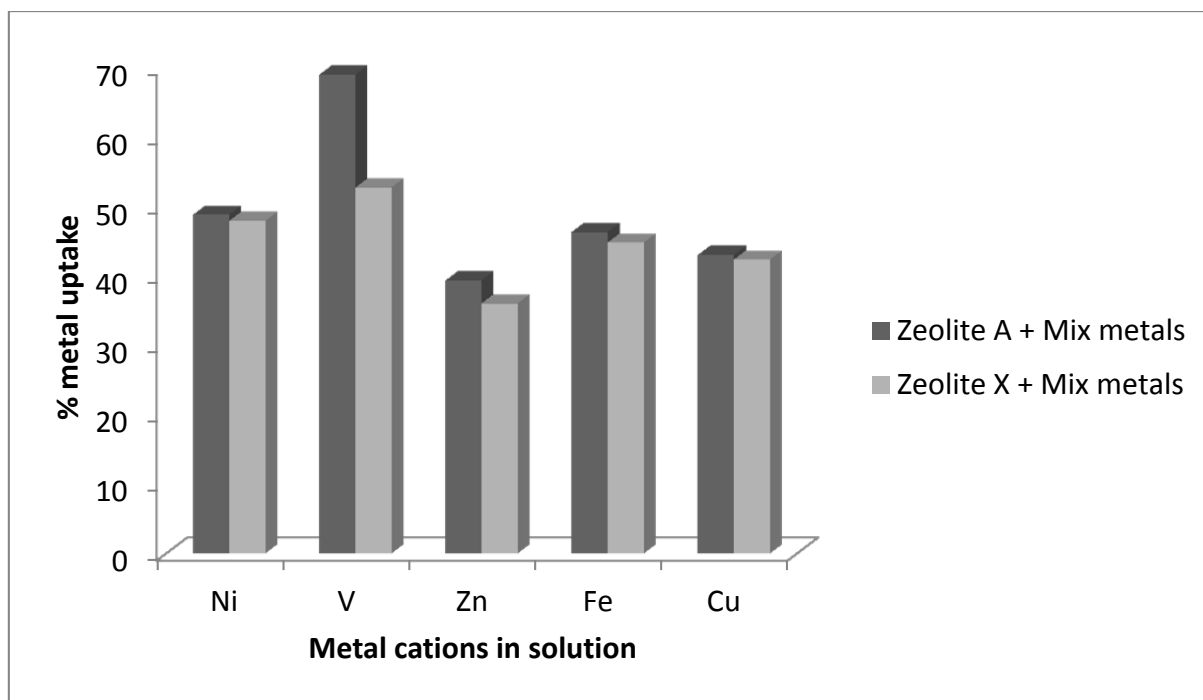
Figure 4.30: Selective removal of metal ions from Mix-metals system

4.2.6.1. PRXD Characterisation of zeolites after selective metal uptake

The zeolites were characterised after the selective metal removal using PXRD. The PXRD patterns obtained (figure 4.31-4.32) showed little or no shift in the patterns but rather a decreased intensity of the reflections compared to that of the parent zeolite. This may be an evidence that metal ion exchange had occurred or degradation of the zeolites as evidenced by a reduction in crystallinity due to the pH of the solution.
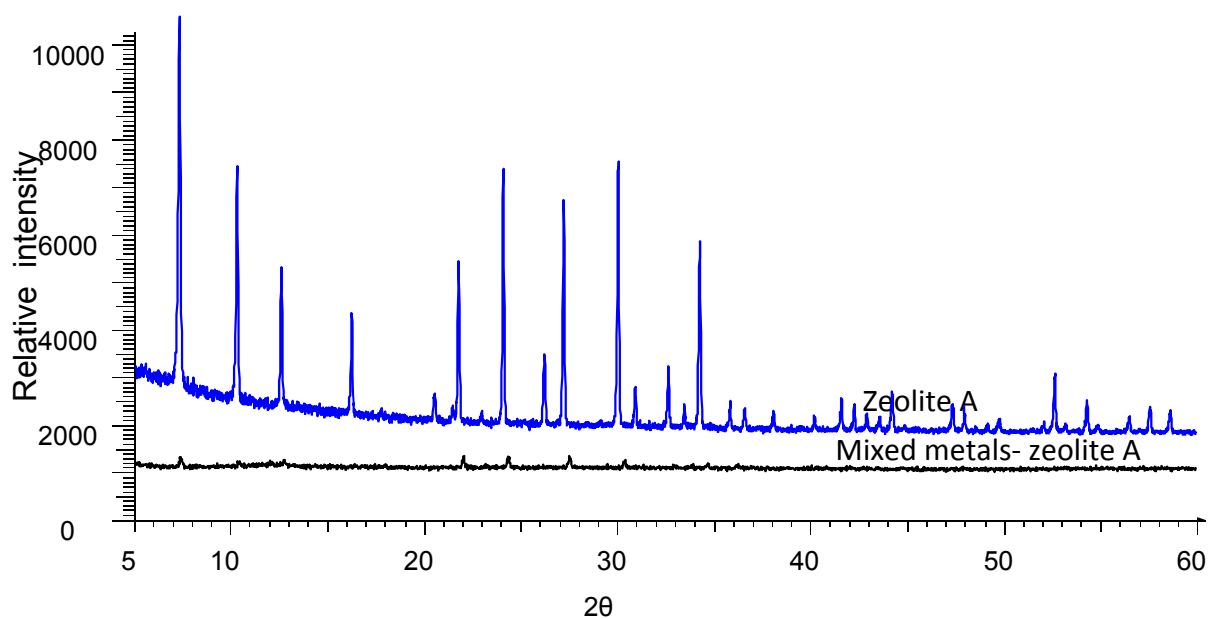
Figure 4.31: PXRD patterns for mixed metal-zeolite A compared with parent zeolite A
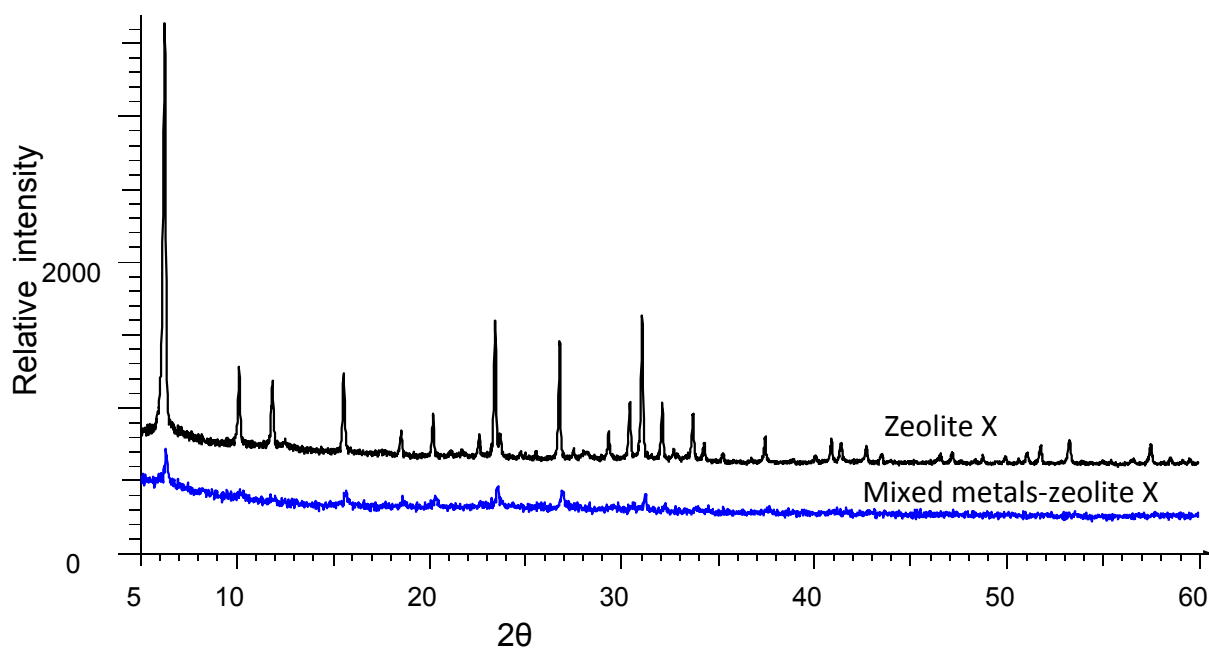
Figure 4.32: PXRD patterns for mixed metals-zeolite X compared with parent zeolite X

4.3. Conclusion

The nickel and vanadium ion exchange carried out and reported in this chapter showed zeolite X to be effective ion-exchanger for nickel (II) from aqueous solution. Zeolite A and X though recorded high percent removal for V (IV), cannot be said to be effective at removing the metal ions from solution as the materials collapse after the V (IV) ion exchange. One of the objectives of this research work is to identify zeolitic materials with high exchange capacity and selectivity for V (IV) and Ni (II), resistance to poisoning and thermal and chemical stability. Thus for the zeolitic materials considered in this work, zeolite X is shown to be effective not only at exchanging with Ni (II) from solution, but also show the potential to be regenerated or recycled after the ion exchange process. Zeolite A and X on the other hand did not have the potential for regeneration after V (IV) exchange so could not be termed ''effective'' since their zeolitic structures were not maintained after the V (IV) exchange. However, if the vanadium (IV) solution is buffered and the of pH solution controlled, the vanadium (IV) exchange with the zeolites could be effective with high V^{4+} uptake as well as maintaining the zeolite's framework structure. K- and Li-zeolites prepared, showed little or no improvement at Ni (II) ions uptake at higher nickel (II) concentration (0.1M), however at lower concentration (0.01M), they showed a significant increase in the nickel (II) exchange from solution. Thus at lower concentrations (0.01M) of Ni (II), K- and Li-zeolites could be used to remove Ni (II) from solution at higher efficiency compared to the parent zeolite. Zeolite Y was not very effective at removing either of the metal ions studied here.

References

1. C.P.C. Poon, in: H. Mislin, O. Ravera (Eds.), Cadmium in the Environment, Birkha User, Basel, Switzerland, 1986.

2. V. Flores, C. Cabassud, Desalination, 1999, 126, 101–108.

3. J.W. Patterson, Industrial Wastewater Treatment Technology, Butterworth Publishers, Stoneham, MA, 1985.

4. M. Amini, H. Younesi, N. Bahramifar, Colloids Surf. A, 2009, 337, 67–73.

5. S. Hao, Y. Zhong, F. Pepe, W. Zhu, Chem. Eng. J., 2012, 189–190, 160–167.

6. E. Maliou, M. Malamis, P.O. Sakellarides, Water Sci. Technol., 1992, 25, 133–138.

7. M.A.S.D. Barros, E.A. Silva, P.A. Arroyo, C.R.G. Tavares, R.M. Schneider, M. Suszek, E.F. Sousa-Aguiar, Chem. Eng. Sci., 2004, 59, 5959–5966.

8. A. Dyer, An Introduction to Zeolite Molecular Sieves, John Wiley & Sons, Chichester, 1988.

9. R. Szostak, Molecular sieves, Principles of Synthesis and Identification, Van Nostrand Reinold, New York, 1989.

10. F. A. Mumpton, L. B. Sand, F. A. Mumpton, A new industrial mineral commodity. Natural Zeolites: Occurrence, Properties, Use, Pergamon Press, New York, USA, 1978.

11. D. W. Breck, Zeolite Molecular Sieves, Structure Chemistry and Use, Wiley, New York, 1974.

12. H. Van Bekkum, E. M. Flanigen, P. A. Jacobs, J. C. Jansen, Introduction to zeolite science and practice. Studies in Surface Science and Catalysis, Elsevier Science Publishers, Amsterdam, 2001.

13. M. I. Occelli and H. Kessler, Synthesis of Porous Materials: Zeolites, Clays and Nanostructures, CRC Press, New York, 1997.

14. R. M. Barrer, Zeolites, 1981, 1, 130.

15. J. B. Nagy, P. Bodart, I. Hannus, I. Kiricsi, Synthesis, Characterization and Use of Zeolitic Microporous Materials., DecaGen publishers Ltd, Szeged, Hungary, 1998.

16. G. Blanchard, M. Maunaye, G. Martin, Water Res., 1984, 18, 1501–1507.

17. M.J. Zamzov, J.E. Murphy, Water Sci. Technol., 1992, 25 133–138.

18. S. Komarneni, Nucl. Chem. Waste Manage., 1985, 5, 247–250.

19. M.J. Zamzov, B.R. Eichbaum, K.R. Sandgren, D.E. Shanks, Sep. Sci. Technol., 1990, 25, 1555–1569.

20. E. Passaglia, P. Miselli, Mater. Eng., 1994, 5, 357–374.

21. A. Shanableh, A. Kharabsheh, J. Hazard. Mater., 1996, 42, 207–217.

22. M. Pansini, Miner. Deposita, 1996, 31, 563–575.

23. D.H. Lee, H. Moon, Korean J. Chem. Eng., 2001, 18 (2), 247– 256.

24. M.J.T. Carrondo, J.N. Lester, R. Perry, J. Water Pollut. Control. Fed., 1981, 53, 344–351.

25. H.E. Allen, S.H. Cho, T.A. Neubecker, Water Res., 1983, 17, 1871–1879.

26. E.A. Daniels, M. Puri, J. Radioanal. Nucl. Chem. Lett., 1985, 94, 17–24.

27. A. Dyer, J.K. Abou-Jamous, J. Radioanal. Nucl. Chem., 1994, 183, 225–233.

28. A. Dyer, T. Shaheen, Sci. Total Environ., 1995, 173/174, 301–311.

29. G. Patane, S. Di Pasquale, F. Corigliano, L. Mavilia, Annal. Chimi., 1996, 8, 87– 98.

30. B. Biškup, B. Suboti´c, Stud. Surf. Sci. Catal., 1999, 125, 745–752.

31. B. Biškup, B. Suboti´c, Phys. Chem. Chem. Phys., 2000, 2, 4728–4733.

32. M.A. Keane, Colloids Surf. A: Physicochem. Eng. Aspects, 1998, 138, 11–20.

33. D.W. Breck, Zeolite Molecular Sieves: Structure, Chemistry and Use, John Wiley & Sons, New York, 1974.

34. M.A.S.D. Barros, P.A. Arroyo, E. Sousa-Aguiar, C.R.G. Tavares, Adsorption, 2004, 10, 227–235.

35. J.S. Kim, M.A. Keane, J. Chem. Technol. Biotechnol., 2002, 77, 633–640.

36. I.C. Ostroski, C.E. Borba, E.A. Silva, P.A. Arroyo, R. Guirardello, M.A.S.D. Barros, J. Chem. Eng. Data, 2011, 56, 375–382.

37. S. Malamisa, E. Katsoua, J.Hazard. Mater. 2013, 252– 253, 428 – 461.

38. S. Bendenia, I. Batonneau-Gener, J.D. Comparot, K. Marouf-Khelifa, H. Hammoudi, A. Khelifa, Micropor. Mesopor. Mater., 2012, 159, 111-118.

39. D. Bae, K. Seff, Micropor. Mesopor. Mater., 2000, 40, 219-232.

40. I. Rodrıguez-Iznaga, V. Petranovskii, G. Rodrıguez-Fuentes, J. Environ. Chem. Eng. 2014, 2, 1221–1227.

41. N. Rajic, D. Stojakovic, M. Jovanovic, N. Z. Logar, M. Mazaj, V. Kaucic, Appl. Surf. Sci. 2010, 257, 1524–1532.

42. M.A. Zanjanchi, A. Ebrahimian, J. Mol. Struc. 2004, 693, 211–216

43. C. M. Pascual, A. Argüelles, M. Leoni, S. A. Khainakov, J. A. Blanco, Appl. Clay Sci. 2014, 91–92, 79–86.

44. N. Dizge, B. Keskinler, H. Barlas, J. Hazard. Mater., 2009, 167, 915–926.

45. N. H. Shaidan, U. Eldemerdash, S. Awad, J. Taiwan Inst. Chem. Eng. 2012, 43, 40–45.

46. B. Alyüz, S.Veli, J. Hazard. Mater. 2009, 167, 482–488.

47. E.D. Vega, J.C. Pedregosa, G.E. Narda, P.J. Morando, Water Res., 2003, 37, 1776–1782.

48. M. Jansson-Charrier, E. Guibal, J. Roussy, B. Delanghe, P. LeCloirec, Water Res., 1996, 30, 465-75.

49. B. Wehrli, W. Stumm, Langmuir, 1988, 4, 753.

50. A. Naeem, P. Westerhoff, S. Mustafa, Water Res., 2007, 41, 1596 – 1602.

51. C. F. Baes and R. E. Mesmer, The Hydrolysis of Cations, John Wiley, New York, 1976.

52. C. l. Peacock and D. M. Sherman, Geochimica et Cosmochimica Acta, 2004, 68 (8), 1723–1733.

53. D. W. Breck, Zeolite molecular sieves, John Wiley & Sons, New York, 1974, pg. 93-94.

54. D.W. Breck, Zeolite Molecular Sieves: Structure, Chemistry and Use, John Wiley & Sons, Inc., New York, 1974, pg. 657.

55. H. Sherry, J. Phys. Chem., 1966, 70, 1158.

56. A. Komura, M. Hayashi and H. Imanaga, Bull. Chem. Soc. Jpn., 1977, 50 (11), 2927-2931.

Chapter 5: Syntheses and Characterisation, metal ion adsorption studies of ligand modified zeolite Y and zeolites adsorption of nickel from Ni-tetraphenylporphyrin

5.0. Introduction

Zeolites are well-known for their adsorption and ion exchange properties. In addition to these properties, zeolites have the ability to act as inorganic supports [1-5]. Dealuminated zeolites like; zeolite Y, ZSM-5, clinoptilolite etc. with relatively high Si/Al ratio might not be considered as good ion exchangers, however due to their high porosity, surface area and Si/Al ratio, they are able to make available high concentration of surface hydroxyl groups that can serve as adsorption sites [6-7]. These zeolites can thus be used as inorganic supports to attach organic ligands which can then be used for the irreversible immobilisation of metal ions [8-9]. Surface functionalised framework materials have been successfully used to selectively immobilise metal ions from solutions [10-15]. These studies include; the immobilisation of Zn (II), Cd (II), Ni (II), Cu (II), Fe (III), and Pb (IV), from solutions of single salts and their mixture using ligand grafted clay mineral composites [10], selective removal of Hg (II), from aqueous solution using mesoporous silica gel modified with 2-aminothiazole [11] and the immobilisation of Cu (II), from aqueous solution using the amine-functionalized mesoporous silica (AMS) [12]. Others include the selective adsorption of Cu (II), Cd (II), and Pb (II), from single metal solutions using succinylated mercerized cellulose modified with triethylene- tetramine [13], adsorption of Pb (II), and Cu (II), onto grafted silica [14] and adsorption studies of Cd (II), Cu (II), Ni (II), Pb (II), and Zn (II), onto modified silica gel [15]. Much of the work and successes is reported on mesoporous compared to microporous materials such as zeolites, the reason that microporous materials feature rarely in this field is that the amount of material which can be grafted is relatively small, although roughening experiments with mild acids have shown significant improvements in grafting levels [16]. For the purpose of this research, the quantity of target ions in oil is so low that using materials which are more easy characterised and prepared at lower cost has significant advantages as the temperatures used in oil processing are challenging for the mesoporous counterparts with lower thermal stability. The present chapter reports on the immobilisation of metal ions from aqueous solution using ligand grafted zeolite Y as compared to the parent zeolites Y. Amongst the zeolites considered in this work (zeolite A, X, Y, sodalites); zeolite Y had a higher Si/Al ratio thus a lower exchange capacity. For this

reason, zeolite Y was chosen for the grafting experiment with the aim of improving its metal ions uptake from solution and hence from crude oil as compared to the parent zeolite Y.

This chapter also reports the use of porphyrin containing nickel cations as a model compound to mimic the extraction and removal of metal ions from crude oil. As described in chapter 1, the ions in crude oil are associated with the asphaltene and part of the challenge in this work is the point at which these ions are liberated from these materials and the ability to remove them before damage occurs to the catalysts. Amongst the model compounds that have been in use for adsorption studies, tetraphenylporphyrin is one of the most commonly used in the oil industry as the mimic for the hydrodemetallation process (HDM) [17] since the materials found in the oil are often described as 'porphyrin-like'. Reports have shown that in the presence of sulphided catalysts, nickel - 5, 10, 15, 20 - tetraphenylporphyrin (Ni-TPP), vanadyl-5, 10, 15, 20 - tetraphenylporphyrin (VO-TPP) and analogues thereof demetallate through a reversible sequential mechanism via hydrogenated intermediates[17-20]. The mechanism of the reaction suggests a link to the porphyrin molecule and is less dependent on the applied catalyst and its chemical state (i.e. sulphided, reduced, or oxidic) [21-23]. Investigations into the thermal degradation of H_2-TPP, Ni-TPP, VO-TPP, Ni-OEP and mixtures of petroporphyrins in refluxing 1-methylnaphthalene at 239.85 ^{o}C in the presence of H_2 and H_2S showed that, with only H_2 or H_2S little or no hydrogenated metalloporphyrins were found whereas in the presence of both H_2 and H_2S, traces of hydrogenated metalloporphyrins, porphyrin type species and polypyrrolics were found [24]. Autoclave experiments at 350 ^{o}C and 400 ^{o}C were shown to give a significant conversion of the metalloporphyrins to metallochlorins, however in the presence of CoMo/Al_2O_3 catalyst, although the rate of reaction was enhanced greatly, the total Ni or V content of the reaction mixtures remained relatively constant. Only at elevated pressures (7MPa) and temperatures above 200 ^{o}C in the presence of a sulphided CoMo/Al_2O_3 catalyst that demetallation occurred [24]. Little attention is given to the use of hydrogen donor solvents for the hydroconversion of Ni-TPP to investigate the removal of metal ions from porphyrinic fractions by zeolites. Thus this chapter, reports the use of hydrogen donor solvent for the dissolution of a porphyrinic model compound (Ni-TPP) and subsequent removal of Ni (II) by zeolites.

This chapter is divided into two parts; part I reports the synthesis of ligand [3-aminopropyltriethoxysilane (APTES)] grafted zeolite Y ($Na_{54.91}Al_{56}Si_{136}O_{384}.246.5H_2O$) and the effectiveness of using the grafted zeolite Y in removing metal ions from solution as compared to the parent zeolite Y. Part II covers the synthesis and hydroconversion of Ni-TPP using hydrogen donor solvents and subsequent removal of the nickel (II) metal ion from the system by use solvent systems/zeolites.

PART I

5.1. Ligand modified zeolite Y

The ligand attachment on zeolite Y was carried out as shown by the schematic diagram in figure 5.1. The ligand modification was carried out in three different solvents (hexane, toluene and acetone) in accordance with procedure described by Mitchell, Bonilla and Pérez-Ramírez [25] with slight changes in reaction conditions.
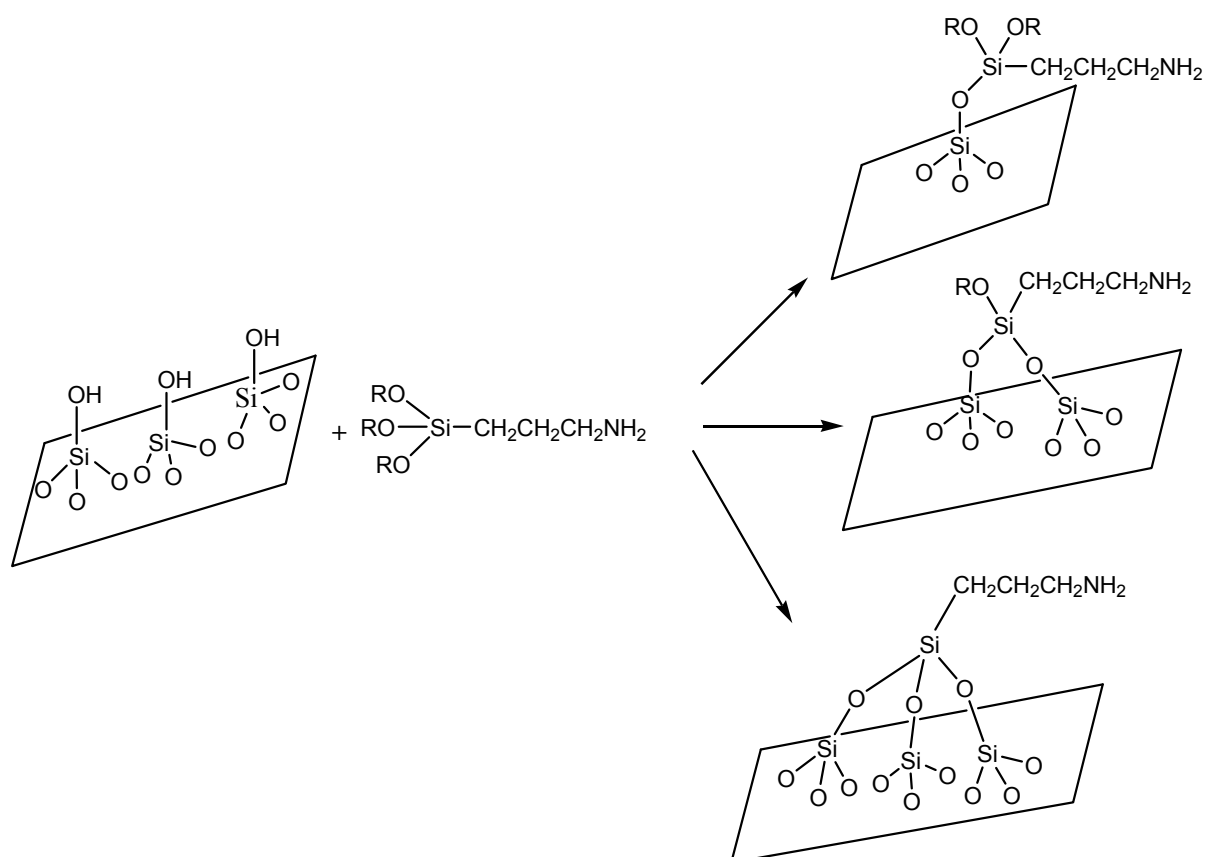

Figure 5.1: Schematic representation of ligand attachment on zeolites surfaces

5.1.1. Experimental

5.1.1.1. Synthesis of ligand grafted zeolites

5 g of zeolite Y was converted to the protonic form by exchanging with 0.1M NH_4NO_3 solution and heating the product at 350 ^{o}C to drive off NH_3 leaving behind H^+. Exactly 2.5 g (1.455 x 10^{-4} moles) of the protonic zeolite Y was now suspended in 40 mL of the appropriate solvent in a round bottom flask and stirred under reflux for 1 h at 40 ^{o}C. 6 mL (2.568 x 10^{-2} moles) of APTES was added drop wise to the mixture under stirring using a dropping pipette. The mixture was then refluxed for 24 h at 40 ^{o}C. Once the reaction was complete, the functionalized zeolite Y was filtered washed with the appropriate solvent followed by distilled water and dried at 80 ^{o}C overnight.

5.2.1.2. Nickel uptake by modified zeolites

Nickel (II) cation uptake by the modified zeolite Y was investigated by treating the modified zeolites with nickel (II) solution at three different concentrations (0.01 M, 0.05 M, and 0.1 M) of 300 mL each, using a roller mixer. After equilibration, the samples were removed, filtered by gravity through fluted filter paper and the mixing bottles washed twice with (50 mL) distilled water through the filter. The zeolite material was then dried overnight at 80 ^{o}C and characterised.

5.2.1.3. Comparison of the selective removal of metal ions from mix metal solution by zeolites

The selective removal of metal ions by grafted zeolite was carried out using a similar procedure as that reported for Ni (II) ions in chapter 4. A solution containing a mixture of five metal cations (Ni (II), V (IV), Zn (II), Fe (II), and Cu (II)), where each metal ion had concentration of 0.05M was prepared and ion exchange carried out with the grafted zeolite Y. 10 mL of 0.05 M solutions each of the Ni (II), V (IV), Zn (II), Fe (II), and Cu (II) were measured into polyethylene bottles containing 0.5 g each of the zeolites and left to equilibrate on the roller mixer for 24 h. This was again done in triplicate. The mixture was filtered after equilibration for 24 h, washed and dried overnight at 80 ^{o}C. Characterisation of the solid product was carried out using PXRD while the amounts of cations remaining in solution were determined by ICP-OES.

5.1.2. Results and discussion

5.1.2.1. Characterization of ligand modified zeolites

The ligand modified zeolites were characterized using; elemental analysis (CHN), powder X-ray diffraction (PXRD), Solid State NMR (SSNMR), Fourier Transformed Infrared (FTIR) spectroscopy and Thermogravimetric analysis (TGA).

5.1.2.1.1. Elemental Analysis (CHN)

The CHN analysis of the modified zeolites showed that the highest loading of the ligand on the zeolite was found for hexane, closely followed by toluene. The ligand loading for acetone was significantly lower (Table 5.1). This indicates that solvent polarity plays an important role in the successful grafting of ligands on porous inorganic materials. Less polar solvents are more effective at attaching organic ligands on porous inorganic surfaces. The high % C, % H and % N for zeolite Y after the ligand grafting indicates some level of attachment on the zeolite material.

Table 5.1: Elemental analysis of the modified zeolites

Zeolites	Hexane			Toluene			Acetone		
	% C	% H	% N	% C	% H	% N	% C	% H	% N
Y $(Na_{54.91}Al_{56}Si_{136}O_{384}.$ $246.5H_2O)$	5.08	2.11	1.82	4.97	2.24	1.64	1.52	1.89	0.0

5.1.2.1.2. Powder X-ray diffraction (PXRD)

PXRD data of the grafted zeolite Y did not differ significantly from that of the parent zeolite Y. This could be due to the small amount of ligand loading on the zeolite meaning that there is no ordered long range structure. No crystalline impurities were formed. The only observed scattering was that for zeolite Y; thus the data (figure 5.2) compared against the ICDD database for the theoretical pattern for the phase zeolite Y (01-070-4285, $Na_{54.91}Al_{56}Si_{136}O_{384}.$ $246.5H_2O)$ clearly suggest that the zeolite framework structure is kept intact after the modification. This is in agreement with earlier investigations with functionalised mesoporous materials [25, 26].
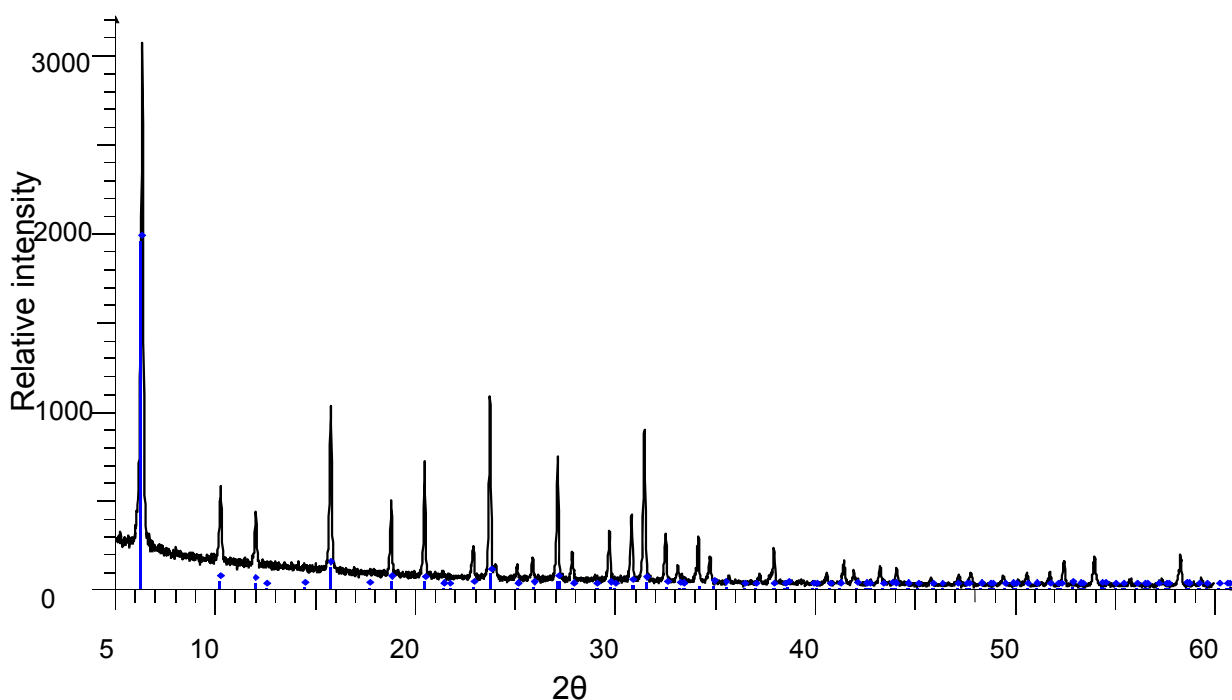
Figure 5.2: PXRD of the modified zeolite Y compared against the ICDD database

5.1.2.1.3. Solid State NMR (SSNMR)

The ^{29}Si MAS NMR spectrum of the ligand grafted zeolites Y is shown in figure 5.3. The ^{29}Si MAS NMR spectrum of zeolites is known to show up to five resonances (-105)-(-107) = Q^4, (-95)-(-105) = Q^3, (-88)-(-95) = Q^2, (-86)-(-92) = Q^1, (-80)-(-86) = Q^0 depending on the chemical shift ranges (ppm) of the silicon environment in the zeolite[27-29]. The cross polarisation (CP) spectrum for zeolite Y following the grafting (figure 5.3) clearly shows additional signal at about -50 and -60 besides the possible signals at Q^2, Q^3 and Q^4. The additional signals correspond to T^2 = [Si (OSi) $_2$ (OH) R] and T^3 = [Si (OSi) $_3$ R] where R= (CH$_2$)$_3$ NH $_2$ [28,30]. The signal with the highest intensity (T^3) is an indication that most of the ligand molecules are covalently bonded to the zeolite Y by tridentate bonds (figure 5.1 insertion c). This result is in good agreement with earlier studies of inorganic-organic hybrids between ligand and vermiculite clay [30].

The ^{13}C CP/MAS NMR spectrum for the ligand loaded zeolite Y is as presented in figure 5.4. The CP/MAS NMR spectrum for zeolite Y gave broad peaks at 09 ppm, 23 ppm and 44 ppm attributed to propyl spacer chain[31-32], again suggesting that there has been some surface modification which is due to the ligand grafting.
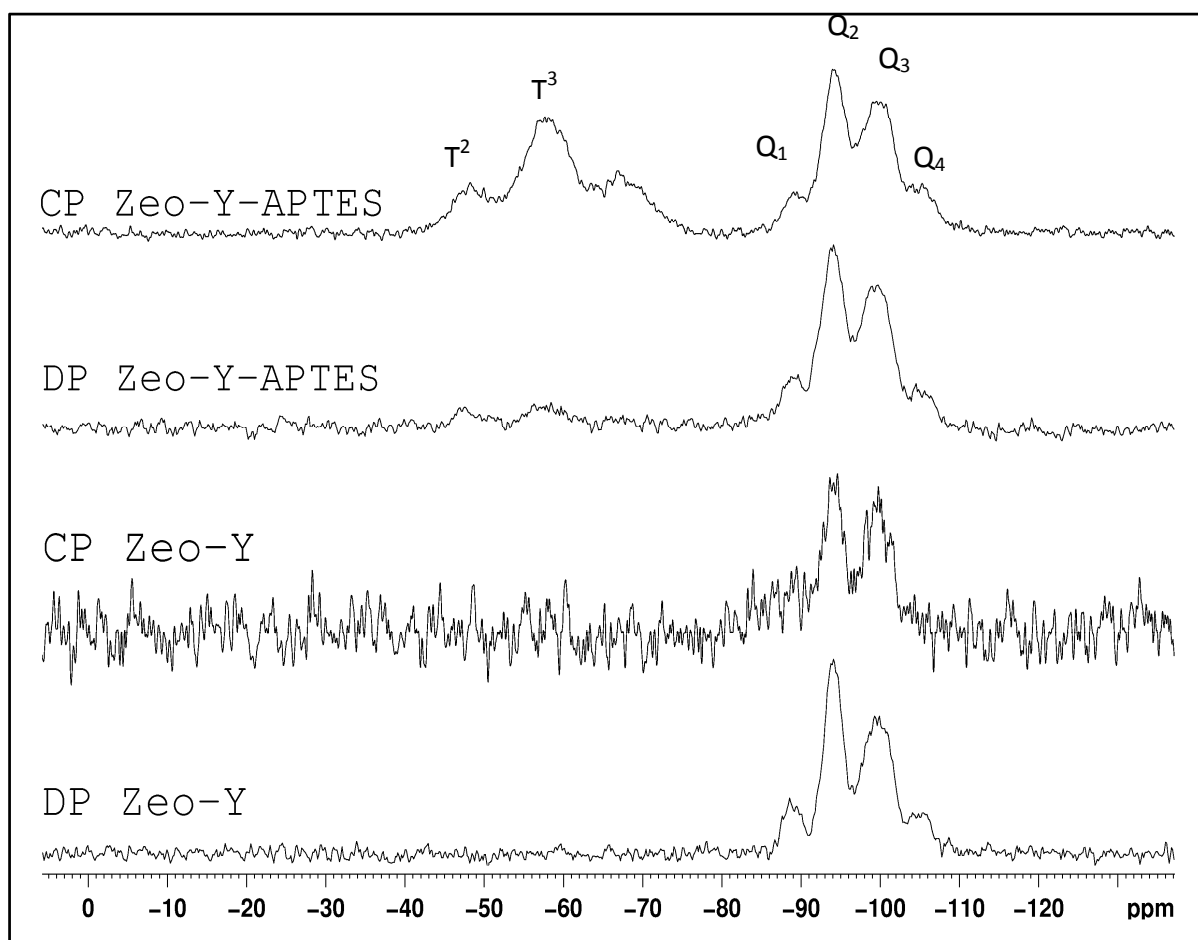
Figure 5.3: ^{27}Si CP and DP MAS NMR spectra for zeolite Y
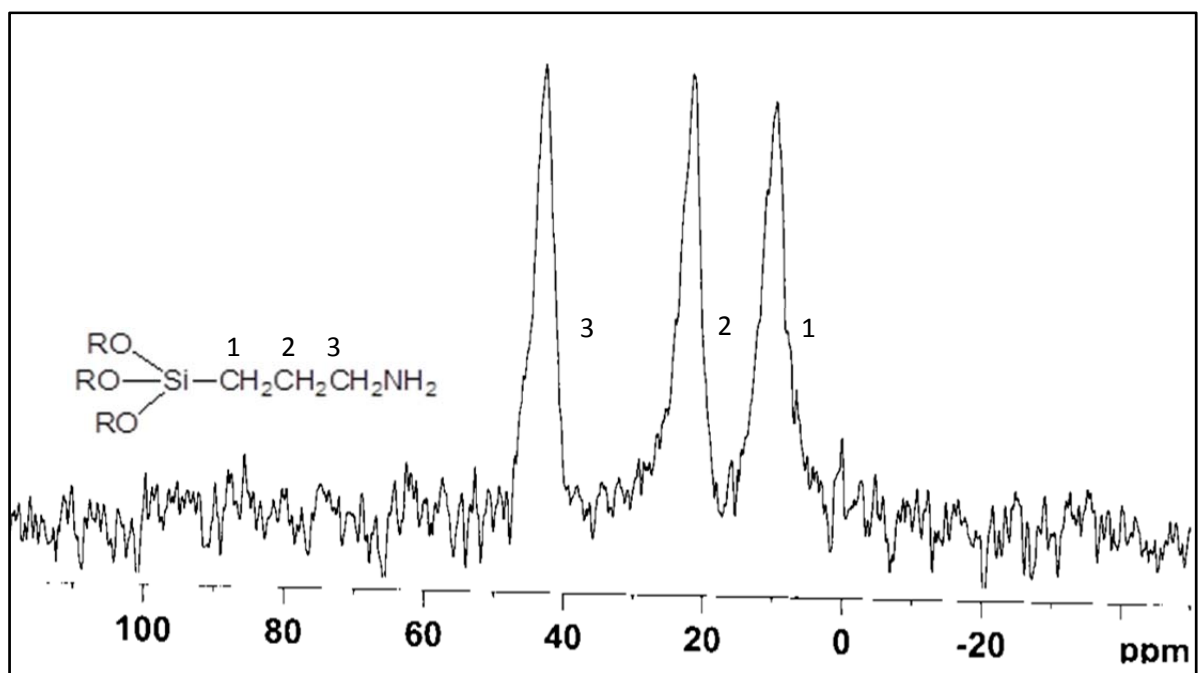
Figure 5.4: ^{13}C CP /MAS NMR spectra of modified zeolite Y

5.1.2.1.4. Fourier Transformed Infrared (FTIR)

The infrared spectroscopy studies of the grafted zeolites showed good evidence of successful grafting of the ligand on zeolite Y (figure 5.5) as shown by the absorption bands typical of functional groups present in the ligand. The broad absorption band at 3491 cm^{-1} was attributed to the OH stretching modes of the surface water and silanol groups. This absorption band is less broad for the grafted zeolite Y compared to the parent zeolite Y. The band at 1644 cm^{-1} was assigned to the angular vibration of the water bonded to the zeolite framework while the weak bands at 1384 cm^{-1} and 1476 cm^{-1} were assigned to N-C and N-H bonds corresponding to the amine group in the ligand, thus agreeing to the success of the ligand grafting in the final product.
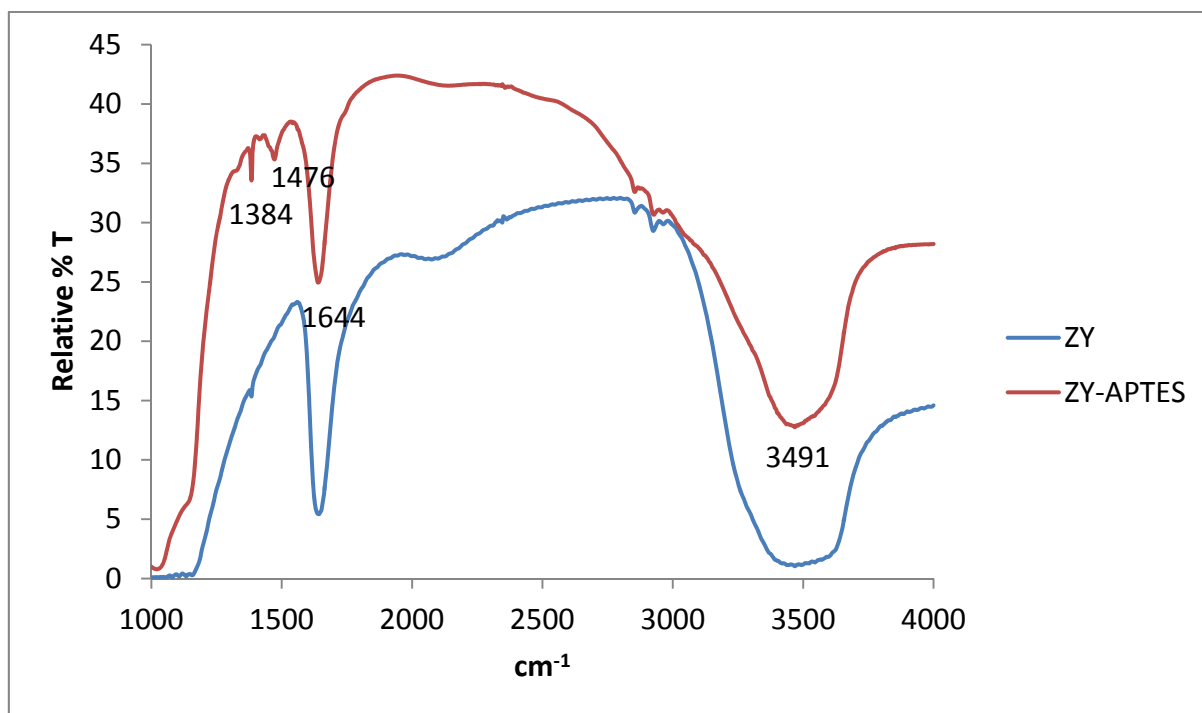
Figure 5.5: FT-IR spectrum of modified zeolite Y compared with the unmodified zeolite Y

5.1.2.1.5. Thermal Analysis (TGA)

The data from the TGA further supports the observations made from the solid state NMR, where there is an observed weight loss for zeolite Y at two distinct stages at separated distances (figure 5.6). The two distinct weight losses observed for the ligand grafted zeolite Y suggest losses due to two different compounds which may be water and the ligand respectively.

PXRD data of the thermal treated sample of the ligand grafted zeolite Y showed that the zeolite framework remained intact at both 200 ^{o}C and 400 ^{o}C where the losses occurred indicating that the weight losses were not as a result of any phase change hence it is likely due to water and the ligand (APTES) respectively.
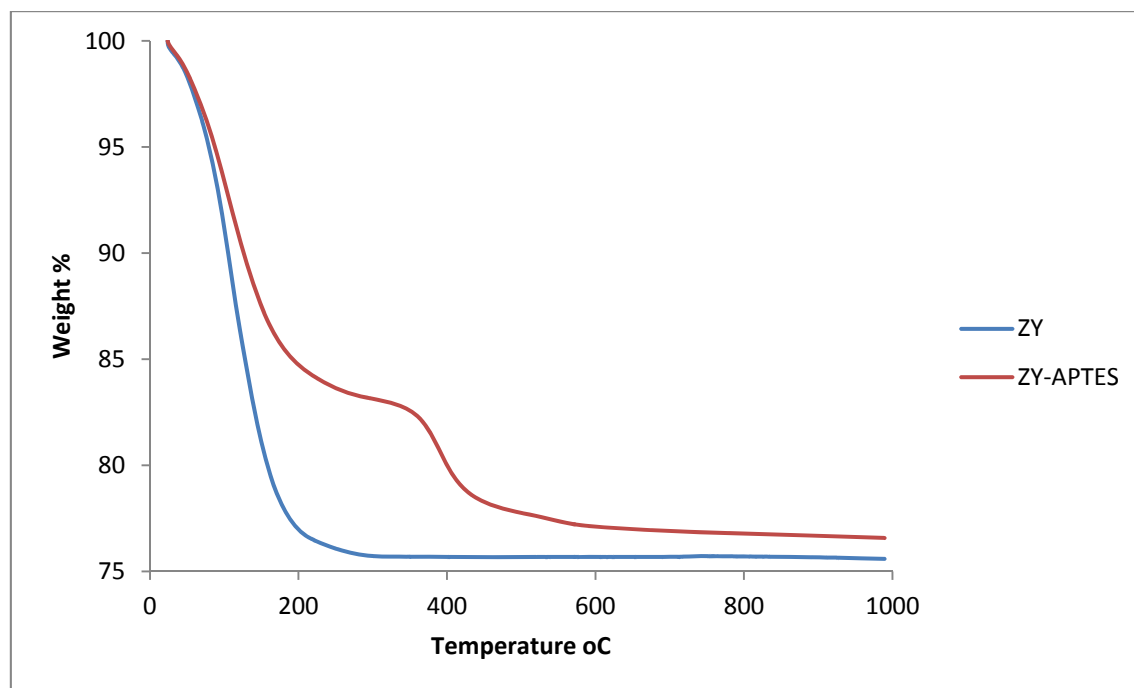
Figure 5.6: TGA of ligand grafted zeolite Y compared with parent zeolite Y

5.1.2.2. Nickel uptake by modified zeolite Y

Analysis of the modified and unmodified zeolite Y (ZY) and sample solutions after treatment with nickel (II) solutions at three different concentrations (0.01 M, 0.05 M, and 0.1 M) shows that the metal cations were adsorbed at all the concentrations (figure 5.7).
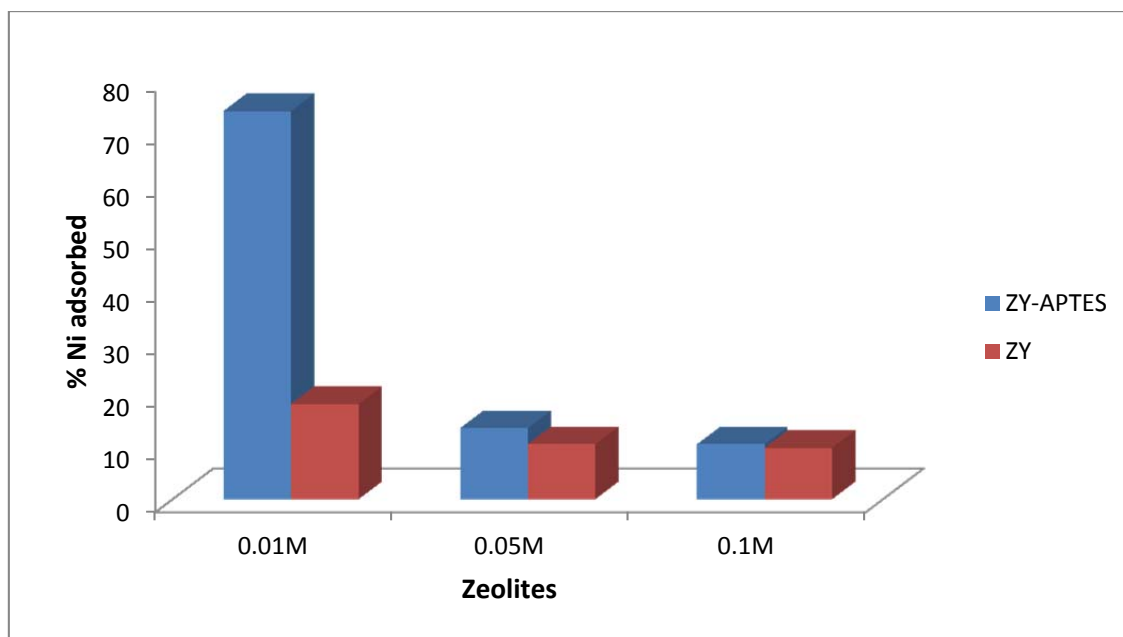
Figure 5.7: Percent nickel adsorbed by modified and unmodified ZY

An increase in the nickel (II) solution concentration lowered the affinity of the zeolites for the in-going Ni (II) ions, which agrees with data presented previously [33, 34]. This was a general trend observed for both the ligand modified and unmodified zeolite Y, however there was a marked increase in the amount of nickel ions adsorbed by the ligand modified zeolite Y as compared to zeolite Y, which could be attributed to the additional immobilization effect of the ligand (APTES) grafted on the zeolite. This is in line with earlier studies by Keane [34] where alkali metal modified zeolite Y was shown to increase the efficiency of metal uptake. Hence the uptake decreases in the order LiY > NaY > KY > RbY > CsY. Data from this analysis shows the metal loading on the modified zeolite to be higher than the ligand loading (Table 5.2) which agrees fairly well with previous work carried out[15] indicating that the Ni (II) ion uptake might not only be due to the immobilisation by the ligand, but also exchange with counter-ions present in the zeolite.

Parent zeolite A and X might be more efficient at exchanging Ni (II) ions from aqueous solution than zeolite Y. However, when the zeolite Y is modified with alkali metals (K^+, Li^+) and the organic ligand (APTES), its efficiency could be significantly improved to match or perform better than those zeolites with low Si/Al ratio (zeolite X and A).

Table 5.2: Comparison of the ligand loading and metal loading for zeolite Y

Sample	moles present (moles)	Ligand loading (moles)	Metal loading (moles)
Ligand-zeolite Y/0.5g	-	0.000235	-
0.01M Ni/300mL	0.003	-	0.001845
0.05M Ni/300mL	0.015	-	0.001663
0.1M Ni/300mL	0.03	-	0.000019

5.1.2.3. Result of selective removal of metal ions from a mix metal solution by zeolites

Analysis of the modified zeolite Y after treatment with a mixture of metal ions (Ni (II), V(IV), Fe (II), Cu (II) and Zn (II)) to investigate the selective adsorption of these metal ions, shows metal cations adsorption for all zeolites tested (figure 5.8).

Figure 5.8: Selective removal of metals by ligand-modified zeolite

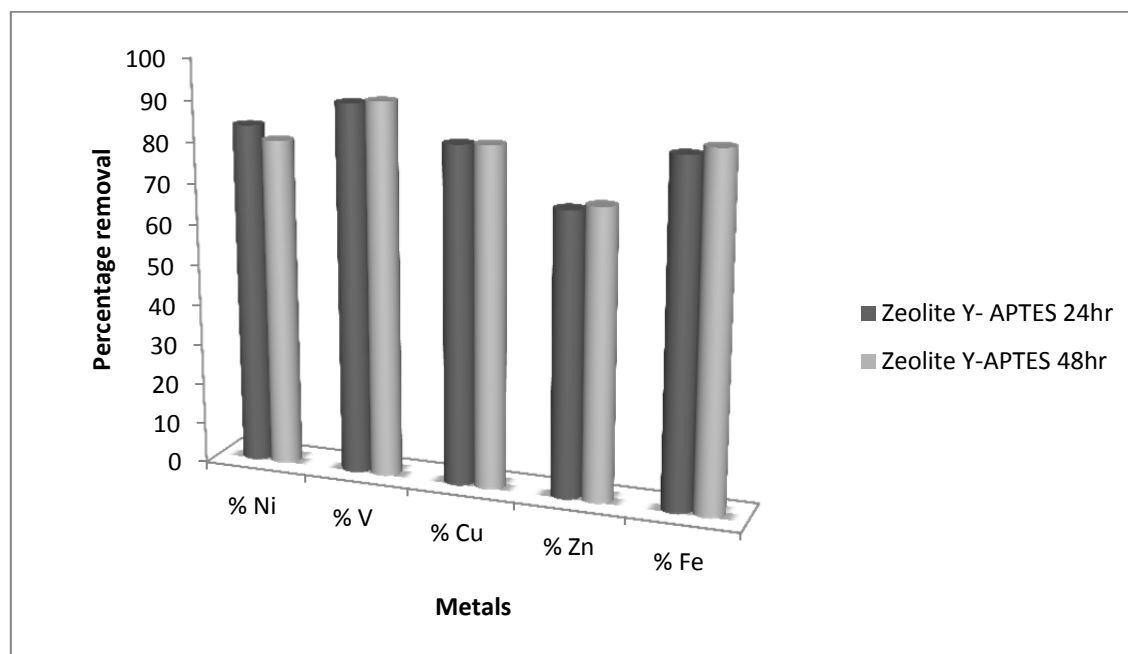The highest adsorption was observed for vanadium ions while zinc ions were found to show the weakest adsorption. The graph displayed in figure 5.8 shows that time has very little or no effect on the adsorption of the metal ions by the modified zeolite Y.

PART II

5.2. Synthesis of nickel tetraphenylporphyrin (Ni-TPP)

5.2.1. Experimental

5.2.1.1. Synthesis of Ni-TPP

The Ni-TPP was synthesized as reported in the literature[35]. Nickel (II) chloride hexahydrate was first dehydrated by heating the crushed solid in an evaporating dish until it lost all its water of hydration and its color turned yellow-orange. 0.0107 g TPP was dissolved in 15.2 mL DMF in a 50 mL round bottom flask. 0.051 g anhydrous nickel (II) chloride was then added, a condenser attached and the mixture heated under reflux at 50 ^{o}C for 5 d.

5.2.1.2. Hydroconversion of Ni-TPP

The hydroconversion of the Ni-TPP was carried out by solvent treatment at elevated temperatures and pressure as described in the literature[36]. The process involves the treatment of Ni-TPP with a hydrogen donor solvent (isopropyl alcohol). Isopropyl alcohols having α-hydrogen atom under favourable conditions, promotes the dissolution of Ni-TPP by hydrogen donor activity forming a liquid extract and an undissolved Ni-TPP residue. 0.0420 g of the Ni-TPP was used, 5 g of isopropyl alcohol and 0.1760 g KOH added in a stainless steel autoclave. The base (KOH) was added to furnish the system with a catalytically active amount of alcoholate anion that could facilitate the dissolution of Ni-TPP as shown in the chain process in equations 5.1-5.3. The experiment was carried out at 335 ^{o}C for 48h and 1 h cool-down time. The reaction mixture was then filtered, washed with the alcohol until the filtrate became clear. The overall filtrate was then transferred to a 50 mL round bottom flask and the solvent evaporated off using rotary evaporator. The greenish solid left after complete evaporation of the solvent was dissolved in distilled water, transferred into 100 mL volumetric flask and made up to the mark ready for treated with zeolite materials.

$OH^- + HOCHRR^1 \rightleftharpoons H_2O + {}^-OCHRR^1$ Equation 5.1

${}^-OCHRR^1 + Ni\text{-}TPP \longrightarrow O=CRR1 + Ni\text{-}TPPH^-$ Equation 5.2

$Ni\text{-}TPPH^- + HOCHRR1 \longrightarrow Ni\text{-}TPPH_2 + {}^-OCHRR^1$ Equation 5.3
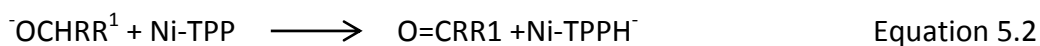
5.2.1.3. Nickel uptake from Ni-TPP by zeolites

The adsorption of Ni (II) from Ni (TPP) H_2 solution by zeolites was investigated using; zeolite A ($Na_{12}Al_{12}Si_{12}O_{48}.24.2H_2O$), zeolite X ($Na_{88}Al_{88}Si_{104}O_{384}.238.8H_2O$), and zeolite Y ($Na_{54.91}Al_{56}Si_{136}O_{384}.246.5$) modified by 3-aminopropyltriethoxysilane (ZY-APTES). The zeolites were treated with 20 mL each of hydrogenated nickel- tetraphenylporphyrin solution. The solutions were analysed before and after treatment with the different zeolite samples and the nickel (II) ion uptake determined.

5.2.2. Results and discussion

5.2.2.1. Characterization of Ni-TPP

The synthesized Ni-TPP was characterized using the UV-visible, elemental analysis (CHN) on an Exeter analytical ink (EAI) CE-440 elemental analyzer and visual observation.

5.2.2.1.1. UV-visible

The absorption spectra of Ni-TPP compared with TPP are as shown in figure 5.9. The H_2 (TPP) had intense absorption at 514 nm and more weak absorptions at 548.00 nm, 590 nm and 646 nm. The absorption at 526 nm is attributed to Ni-TPP. This absorption spectra are in good agreement with work carried out by Marsh and Mink[37] where the intense absorption between 500-550nm and weakly absorption between 590-650nm were attributed to the red-violet H_2 (TPP) whereas the absorption at 525nm was reported to be due to Ni-TPP. On metalation, the porphyrinic ring system deprotonates, forming a di-anionic ligand. The nickel metal ions in this case behave like Lewis acids accepting lone pairs of electrons from the porphyrin ligand (figure 4.10). The Ni-TPP are shifted to shorter wavelength due to the dπ-π* backbonding of the porphyrin. The spectrum on metalation has fewer peaks as a result of an increased symmetry compared with that without metal ion.
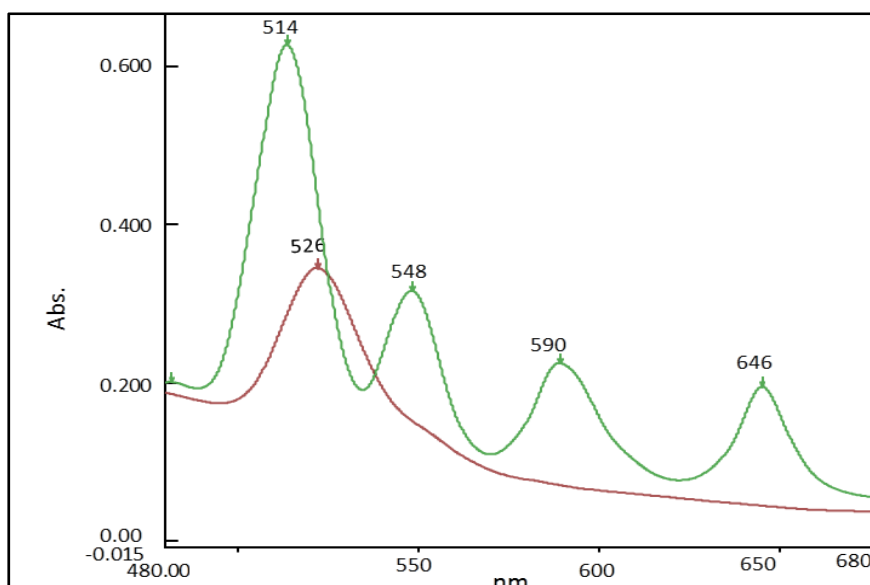
Figure 5.9: Absorption spectra of H_2 (TPP) and Ni (TPP)
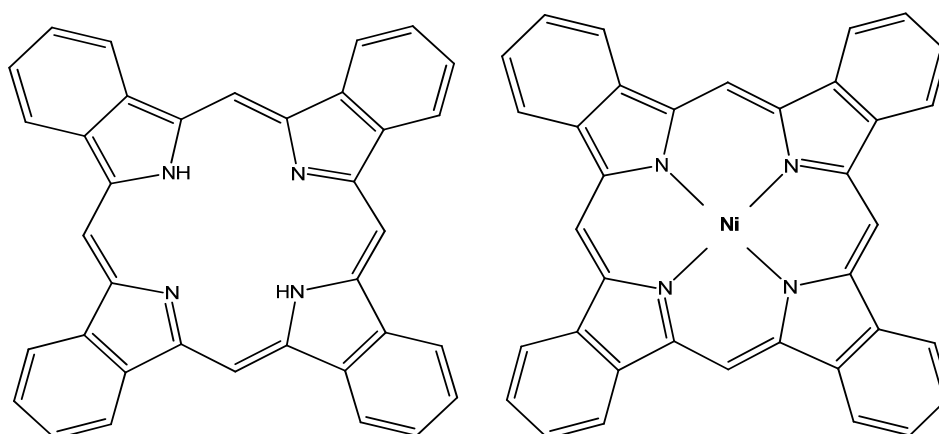
Figure 5.10: H_2 (TPP) before (left) and after (right) metalation

The absorption spectra of hydroconverted Ni-TPP compared with that of Ni-TPP and TPP are as presented in figure 5.11. The UV-vis spectrum of the hydroconverted Ni-TPP is dominated by two major absorptions at around 600 nm and 540 nm. According to literature [38, 39], the absorption at around 600 nm is attributed to the hydrogenated form of Ni-TPP (Ni-TPC) while that around 540 nm is due to Ni-TPP. The data from this work is in good agreement with earlier studies [40, 41] where the absorption at 528 nm and 616 nm were assigned to Ni-TPP and Ni-TPC respectively. A shoulder was observed at 596 nm which was attributed to nickel-5, 10, 15, 20 - tetraphenylisobacteriochlorin

(Ni-TPiB). The UV-vis spectrum in this study gave a broad absorption at around 600 nm which may be due to the combined absorption of Ni-TPC and Ni-TPiB.
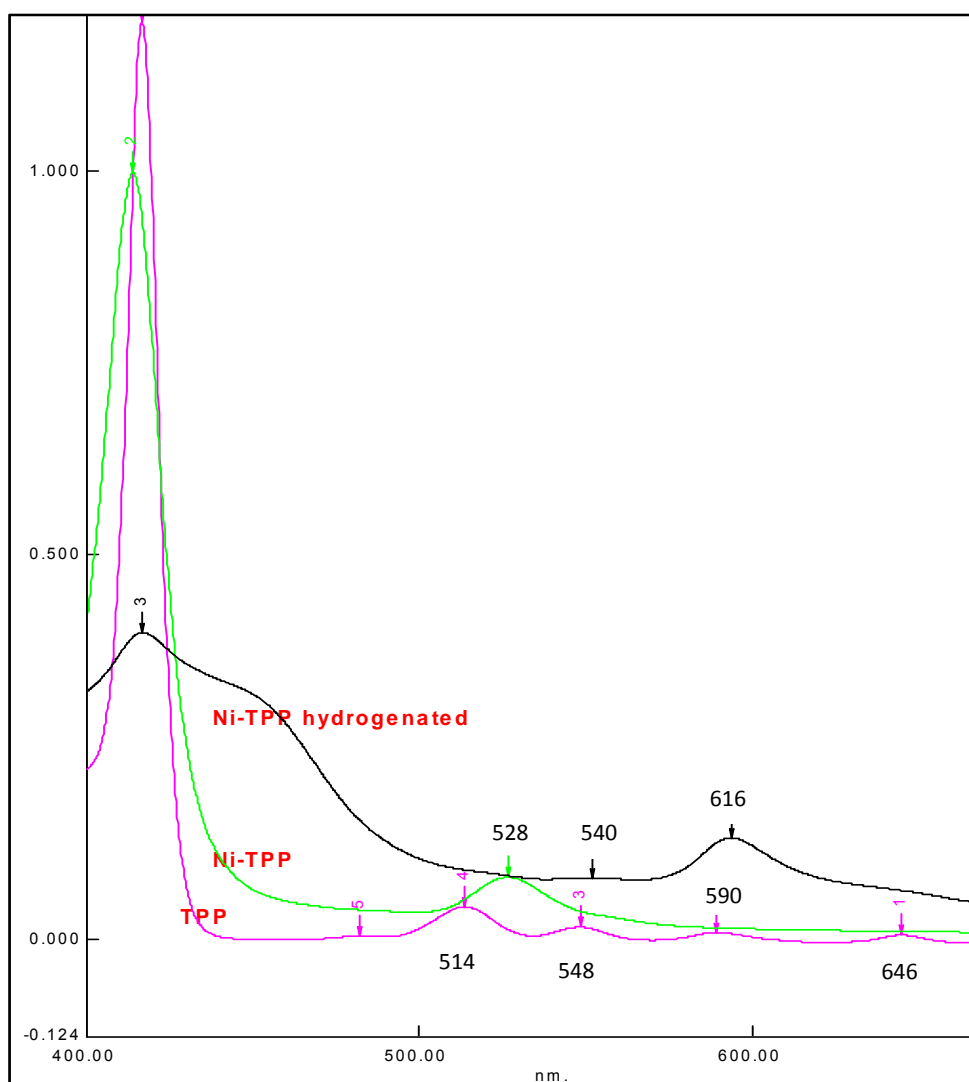
Figure 5.11: Absorption spectra of H_2 (TPP), Ni (TPP) and Ni (TPP) H_2

5.2.2.1.2. Colour change

The observed colour change of the different compounds made was also an indication and further confirmation with the data from UV-Vis characterization, that the reaction had proceeded to completion. Figure 5.12, shows the different color changes;
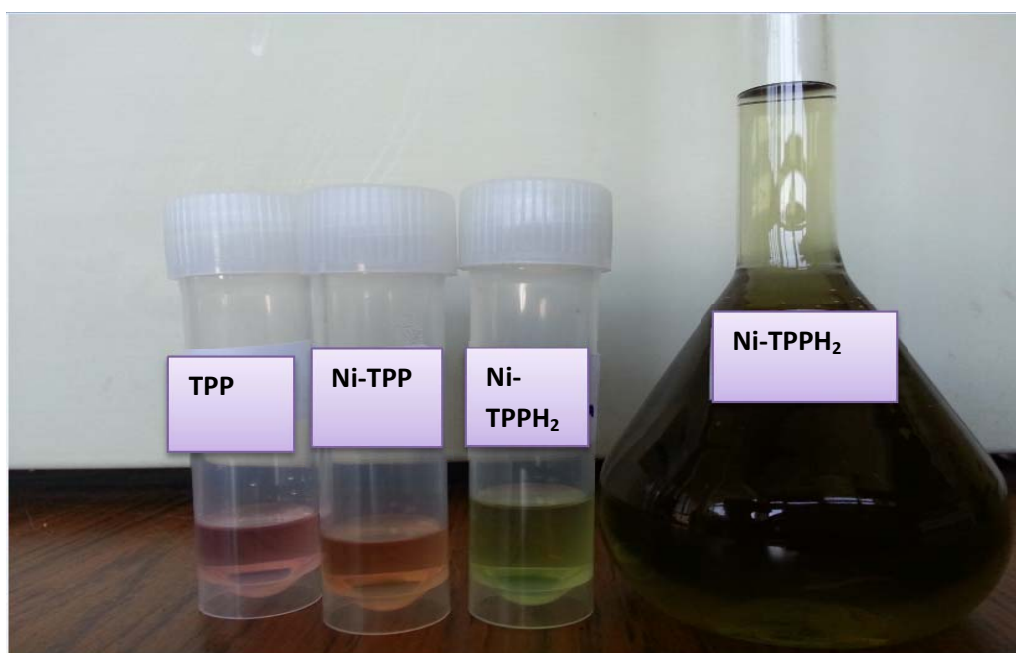
Figure 5.12: Observed colour changes for TPP (pink), Ni-TPP (orange) and Ni (TPP) H$_2$ (green)

5.2.2.1.3. Elemental analysis (CHN)

The elemental analysis (CHN) of tetraphenylporphyrin and nickel-tetraphenyl porphyrin are shown in table 5.4.

Table 5. 4: Elemental analysis of tetraphenylporphyrin and nickel-tetraphenylporphyrin

	% C	% H	% N
Tetraphenylporphyrin	85.72	4.76	9.06
Nickel-tetraphenylporphyrin	78.59	3.86	6.60

The elemental analysis of the two compounds shows that the metalloporphyrin has been produced as seen by the decrease in the percent carbon due to an added weight of nickel to the molecular weight of the compound.

5.2.2.2. Comparative uptake of nickel from Ni (TPP) H$_2$ by zeolites

Analysis of the Ni (TPP) H$_2$ solution before and after treatment with the different zeolite samples shows that the Ni (II) from the solution was taken up by all the zeolites (figure 5.13).
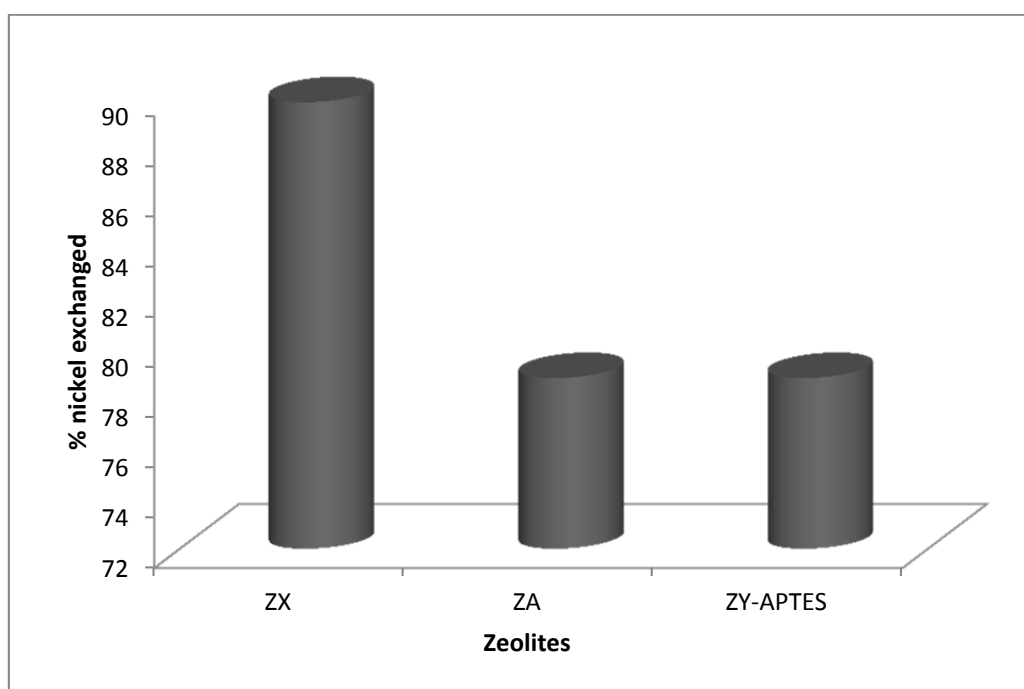
Figure 5.13: Percent nickel removal by zeolites from Ni-TPPH$_2$ solution

The highest uptake was found for zeolite X (~90 %). This result is in good agreement with the aqueous Ni (II) ions exchange with zeolites A, X and Y reported in the previous chapter. Zeolite X has consistently shown good efficiency for Ni (II) removal from solution. The high uptake of Ni (II) ions from a model porphyrinic compound of nickel by zeolite X, shows that the material has the potential to provide methods for the removal of Ni (II) from the porphyrinic complexes in crude oil.

5.3. Conclusion

Ligand modified zeolites Y and Ni-tetrphenylporphyrin (Ni-TPP) were successfully synthesised. The Ni (II) ions adsorption by the ligand modified zeolite was investigated compared to that of the as synthesised zeolite Y. The nickel uptake from the Ni-tetrphenylporphyrin solution was also studied using the different zeolites. At lower concentrations of nickel, the ligand modified zeolite Y was found to be more efficient at nickel ion removal compared with the parent zeolite. Selective adsorption studies of a mixture containing five metal ions (Ni (II), V(IV), Cu(II), Zn(II), and Fe(II),) showed that Fe and Cu ions are possible interfering ions particularly for nickel uptake. Zeolite X and A were shown to have high efficiency at removing nickel ions from Ni-TPP.

References

1. R. Szostak, Molecular sieves, Principles of Synthesis and Identification, Van Nostrand Reinold, New York, 1989.

2. F.A. Mumpton, L.B. Sand, F.A. Mumpton, A new industrial mineral commodity. Natural Zeolites: Occurrence, Properties, Use, Pergamon Press, New York, USA, 1978.

3. D.W. Breck, Zeolite Molecular Sieves, Structure Chemistry and Use, Wiley, New York, 1974.

4. H. Van Bekkum, E.M. Flanigen, P.A. Jacobs, J.C. Jansen, Introduction to zeolite science and practice. Studies in Surface Science and Catalysis, Elsevier Science Publishers, Amsterdam, 2001.

5. M.I. Occelli and H. Kessler, Synthesis of Porous Materials: Zeolites, Clays and Nanostructures, CRC Press, New York, 1997.

6. E. Erdem, N. Karapinar, R. Donat, J. Coll. Inter. Sci., 2004, 280, 309.

7. P.W. Schindler, B. Fuerst, R. Dick, P.U. Wolf, J. Coll. Inter. Sci., 1976, 55, 469.

8. S.M. evangelista, E.Oliveira, G.R.castro, L.F.Zara, A.G.S. Prado, Surf. Sc., 2007, 601, 2194-2202.

9. Y. jiang, Q.Gao, H.Yu, Y.Chen, F.Deng, Micropor. Mesopor. Mater., 2007, 103, 316-324.

10. M. Addy, B. Losey, R. Mohseni, E. Zlotnikov , A. Vasiliev, Applied clay Sc., 59-60 (2012) 115-120

11. P.Tzvetkova, R.Nickolov, J. Chem. Technol. Metall., 2012, 47, 5, 498-504.

12. Z. Hu, X. Zhang, D. Zhang, Ji-xiao Wang, Water Air Soil Pollut., 223,(2012) 2743–2749.

13. Leandro Vinícius Alves Gurgel, Laurent Frédéric Gil, J. Carbohydr. Polym. 77 (2009) 142–149.

14. R. Guilet, N. Chiron, E. Deydier, J. Water Res., 37 (2003) 3079–3086.

15. A.N. Vasiliev, L.V. Golovko, V.V. Trachevsky, G.S. Hall, J.G. Khinast, Micropor. Mesopor. Mater., 118 (2009) 251–257.

16. Z. Xu, Y. Huang, C. Zhang, L. Liu, Y. Zhang, L. Wang, Composites Science and Technology, 2007, 67, 3261-3270.

17. J. Weitkamp, W. Gerhardt, R. Rigoni, H. Dauns, Erdöl, Kohle-Erdgas-Petrochem. 36 (1983) 569.

18. R.A. Ware, J. Wei, J. Catal. 93 (1985) 122.

19. R.L.C. Bonné, P. van Steenderen, J.A. Moulijn, Bull. Soc. Chim. Belg. 100 (11/12) (1991) 877.

20. R.L.C. Bonné, P. van Steenderen, J.A. Moulijn, ACS, Prepr., Div. Fuel Chem. 36 (4) (1991) 1853

21. R.A. Ware, J. Wei, J. Catal. 93 (1985) 100.

22. R.A. Ware, J. Wei, J. Catal. 93 (1985) 135.

23. R.A. Ware, J. Wei, ACS Prepr. Div. Petr. Chem. 30 (1985) 62.

24. L.A. Rankel, ACS Prepr. Div. Petr. Chem. 26 (1981) 689.

25. S. Mitchell, A. Bonilla, J. Pérez-Ramírez, Mater. Chem. Phys 127 (2011) 278–284.

26. J. Aguado, J. M. Arsuaga, A. Arencibia, M. Lindo, V. Gascón, J. Hazard. Mater. 163 (2009) 213-221.

27. X. Bao, Z.Yan, D. Ma, J. Zhuang, X. Liu, X. Liu, X. Han, F. Chang, L. Xu, Z. Liu, J. Mol. Catal. A: Chem. 194 (2003) 153-167.

28. T. Bein, R.F. Carver, R.D.Farlee and G.D Stucky, J.Am.Chem. Soc. 110 (1988) 4546-4553.

29. M.A. Khadin and M.A.AL-Shafei, Solid State NMR Spectroscopy and refinery catalysts. Research and development Centre, Saudi Aramco, Dhahran, 31311, Saudi Arabia.

30. A.P.M. Alves, M.G. Fonseca and A.F. Wanderley, Materials Research, 16, 4 (2013) 891-897.

31. X. Wang, K.S.K. Lin, J.C.C. Chan, S. Cheng, J. phys. Chem. B, 109 (2005)1763-1769.

32. S. Ek, E.I. Iiskola, L. Niinistö, J. Vittinen, T.T. Pakkanen and A. A Root, J. phys. Chem. B, 108 (2004)11454-11463.

33. A. Dyer, An Introduction to Zeolite Molecular Sieves, John Wiley & Sons, Chichester, 1988.

34. M.A. Keane, Colloids Surf. A: Physicochem. Eng. Aspects, 1998, 138, 11–20.

35. D.F. Marsh and L.M. Mink, J. Chemical education, 73, 1996, 1188-1190.

36. D.S. Ross, P. Alto, J.E. Blessing and M. Park, Alcohols as hydrogen-donor solvents for treatment of coal. Patent number 4298450, 1981.

37. D. F. Marsh and L. M. Mink, J. Chemical education., 73,1996, 1189

38. R.L.C. Bonné, P. van Steenderen, J.A. Moulijn, Applied Catalysis A: General 206, 2001, 171–181

39. A. J. Garcı́a-Lo´pez, R. Cuevas, J. Ramı́rez, J. Ancheyta, A.A. Vargas-Tah, R. Nares, A. Gutie´rrez-Alejandre, Catalysis Today 107–108, 2005,545-550.

40. R.L.C. Bonné, P. van Steenderen, J.A. Moulijn, Applied Catalysis A: General 206 (2001) 174

41. A.J. Garcı́a-Lo´pez, R. Cuevas, J. Ramı́rez, J. Ancheyta, A.A. Vargas-Tah, R. Nares, A. Gutie´rrez-Alejandre, Catalysis Today 107–108 (2005) 548.

Chapter 6: Crude oil characterisation

and solvent extraction of metal ions

from crude oil

6.0. Introduction

Ion exchange in a solvent medium can only occur if the exchanging species are soluble in the solvent used. The high dielectric constant of water makes it an excellent solvent for most ion exchange reactions. Other solvents with large dielectric constants compared to water are as shown in table 6.1. These solvents may also allow ion exchange to occur.

Table 6.1: solvents with dielectric constants compared to water

Solvents	Dielectric constant	Dipole moment
Water	80	1.8
Methanol	32.7	1.7
Ethanol	24.5	1.69
Liquid ammonia	25	1.46
Acetone	20.7	2.85
Isopropyl alcohol	17.9	1.66
Formamide	111	3.37
Dimethylsulfoxide	46.7	3.9

Ion exchange using polar protic solvents and mixed solvents offers interesting possibilities for the separation and extraction of metal cations [1]. The investigation into the ion exchange using mixed solvents started as early as the 1920's with the ion exchange of alkali metal ions in water-ethanol solution on calcium permutite[2]. However, the renewed interest in this field of study only arose in the late 1940's with the investigation into the exchange of alkali ions and ammonium ions on phenolsulphonate resins using ethanol and acetone[2]

Ion-exchange in mixed solvents has been extensively investigated in recent years for both organic and inorganic exchangers, with the hope of achieving compositions currently inaccessible by aqueous ion exchange[3].

Investigations into ion-exchange using polar solvents have been extensively carried out on resins as the exchanger[1, 4-8]. However, until recently only a few reports have been presented for ion-exchange in polar solvents using zeolites [9-11]. Ion exchange of Co (II) for Na^+ in zeolite A and zeolite X using solvents with composition range from

water to completely dried formamide shows that the extent of ion exchange is proportional to the water content at $[H_2O]<1.5$[9]. Small amounts of water in formamide disproportionately increased the ion exchange while small amount of formamide in water disproportionately hinders ion exchange. The pure organic solvent was not suitable for ion exchange in zeolites[9]. Radak and Susic studied the ion exchange behaviour of alkali metal ions on synthetic zeolite 4A as a function of dielectric constant in the water-methanol system. The thermodynamic affinity sequence, based on the standard free energies of exchange was shown to be $Na^+>K^+>Rb^+>Cs^+>Li^+$ [10]. Investigation of the possibility of ion exchange of heavy metal ions in polar organic solvents using natural zeolite (clinoptilolite), shows that the metal ions exchange using zeolite is possible in polar organic solvents and that the selectivity can be totally changed as compared to water[11]. The results of these varied research studies demonstrate the possibility of ion exchange in resin-polar mixed solvent and zeolite-polar mixed solvent systems as well as points to the fact that the addition of polar solvents to the aqueous phase can enhance the affinity of the cations in solution toward the exchanger. The use of the right solvent mixture could therefore be used to improve the selectivity of one cation over another by the addition of polar solvents to an aqueous solution of the metal ions[12]. The selectivity can be explained in terms of the dielectric constants of the solvents, solvation of ions and ion association[2].

Literature reports have shown that pure organic solvents are not suitable for ion exchange in zeolites[9, 12]. The investigation into the ion exchange in a range of solvents; CuCl, $CuCl_2$ and $CuSO_4$ in acetonitrile and of $CuCl_2$ in methanol, dimethylsulfoxide solutions of Pb $(NO_3)_2$ and at 140 ^oC, KNO_3 and finally HgS in liquid sulphur on zeolite A and zeolite X, showed no ion exchange occurred for any of the cases[12]. The inability of the cations to enter or leave sites within the zeolites was thought to be as a result of the fact that their solvation complexes were less stable relative to the outgoing cation[12]. Ion-exchange was however shown to have occurred in a non-aqueous ammonia system with alkali metal nitrates as the cationic species albeit with additional adsorption of ammonia at the same time[13]. The structural stability of the zeolites under investigation might be an issue of concern since zeolites are not stable in highly alkaline environments. Despite the stability of the zeolites, these results

suggest that only solvents with large dipole moments (e.g. water and ammonia) that are able to create a suitable coordination sphere for cations in the solvent and therefore stabilise both the outgoing and incoming cations at their intermediate states, are able to allow ion-exchange to effectively occur. Furthermore, fully/partially hydrated or ammoniated cations are capable of forming hydrogen bonds to the oxygen of the zeolites framework and with themselves, thus stabilising furthermore, their transitional states[13].

The literature reviewed in this chapter had the ion-exchange carried out between a solid ion exchanger and the metal ions containing solvent mixture. It is expected that, the solvents and aqueous solutions used in this study, will extract the metal ions from crude oil and then subsequent ion exchange occurs between the zeolites and the metal ion containing solvent mixture.

6.1. Experimental

6.1.1. Characterisation of the crude oil

General characterisation studies were carried out on the crude oil to determine the physicochemical properties as well as the hydrocarbon fingerprinting of the crude oil. The characterisations carried out include: density measurement, API gravity, transition metal cation content Ni (II) & V (IV), sulphur content and the gas chromatographic analysis.

6.1.1.1. API of crude oil

The American Petroleum Institute (API) gravity of the crude oil was determined using the measured density of the crude oil.

6.1.1.2. Metal ions [Ni (II) & V (IV)], and sulphur content in crude oil

The metal cations content in the crude oil was determined using the X-ray fluorescence analysis (XRF) on the ashed crude oil samples. 100 mL of the crude oil sample was weighed into an alumina crucible and heated on a hot plate in a fume cupboard until the residue stopped fuming. The alumina crucible containing the oil residue was then transferred into a muffle furnace at 600 ^{o}C for 3 h. This was then

removed from the furnace, allowed to cool and finely ground using a mortar and pestle, ready for XRF analysis.

6.1.1.3. Gas Chromatographic analysis on the crude oil

The crude oil sample was subjected to a full scan of 50-600 mass units using the GC 8000 series MD 800 Gas Chromatograph, equipped with the column 30 m DB5MS. A sample injection volume of 1 μL was used. The injector temperature and transfer temperature were both kept at 250 ^{o}C. The oven temperature was programmed from 35 ^{o}C to 300 ^{o}C at 10 ^{o}C/min with an initial hold time of 10 min.

6.1.2. Extraction of metal ions from crude oil

Water (H_2O), Isopropylalcohol [$CH_3CHOHCH_3$ (IPA)], aqueous solution of Na-EDTA (0.05 M) and aqueous solution of H_3PO_4 (0.05 M), were used to investigate the extraction of the metal cations from crude oil. These extracting media were chosen based on their effectiveness in earlier investigations[5, 6, 14, 15]. 50 mL crude oil was measured into a round bottom flask containing 100 mL H_2O and refluxed for 24 h at 110 ^{o}C. The mixture was then transferred into a 250 mL separating funnel and left standing overnight. Distinct layers were carefully separated; the organic layer was then ashed for XRF analysis. The same procedure was repeated for aqueous solution of H_3PO_4 (0.05M) and aqueous solution of Na-EDTA (0.05M). A ratio of 1:1 for $CH_3CHOHCH_3$ (IPA) and water was used in the case of IPA and the rest of the procedure remained the same. A similar investigation in the presence of the zeolite materials (Zeolite A, Zeolite X and Zeolite Y-APTES) using $CH_3CHOHCH_3$ (IPA), H_3PO_4 (0.05 M) and EDTA (0.05 M) as the extracting media, was also carried out. Zeolite Y - APTES represents the ligand [3-amino propyltriethoxylsilane] attached zeolite Y and was chosen for this investigation, rather than the parent zeolite Y, due to its improved metal ion uptake efficiency compared to the parent zeolite Y. 50 mL crude oil was measured into a round bottom flask containing 0.5 g zeolite A and 100 mL H_3PO_4 (0.05 M) and refluxed for 24 h at 110 ^{o}C. The mixture was then transferred into a separating funnel and left standing for at least 1 h after which the distinct layers were carefully separated and filtered under gravity to recover the zeolite; the organic layer was then ashed for XRF

analysis. The same procedure was carried out in IPA and EDTA for each of the zeolites (zeolite A, zeolite X and Zeolite Y-APTES).

6.2. Results and discussion

6.2.1. General characteristics of the studied crude oil

The specific density, API gravity, trace metals and sulphur contents of crude oil are important parameters used for the classification of crude oils. GC–MS on the other hand is used for the selective separation, identification, and quantification of components of complex organic mixtures. It is a fingerprinting technique used for oil characterisation by evaluating the range of hydrocarbons in crude oil[16]. Table 6.2 presents the physicochemical parameters of the crude oil studied.

The API gravity gives information on the grade/quality of crude oil. According to the American Petroleum Institute (API) gravity standard, crude oils with API gravity > 31 are classified as light, those with API gravity of 22 to 31 as medium and those with API gravity ≤ 20 as heavy crude oils[17]. The value of the API gravity for the crude oil in this study compared with that of the API standard shows that the crude oil studied is medium crude oil category. It's worth noting here that the demand /market value for crude oil decreases from light – heavy crude oils. As the oil tends towards being heavy, the more expensive and difficult is its refining process[17].

The sulphur content of a crude oil on the other hand determines whether the crude oil is sour or sweet. Sweet crude oils are those that meet product specification with sulphur content of less than 0.5 %. Sulphur content greater than this value are said to be sour[18]. The crude oil used in this study has sulphur content of less than 0.5 % (% wt.) thus could be classified as sweet crude.

Trace metal ions are often found in crude oils[19]. These metals are basically a reflection of the metal ions carried along during migration and incorporated into the oil in form of complex species. The metals could also be derived from organic molecules as well as biogenic and abiogenic sources[20]. The nature and abundance of these metals in crude oil are of interest to the petroleum industry as they are the source of catalysts poison, corrosion of equipment and general environmental pollution[21]. The trace

metal analysis revealed eight metal cations in the crude oil used in this study (Nigerian crude) as given in Table 6.3 with their standard deviation values based on the triplicate analysis of the crude oil samples. The result of the analysis showed that the most abundant trace metal ions from the crude oil are nickel, iron and zinc. Other metal cations such as vanadium, chromium, copper, manganese and lead are present at low concentrations ≤ 0.5 ppm. The relatively higher concentrations of nickel and iron observed from the result are expected since these metals are commonly associated with crude oils[22]. The relatively high concentration of nickel, iron and zinc compared to the other metals investigated could be explained based on the fact that most soils associated with the areas where crude oils are found in Nigeria have appreciable deposits of metal ores such as iron ores[23], nickel and vanadium are usually known to be associated with such ores. Additional sources of iron in crude oil even though relatively low compared to metal ores may be contributions from the drilling equipment and machineries. The abundance of nickel in the crude oil could also be explained based on the fact that most of the oil wells in Nigeria are associated with the marine environment where there is abundant input of porphyrin obtained from organic matter derived from algae and bacteria[24]. The low V/Ni ratio 0.05 from Table 6.2, further agrees with the fact that the crude oils used in the study are derived from marine organic matter. The result of the analysis of the crude oil in this study (Table 6.3) is in good agreement with the results of other studies on Nigerian crude oils as shown in Table 6.4 [25-27].

Table 6.2. General characteristics of the studied crude oil sample

Density (g/mL)	0.88057
[a]API gravity	29.2
Sulfur content (ppm)	90.1
Ni (ppm)	10.1
V (ppm)	0.5
V/Ni	0.05

[a]API = (141.5/d)-131.5, where d is a density of crude oil at 608F.

Table 6.3. Trace Metals in Nigerian crude oils from this study

Parameters (mg/L)	Nigerian Crude A (av.)	Nigerian Crude B (Av.)	Average (crude A & B)
Ni	6.14±1.4	14.06±0.0	10.1
V	0.43±0.0	0.51±0.03	0.47
Fe	253.7±41.9	15.06±1.0	134.4
Cr	9.6±0.0	0.49±0.0	5.1
Cu	0.48±0.1	0.53±0.01	0.5
Zn	4.5±1.6	4.67±2.9	4.6
As	0.13±0.09	0.6±0.44	0.37
Mn	0.99±0.0	0.49±0.0	0.74
Pb	0.2±0.08	0.22±0.0	0.21

Values obtained are means of triplicate determination; ± standard deviations of the means.

Table 6.4. Trace Metals in Nigerian crude oils from other studies[25-27]

Parameters (mg/L)	Lit. 1 (Av)	Lit. 2 (Av.)	Lit. 3 (Av.)
Ni	2.66	6.28	7.81
V	0.5	1.27	50.92
Fe	9.36	0.25	65.67
Cr	1.6	0.026	0
Cu	1.99	0.77	25.5
Zn	27.56	0.51	0.1
As	0	0.2	0.2
Mn	0.76	0.35	3.4
Pb	7.96	0.005	0.61

The Gas Chromatograms obtained for the crude oil samples studied show a monomodal distribution pattern for the homologues series of the n-alkanes. The chromatograms show some close similarities as shown in figures 6.1-6.3. They all show high concentrations of moderately high molecular weight hydrocarbons (C_{12}-C_{22}). The chromatogram for the sample in figure 6.2 showed little or no low molecular weight hydrocarbons are present, probably due to evaporation during sample preparation. It is worth noting here that even though the chromatograms share some similarities, they are each uniquely different thus can be used as a fingerprint to provide some information on the source of the hydrocarbon under investigation.
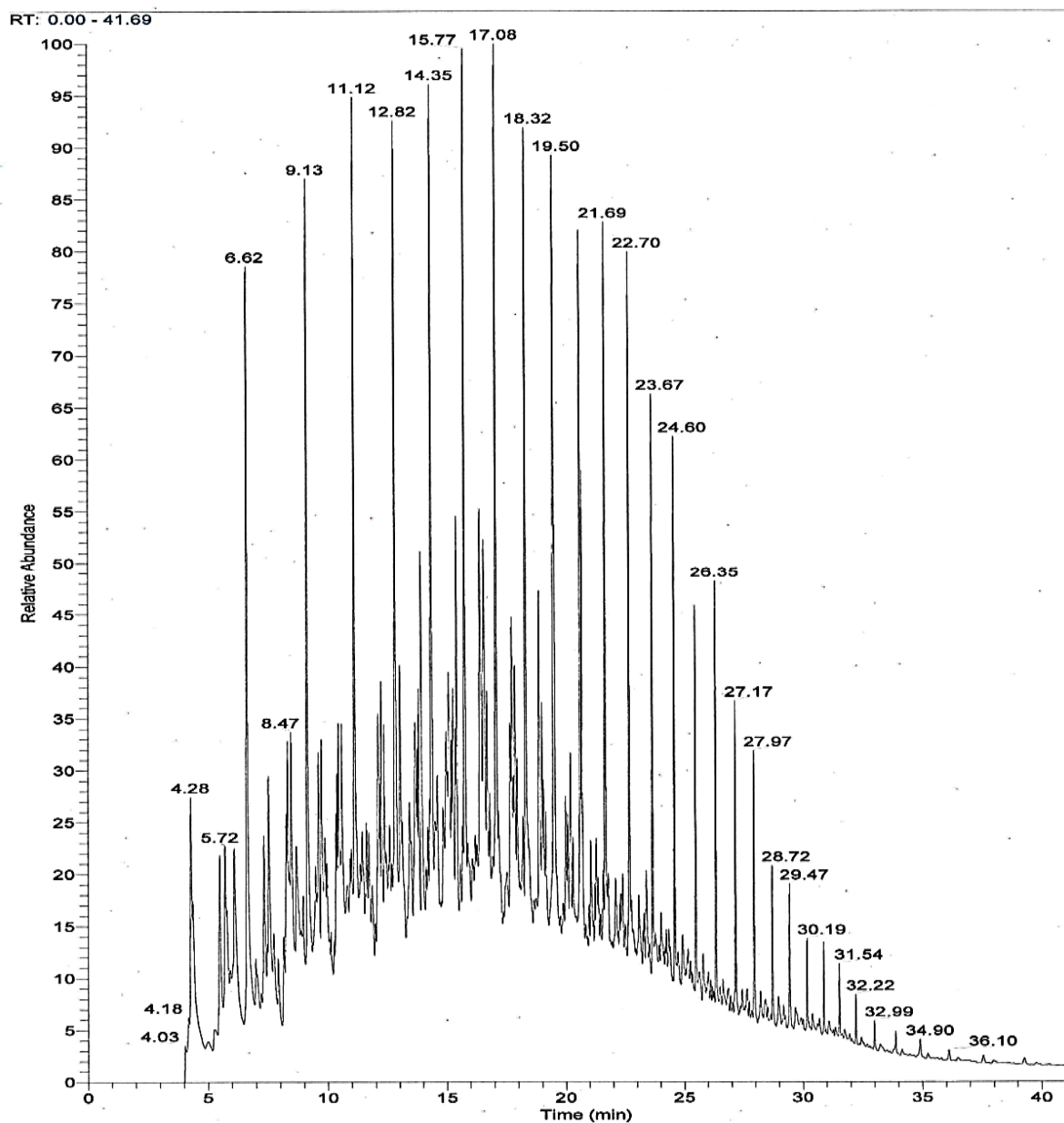
Figure 6.1 Gas chromatographic fingerprint of 'Crude A' oil sample
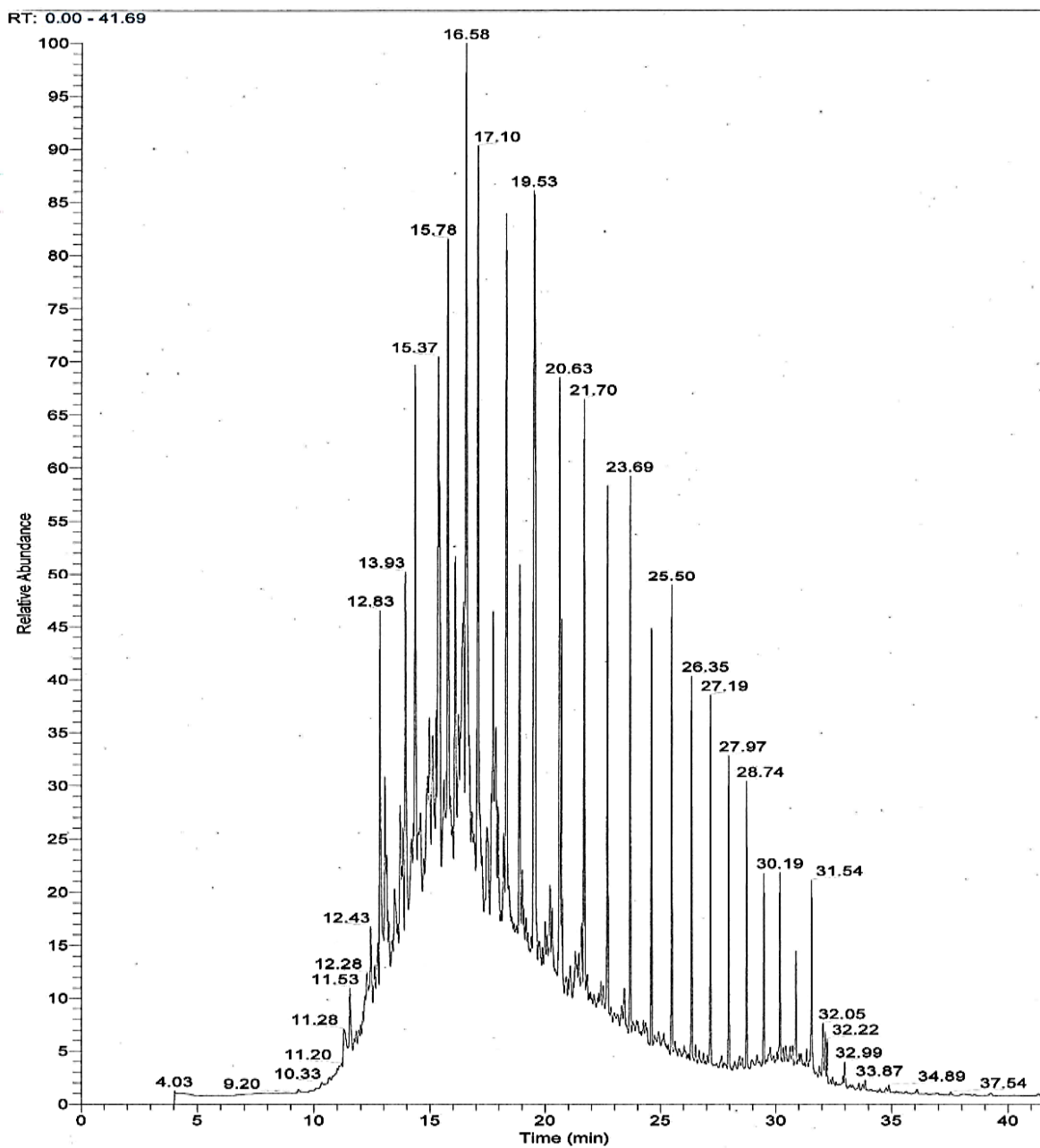
Figure 6.2 Gas chromatographic fingerprint of 'Crude B' oil sample
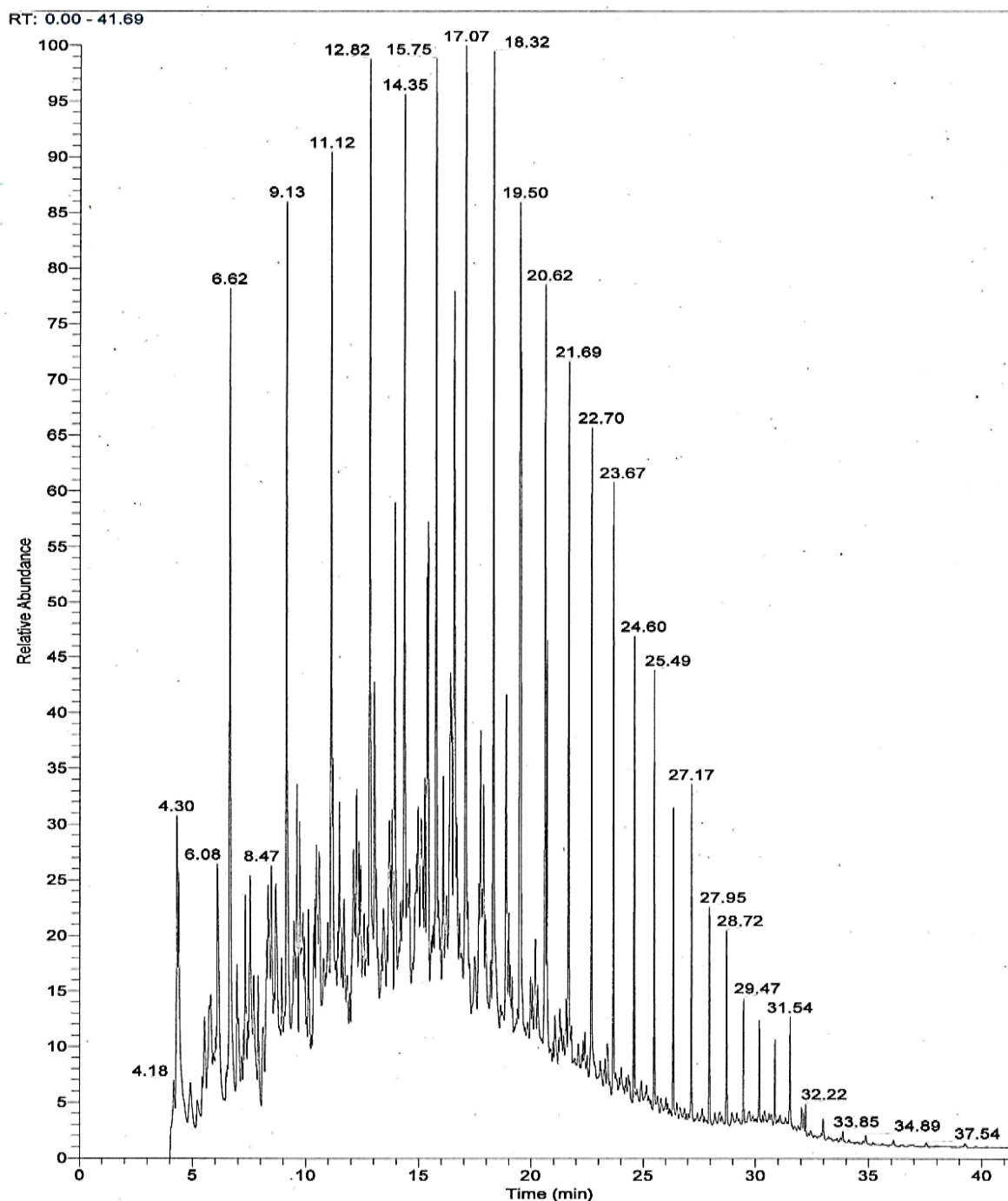
Figure 6.3 Gas chromatographic fingerprint of 'blend' crude oil sample

6.2.2. Solvent extraction of trace metal ions from crude oil

Nickel, Iron and Zinc were the three trace metals extracted from the crude oil because they were the most abundant metal ions found from the crude oil analysis. The result of the solvent extraction of trace metal ions from crude oil is as shown in table 6.5-6.7.

The % extraction indicates how much metal cation is taken out by the solvent mixture and/or complexing agent.

Table 6.5: Extraction of nickel ions from crude oil

| Sample ID	Wt. %	Moles	Conc. (ppm)	% Extr.
Crude oil	$5.9 \times 10^{-3} \pm 2 \times 10^{-4}$	$1 \times 10^{-4} \pm 4 \times 10^{-6}$	5.9 ± 0.2	0
Crude + H_2O	$5.8 \times 10^{-3} \pm 1 \times 10^{4}$	$9.9 \times 10^{-5} \pm 2 \times 10^{-6}$	5.8 ± 0.1	4.4
Crude + H_3PO4	$4.7 \times 10^{-3} \pm 1 \times 10^{-4}$	$8.1 \times 10^{-5} \pm 2 \times 10^{-6}$	4.7 ± 0.1	21.7
Crude + EDTA	$4.4 \times 10^{-3} \pm 1 \times 10^{-4}$	$7.4 \times 10^{-5} \pm 2 \times 10^{-6}$	4.4 ± 0.1	28.3
Crude + IPA	$4.1 \times 10^{-3} \pm 1 \times 10^{-4}$	$7 \times 10^{-5} \pm 2 \times 10^{-6}$	4.1 ± 0.1	32.6
ZA + IPA + crude	$2.4 \times 10^{-3} \pm 9 \times 10^{-5}$	$4 \times 10^{-5} \pm 2 \times 10^{-6}$	$2.4 \pm 9 \times 10^{-2}$	60.9
ZX + IPA + crude	$2.1 \times 10^{-3} \pm 8 \times 10^{-5}$	$3.6 \times 10^{-5} \pm 1 \times 10^{-6}$	$2.1 \pm 8 \times 10^{-2}$	65.2
ZA + crude	$5.7 \times 10^{-3} \pm 1 \times 10^{-4}$	$9.7 \times 10^{-5} \pm 2 \times 10^{-6}$	5.7 ± 0.1	6.52
ZX + crude	$4 \times 10^{-3} \pm 1 \times 10^{-4}$	$6.7 \times 10^{-5} \pm 2 \times 10^{-6}$	4 ± 0.1	34.8
ZA + H_3PO4 + crude	$2.9 \times 10^{-3} \pm 9 \times 10^{-5}$	$4.9 \times 10^{-5} \pm 2 \times 10^{-6}$	$2.9 \pm 9 \times 10^{-2}$	52.2
ZX + H_3PO4 + crude	$3.7 \times 10^{-3} \pm 1 \times 10^{-4}$	$6.3 \times 10^{-5} \pm 2 \times 10^{-6}$	3.7 ± 0.1	39.1
ZY-APTES + H_3PO4 + crude	$2.8 \times 10^{-3} \pm 9 \times 10^{-5}$	$4.7 \times 10^{-5} \pm 2 \times 10^{-6}$	$2.8 \pm 9 \times 10^{-2}$	54.3
ZA + EDTA + crude	$2.6 \times 10^{-3} \pm 9 \times 10^{-5}$	$4.5 \times 10^{-5} \pm 2 \times 10^{-6}$	$2.6 \pm 9 \times 10^{-2}$	56.5
ZX + EDTA+ crude	$5.8 \times 10^{-3} \pm 1 \times 10^{-4}$	$9.9 \times 10^{-5} \pm 2 \times 10^{-6}$	5.8 ± 0.1	4.35
ZY-APTES + EDTA+ crude	$5.8 \times 10^{-3} \pm 1 \times 10^{-4}$	$9.9 \times 10^{-5} \pm 2 \times 10^{-6}$	5.8 ± 0.1	4.35

Table 6.6: Extraction of Iron from crude oil

Sample ID	Wt. %	Moles	Conc. (ppm)	% Extr.
Crude oil	$7.5\times10^{-2} \pm 5\times10^{-3}$	$1.4\times10^{-3} \pm 9\times10^{-5}$	75.1 ± 5	0
Crude + H_2O	$7.4\times10^{-2} \pm 5\times10^{-3}$	$1.3\times10^{-3} \pm 8\times10^{-5}$	74.1 ± 5	1.3
Crude + H_3PO4	$1.7\times10^{-2} \pm 8\times10^{-4}$	$3.1\times10^{-4} \pm 1\times10^{-5}$	17.0 ± 0.8	77.3
Crude + EDTA	$6\times10^{-2} \pm 9\times10^{-4}$	$1.1\times10^{-3} \pm 2\times10^{-5}$	60.1 ± 0.9	20
Crude + IPA	$1.6\times10^{-2} \pm 7\times10^{-4}$	$2.9\times10^{-4} \pm 1\times10^{-5}$	16.0 ± 0.7	78.7
ZA + IPA + crude	$7\times10^{-3} \pm 6\times10^{-4}$	$1.3\times10^{-3} \pm 1\times10^{-5}$	7.0 ± 0.6	90.7
ZX + IPA + crude	$7\times10^{-3} \pm 6\times10^{-4}$	$1.3\times10^{-4} \pm 1\times10^{-5}$	7.0 ± 0.6	90.7
ZA + crude	$1\times10^{-2} \pm 6\times10^{-4}$	$1.8\times10^{-4} \pm 1\times10^{-5}$	10.0 ± 0.6	86.7
ZX + crude	$1.3\times10^{-2} \pm 7\times10^{-4}$	$2.3\times10^{-4} \pm 1\times10^{-5}$	13.0 ± 0.7	82.7
ZA + H_3PO4+ crude	$9\times10^{-3} \pm 6\times10^{-4}$	$1.6\times10^{-4} \pm 1\times10^{-5}$	9.0 ± 0.6	88.0
ZX + H_3PO4+ crude	$5\times10^{-3} \pm 5\times10^{-4}$	$9\times10^{-5} \pm 9\times10^{-6}$	5.0 ± 0.5	93.3
ZY-APTES + H_3PO4 + crude	$1.5\times10^{-3} \pm 7\times10^{-4}$	$2.7\times10^{-4} \pm 1\times10^{-5}$	15.0 ± 0.7	80.0
ZA + EDTA+ crude	$1.3\times10^{-2} \pm 7\times10^{-4}$	$2.3\times10^{-4} \pm 1\times10^{-5}$	13.0 ± 0.6	82.7
ZX + EDTA+ crude	$9\times10^{-3} \pm 6\times10^{-4}$	$1.6\times10^{-4} \pm 1\times10^{-5}$	9.0 ± 0.6	88.0
ZY-APTES +EDTA+ crude	$1.6\times10^{-2} \pm 7\times10^{-4}$	$2.9\times10^{-4} \pm 1\times10^{-5}$	16.0 ± 0.7	78.7

Table 6.7: Extraction of zinc from crude oil

Sample ID	Wt. %	Moles	Conc. (ppm)	% Extr.
Crude oil	$3x10^{-3} \pm 5x10^{-3}$	$4.6x10^{-5} \pm 8x10^{-6}$	3.0 ± 0.5	0
Crude + H_2O	$2.4x10^{-3} \pm 4x10^{-4}$	$3.6 x10^{-5} \pm 6x10^{-6}$	2.4 ± 0.4	21.4
Crude + H_3PO4	$1.5x10^{-3} \pm 1x10^{-5}$	$2.3x10^{-5} \pm 2x10^{-6}$	1.5 ± 0.1	50
Crude + EDTA	$6.5x10^{-4} \pm 1x10^{-5}$	$9.9x10^{-6} \pm 2x10^{-6}$	0.7 ± 0.1	78.6
Crude + IPA	$6.5x10^{-4} \pm 1x10^{-5}$	$9.9x10^{-6} \pm 1x10^{-6}$	0.7 ± 0.1	78.6
ZA + IPA + crude	$6.5x10^{-4} \pm 8x10^{-5}$	$9.9x10^{-6} \pm 1x10^{-6}$	0.7 ± 0.08	78.6
ZX + IPA + crude	ND*			
ZA + crude	$1.5 x10^{-3} \pm 1x10^{-4}$	$2x10^{-5} \pm 2 x10^{-6}$	1.5 ± 0.1	50
ZX + crude	$1.3x10^{-3} \pm 1 x10^{-4}$	$2x10^{-5} \pm 2 x10^{-6}$	1.3 ± 0.1	57.1
ZA + H_3PO4 + crude	ND*			
ZX + H_3PO4 + crude	ND*			
ZY-APTES +H_3PO4 + crude	ND*			
ZA + EDTA+ crude	$4.3x10^{-4} \pm 8x10^{-5}$	$6.6 x10^{-6} \pm 1x10^{-6}$	0.4 ± 0.08	85.7
ZX + EDTA+ crude	$4.3x10^{-4} \pm 8x10^{-5}$	$6.6x10^{-6} \pm 1x10^{-6}$	0.4 ± 0.08	85.7
ZY-APTES + EDTA+ crude	$6.5x10^{-4} \pm 1x10^{-4}$	$9.9x10^{-6} \pm 2x10^{-6}$	0.7 ± 0.1	78.6

ND*=Not-detected

The result of the solvent extraction of nickel, iron and zinc from the crude oil shows that all the metal ions could be extracted by the solvents and aqueous solutions used. The extent/degree of extraction however varies. For nickel cation, the extent of extraction in the order of increasing % extraction is $H_2O<H_3PO_4<Na-EDTA<IPA$. A similar trend is observed when the solvent/solution-crude oil mixture was treated with zeolite A, the nickel extraction in the order of increasing % extraction was found to be $H_3PO_4<Na-EDTA<IPA$. For zeolite X, the order was found to be Na-EDTA<H_3PO_4< IPA. ZY-APTES showed % nickel extraction in the order Na-EDTA<H_3PO_4. The extraction of iron from the crude oil (Table 6.6) showed the extent of extraction of iron in the order of increasing % extraction as H2O=EDT<H_3PO<IPA. Addition of zeolite materials to the system, gave the extent of iron extraction in the order of increasing % extraction for; Zeolite A as EDTA<H_3PO_4<IPA, Zeolite X as EDTA<IPA <H_3PO_4 and Zeolite Y- APTES as

EDTA<H_3PO_4. The extraction of zinc ions from the crude oil (Table 6.7) on the other hand showed the extent of zinc extraction in the order H_2O<H_3PO_4 <CH_3OH=EDTA.

The extracting media were much better at extracting or removing, iron cations (ca.90 %) over nickel cations. This could be due to the size difference between the metal cations which could have resulted in different hydration spheres around the metal ions, thus the difference in their ease of extraction.

The amount of cations extracted by water as compared to IPA shows the alcohol significantly improves the removal of the nickel cations.

The aqueous solution of phosphoric acid also gave a good extraction and removal by the zeolite materials. However, the PXRD on the zeolite samples after removal of the cations from aqueous solution of H_3PO_4 shows that the zeolites fall apart after the extraction and removal process (figure 6.4), except for ZY-APTES. This behaviour is expected since zeolites are not very stable in acid environments.
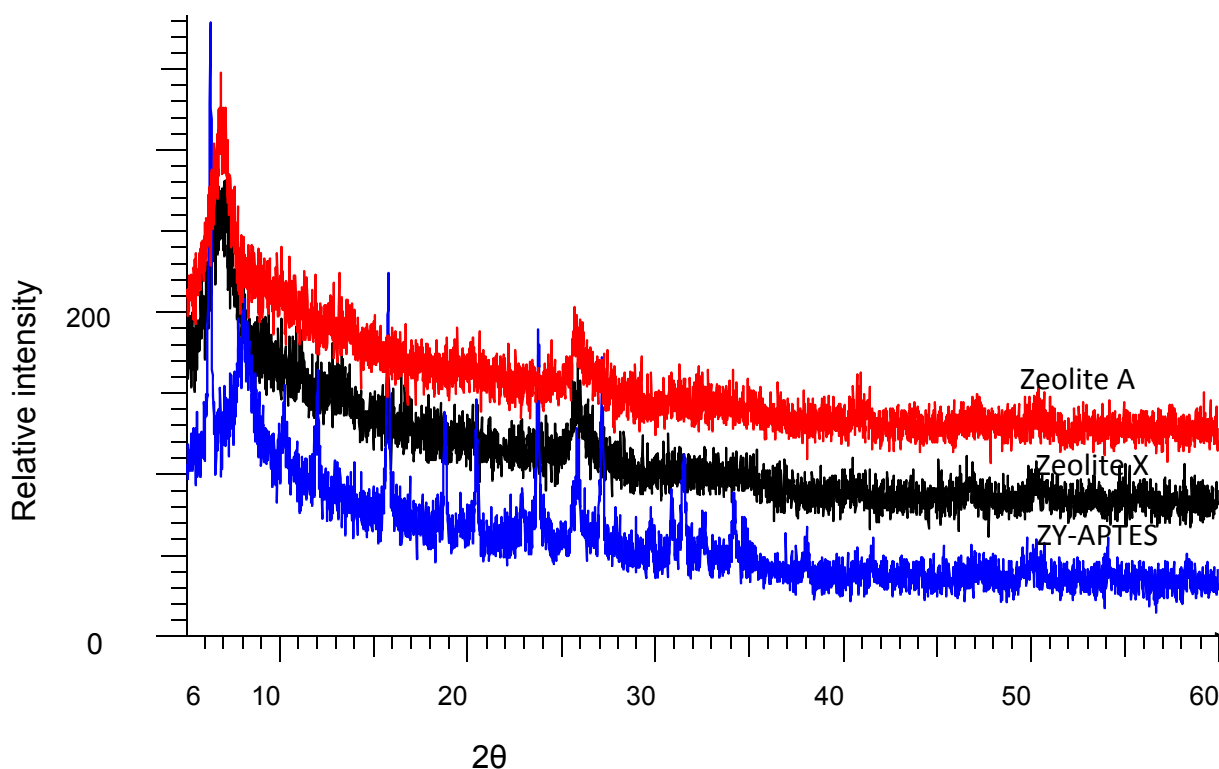

Figure 6.4: PXRD patterns of zeolites A, X and Y after extraction/removal in aqueous solution of H_3PO_4

The alcohol, IPA, was observed to have significant influence on the extraction of the metal ions from crude oil. The effect of the alcohol on the extraction of these metal ions could also be explained based on their high dielectric constants and dipole moments. Isopropanol has a relatively high dielectric constants (18) and high dipole moment (1.66) close to those of water (80 and 1.85), as a result, they are able to provide suitable coordination environment to cations in solution. Another reason may be the ease of solvation of ions in the solvent. The alcohol must have been able to stabilise cations in solution at their intermediate states more effectively compared to the other extraction media used. Also the alcohol (IPA) has relatively high hydrogen bond δH (16.4) and so is able to hydrogen bond to oxygen of the zeolite framework. These results are in good agreement with results obtained in the previous chapters (chapter 4 and 5). The solvent (IPA) used in the treatment of a model Ni-tetraphenylporphyrin (Ni-TPP) compound in chapter 4, was shown to have promoted the dissolution of the Ni-TPP by the α-hydrogen donor activity of the solvent. It is therefore possible that the alcohol used for the extraction of metal ions from crude oil had a similar effect on the metal-complexes in the crude oil.

6.3. Conclusion

Characterisation studies of the crude oil used in this study was carried out. Parameters such as the density, API gravity, sulphur content, trace metal content as well as the gas chromatographic analysis of the crude oil were carried out to determine the physicochemical properties and the hydrocarbon fingerprint of the crude oil. Extraction of metal ions from the crude oil using different extraction media, showed the alcohol, IPA, to be the most efficient at extracting the metal ions from the crude oil.

References

1. C.A. Fleming and A.J. Monhemious, Hydrometallurgy, 1979, 4, 159–167.

2. V. M.Radak and M.V Susic, J. inorg. nucl. chem., 1971, 33, 1927-1931.

3. Z. Dizdar, J. inorg. Nucl. Chem., 1972, 34, 1069-1081.

4. M.M. Awad, A.M.A. Salem and A.A Swelam, Indian J. Chemistry, A: Inorg., Bioorg., Phys., Theor. Anal. Chem., 1996, 35A, 693–701.

5. J.I. Kim, J. Inorg. Nucl. Chem., 1975, 37, 239–245.

6. V.I. Gorshkov and A.I. Vovk, Zh. Fiz. Khim., 1968, 42, 2252–2258.

7. C. Poitrenaud, Bull. Inform. Sci. Tech., 1964, 85, 25–33.

8. J.G. Jones and J.D.R. Thomas, Talanta, 1972, 19, 961–969.

9. D. Bae and K. Seff, Zeolites, 1996, 17, 444–446.

10. V.M. Radak and M.V. Susic, J. Inorg. Nucl. Chem., 1971, 33, 1927–1931.

11. V.J. Inglezakis, M.D. Loizidous, Desalination, 2007, 211, 238-248.

12. K. Ho, H. S. Lee, B. C. Leano, Tao Sun and K. Seff, Zeolites, 1995,15, 377-381.

13. Haruo Uyama, Yasush Kanzaki and Osamu Matsumoto, Mat. Res. Bull., 1987, 22, 157-164.

14. D. Acevedo, Luis F. D'Elia Camacho, Jorge Moncada, Z. Puentes, Fuel, 2012, 92, 264–270

15. D.S. Ross, P. alto, J.E. Blessing and M. Park, Patent number 4298450, 1981.

16. J.M. Hunt, petroleum Geochemistry and Geology. 1996. Freeman and company. New York, USA, 231-238

17. American Petroleum Institute (2011). API Speciation for Materials and Testing for Petroleum Products. API Production Dept. API 14A. Eleventh edition. Dallas: 20-21. AOAC (1984) Official Methods Analytical Chemistry 10th ed: 79-81.

18. H. Volk, S.C. George, H. Middleton and S. Schofield, 36, 2006, (1):29-51.

19. J.M. Fausnaugh, (2002). Using Trace Metals as Abnormally Identification and characterization of crude oil samples. www.Jeotech. Org. retrieved 12/07/2011.

20. A.A. Akinlua, T.R. and B.B. Adeleke, Geochemical journal, 2007, 41,271-281.

21. M.F. Ali, A. Bukharl and M. Saleem, Ind. Eng. Chem. Prod. Res. Dev. 1983, 22,691-694.

22. M.F. Ali and S. Abbas, Technol., 2006, 86, 573-584.

23. Udoessien, E.I. (1997): Pollution in Petroleum and Allied Industries. Mef (Nig) Ltd,Uyo: 5-7

24. A. J. G. Barwise, Energy and Fuels, 1990, 4, 647-652.

25. M.C. Onoja, N.C. Oforka, L.C. Osuji, Energy and fuel research, 2011, 1, 139-146.

26. J.D, Udeme and I.U. Etim, Petroleum and Coal, 2012, 54(3), 243-251.

27. A.A. Olajiri and R.A. Oderinde, Bull. Chem. Soc. Jpn., 1993, 66, 630-632.

Chapter 7: Summary, Conclusion and recommendations

7.1. Summary and Conclusion

The work reported in this thesis is focused on the investigations of zeolites as ion-exchangers/adsorbents for the possible removal of nickel (II) and vanadium (IV) ions from crude oil. Nickel (II) and vanadium (IV) were the target metal ions due to their poisoning effect on the hydroprocessing catalysts.

Amongst the technologies in use to improve production of transportation fuel from heavy oils, hydrocracking is one of the most efficient with high selectivity to middle distillate and low selectivity to coke. Hydrocracking, in most cases combines, with other pre-treatment processes known as hydrotreating processes. The crude oil feeds for hydrocracking most often contain high levels of Ni (II) & V (IV) ions, such that the conventional acid catalysts, used during the hydroprocessing are easily poisoned thus giving additional costs of either catalyst regeneration or replacement to the refinery. These issues necessitates the search for materials that would efficiently reduce the metal cation concentration from crude oil, thus the importance of this research.

Synthetic zeolites A, X and Y having porous framework, large surface area, catalytic, ion exchange and adsorption properties, have been employed in industrial applications like heterogeneous catalysis, water softening and wastewater treatment. The effectinveness of the zeolites for these application was the reason behind their use in this research study.

The efficacy of using sodium based-zeolites A, X and Y for the removal of nickel (II) and vanadium (IV) ions from aqueous solution by batch ion-exchange have been evaluated under non-competitive and competitive conditions. The vanadium ion-exchange gave a much higher metal ion uptake than that for nickel under identical experimental conditions with exchange efficiency of about 90 % for zeolite A. The nickel ion-exchange recorded an exchange efficiency of about 38 % for zeolite X which was shown to have occurred mostly at the exchange sites of the zeolite. The framework structure of the zeolites were maintained even though some amounts of silicon leaching was observed. An ''over ion-exchange'' was observed in the case of vanadium exchange. Characterisation of the vanadium-exchanged zeolite A, showed that all the sodium cations (Na$^+$) within the zeolite were exchanged and in addition, a significant

amount of silicon species (77.4 %) were also exchanged by the vanadium(IV) ions, while the amount of Al (III) ions remain fairly constant. This clearly shows that, the vanadium (IV) ion exchange did not only occur with sodium cations at the exchange sites but also with the framework cations. This resulted to zeolite collapse, so there was a need to improve Ni(II) exchange, hence focus of the remainder of the thesis.

Potassium and lithium-based zeolites were synthesised and tested for the efficacy of the nickel ion removal compared with that of the parent zeolite materials investigated. There was little or no observed increase in the nickel ion exchange activity of the alkali metal zeolites compared to the parent zeolites at higher concentrations of the nickel solutions. However, at lower concentrations there was a marked increase in the nickel uptake by the alkali metal-zeolites. Thus at lower concentration of nickel (0.01M), alkali metal zeolites can be used to remove nickel ions from solution at higher efficiency compared to the parent zeolite.

The optimum conditions for the ion exchange reactions were established. A contact time of 24 h (1440 min) and zeolite dosage of 0.5 g were obtained as the optimum time and dosage for the exchange process.

A further investigation using a ligand grafted zeolite Y was carried out. The ligand (APTES) was successfully grafted on zeolite Y. The ligand grafted zeolite Y gave a Ni (II) ion uptake over 90 % as compared to 35.2 % uptake by the parent zeolite Y. This study suggests that ligand modified zeolite Y could be used to significantly improve the uptake of metal ions from solution, hence crude oil.

A good percentage of the total vanadium and nickel content in crude oil is made up of metalloporphyrins. Thus it is appropriate to use a metalloporphyrins model compound to study the metal ion uptake from crude oil. During hydro-desulphurization and catalytic cracking of crude oil, the feedstock are exposed to H_2 and H_2S and at high temperature and pressure, hydrodemetalization may occur. These metals are deposited on the catalysts, thus poisoning the catalysts. A pre-treatment of the crude oil using a hydrogen-donor solvent and subsequent treatment with zeolite materials before it gets through to the downstream processing units was proposed to be a feasible method of metal ions removal from crude oil.

A model compound of nickel-tetraphenylporphyrin (Ni-TPP) was used to investigate the removal of metal ions from crude oil and modelling of the actual process. The model compound was first synthesised and demetallated. Analysis of the demetallated Ni-TPP solutions before and after treatment with zeolites showed 89.8 % nickel exchange for zeolite X .

The success of the nickel ion exchange in aqueous medium was achieved, particularly for zeolite X. Zeolite A, on the other hand falls apart after the vanadium ion exchange, so cannot be said to be successful. Similarly, ion-exchange in crude oil requires a medium of exchange. Amongst the media of extraction tested for metal ion extraction and removal from crude oil, isopropyl alcohol-water mixture (50:50) gave the highest nickel and iron extraction of about 65 % and 91 % respectively. This result is in good agreement with earlier investigations in this work (chapter 4).

Based on the results of these studies, zeolites materials particularly zeolite X and modified zeolite Y, has the potential to provide methods for the removal of poisoneous metal ions from crude oil.

7.2. Limitations of the study

As the ion-exchange process was carried-out mainly in aqueous media and polar solvent mixture, the results could have been more comparable if the exchange in non-polar media were also considered. Considering our line of research, it was difficult to separate and analyse the individual components for the metal ions using non-polar solvents, since the two are missible. However, the results obtained from this work can be used as a model for other systems.

There was also difficulty in analysing for the metal ions in the liquid crude oil samples since most of the instrumentation available could not tolerate organics. The crude oil had to be ashed before analysis which makes it prone to risks of contamination or loss of analyte due to the formation of volatile compounds.

7.3. Recommendations for future work

The use of a composite zeolite (combining two or more of the zeolites) is recommended. This might improve the uptake of both Ni (II) and V (IV) given the right

medium of extraction. The ligand grafting on the zeolites using different other organic ligand could allow one to compare the different types of ligands and discuss the differences between them e.g donor atoms and chain lengths.

An ion-exchange/extraction method can be developed under similar conditions using non-polar solvents. This might provide a better mimic for the crude oil environment, since it is non-polar in nature. Buffering the vanadium (VI) solution could help regulate the pH of the solution, thus maintaining the framework structure of the zeolites after the vanadium ion exchange.

The use of a column for the continuous ion-exchange process might offer a more efficient and easy way of reactivating the zeolite materials for subsequent reuse and ease of automation of the process. Experiments on the metal ion recovery from the zeolites after the removal process could also be considered, such that the metal ions are recovered and the zeolites reused for the target application.

Appendices

Appendix 1: Alkali metal exchanged zeolites

Sample ID	% K in zeolites	K /Li in Formula	Formula
Potassium zeolite A	57.7±0.4	6.9±0.1	$Na_{5.1}K_{6.9}Al_{12}Si_{12}O_{48}.24.8H_2O$
Potassium zeolite X	42.0±0.5	36.1±0.8	$Na_{51.9}K_{36.1}Al_{88}Si_{106}O_{384}.211.3H_2O$
Potassium zeolite Y	41.9±0.7	23.5±0.6	$Na_{31.4}K_{23.5}Al_{56}Si_{136}O_{384}.215.8H_2O$
Potassium sodalite (0.1 M KNO$_3$)	3.2±0.4	0.3±0.04	$Na_{7.7}K_{0.3}[AlSiO_4]_6Cl_2$
K-SOD(2 M KNO$_3$)	40.9±0.05	3.3±0.04	$Na_{4.7}K_{3.3}[AlSiO_4]_6Cl_2$
K-HydroSOD (2 M KNO$_3$)	43.3±0.05	2.6±0.03	$Na_{3.4}K_{2.6}[AlSiO_4]_6.6H_2O$
K-HydroSOD (2 M KOH)	44.0±0.05	2.6±0.03	$Na_{3.4}K_{2.6}[AlSiO_4]_6.6H_2O$
Lithium zeolite A	29.3±3.9	3.5±0.5	$Na_{8.5}Li_{3.5}Al_{12}Si_{12}O_{48}.29.7H_2O$
Lithium zeolite X	28.7±2.9	24.7±2.7	$Na_{63.3}Li_{24.7}Al_{88}Si_{106}O_{384}.263.2H_2O$
Lithium zeolite Y	17.6±2.6	9.9±1.6	$Na_{45}Li_{9.9}Al_{56}Si_{136}O_{384}.284.6H_2O$
Li-SOD	38.3±0.2	3.1±0.05	$Na_{4.9}Li_{3.1}[AlSiO_4]_6Cl_2$
Li-HydroSOD	41.4±0.2	2.5±0.04	$Na_{3.5}Li_{2.5}[AlSiO_4]_6.6H_2O$

Appendix 2: Zeolitic exchange with nickel (II)

| Zeolites	Molar Conc.	% Ni^{2+} in zeolites	Ni^{2+} in formula	Formula
Zeolite A	0.01M	28.8 ± 1	3.7 ± 0.3	$Na_{4.6}Ni_{3.7}Al_{12}Si_{12}O_{48}.24.2H_2O$
	0.025M	22.7 ± 0.3	2.9 ± 0.1	$Na_{7.2}Ni_{2.9}Al_{12}Si_{12}O_{48}.24.2H_2O$
	0.05M	20.8 ± 0.3	2.7 ± 0.1	$Na_{6.7}Ni_{2.7}Al_{12}Si_{12}O_{48}.24.2H_2O$
	0.075M	19.5 ± 0.2	2.5 ± 0.08	$Na_{7.0}Ni_{2.5}Al_{12}Si_{12}O_{48}.24.2H_2O$
	0.1M	23.4 ± 0.09	3.0 ± 0.08	$Na_{6.0}Ni_{3.0}Al_{12}Si_{12}O_{48}.24.2H_2O$
Zeolite X	0.01M	37.5 ± 1	39.8 ± 2	$Na_{8.4}Ni_{39.8}Al_{88}Si_{106}O_{384}.238.8H_2O$
	0.025M	32.9 ± 0.4	35 ± 1	$Na_{18.0}Ni_{35.0}Al_{88}Si_{106}O_{384}.238.8H_2O$
	0.05M	36.3 ± 0.3	38.6 ± 1	$Na_{10.8}Ni_{38.6}Al_{88}Si_{106}O_{384}.238.8H_2O$
	0.075M	37.6 ± 0.2	40 ± 1	$Na_{8.0}Ni_{40.0}Al_{88}Si_{106}O_{384}.238.8H_2O$
	0.1M	35.9 ± 1	38.1 ± 1	$Na_{11.8}Ni_{38.1}Al_{86}Si_{106}O_{384}.238.8H_2O$
Zeolite Y	0.01M	18.1 ± 1	18.7 ± 2	$Na_{17.5}Ni_{18.7}Al_{56}Si_{136}O_{384}.246.5H_2O$
	0.025M	11.2 ± 1	11.5 ± 2	$Na_{31.9}Ni_{11.5}Al_{56}Si_{136}O_{384}.246.5H_2O$
	0.05M	10.4 ± 3	10.8 ± 4	$Na_{33.3}Ni_{10.8}Al_{56}Si_{136}O_{384}.246.5H_2O$
	0.075M	9.5 ± 0.7	9.8 ± 0.9	$Na_{35.3}Ni_{9.8}Al_{56}Si_{136}O_{384}.246.5H_2O$
	0.1M	9.8 ± 0.5	10.1 ± 0.7	$Na_{34.7}Ni_{10.0}Al_{56}Si_{136}O_{384}.246.5H_2O$

Appendices

Appendix 3: Zeolitic exchange with vanadium (IV)

Zeolites	Molar Conc.	V^{4+} in zeolites (ppm)	V^{4+} in zeolites (moles)	% V^{4+} in zeolites	V in formula
Zeolite A	0.01M	426±4.1	$2.5 \times 10^{-3} \pm 3 \times 10^{-5}$	84±0.9	10.0±0.3
	0.025M	1060±1.7	$6.3 \times 10^{-3} \pm 1 \times 10^{-5}$	83±0.2	10.1±0.2
	0.05M	2225±3.7	$1.3 \times 10^{-2} \pm 2 \times 10^{-3}$	87±0.2	11.2±0.3
	0.075M	2844±5.1	$1.7 \times 10^{-2} \pm 3 \times 10^{-5}$	75±0.2	9.6±0.2
	0.1M	4058±16.7	$2.4 \times 10^{-2} \pm 1 \times 10^{-5}$	80±0.4	10.2±0.3
Zeolite X	0.01M	212±4.8	$1.3 \times 10^{-3} \pm 3 \times 10^{-5}$	42±1.0	44.3±2
	0.025M	634±5.3	$3.7 \times 10^{-3} \pm 3 \times 10^{-5}$	50±0.5	53.0±2
	0.05M	1577±7.6	$9.3 \times 10^{-3} \pm 5 \times 10^{-5}$	62±0.4	65.8±2
	0.075M	1895±8.2	$1.1 \times 10^{-2} \pm 5 \times 10^{-5}$	50±0.3	52.7±1
	0.1M	2390±15	$1.4 \times 10^{-2} \pm 8 \times 10^{-5}$	47±0.4	49.9±1.4
Zeolite Y	0.01M	132±5.2	$7.7 \times 10^{-4} \pm 3 \times 10^{-5}$	26±1.1	3.8±0.2
	0.025M	412±7.5	$2.4 \times 10^{-3} \pm 4 \times 10^{-5}$	32±0.6	4.8±0.2
	0.05M	681±12.1	$4 \times 10^{-3} \pm 7 \times 10^{-5}$	27±0.5	4.0±0.2
	0.075M	1064±10.2	$6.3 \times 10^{-3} \pm 6 \times 10^{-5}$	28±0.3	4.1±0.1
	0.1M	977±17.3	$5.8 \times 10^{-3} \pm 1 \times 10^{-3}$	19±0.4	2.9±0.1

Appendix 4: SEM chromatograms of zeolite X after Ni^{2+} exchange
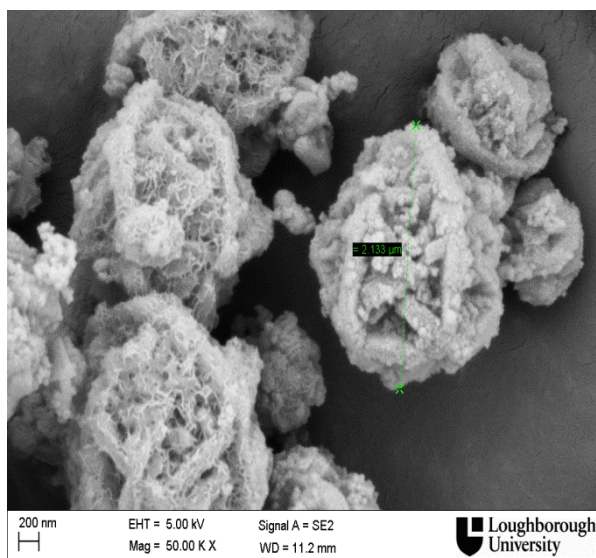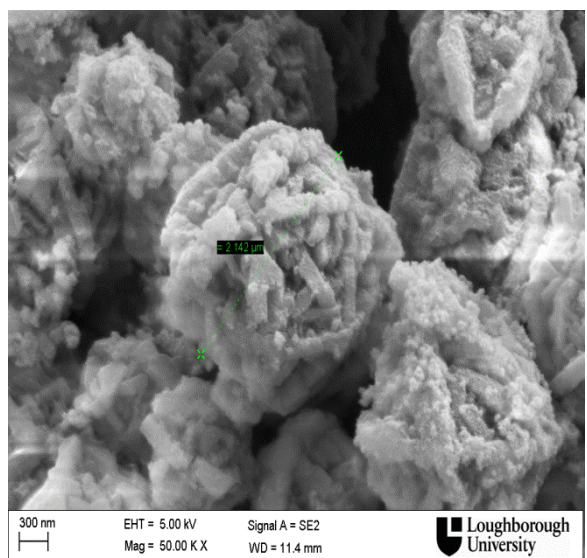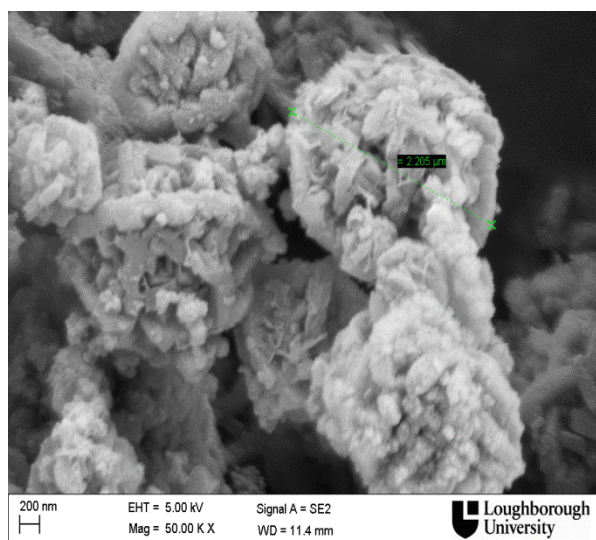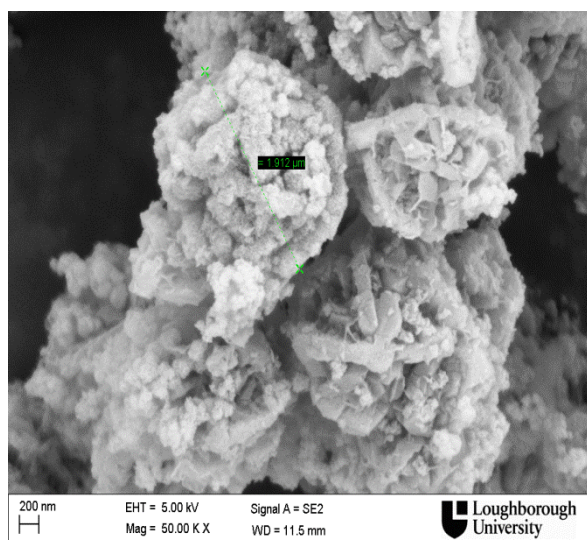
Appendix 5: SEM chromatograms of zeolite A after vanadium exchange
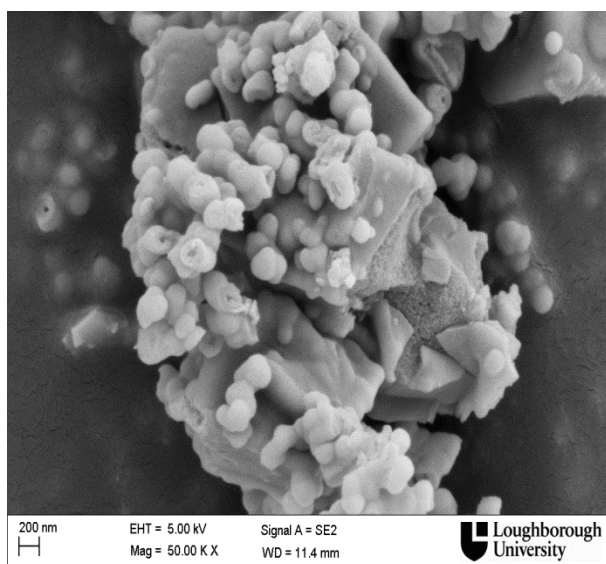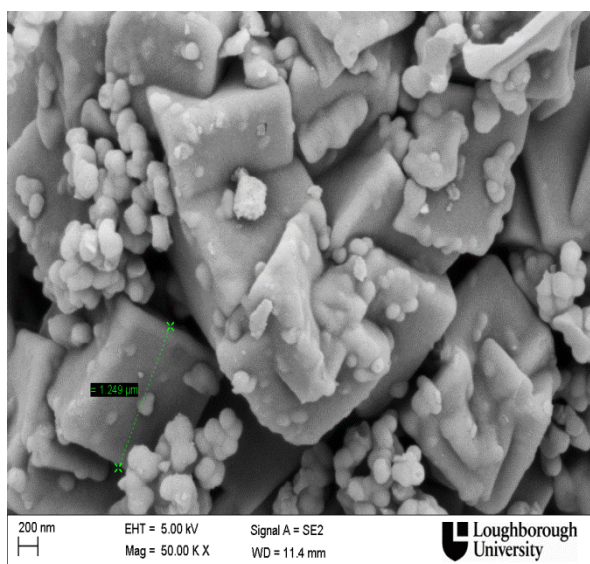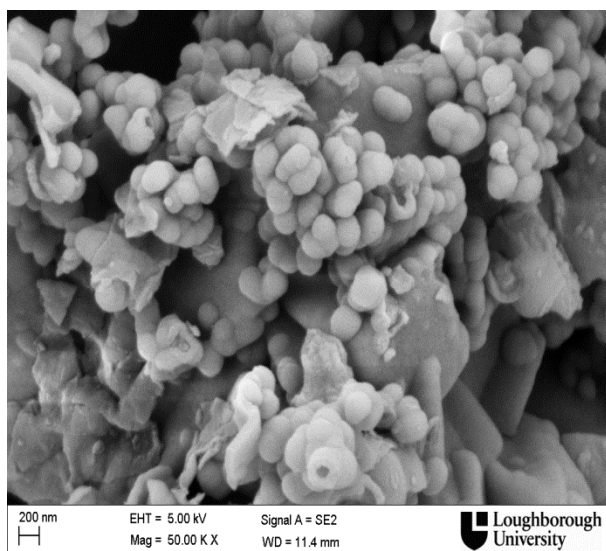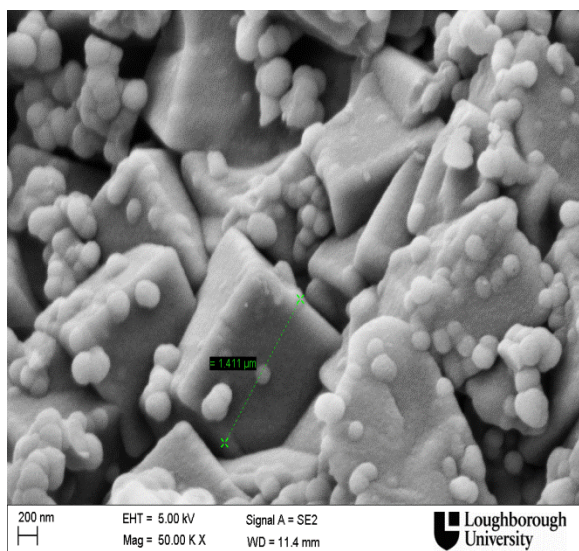
Drafts for publication

R.E. Ikyereve, S.E.Dann, Organic ligand grafted zeolites for the removal of metal ions from solution, Drafted document.

R.E. Ikyereve, S.E.Dann, Ni-tetraphenylporphyrin; synthesis, hydrodemetallation and nickel removal by zeolites, Drafted document.

R.E. Ikyereve, S.E.Dann, Ion Exchange of nickel (II) and vanadium (IV) from aqueous solution, Drafted document.